Fabrication of a Biodegradable Polymeric Nanostructural Carrier Mediated Target Specific Drug Delivery System for the Treatment of Lung Cancer

Thesis submitted by

LEENA KUMARI

DOCTOR OF PHILOSOPHY (PHARMACY)

Department of Pharmaceutical Technology

Faculty Council of Engineering and Technology

Jadavpur University

Kolkata, India

2023

INDEX NO. 268/18/Ph

1. **Title of the thesis:** Fabrication of a Biodegradable Polymeric Nanostructural Carrier Mediated Target Specific Drug Delivery System for the Treatment of Lung Cancer

2. **Name, Designation and institution of supervisor:**

Professor (Dr.) Biswajit Mukherjee

Professor,

Department of Pharmaceutical Technology,

Jadavpur University,

Kolkata-700032, India.

3. **List of publications (related to thesis)**

(i) **Leena Kumari,** Iman Ehsan, Arunima Mondal, Ashique Al Hoque, Biswajit Mukherjee, Pritha Choudhury, Arunima Sengupta, Ramkrishna Sen, Prasanta Ghosh, Cetuximab-conjugated PLGA nanoparticles as a prospective targeting therapeutics for non-small cell lung cancer, Journal of Drug Targeting 31 (2023) 521-536. https://doi.org/10.1080/1061186X.2023.2199350 **(Impact Factor: 5.016)**

Other Publications

(ii) Iman Ehsan, **Leena Kumari**, Ramkrishna Sen, Ashique Al Hoque, Biswajit Mukherjee, Alankar Mukherjee, Prasanta Ghosh, Sanchari Bhattacharya, J591 functionalized Paclitaxel loaded PLGA nanoparticles successfully inhibited PSMA overexpressing LNCaP cells, Journal of Drug Delivery Science and Technology, 75 (2022) 103689. https://doi.org/10.1016/j.jddst.2022.103689 **(Impact Factor: 5.062)**

(iii) Nabanita Kar, Santanu Ghosh, **Leena Kumari,** Shreyasi Chakraborty, Tanmoy Bera, Search for new antileishmanial chemotherapeutics, International Journal of Pharmacy and Pharmaceutical Sciences, 10 (2018) 46-52. https://doi.org/10.22159/ijpps.2018v10i1.20859

(iv) Shreyasi Chakraborty, Nabanita Kar, **Leena Kumari**, Asit De, Tanmoy Bera, Inhibitory effect of a new orally active cedrol-loaded nanostructured lipid carrier on compound 48/80-induced mast cell degranulation and anaphylactic shock in mice, International Journal of Nanomedicine, 12 (2017) 4849-4868. https://doi.org/10.2147/IJN.S132114 **(Impact Factor: 8.0)**

Book Chapters

(i) Biswajit Mukherjee, Lopamudra Dutta, **Leena Kumari**, Manasadeepa Rajagopalan, Sanchari Bhattacharya, Manisheeta Ray, Shreyasi Chakraborty, Nonionic surfactant nanovesicles for cosmeceutical applications, In: Nanocosmeceuticals, Academic Press, 2022, pp. 327-345. https://doi.org/10.1016/B978-0-323-91077-4.00015-6

(ii) Biswajit Mukherjee, **Leena Kumari**, Iman Ehsan, Prasanta Ghosh, Soumyabrata Banerjee, Samrat Chakraborty, Manisheeta Ray, Ashique Al Hoque, Ratan Sahoo, Guar gum-based nanomaterials in drug delivery and biomedical applications, In: H. Bera, C. M. Hossain, S. Saha (Eds.), Biopolymer-Based Nanomaterials in Drug Delivery and Biomedical Applications, Academic Press, 2021, pp. 143-164. https://doi.org/10.1016/B978-0-12-820874-8.00016-6

(iii) Biswajit Mukherjee, Samrat Chakraborty, Iman Ehsan, Apala Chakraborty, **Leena Kumari**, Alankar Mukherjee, Shounak Sarkhel, Conventional and nonconventional approaches to site-specific targeting of nanotherapeutics in some infectious diseases and metabolic disorders. In: S. Talegaonkar, M. Rai (Eds.) Nanoformulations in human health, Springer Nature Switzerland AG, 2020, pp. 111-132. https://doi.org/10.1007/978-3-030-41858-8_6

(iv) Biswajit Mukherjee, Soma Sengupta , Soumyabrata Banerjee, Moumita Dhara, Ashique Al Hoque, **Leena Kumari**, Ray, Manisheeta Ray, Iman Ehsan, Alankar Mukherjee, Transdermal Nanomedicines for Reduction of Dose and Site-Specific Drug Delivery, 2020. In: M. K. Das, Y. V. Pathak (Eds.), Nano

Medicine and Nano Safety, Springer, Singapore, 2020, pp. 175-211. https://doi.org/10.1007/978-981-15-6255-6_8

(v) Biswajit Mukherjee, Ashique Al Hoque, Shreyasi Chakraborty, **Leena Kumari**, Roy S, Paul P. Nanomedicine: Could It Be a Boon for Pulmonary Fungal Infections?. In: Nanomedicine for the Treatment of Disease 2019 Sep 25 (pp. 141-164). Apple Academic Press.

4. List of patents: Nil

5. List of Presentations in National/ International/ Conferences/Workshops:

National:

National Seminar on Pharmacy & Healthcare: Traditional Knowledge to Modern Techniques held on 14th September, 2018 at Jadavpur University, Kolkata.

International:

International e-conference on 'Research advancement resilience in the pandemic era-A drive for innovative transformation' held on 26th-27th August, 2021 at School of Health Sciences, NSHM Knowledge Campus, Kolkata, India.

3rd Pharm. Tech. IAPST International Conference on 'Molecular mechanism of diseases and novel therapeutic approaches' held on 19th-20th January, 2019 at School of Pharmacy and Life Sciences, Centurion University of Technology and Management, Bhubaneswar, India.

"Statement of Originality"

I **Leena Kumari** registered on **18.05.2018** do hereby declare that this thesis entitled **"Fabrication of a Biodegradable Polymeric Nanostructural Carrier Mediated Target Specific Drug Delivery System for the Treatment of Lung Cancer"** contains literature survey and original research work done by the undersigned candidate as part of Doctoral studies.

All information in this thesis have been obtained and presented in accordance with existing academic rules and ethical conduct. I declare that, as required by these rules and conduct, I have fully cited and referred all materials and results that are not original to this work.

I also declare that I have checked this thesis as per the "Policy on Anti Plagiarism, Jadavpur University, 2019", and the level of similarity as checked by iThenticate software is **8%**.

Signatures of Candidate: *Leena Kumari*
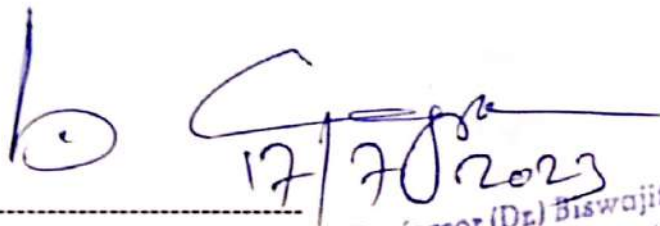
Date: 17/07/2023

Certified by Supervisor:

(Signature with date, seal)

17/ 7/ 2023

Professor (Dr.) Biswajit Mukherjee
Department of Pharmaceutical Technology
Jadavpur University
Kolkata-700032, India

CERTIFICATE FROM THE SUPERVISOR

This is to certify that the thesis entitled **"Fabrication of a Biodegradable Polymeric Nanostructural Carrier Mediated Target Specific Drug Delivery System for the Treatment of Lung Cancer"** submitted by **Ms. Leena Kumari** who got her name registered on **18.05.2018** for the award of Ph.D. (Pharmacy) degree of Jadavpur University is absolutely based upon her thesis nor any part of the thesis has been submitted for any degree/diploma or any other academic award anywhere before.

Signature of the Supervisor
and date with Office Seal

Professor (Dr.) Biswajit Mukherjee
Department of Pharmaceutical Technology
Jadavpur University
Kolkata-700032, India

ACKNOWLEDGEMENTS

Coming to this stage of my academic carrier, I express my heartfelt gratitude to the Almighty for blessing and directing me to successfully accomplish my long cherished dream of this thesis. I would like to acknowledge each and everyone, not only those who have supported me during these years of my life but also those who have always kept believe in me.

First of all, I would like to thank my Guide, **Prof. (Dr.) Biswajit Mukherjee** for giving me an opportunity to work under his guidance. His encouraging, patient and insightful guidance towards innovative and quality work has pervaded in me the essence of dedication, hard work, morality and sincerity towards research and investigation. He always had the confidence in me and my abilities, which encourage me to grow as a future researcher and face further challenges of life.

I would like to acknowledge our Head of the Department **Prof. (Dr.) Sanmoy Karmakar** for his support and technical help. I also want to owe my sincere gratitude to **Prof. Amalesh Samanta Sir, Dr. Arunima Sengupta Madam and Dr. Manas Bhowmik Sir** for providing me the technical help whenever it was required. I also want to extend my sincere thanks to all the teaching and non-teaching staffs at the Department of Pharmaceutical Technology, Jadavpur University.

I want to extend my special gratitude to **Dr. Hemant Ramchandra Badwaik** who had guided me during the B. Pharm. degree course. He is not only my teacher but my friend and philosopher as well. He always helped me in my tough times.

I convey my sincere thanks to **Department of Science and Technology (DST PURSE-II)** for providing financial assistance from 2016 to 2018 [Reference no. P-1/Rs/81/16]. I would like to express my sincere gratitude to the **Council of Scientific & Industrial Research (CSIR), New Delhi**, India, for providing technical assistance from 2018 to 2021 [File no. 09/096(0928)/2018-EMR-I].

I want to thanks from core of my heart my lab mates Ashique, Iman, Ramkrishna, Brahamacharry, Apala, my seniors, **Laboni Di, Moumita Di, Debasmita Di, Sanchari Di, Paramita Di, Lopa Di, Dipika Di, Soma Di, Shreyasi Di, Prasanta Da, Soumya Da, Tapan Da, Bhabani Da** and my juniors, **Manisheeta, Alankar, Deepayan, Sahajit, Nobila, and Sandipan** for their friendship, motivation and sharing of knowledge and experiences. I owe special thanks to **Samrat Sir** for always providing me technical help and support during the course of my research study.

I convey my special thanks to **Nabanita Di, Santanu Da, Suman Da, Asit Da, Arunima, Rajkumar and Ahana**. I want to acknowledge that without their friendship, support and motivation it was not easy to overcome during the tough times.

Words are not enough to extend my special thanks to my dear friends **Barnali, Sinjini, Anindita and Tanjina** for technical help, moral support and motivational words.

I dedicate this thesis to **my beloved parents** for their unconditional love, patience and support. You are always present in all the important moments of my life for making me the person that I am today. Thank you and love you.

Date: 17/07/2023
Place: KOLKATA (W.B.)

Leena Kumari
Leena Kumari

Dedicated to

My Beloved Parents,

&

My Guide (Prof. Biswajit Mukherjee)

PREFACE

Non small cell lung cancer (NSCLC) is among the most menacing forms of malignancy and has a poor prognosis, with a low overall survival rate due to delayed detection and ineffectiveness of conventional therapy. The conventional management of NSCLC includes different medical interventions like chemotherapy, surgical removal, and radiation therapy. However, conventional chemotherapeutic agents are nonspecifically distributed in the body where they affect both cancerous and neighbouring normal cells, thereby limiting the achievability of dose within the tumor cells and thus resulting in suboptimal treatment due to excessive toxicities. Compounds which are highly effective, such as Taxol (PTX formulation), and Taxotere (DTX formulation) for the treatment of lung cancer, are also toxic to healthy cells, and current delivery strategies are unable to target just the tumor cells, leading to side effects. Lately, nanotechnology has emerged as a promising intervention in the management and treatment of lung cancers. It has revolutionized the existing modalities and focuses primarily on reducing toxicity and improving the bioavailability of anticancer drugs to the target tumor cells.

This thesis provides an insight into the development of site-specific targeting based drug delivery for lung cancer therapy. The monoclonal antibody-conjugated nanoparticles (Cet-DTX NP) were formulated to target specifically to lung cancer cells, thereby minimizing the adverse effects on the healthy tissues. The optimized nanoformulation, DTX-loaded Poly (D, L-lactide-co-glycolide) (PLGA) nanoparticles (DTX NP) were prepared by multiple emulsion solvent evaporation technique and further conjugated with anti-EGFR antibody [Cetuximab (Cet)] by means of EDC/NHS coupling chemistry. Cet antibody is an already established predictive marker against EGFR-mediated targeted drug delivery. PLGA is USFDA approved biodegradable and biocompatible polymer for the fabrication of delivery system against a variety of human diseases. DTX is already proven to be a very potent chemotherapeutic agent against numerous cancers, including lung cancer. We have mainly focused on emphasizing on *in vivo* animal studies to demonstrate the significant potential of our nanoformulations. The obtained results supported our hypothesis, since the nanoparticles were successfully internalized within the lung cancer cells to release the drug in a sustained manner for an extended period of time, thereby improving anti-tumor efficacy against non-small cell lung adenocarcinoma. However, further investigations on the potential of these nanoparticles are warranted to bring them from bench to bedside, to serve mankind in a better way.

LIST OF ABBREVIATIONS

°C	Celsius
Abs	Absorbance
AEC	Animal Ethics Committee
ALP	Alkaline phosphatase
ANOVA	Analysis of variance
AUC	Area under the curve
AUMC	Area under the moment curve
B(a)P	Benzo[a]pyrene
bp	Base pair
BSA	Bovine serum albumin
cDNA	Complementary DNA
Cet	Cetuximab
Cet-DTX NP	Cetuximab antibody conjugated Doccetaxel loaded nanoparticles
CK	Carbon counts
C_L	Clearance
DAPI	4',6-diamidino-2-phenylindole
DCM	Dichloromethane
DMEM	Dulbecco's Modified Eagle Medium
DMSO	Dimethyl Sulfoxide
DNA	Deoxyribonucleic Acid
DTA	Data Transfer Assistance
DTX	Docetaxel
DTX NP	Docetaxel loaded PLGA nanoparticles
EDC	1-(3-dimethylaminopropyl)-3-ethylcarbodiimide hydrochloride
EDTA	Ethylenediamine tetraacetic acid
EDX	Energy dispersive X-Ray
EGFR	Epidermal Growth Factor Receptor
ELISA	Enzyme-linked immunosorbent assay
EMA	European Medicines Agency

EPR	Enhanced permeability and retention
FACS	Fluorescence Activated Cell Sorter
FBS	Fetal bovine serum
FESEM	Field emission scanning electron microscopy
FITC	Fluorescein Isothiocyanate
FTIR	Fourier Transform Infrared Spectroscopy
g	gram
GAPDH	Glyceraldehyde-3-phosphate dehydrogenase
GTP	Guanosine triphosphate
HRP	Horseradish peroxide
I.V.	Intravenous
IC_{50}	Inhibitory Concentration
ICH	International Council for Harmonizationm
ISO/TR	International Organization for Standardization/Technical Report
KBr	Potassium bromide
K_D	Dissociation constant
kDa	Kilo Dalton
LC-MS/MS	Liquid Chromatography and Mass Spectroscopy
L_D	Lethal dose
LPO	Lipid peroxidation
mAbs	Monoclonal antibodies
mg	milligram
ml	milliliter
mm	millimeter
mRNA	Messenger ribonucleic acid
MRT	Mean residence time
MST	Mean survival time
MTD	Maximum tolerated dose
MTT	3-(4,5-dimethylthiazol-2-yl)-2,5-diphenyltetrazolium bromide
mV	Millivolt
ng	Nanogram

NHS	N-hydroxysuccinimide
NK	Nitrogen counts
nM	Nanomolar
nm	Nanometer
NPs	Nanoparticles
NSCLC	Non small cell lung cancer
OD	Optical density
OK	Oxygen counts
PAHs	Polycyclic aromatic hydrocarbons
PBS	Phosphate buffer saline
PCL	Polycaprolactone
PDI	Polydispersity index
PDLA	Poly D-lactic acid
PGA	Polyglycolic acid
PI	Propidium iodide
PLGA	Poly Lactic Co-Glycolic Acid
PLLA	Poly L-lactic acid
PTX	Paclitaxel
PVA	Polyvinyl alcohol
R^2	Coefficient of determination
RES	Reticuloendothelial system
RH	Relative humidity
RIPA buffer	Radioimmunoprecipitation assay buffer
ROS	Reactive oxygen species
RPM	Rotation per minute
RPMI	Roswell Park Memorial Institute Medium
RT-PCR	Real-time reverse transcriptase-polymerase chain reaction
SCLC	Small cell lung cancer
SD	Standard deviation
SDS-PAGE	Sodium dodecyl sulfate-polyacrylamide gel electrophoresis
SGOT	Serum Glutamic Oxaloacetic Transaminase

SGPT	Serum Glutamic Pyruvic Transaminase
SK	Sulphur counts
$t_{1/2}$	Half-life
TBARS	Thiobarbituric acid reactive substance
TEM	Transmission Electron Microscopy
TGF-α	Transforming growth factor-alpha
TKIs	Tyrosine kinase inhibitors
TMB	Tetramethylbenzidine
USFDA	United States Food and Drug Administration
UV/vis	Ultraviolet-visible spectroscopy
v/v	Volume/volume
VEGF	Vascular endothelial growth factor
V_{ss}	Steady State Volume Distribution
w/v	Weight/volume
WHO	World Health Organization
λ_{max}	Wavelength of maximum absorbance
μg	microgram
μl	microliter
μM	Micromolar

CONTENTS

LIST OF FIGURES

LIST OF TABLES

1. Introduction

1.1. Lung cancer

Lung cancer is among the leading deadly cancers prevailing in human beings, all over the globe. Its mortality rate is more than the rates of the other most prevalent cancers such as pancreatic, colon and breast cancer. According to the WHO, non small cell lung cancer (NSCLC) and small cell lung cancer (SCLC) are the two broad subtypes of lung cancer, and accounts for around 85% and 15% of all the cases, respectively. NSCLC is further divided into adenocarcinoma, squamous cell carcinoma and large cell carcinoma (Zappa and Mousa, 2016; Thandra et al., 2021). Squamous cell carcinoma causes 25–30% of all instances of lung cancer. It develops from early stages of squamous cells in the bronchial tubes. Strong links between this subtype of NSCLC and cigarette smoking have been found (Furrukh, 2013). The most prevalent form of lung cancer, which accounts for about 40% of cases, is adenocarcinoma. It originates from tiny airway epithelium type II alveolar cells that secrete mucus (Denisenko et al., 2018). Regardless of age, it is the commonest type of lung cancer among men and women, smokers and non-smokers. It typically develops in the peripheral region of lungs, which might be due to the fact that the filters present in the cigarettes prevent larger particles from invading the lungs. This might lead to the formation of peripheral lesions due to deeper inhalation of cigarette smoke (Li et al., 2018). Compared to other forms of lung cancer, adenocarcinoma progresses more slowly and is prone to be detected early on before it advances to adjacent organs. The large cell (undifferentiated) carcinomas accounts for around 5-10% of the lung cancer. Large cell carcinoma typically originates in the center of the lungs, although it can sporadically spread to neighbouring lymph nodes, the thoracic wall, and neighboring organs. Large cell carcinoma tumors are strongly correlated with smoking (Rajdev et al., 2018).

1.2.   Causes of lung cancer

1.2.1. Smoking

Lung cancer is primarily caused by smoking, by far. Approximately 80% of lung cancer fatalities are related to smoking, and indirect smoke exposure contributes to many more cases. The biggest risk factor for lung cancer is undoubtedly smoking, but other factors frequently interact with it as well. Cigarette users are considerably more at risk if they are also exposed to established risk factors like asbestos and radon. Since not every

smoker develops lung cancer, it is likely that additional factors, such as genetics, are also involved (Hecht, 2002; Pesch et al., 2012).

1.2.2. Lung cancer in non-smokers

Lung cancer does not only affect smokers. While many lung cancer patients were once smokers, many others never smoked at all. Exposure to radon, indirect smoke, air pollution, or other causes can result in lung cancer in nonsmokers. In certain persons who do not smoke, occupational exposure to asbestos, diesel exhaust, or other specific substances can also result in lung cancer. The lung cancer occurring in non-smokers frequently differs from smokers' lung cancer in some respects. They usually occur when people are younger. Nonsmokers lung cancer frequently has specific gene alterations that are different from those found in smokers lung tumor (Couraud et al., 2012).

1.2.3. Gene changes that may lead to lung cancer

Our genes are made up of DNA, a material found in each and every cell. Lung cancer risk factors may change the DNA of lung cells. These alterations have the potential to cause cancer and aberrant cell development. Since our DNA comes from our parents, we typically resemble them. Some genes contain instructions that determine when cells divide to create new cells and when they will die. Oncogenes promote the survival, division, and growth of tumor cells (Brennan et al., 2011; Chen et al., 2014).

Inherited gene changes

The chance of getting some cancers is considerably increased by inherited DNA mutations. Nevertheless, the bulk of lung cancers are not expected to be caused only by genetic abnormalities. In certain families with previous cases of lung cancer, genes do appear to be involved (Kanwal et al., 2017).

Acquired gene changes

Rather than being inherited, gene alterations linked to lung cancer typically occur during life. Lung cell acquired mutations are frequently the result of exposure to environmental factors, such as the carcinogens found in cigarette smoke. However, some gene alterations might simply be chance occurrences that occasionally take place inside a cell without an external cause (Wistuba and Gazdar, 2003).

1.2.4. Diet and food supplements

Consumption of fruits and vegetables that are a rich source of vitamins, antioxidants and other micronutrients, such as carotenoids, may decrease the potential of lung cancer risk (Takata et al., 2013). Despite some investigations suggest carotenoids reduce the risk of developing lung cancer, the findings are conflicting, and few research studies have suggested that supplements at high doses may be harmful (Shareck et al., 2017). Although there was a protective trend for α-carotene, lycopene, zeaxanthin and lutein; β-cryptoxanthin has a more consistent protective effect. Vitamins C and E may also play a preventive function. Regardless of smoking status, no associations between total or specific types of fat consumption and risk of lung cancer were discovered. On the other hand, deep-fried food, chilli and cured meat are associated with more likelihood of developing lung cancer (Butler et al., 2013).

1.2.5. Alcohol

According to recent epidemiological research, people who drink alcohol, especially beer, are more prone to the development of lung cancer. It is unclear how alcohol consumption affects gender, race, smoking status, and histological type. According to reports, the link between alcohol and lung cancer is stronger in people who don't consume enough vegetables, vitamin A, or carotenoids. However, two chemoprevention trials found a link between alcohol consumption and elevated lung cancer prevalence among smokers linked to vitamin supplementation, including β-carotene. These paradoxical results may be explained by the fact that ethanol has been demonstrated in experimental investigations to both cause a shortage of vitamin A and aggravate its toxicity as well as that of β-carotene. Investigations should make an effort to explore enough lung cancer cases to thoroughly analyze the association between alcohol use and other dietary parameters, including smoking status, carotenoids intake, sex, race, and histological type (Bagnardi et al., 2011; Fehringer et al., 2017).

1.2.6. Air pollution

Air pollution damages the lungs and is a major issue for world health. Airborne fine particulates from industry and vehicle exhausts have been correlated to lung cancer. The exposure of asbestos, hazardous metals and polycyclic aromatic hydrocarbons (PAHs) to the workers might also lead to the development of lung cancer. Lung cancer rates are increased by inhaling cigarette smoke, cooking fumes, and radioactive waste products. Additionally, bacteria and viruses are significant risk factors for cancer and lung inflammation. Lung

inflammation, DNA damage, and epigenetic regulation are specific impacts of air pollution-induced lung cancer (Christiani , 2021; Xue et al., 2022).

1.2.7. Occupational exposure

Workers may have been exposed to carcinogens in a variety of work environments, increasing their chance of developing lung and other cancers. Individuals who are subjected to the widely known human carcinogens, chrysotile asbestos and crystalline silica are at an elevated risk of developing lung cancer. Due to exposure to radioactive particle matter, employees at nuclear uranium mines and power plants are also more prone of developing lung cancer (Shankar et al., 2019; Kwak et al., 2020).

1.3. Current treatment strategies for NSCLC

The current treatment options for the management of NSCLC include surgery, chemotherapy, radiotherapy and targeted therapy **(Figure 1.1)**.
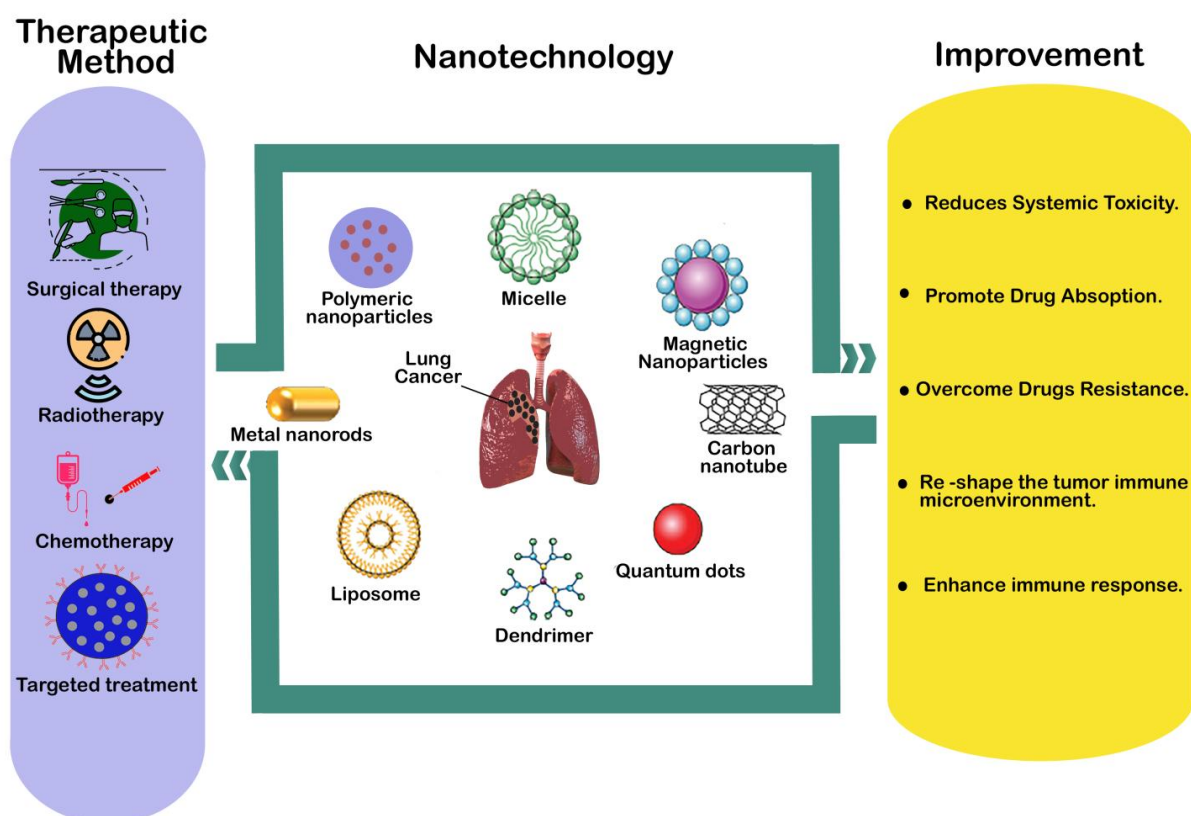
Figure 1.1. Schematic representation of advantages of nanoformulations over conventional treatment strategies for lung cancer therapy [Adapted with permission from Li et al., 2021]

1.3.1. Surgery

Surgery is the only reliably efficient and successful therapy for lung cancer patients. This approach can only be used if the cancer can be completely removed, and the patient must be strong enough to endure the indicated surgery. Resectability concerns involve preoperative staging, which may include imaging tests and biopsies, whereas operability concerns involve assessing patient condition and using medical techniques that reduce risk of surgery and morbidity. Patients with stage I, II and IIIA NSCLC frequently undergo surgery for tumor removal if it is found to be resectable and the patient is healthy enough to undergo surgery. Surgery is used to remove a lobe or section of the lung harboring the tumor. To determine whether the tumor is resectable, biopsies and imaging tests are performed, together with a patient assessment to determine operability (Lang-Lazdunski, 2013; Hoy et al., 2019).

1.3.2. Chemotherapy

Patients with stage IV lung cancer make up about 40% of newly diagnosed cases. The goals of treatment for these patients are to increase survival and reduce adverse disease-related consequences. The first-line therapy for stage IV NSCLC is anticancer combination chemotherapy (Molina et al., 2006). Since the advent of adjuvant chemotherapy, which is suggested to be quite efficient in lung cancer treatment, the role of chemotherapy in the treatment of lung cancer has grown dramatically. Chemotherapy appears to provide symptomatic relief in individuals with decreased performance status for advanced stage NSCLC, and it prolongs patients survival and enhances their quality of life with excellent performance status. The patients suffering from advanced stage NSCLC are preferably treated with platinum-based combination chemotherapy regimens, however non-platinum-based combination treatments are acceptable alternatives in some populations (Cortés et al., 2015). Bevacizumab, an inhibitor of vascular endothelial growth factor (VEGF), and chemotherapy can increase survival in lung cancer patients. Moreover, the survival of lung cancer patients might improve as a result of the development and testing of drugs like tyrosine kinase inhibitors (TKIs), monoclonal antibodies (mAbs) and direct inhibitors of proteins involved in lung cancer proliferation (Assoun et al., 2017; Keedy and Sandler, 2007).

1.3.3. Radiotherapy

In radiotherapy, high-energy rays are employed to damage and destroy the DNA of cancer cells. With the implementation of this therapy, tumors that are located in specific areas of the body may shrink or disappear. Patients with locally progressing NSCLC who are unable to have the tumor surgically removed may benefit from radiotherapy. Radiotherapy may be incorporated into palliative care for NSCLC patients who cannot tolerate chemotherapy or surgery. Internal radiation therapy and external radiation therapy are the two different types of radiation therapy (Baskar et al., 2012; Simone and Jones, 2013). Both employ high-energy X-rays or other radiation types to either eradicate tumor cells or at least retard their growth. An external radiation therapy is administered via equipment. Small radioactive "seeds" must be injected into or close to a cancerous tumor during internal radiation therapy to aid in tumor reduction. The majority of NSCLC patients undergo external radiation therapy. On the basis of the type of lung cancer and its stage, external radiation may be used to treat NSCLC by different approaches. In cases where the tumor cannot be removed surgically or when the patient is not healthy enough for surgery, radiotherapy can be utilized in its place. Chemotherapy can be combined with it to treat Stage III malignancies. Radiation therapy and chemotherapy can be administered together in such cases. In order to minimize symptoms and relieve discomfort in patients with advanced lung cancer, it can also be used as palliative therapy (Baker et al., 2016; Vinod and Hau, 2020).

1.3.4. Targeted therapy for lung cancer

Despite claiming of modern medical techniques including surgery, radiation and chemotherapy, several hurdles are being faced to reduce the number of mortalities caused by lung cancer. Owing to the rapid first-pass metabolism, the conventional methods are inaccurate and only deliver small quantities of drugs. Most chemotherapeutic drugs affect the healthy tissues, since they are non-targeting, which can have adverse effects. The investigation and hunt for more modern, tailored therapeutic techniques has resulted from this gap in medical innovation. Approaches for targeted drug delivery have gained an increasing interest to solve this issue (Yuan et al., 2019; Imyanitov et al., 2021). Drug carriers can carry drugs to the lungs, control their dose, extend their release, and reduce the likelihood of untoward effects and

complications in patients. This targeted strategy limits the distribution of drugs to normal organs and tissues while delivering it to the diseased ones (Majeed et al., 2021; Chung et al., 2023).

The advent of nanotechnology in recent decades has opened up new possibilities for site-specific drug targeting and contributed to the advancement of nanoparticulate drug delivery carriers. These nano devices prevent anticancer drugs from accumulating up in healthy tissues while delivering high doses of drugs directly to the tumor site. The nanocarriers were developed to release drugs more slowly, prolong their effect, and shield therapeutic agents from the clearance of phagocytic cells and early destruction. Since, the respiratory system has a vast surface area and enables skipping the first-pass metabolism and enhances the initiation of quick pharmacological effect, it is suited for targeted drug administration. Nanoparticles make it easier for therapeutic drugs to be released into the lung tissue in a controlled manner, which lowers the frequency of dose and increases patient compliance (Li et al., 2021; Shen et al., 2023).

1.3.4.1. Polymeric nanoparticles

Polymeric nanoparticles have become a successful method of treating cancer in the realm of nanotechnology because they can be customized in terms of composition and form. Chitosan, alginates, polylactide-co-glycolide (PLGA) and polycaprolactone (PCL) are some of the polymers used to treat lung cancer. Nanoparticles synthesized by PCL or PLGA have more efficacy and lower toxicity than conventional methods of delivering chemotherapeutic drugs (Garg, 2022; Liu et al., 2023). Nanoparticle formulations can be targeted actively or passively, thereby accumulating in malignant tissue with substantially less excretion from the body **(Figure 1.2)**. Owing to a poorly developed lymphatic drainage system and leaky vasculature, the nanoparticles are able to penetrate the tumors by extravasation. The reticuloendothelial system (RES) will take up nanoparticles that have been poorly engineered. The liver, spleen, and lungs quickly absorb nanoparticles with a hydrophobic surface, whereas those with a hydrophilic surface take longer for the body to circulate them. Therefore, nanoparticles must be 100 nm or smaller to limit macrophage clearance for prolonged circulation in bloodstream and hence improve targeting (Najlah et al., 2017; Sharma et al., 2022).
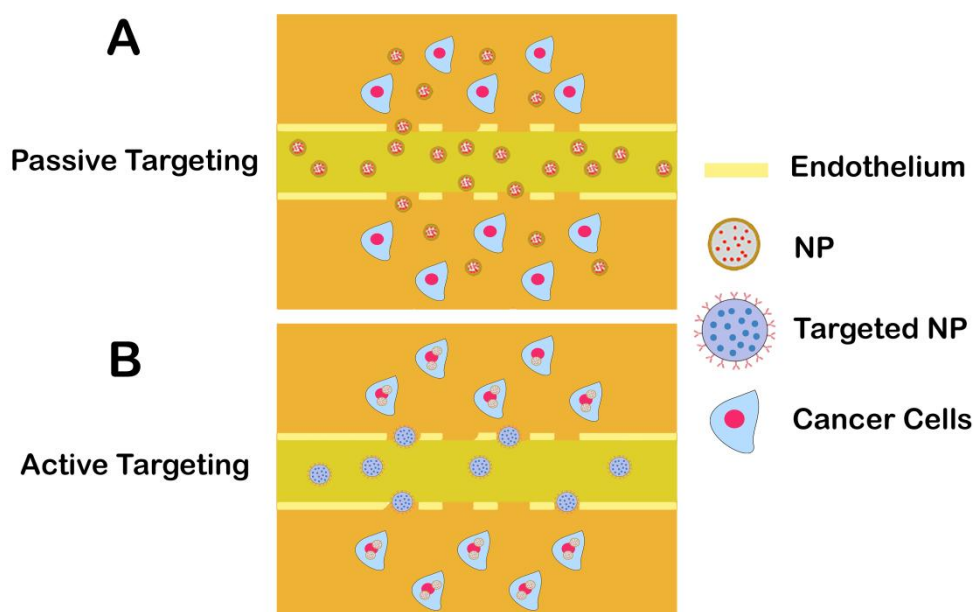
Figure 1.2. Passive and active targeting of nanoparticles to tumor cells [Adapted with permission from Alexis et al., 2008]

Passive targeting

The benefit of the permeability of tumor tissues is utilized in passive targeting. To accomplish passive targeting of chemotherapeutic drugs, it is possible to take the advantage from the leaky vasculature of rapidly growing malignant tumors. This is referred to as the enhanced permeation and retention effect, or EPR effect. The majority of polymeric NPs exhibit the EPR, as seen in the passive targeting of Genoxol-PM and the poly(lactic acid)-block poly(ethylene glycol) polymeric micelles loaded with paclitaxel (Oerlemans et al., 2010). Recently, individuals with advanced NSCLC participated in a phase II trial to examine this nanocarrier technology. Certain drugs can be given as prodrugs, or inert medications, which can then be activated once they enter the tumor environment. The matrix metalloproteinase-2 effectively released free doxorubicin from the albumin-bound form. Redox potential and pH can also trigger the release of drug at the location of lung tumor (Guo and Szoka, 2003; Sarkar et al., 2017).

Active targeting

The polymeric nanoparticles are conjugated to a targeting ligand to achieve active targeting, which enables the site-specific delivery of chemotherapeutic drugs to cancerous tissues. Proteins such as transferrin, folate, aptamers, mAbs, etc. are all examples of the targeting

ligands (Yu et al., 2010; Attia et al., 2019). The strategy relies on certain interactions, like antibody-antigen, ligand-receptor and lectin carbohydrate interactions by utilizing receptor-mediated endocytosis for drug delivery and targeting with nanoparticles. Through ligand-receptor interaction, tumor cells are made to internalize the drug-loaded nanoparticles. Depending on the form of the cleavable link, the drug will be delivered intracellularly when it is exposed to lysosomal enzymes or at lowered pH. In a research work, mice with A549-luc-C8 lung tumors were injected with PGA nanoparticles filled with paclitaxel palmitate and coated with cetuximab mAb for targeting. Compared to the control group, the treated mice had a dramatically higher survival rate (Karra et al., 2013).

1.4.   EGFR as a target receptor for NSCLC

The tyrosine kinase type I receptor family includes the EGFR (Epidermal growth factor receptor), whose gene is found on the short arm of human chromosome 7. The EGFR gene contains 28 exons that work together to generate a protein that is present on the cell membrane of different epithelial cells. This protein links to heparin-binding EGF or epidermal growth factor to control cell proliferation. The EGFR and its downstream genes are activated and regulated to cause cell proliferation, cell death, and angiogenesis. The overexpression of EGFR in NSCLC has been associated with angiogenesis and a poor prognosis. Tyrosine kinase inhibitors are recognized as highly effective drugs against NSCLC. Several drugs, including panitumumab, cetuximab, erlotinib and gefitinib target the EGFR (Liu et al., 2017; Aran and Omerovic, 2019).

1.5.   Monoclonal antibody conjugated nanoparticles

Nowadays, ligands are conjugated with monoclonal antibodies (mAbs) on the surface of nanoparticles (NPs) to achieve targeting to tumor region, thereby reducing accumulation of drugs to non-targeted sites. Tyrosine kinase inhibitors and monoclonal antibodies are the primary forms of treatment employed as a targeted strategy against NSCLC (Thomas et al., 2012). Bevacizumab and Cetuximab are mAbs that are used to treat NSCLC. The binding of cetuximab to the EGFR receptors suppresses the activity of the receptor-associated tyrosine kinase, which in turn targets the EGFR pathway. These antibodies have the ability to adhere to and specifically bind to receptors on cancer cells as well as normal substrates that aid in the proliferation of cancer cells. Antibody binding to certain

receptors or substrates can kill cancer cells, stops its growth, or retards its spreading (Bonomi et al., 2013).

The nanoparticles conjugated with antibody on their surface have possible advantages over existing methods because they can avoid some problems with direct conjugates, such as the requirement for drug release after internalization into endosomal/lysosomal vesicles. Additionally, antibody-conjugated NPs have the potential for significantly larger drug to antibody ratios, thereby maximizing the amount of drug that may be directed at the impacted region (Patel et al., 2018).

1.6. Antibody conjugated PLGA nanoparticles for targeted delivery of anticancer drugs

Therapeutic agents can be incorporated into PLGA nanoparticles, including proteins, nucleic acids, hydrophilic and hydrophobic molecules, etc. The Food and Drug Administration (FDA) and European Medicines Agency (EMA) have both affirmed their consent for utilization of PLGA in pharmaceutical products. The most efficient and simple strategy to improve the therapeutic efficacy of cytostatic drugs like taxanes is to incorporate them into the polymeric nanoparticles (Ma and Mumper, 2013). Currently, paclitaxel and docetaxel are often utilized in healthcare facilities to treat a range of cancers. Both drugs have cytostatic effects on cancer cells by stabilizing microtubules in the cytoskeleton and binding to beta-tubulin, which causes cell cycle arrest at G2/M phase, mitotic suppression, and consequent cellular apoptosis. The extremely poor solubility of taxanes in aqueous media is a significant drawback. Solubilizers must be added when being utilized in a clinic, such as polysorbate-80 for DTX. These solubilizers frequently result in severe toxic and allergic reactions, which restrict their usage (Belani, 2000; Che et al., 2013). When an antibody is conjugated to the surface of a PLGA nanoparticle, its terminal groups plays a major role. Two different kinds of terminal groups are present in commercially available PLGA. The PLGA with free terminal –COOH group, is the first type. The PLGA with terminal esterified groups, is the second type. The 1-ethyl-3-[3-dimethylaminopropyl] carbodiimide hydrochloride/N-hydroxysuccinimide (EDC/NHS) coupling process is one of the extremely effective methods for conjugating ligands onto the surface of nanoparticles. Various DNA or antibodies are frequently attached to the nanoparticles using this method (Mondal et al., 2019; Ehsan et al., 2022). The cetuximab mAb has been demonstrated in numerous studies to be capable of

being conjugated to nanoparticles, enabling the drug-loaded nanoparticles to be administered precisely to lung cancer cells (Karra et al., 2013; Patel et al., 2018).

1.7.   Research envisaged

The goal of this research study is to develop Cetuximab antibody conjugated Doccetaxel loaded nanoparticles (Cet-DTX NP) that can target specific lung tumors and offer a definite therapeutic advantage. For the purpose of accumulating lung tumor-specific nanoparticles in an experimental mouse model, we have developed DTX-loaded Poly (D, L-lactide-co-glycolide) (PLGA) nanoparticles conjugated with anti-EGFR antibody (Cet). Cet has already been discovered as a predictive marker against EGFR-targeted site-specific delivery. The biodegradability of PLGA for human usage and the effectiveness of DTX have already been proven. We made an effort to concentrate on *in vivo* outcomes to demonstrate how the optimized nanoformulation should be used. These results supported our prediction because the drug reached the affected tissues with increased and sustained availability and had improved anti-tumor efficacy against non-small lung adenocarcinoma.

2. Literature Review

2.1. Information on lung cancer

Lung cancer prevails as a commonest type of cancer that affects a large percentage of the population globally. On the basis of origin of cells, around 80 to 85 percent of lung cancer cases are NSCLC. On the basis of their histological features, NSCLC is subdivided into lung adenocarcinomas, squamous cell carcinomas, and large cell carcinomas. Precisionlized oncology, as opposed to conventional chemotherapy, has aided in improving lung cancer therapy (Herbst et al., 2018; Mithoowani and Febbraro, 2022). Clinicians may now tailor the available treatments owing to recent advancements in the understanding of pathways, strategies for identifying genetic defects, and novel drugs that inhibit the activity of the pathways. There are several primary targetable pathways in lung cancer, including the NTRK/ROS1, RAS-MAPK, PI3K/AKT/mTOR and EGFR pathways. A number of drugs with proven clinical efficacy have been directed targeting via these pathways. Some of these, including the NTRK/ROS1 inhibitors (entrectinib), the PI3K/AKT/mTOR inhibitors (everolimus), and EGFR inhibitors (gefitinib and erlotinib), have taken the place of chemotherapy as the first line of therapy (Yuan e al., 2019; Wang et al., 2022).

2.2. EGFR pathways

The transmembrane tyrosine kinase receptor EGFR belongs to the ErbB family. The extracellular domain of EGFR is a target for the ligands transforming growth factor-alpha (TGF-α) and EGF. The interaction of ligands with the receptor results in a conformational change and dimerization, that activates the intracellular tyrosine kinase (Wieduwilt and Moasser, 2008; Du and Lovly, 2018). The proliferation of cells, its invasion, metastasis, angiogenesis, and reduced cell death are the outcomes of the subsequent intracellular events cascade. In many malignancies, the EGFR is dysregulated. Up to 85% of NSCLC tumors exhibit EGFR expression, which has been linked to tumor growth, invasion, metastasis, and a poor prognosis. In individuals with advanced NSCLC, EGFR blocking may thereby enhance outcomes (Prabhakar, 2015).

Monoclonal antibodies and TKIs can be used to block the EGFR function (Dassonville et al., 2007). TKIs and antibodies both have diverse modes of action, pharmacokinetics, and pharmacodynamics. Monoclonal antibodies bind to the EGFR's surface, competing with EGF to prevent it from binding. Complexes with antibody receptors are internalized and broken

down. As a result, the EGFR on tumor cell surface is downregulated. Additionally, monoclonal antibodies may exert their effects through immunological pathways including antibody-dependent cellular cytotoxicity (Pirker and Filipits, 2011).

2.3. Overexpression of EGFR receptors on lung cancer

Cells having a high rate of growth are cancerous cells. This characteristics result in the development of a number of receptors that significantly increase proliferative activity in these cells compared to normal cells. This receptor overexpression has been used by researchers to develop active, tailored drug delivery systems. Lung cancer has an overexpression of various receptors, including EGFR receptor (Selvaggi et al., 2004).

2.4. EGFR-directed monoclonal antibodies

Patients with NSCLC are now undergoing various levels of clinical development for EGFR-directed monoclonal antibodies, particularly when combined with palliative treatment. Cetuximab, matuzumab, panitumumab, etc. are few examples of the monoclonal antibodies (Pirker and Filipits, 2011; Takeda and Nakagawa, 2015).

2.5. Cetuximab

Cetuximab, which is sold under the brand name Erbitux®, is a chimeric human-murine monoclonal IgG1 antibody. In addition to inhibiting signal transmission, it also affects cells through immunological processes such as complement- and antibody-dependent cytotoxicity (Bou-Assaly and Mukherji, 2010). Combining radiation therapy with cetuximab is authorized for treating either locally or regionally progressed neck or head squamous cell carcinoma. It is indicated for the carcinoma that has spread or returned after receiving platinum-based therapy. Patients with advanced NSCLC have participated in phase II and phase III clinical trials that investigated cetuximab combined with chemotherapy. It has also been studied in conjunction with chemoradiotherapy and as a standalone treatment in these patients with stage III NSCLC. A loading dosage of 400 mg/m^2 of cetuximab are administered intravenously, followed by 250 mg/m^2 of weekly doses (Blumenschein et al., 2011; Zhao et al., 2016). The structure of cetuximab is shown in **Figure 2.1**.
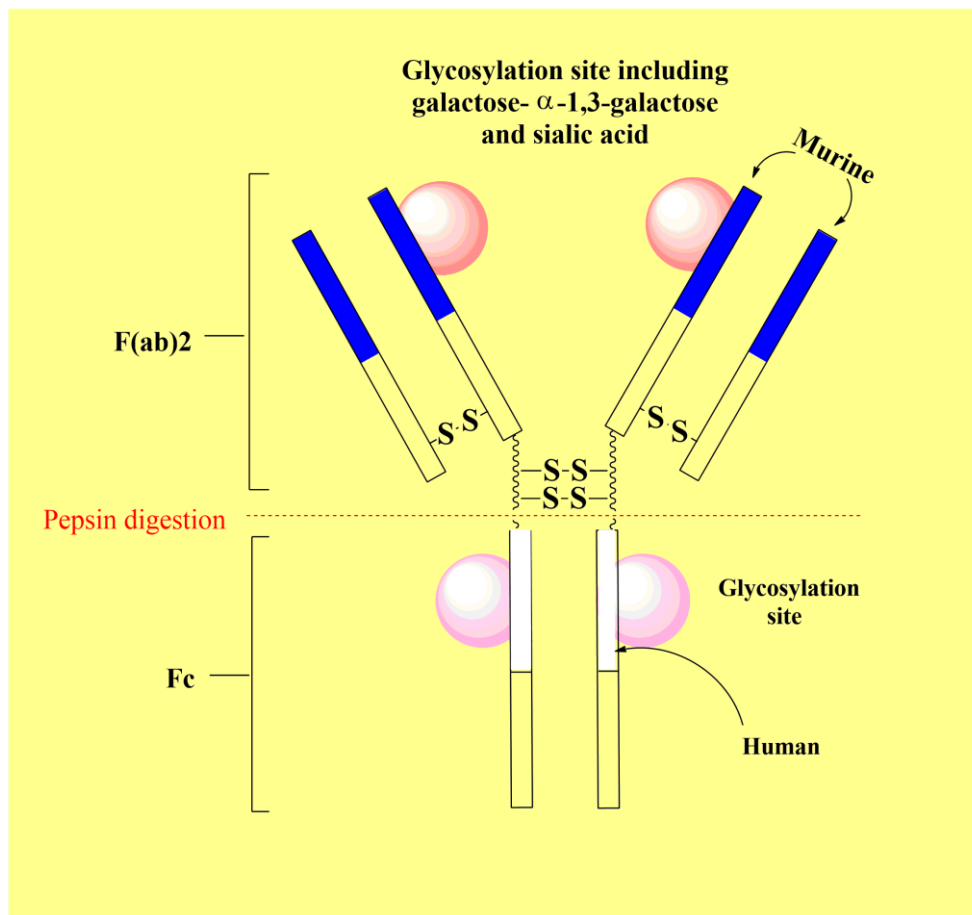
Figure 2.1. Structure of Cetuximab [Reproduced (with slight modifications) with permission from Chung et al., 2008, Copyright Massachusetts Medical Society]

2.5.1. Mechanism of action

Cetuximab preferentially binds to the EGFR on the tumor cells in order to competitively prevent the interaction of EGF and other ligands produced by cancerous cells. It inhibits the activation of EGFR and the activation and phosphorylation of receptor-associated kinases (Jak/Stat, PI3K/Akt and MAPK) after interacting to domain III of the EGFR. Inhibiting the EGFR signalling pathway ultimately prevents cancer cell motility and invasion as well as the progression of the cell cycle. Additionally, cetuximab causes cell death and reduces the synthesis of VEGF and matrix metalloproteinase. Cetuximab has been demonstrated to prevent cancer angiogenesis *in vitro*. Furthermore, internalization of the antibody-receptor complex brought on by cetuximab binding to EGFR resulted in a general downregulation of EGFR expression (Rossi et al., 2006).

2.5.2. Metabolism

Cetuximab is anticipated to undergo protein catabolism by a target-mediated disposal pathway and lysosomal breakdown by the reticuloendothelial system, similar to other monoclonal antibodies (Ryman and Meibohm, 2017).

2.5.3. Toxicity

For mice, the i.v. LD_{50} is >300 mg/kg, while for rats, it is >200 mg/kg. Much information is not available regarding cetuximab overdose. Cetuximab has been linked in clinical trials to significant dermatologic toxicities, cardiac arrest, and fatal infusion responses (Saif and Kim, 2007).

2.6. Docetaxel (DTX)

Docetaxel (DTX), a semi-synthetic analogue of Paclitaxel, is an anticancer drug from the second generation of the taxoid family. DTX is produced semi-synthetically from the precursor molecule 10-deacetylbaccarin-III, which is derived from Pacific yew tree *Taxus baccata* (Sohail et al., 2018). The substance is nearly insoluble in water due to its high lipophilicity; nevertheless, compared to paclitaxel, it has superior water solubility because of its chemical structure, which includes a hydroxyl group on C-10 and a tertbutyl carbamate ester on the side chain of phenylpropionate. DTX may inhibit disassembly and microtubule depolymerization, leading to cell cycle arrest in G1/M phase and eventually cellular apoptosis. This is achieved via attaching to tubulin, which then helps to stabilize it. The mechanism of action of DTX is depicted in **Figure 2.2**. Additionally, it has the ability to upregulate the expression of the cell cycle inhibitor p27 and downregulate that of the anti-apoptotic gene Bcl-2, rendering DTX the ability to suppress the growth of a number of malignancies, including non-small cell lung, ovarian, breast, gastric and prostate cancer. There are certain substantial adverse effects associated with the commercially available forms of DTX (Taxotere), including nasolacrimal duct stenosis, musculoskeletal toxicity, peripheral neuropathy, hypersensitivity responses and neutropenia. Its anticancer potential has been improved and associated adverse effects have been overcome by the use of a number of approaches, including the development of novel delivery methods (Imran et al., 2020). The drug profile of docetaxel is given in **Table 2.1**.
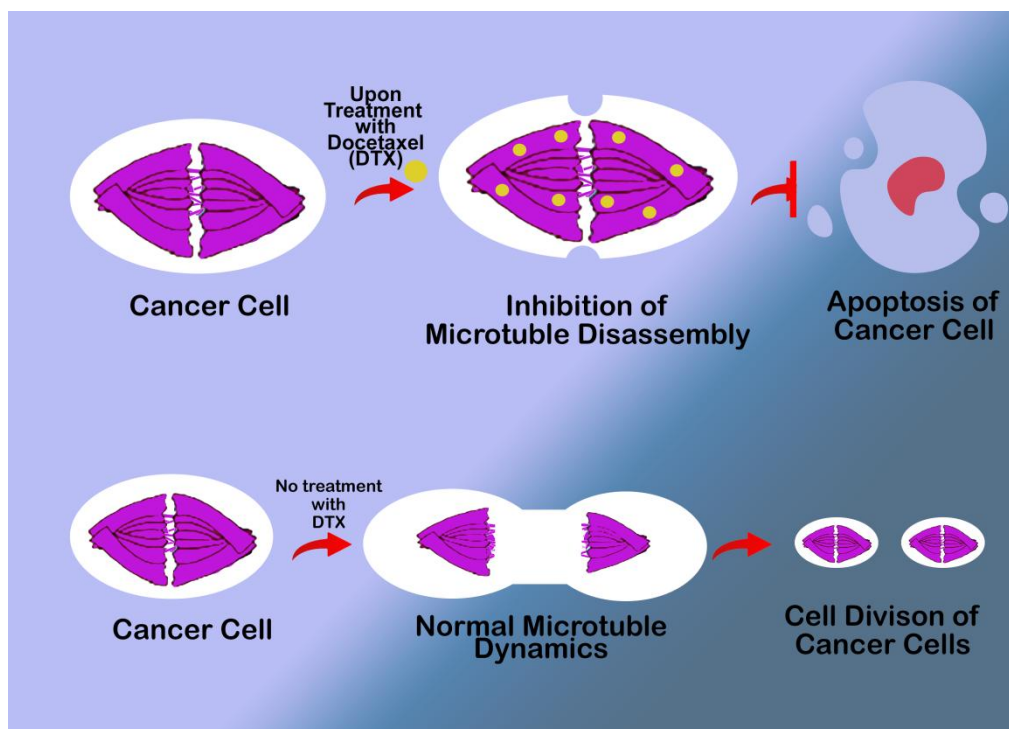
Figure 2.2. Schematic representation of the mechanism of action of DTX on tumor cells [Adapted with permission from Imran et al., 2020]

Table 2.1. Drug profile of Docetaxel (Montero et al., 2005; Imran et al., 2020)

Generic name of the drug	Docetaxel
Brand name	Taxotere
IUPAC name	1,7β,10β-trihydroxy-9-oxo-5β,20-epoxytax-11-ene-2α,4,13α-triyl 4-acetate 2-benzoate 13-{(2R,3S)-3-[(tert-butoxycarbonyl)amino]-2-hydroxy-3-phenylpropanoate}
Molecular formula	$C_{43}H_{53}NO_{14}$
Chemical structure	
Molecular weight	807.8792

State	Solid
Physical appearance	White or off white powder
Melting point	232 °C
Log P	2.4
Solubility	Soluble in DMSO, ethanol, chloroform, dichloromethane, ethyl acetate, methanol. Water solubility is very low (0.0127 mg/mL)
pKa (Strongest acidic)	11.9
Indication	Following the failure of earlier chemotherapy, it is used to treat patients with locally advanced or metastatic breast cancer. It is also utilized to treat locally advanced or metastatic NSCLC. Additionally, it is used in conjunction with prednisone to treat patients with metastatic prostate cancer that is androgen independent (hormone refractory). Docetaxel is also used to treat head and neck cancer as well as stomach adenocarinoma.
Dose	75 mg/m^2 IV over 1 h every 3 weeks
Mechanism of action	The typical function of microtubule growth is disrupted by docetaxel. It hyper-stabilizes their structure and stops their function. Consequently, the cell is unable to utilize its cytoskeleton flexibility. Docetaxel selectively attaches to β-subunit of tubulin. The resulting complex is a microtubule/docetaxel that cannot be broken down.
Half-life	The terminal elimination half-life was 116 h with plasma sampling occurring up to 8 to 22 days following docetaxel injection. A triphasic elimination profile is produced by doses between 70 and 115 mg/m^2 with infusion periods between 1 and 2 h. The α, β, and γ forms have respective half-lives of 4 min, 36 min, and 11.1 h.
Absorption	Dose ranging from 70 mg/m^2 to 115 mg/m^2 with infusion periods of 1-2 h resulted in dose-proportional increase in AUC.
Volume of distribution	The volume of distribution of docetaxel at steady state is 113 L. A three-compartment pharmacokinetic model can be used to explain its pharmacokinetic profile.

Protein binding	Studies conducted *in vitro* revealed that 94% of the protein was bound, primarily to albumin, lipoproteins, and α1-acid glycoprotein. Docetaxel has been found to be 97% bound to plasma protein in cancer patients.
Metabolism	Hepatic metabolism. Docetaxel is metabolised by the CYP3A4 isoenzyme, according to *in vitro* drug interaction studies (one major, three minor metabolites).
Route of elimination	Primarily in the faeces and urine.
Clearance	After the cancer patients receive 20–115 mg/m^2 via IV route, the total body clearance was 21 L/h/m^2.
Toxicity	The oral LD_{50} in rats is greater than 2000 mg/kg. The following side effects of overdosage are anticipated: mucositis, peripheral neurotoxicity, and bone marrow suppression. Two overdose reports involved patients who received infusions of 150 and 200 mg/m^2 over the course of an hour. Both patients underwent cutaneous responses, severe neutropenia, minor asthenia, mild paresthesia, and recovered normally.

2.6.1. DTX as a potent chemotherapeutic agent against NSCLC

DTX exerts its anti-cancer effect to treat NSCLC by specifically attaching to its intracellular target, the β-subunit of polymerized tubulin. This boosts the polymerization of tubulin, which ultimately leads to distorted microtubule assembly and blocks their depolymerization (Wang et al., 2021). The ability of DTX to trigger the G2/M phase arrest that leads to apoptosis or other types of cell death is the basic mechanism by which it works to treat lung cancer. Guanosine triphosphate (GTP) is needed for the energy-driven process that creates microtubules, however DTX has the capacity to polymerize tubulin and develop microtubules even in the lack of GTP. This distortion in the stability of the microtubules disrupts the regular mitotic process, ultimately leading to cell death (Morse et al., 2005). DTX also has the capacity to phosphorylate bcl-2 that promotes apoptosis by inactivating following phosphorylation (Kraus et al., 2003).

2.7. PLGA profile

Poly (D, L-lactide-co-glycolide) (PLGA) is a copolymer comprising poly lactic acid (PLA) and poly glycolic acid (PGA). It is an excellent biopolymer widely employed in the field of drug delivery. An asymmetric α-carbon present in poly lactic acid is typically referred to as the D or L form, though it may also be referred to as the R or S form. The enantiomeric forms of the PLA polymer are poly D-lactic acid (PDLA) and poly L-lactic acid (PLLA) (Makadia and Siegel, 2011; Kapoor et al., 2015). The structure of PLGA and its monomers is depicted in **Figure 2.3**.
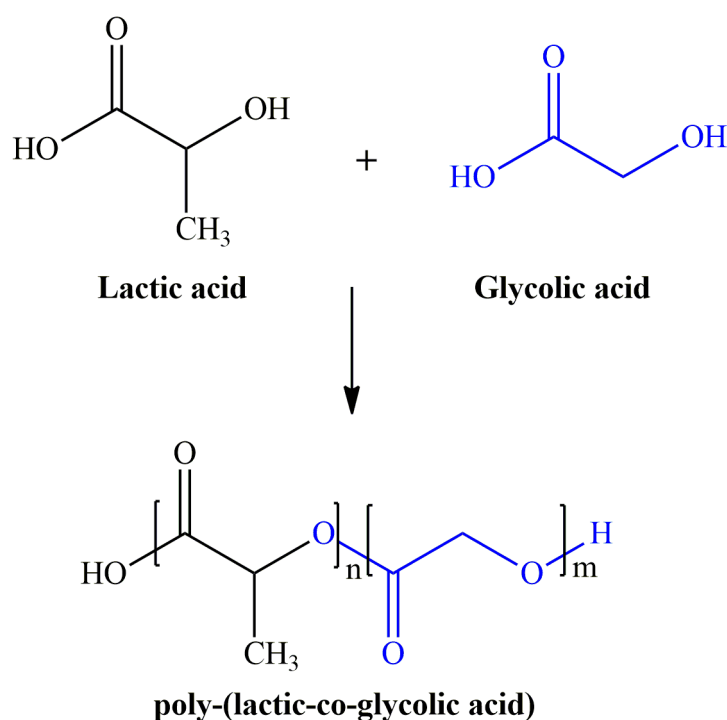
Figure 2.3. Structure of Poly-lactic-co-glycolic acid and its monomers

2.7.1. Physico-Chemical Properties

PLGA can enclose drug molecules of any form and size. Its solubility is reported in various solvents, including ethyl acetate, chlorinated solvents, tetrahydrofuran and acetone. During biodegradation in water, the ester linkages in PLGA are hydrolyzed. Due to the presence of methyl side groups, lactide-rich PLGA copolymers are less hydrophilic than PGA, which causes them to absorb less water and degrade more gradually. The alteration in PLGA properties during polymer biodegradation affects the release rates of drugs incorporated into PLGA. The ratio of lactide to glycolide, initial molecular weight, storage temperature and the

size of the device might govern the physical properties of PLGA (Azimi et al., 2014; Malek-Khatabi et al., 2023). The mechanical durability of the PLGA is influenced by its physical properties, including polydispersity index and molecular weight. These characteristics may regulate the rate of device deterioration and hydrolysis and have an impact on the device's capacity to be designed as a delivery vehicle. However, according to recent research, the type of drug also affects the release rate (Elmowafy et al., 2019). The swelling behavior, mechanical strength, capacity to undergo hydrolysis, and rate of biodegradation of the polymer are all directly influenced by the degree of crystallinity of the PLGA. Upon co-polymerization with PLA, crystallized PGA reduces the level of crystallinity in PLGA, speeding up the process of hydration and hydrolysis. The intrinsic viscosity of commercially available PLGA polymers, which is correlated with their molecular weights, is typically used to describe them (Makadia and Siegel, 2011; Xu et al., 2017).

2.7.2. Pharmacokinectics and Biodistribution of PLGA

A non-linear and dose-dependent profile governs the biodistribution and pharmacokinetics of PLGA. Additionally, past research indicates that the dose and makeup of PLGA carrier systems may affect both uptake by the mononuclear phagocyte system (MPS) and blood clearance. Some PLGA formulations, like nanoparticles, quickly build up in the spleen, liver, lymph nodes, bone marrow, and peritoneal macrophages (Rafiei and Haddadi, 2017). The early stage of the PLGA nanocarriers breakdown occurs quickly (by about 30%), and it then progresses slowly until it is eventually eliminated. The surface modification of nanoparticles also enhances its circulation time in blood (Singh and Pai, 2014; Parmar et al., 2022).

2.7.3. Drug release behavior

Biphasic Release

The combined processes of surface erosion and bulk erosion may lead to the deterioration of PLGA copolymers. The lactide to glycolide ratio, the polymer's molecular weight, its degree of crystallinity, and its Tg all affect how quickly the PLGA copolymers degrade. Due to biodegradation of PLGA, the drug release has been demonstrated to exhibit the following pattern: (Hussein et al., 2013; Hines and Kaplan, 2013; Keles et al., 2015)

> (i)   The concentration and type of drug, and polymer hydrophobicity are connected to the initial burst release of drug. As a result of the drug's solubility and the degree

to which water penetrates the polymer matrix, drug attached to the surface is released in the medium. Randomly splitting PLGA greatly reduces its molecular weight.

(ii)   In the subsequent stage, drug is progressively released through the thicker drug-depleted layer. PLGA is hydrolyzed by aqueous medium in the matrix to produce soluble monomeric and oligomeric components. It opens a channel for drug release through erosion and diffusion of the polymer.

2.7.4. Toxicology

PLGA devices may cause local tissue responses. Even though PLGA has been proven to be incredibly safe biomaterial, there might be special precautions needed when employing it in the field of nanotechnology. However, these reactions are often minor (Makadia and Siegel, 2011).

2.8. Nanotechnology tools for the delivery of DTX in the treatment of cancers

By utilizing their limits to improve therapeutic outcomes, nanotechnology has recently attracted increasing attention for the delivery of pharmaceuticals. A significant improvement in drug delivery has been brought about by intelligent use of nanotechnology, particularly in the area of cancer treatment (Patra et al., 2018; Farjadian et al., 2019; Haleem et al., 2023). There are a variety of problems with the administration of anti-cancer drugs via systemic routes and conventional ways. Drugs administered through conventional therapies are unable to pass through a number of biological barriers, including the tumor micro-environment. Nanotechnology-based targeted drug delivery for anticancer drugs is necessary to get around these problems with conventional therapies because they permit active and passive drug targeting and avoid reticuloendothelial system (RES) clearance (Yao et al., 2020; Sabit et al., 2022). Such nanoparticles are superior to conventional therapeutics in that they improve bioavailability through targeted administration, resolve solubility and permeability barriers, and protect the drug from deterioration due to an unfavorable microenvironment at the targeted region. They can also maintain the necessary drug concentration in plasma for efficient anticancer therapy and offer a retarded drug release for a prolonged duration (Yetisgin et al., 2020).

Thus, the delivery method based on nanotechnology offers a viable substitute for current technologies for anticancer drug delivery. In order to lessen the numerous forms of toxicities

related to the usage of anti-cancer drugs, these nanocarriers can be made utilizing a variety of components, including inorganic solvents, metals, lipids, proteins and surfactants. In order to target NSCLC, a variety of nanocarriers have been thoroughly discussed, including self-assembled nanoparticles (Barak et al., 2022), nanostructured lipid carriers (NLC) (Guo et al., 2019; Rawal et al., 2021), polymeric nanoparticles (Shukla et al., 2020; Zhang et al., 2021), solid lipid nanoparticles (SLN) (Ahmed et al., 2020), polymeric micelles (Wang et al., 2021), liposomes (Park et al., 2021), nanocapsules (Rudnik et al., 2020) and nanosuspensions (Zhang et al., 2022). These technologies offer a new platform that can be used to target different cancers.

2.8.1. DTX loaded polymeric nanoparticles

DTX can be incorporated into polymeric nanoparticles by entrapment within the polymeric core or conjugation to the polymeric molecules. These nanoparticles can be used to deliver pharmaceuticals to target areas by diffusion through matrix, swelling followed by diffusion, stimulation by external stimuli or bulk erosion (Rafiei and Haddadi, 2017; Zhang and Zhang, 2013). Zhang et al. developed DTX-Tmab-PLNs, which demonstrated targeted delivery to breast cancer cells that expressed the human epidermal growth factor receptor-2 (HER-2) protein. The cytotoxicity and cellular uptake studies demonstrated that DTX-Tmab-PLNs effectively delivered DTX to HER-2 positive breast cancer cells, increasing the drug ability to combat cancer (Zhang et al., 2019). Wang et al. synthesized DTX-loaded PAMAM-based Poly (γ-benzyl-L-glutamate)-b-D-α Tocopherol Polyethylene Glycol 1000 Succinate nanoparticles (DTX-PAM-PBLG-b-TPGS NPs) and observed higher cytotoxicity against MCF-7 cell line, when compared to free DTX, thereby suggesting greater efficacy of the developed nanoparticles (Wang et al., 2019). For the treatment of NSCLC, Chisti et al. developed DTX-loaded poloxamer (PLX-188) coated poly (lactic-co-glycolic acid) (PLGA) NPs administered through pulmonary route. When compared to free DTX, these nanoparticles demonstrated higher cytotoxicity and regulated drug release, thereby enhancing its therapeutic efficacy (Chishti et al., 2019). For the combined management of prostate cancer, Li et al. developed tailored nanoparticles for the delivery of doxorubicin (DOC) and DTX (DDC-NPs). These NPs demonstrated a reduction in *in vivo* toxic effects and enhanced the outcomes of DOC and DTX. The enhanced anti-cancer potential, according to the researchers, was caused by DTX-DOX's greater internalization in tumor cells due to targeted administration of drug-loaded nanoparticles (Li et al.; 2019). Zhao et al. synthesized DTX-

loaded NPs with polypyrrole, hyaluronic acid and some phase transition material. Such nanoparticles demonstrated photoacoustic characteristics that facilitated accurate real-time photothermal therapy and drug localization in tumors. The outcomes in the 4T1 mouse model demonstrated the cytotoxic effect and tumor-inhibiting properties of nanoparticles (Zhao et al., 2019). Ionically cross-linked nanoparticles based on chitosan and sodium tripolyphosphate were described by Mahmood et al. for the sustained administration of DTX. When tested for safety in wistar rats, these NPs showed increased DTX tolerance without any oral acute toxicity, tissue disruption and histological alterations (Mahmood et al., 2019). To improve radiotherapy in a xenografted prostate tumor model, Loiseau et al. formulated DTX-loaded titanium nanotubes modified with gold nanoparticles. With the aid of titanium nanotubes, the combination emphasised on delivering gold nanoparticles to tumors in an *in vivo* PC-3 xenografted model for 20 days. In an *in vitro* experiment, The the prostate adenocarcinoma cells showed enhanced cytotoxicity on tumor cells as well as prevented tumor genesis and proliferation (Loiseau et al., 2019). Gaio et al. employed hyaluronic acid coated nanoparticles to deliver DTX and a photosensitizer in conjunction for chemotherapy and photodynamic therapy to destroy breast cancer cells (Gaio et al., 2020). DTX-loaded transferrin conjugated PLGA nanoparticles were developed by Jose et al. for targeted delivery in the treatment of breast cancer. The G2/M phase arrest validated the targeted nanoparticles, confirming that these nanoparticles exhibited greater cellular cytotoxicity against MCF-7 cell lines (Jose et al., 2019). Abou-El-Naga et al. showed that DTX-loaded polymeric nanoparticles can overcome multidrug resistance in breast cancer cells. These DTX-PLGA-NPs showed increased cell cytotoxicity and restricted DTX efflux by decreasing ABCG2 and MDR1 expression, which were both known to be greater in free DTX (Abou-El-Naga et al., 2022). To observe the combined synergistic effect of DTX resveratrol in NSCLC, Song et al. synthesized EGFR linked lipid polymeric nanoparticles. According to *in vitro* and *in vivo* tests, the results showed highest cytotoxicity towards cancerous cells and negligible systemic toxicity (Song et al., 2018). In order to treat prostate cancer, Sokol et al. combined abiraterone acetate (Abr A) with DTX in polymeric (PLGA) nanoparticles. They found that this combination was more internalized in endosomal compartments and more hazardous to the LNCaP prostate cancer cell line than free drugs. Prostate cancer treatment with the combination showed synergy and offered better therapeutic results (Sokol et al., 2019). For the simultaneous delivery of DTX and doxorubicin hydrochloride to treat cancer, Mattu et al. designed polymeric nanoparticles. As compared to free drugs, these nanoparticles

showed an increased internalization of both drugs in tumors by about 11 folds. They have higher concurrent accumulation in tumors, which leads to better outcomes for cancer patients (Mattu et al., 2018).

2.9.   Polymeric nanoparticles with monoclonal antibody for lung cancer

Polymeric nanoparticles are the drug delivery systems of nanoscale size range that employs polymers to encapsulate drugs. These nanoparticles are extensively used for active and passive drug targeting to desired organs and tissues. In addition, a number of advancements in polymeric nanoparticles for active targeted delivery systems for lung cancer therapy have been made, for instance, use of monoclonal antibodies as ligands attached to their surface (Wathoni et al., 2022). Demethoxycurcumin was encapsulated in anti-EGFR-ligand-coated chitosan nanoparticles. Rats were used for both *in vivo* and *in vitro* testing of these nanoparticles on the A549 cell line. These nanoparticles successfully delivered drugs to EGFR receptors, leading to an eight-fold reduction in tumor burden in experimental animals when compared to the control group (Huang et al., 2015). DTX and Cet were successfully entrapped in ligand conjugated PLGA nanoparticles to target the drug molecules to the EGFR receptor. According to *in vitro* research, these nanoparticles may release 25% of the drug after 48 h at a pH of 5.5. These nanoparticles were also able to cause apoptosis and reduce the viability of the A549 cell line. According to the *in vivo* results on mice with 150 mm^3 tumor volumes, these nanoparticles significantly slowed the growth of the tumors, and the tumor volume decreased by roughly 81% (Patel et al., 2018). DOX is incorporated in polymeric nanoparticles made of hyaluronic acid and amphipathic cationic starch. Anti-EGFR ligands erlotinib, apatinib, and icotinib were used to assess their effects on the PC9, NCI-H1975 and A549 cell lines. For *in vivo* research, rats were employed as experimental animals. The data demonstrated that icotinib was the most efficient ligand when compared to others. The cytotoxic action of icotinib nanoparticles, with a particle size of 65.7 nm, was enhanced, and cancer cell types were stopped from migrating. The results of the *in vivo* tests showed that the target region had a higher concentration of nanoparticles and had improved drug selectivity (Li et al., 2020). Additionally, paclitaxel palmitate nanoparticles were delivered via anti-EGFR. The therapeutic efficacy of A549-luc-C8 in metastasizing lung tumors was improved *in vitro* and *in vivo* with Cet administration in this system (Karra et al., 2013). Another monoclonal antibody, LFC131, targets the CXCR4 receptor, which is prominently expressed in lung cancer. LFC131 can effectively deliver medicines to A549 cells and increase the

internalization of DOX nanoparticles composed of PLGA polymer (Chittasupho et al., 2014). In a different investigation, chitosan polymer and Tn antigen were combined to produce nanoparticles that delivered doxorubicin. Tn antigen is a lung cancer-specific antigen that is frequently used to target antibodies. The findings showed that the cell viability reduced with an increase in the internalization of the nanoparticles within the tumor cells (Castro et al., 2021).

3. Objectives and plan of study

3.1. Objectives

The objectives of this research work is to develop Docetaxel (DTX) loaded Poly (D, L-lactide-co-glycolide) (PLGA) nanoparticles and further conjugating it with cetuximab (Cet) mAb that can target specifically to non small cell lung cancer (NSCLC).

This research study is divided into following sections:

- Preparation of Docetaxel loaded PLGA nanoparticles (DTX NP) and further conjugation with anti-EGFR antibody (Cet) for targeted drug delivery. The physicochemical characterization of the optimized nanoparticles will be carried out.
- *In vitro* cytotoxicity studies, cellular internalization, cell cycle analysis and cellular apoptosis study will be performed on EGFR-overexpressed lung cancer cells (A549 and NCI-H23) and normal lung epithelial cells (L-132).
- Further, *in vivo* pharmacokinetics study, *in vivo* biodistribution study, survival studies and lung histopathology will be assessed in benzopyrene (B(a)P) induced lung cancer mice model.

3.2. Plan of study

The plan of study is described as follows:

- ➢ Preformulation studies
    - Estimation of standard calibration curve of Docetaxel by UV-Visible spectroscopy
    - Drug-excipients interaction study by Fourier transform infrared spectroscopy (FTIR)
- ➢ Preparation and optimization of Docetaxel loaded PLGA nanoparticles
    - Preparation of Docetaxel loaded PLGA nanoparticles by multiple emulsion solvent evaporation technique
    - Development of anti-EGFR antibody-conjugated DTX-loaded nanoparticles and its various physicochemical characterization
    - Confirmation of the antibody conjugation onto the surface of the nanoparticles by SDS-PAGE

- Morphological characterization of the optimized nanoaprticles by field emission scanning electron microscopy (FESEM) and transmission electron microscopy (TEM)
- Investigation of the stability studies of the nanoparticles by accelerated stability analysis and assessment of hydrolytic stability study

➢ *In vitro* drug release study

- *In vitro* drug release study of the optimized nanoparticles in phosphate buffer saline (PBS) (pH 7.4) with 0.1% w/v tween 80, citrate buffer (pH 3), acetate buffer (pH 5) and bicarbonate buffer (pH 10)
- Evaluation of various drug release study and assessment of the regression coefficient (R^2) by different release kinetics model

➢ *In vitro* cellular studies in various lung cancer cells (A549 and NCI-H23) and normal lung epithelial cells (L-132)

- Cell culture of human lung cancer cell lines
- Detection of mRNA by RT-PCR
- Determination of dissociation constant (K_D) by ELISA method
- *In vitro* cytotoxicity assay using MTT reagent
- *In vitro* cellular uptake study by confocal microscopy and flow cytometer
- *In vitro* cellular apoptosis study
- *In vitro* cell cycle analysis

➢ Hemolysis study

➢ *In vivo* evaluation of the nanoparticles

- Assessment of the maximum tolerated dose (MTD) of drug and experimental nanoparticles in normal male Swiss albino mice
- *In vivo* pharmacokinetics study of the experimental nanoparticles in normal mice
- *In vivo* biodistribution study in B(a)P induced lung cancer mice model
- Determination of survival time of experimental mice
- Caspase-3 activity, ROS and LPO levels of experimental mice after treatment with the nanoformulations
- Lung histopathology analysis

➢ **Statistical analysis**

- Student's t-test and one-way ANOVA will be used for the statistical analysis, and Graph Pad Prism will be used to generate the graphs

4. Materials and Equipments

4.1. Chemicals used in the study

Table 4.1. List of materials/chemicals used in the study

Serial No	Name	Source
1.	Acetone	Merck Life Science Pvt. Ltd, Bengaluru, India
2.	Acetonitrile	Merck Life Science Pvt. Ltd, Bengaluru, India
3.	Cell lysis buffer	Abcam
4.	Cetuximab	Ideal Chemicals, Kolkata, India
5.	Chloroform	Merck Life Science Pvt. Ltd, Bengaluru, India
6.	Citric acid	Merck Life Science Pvt. Ltd, Bengaluru, India
7.	4',6' Diamidino-2-phenylindole (DAPI)	Thermo Fisher Scientific, Mumbai, India
8.	Dichloromethane (DCM)	Merck Life Science Pvt. Ltd, Bengaluru, India
9.	Disodium hydrogen phosphate	Merck Life Science Pvt. Ltd, Bengaluru, India
10.	Dimethylsulfoxide (DMSO)	Merck Life Science Pvt. Ltd, Bengaluru, India
11.	Dulbecco's Modified Eagle Medium (DMEM)	Thermo Fisher Scientific, Waltham, USA
12.	Ethylene diamene tetra acetic acid (EDTA)	Merck Life Science Pvt. Ltd, Bengaluru, India
13.	1-(3-dimethylaminopropyl)-3-ethylcarbodiimide hydrochloride (EDC)	Himedia Laboratories Pvt. Ltd., Maharashtra, Mumbai, India.
14.	Ethyl Acetate	Merck Life Science Pvt. Ltd, Bengaluru, India India
15.	Fetal bovine serum (FBS)	HiMedia Laboratories, Mumbai, India

Serial No	Name	Source
16.	Fluorescein isothiocyanate (FITC)	HiMedia Laboratories, Mumbai, India
17.	FITC annexin V/dead cell apoptosis kit	Thermo Fisher Scientific,Waltham, MA, USA
18.	Glacial acetic acid	Merck Life Science Pvt. Ltd, Bengaluru, India
19.	Methanol	Merck Life Science Pvt. Ltd, Bengaluru, India
20.	3-(4,5-dimethylthiazol-2-yl)-2,5-diphenyltetrazolium bromide (MTT)	HiMedia Laboratories, Mumbai, India
21.	N-hydroxysuccinimide (NHS)	Himedia Laboratories Pvt. Ltd., Maharashtra, Mumbai, India.
22.	Docetaxel (DTX)	A gift samples provided by Fresenius Kabi Oncology, Kolkata, West Bengal, India with 99.95% purity
23.	Penicillin-Streptomycin	HiMedia Laboratories, Mumbai, India
24.	Acid-terminated Poly lactic-co-glycolic acid (ratio, 75:25; molecular weight, 4,000–15,000 Da)	Sigma-Aldrich Co, St Louis, MO, USA.
25.	Potassium dihydrogen phosphate	Merck Life Science Pvt. Ltd, Bengaluru, India
26.	Polyvinyl alcohol (M.W. 85,000- 1,24,000) (M.W. 150,000)	SD Fine-Chemicals limited, Mumbai, India
27.	Roswell Park Memorial Institute Medium (RPMI 1640)	HiMedia Laboratories, Mumbai, India
28.	Sodium acetate	Merck Life Science Pvt. Ltd, Bengaluru, India
29.	Sodium bicarbonate	Merck Life Science Pvt. Ltd, Bengaluru, India

Serial No	Name	Source
30.	Sodium carbonate	Merck Life Science Pvt. Ltd, Bengaluru, India
31.	Sodium citrate	Merck Life Science Pvt. Ltd, Bengaluru, India
32.	Sodium hydroxide	Merck Life Science Pvt. Ltd, Bengaluru, India
33.	Trypsin	HiMedia Laboratories, Mumbai, India
34.	Tween 80	SD Fine Chemicals limited, Mumbai, India
35.	Water for HPLC Corp. Billerica, MA, USA 41. Millex-GP Syringe Filter Unit, 0.22 μm, polyethersulfone, 33 mm, gamma sterilized Millipore Corp. Billerica, MA, USA	Merck Life Sc. Pvt. Ltd., Mumbai, Maharashtra, India
36.	Milli-Q water Millipore	Corp. Billerica, MA, USA

4.2. Animals and different cells used in the study

Table 4.2 The source of animals and different cells used in the study

Animals	Source
Swiss albino male mice	National Institute of Nutrition (NIN), Hyderabad, Telangana, India.154/GO/RBiBt-S/RL/99/CPCSEA
Human Cells	**Source**
A549 cells, NCI-H23 cells and L-132 cells	National Centre for Cell Sciences, Pune, India

4.3. Instruments

Table 4.3 List of instruments and equipments used in the study

Serial No	Name	Source
1.	Bath sonicator	Trans-O-Sonic, Mumbai, India
2.	FAC Scan Flow Cytometer	BD biosciences, San Jose, CA,USA
3.	CO_2 incubator	Thermo Fisher Scientific, Waltham, MA USA
4.	Cold centrifuge	HERMLE Labortechnik GmbH, Wehingen, Germany
5.	Confocal microscope	TCS-SP8 confocal microscope, Leica, Germany
6.	Digital pH meter (EUTECH)	Thermo Fisher Scientific India Pvt. Ltd., Hiranandani Business Park, Mumbai India
7.	Digital weigh balance	Sartorius Corporate Administration, Otto-Brenner-Straße 20, Goettingen, Germany
8.	Disposable syringe (Dispo Van)	Hindustan Syringes and Medical Devices Limited, Ballabgarh, Faridabad, Haryana, India
9.	FTIR instrument	Magna-IR 750, Series II, Nicolet Instruments Inc, Madison, Wisconsin, USA
10.	Normal Freezer	LG double door, Yeouido-dong, Seoul, South Korea
11.	-80° C Freezer (Model no U410-86)	New Brunswick Scientific, Eppendorf House, Arlington Business Park, Stevenage, UK

Serial No	Name	Source
12.	High speed homogenizer	IKA Laboratory Equipment, Model T10B Ultras-Turrax, Staufen, Germany
13.	Incubator shaker	BOD-INC-1S, Incon, India
14.	Laminar airflow bio-safety hood	Thermo Fisher Scientific, Waltham, MA USA
15.	Tandem liquid chromatography and mass spectrophotometry (LC–MS/MS)	LC: Shimadzu Model 20AC, MS: AB-SCIEX, Model: API4000, Software: Analyst 1.6
16.	Laboratory Freeze Dryer (lyophilizer)	Instrumentation India, Kolkata, India
17.	Magnetic stirrer	Remi Sales & Engineering Ltd, Ganesh Chandra Avenue, Bando House, Dharmatala, Kolkata, India
18.	0.22 µ membrane filter	Merck Life Science Pvt. Ltd, Mumbai, India
19.	Microplate reader	Spectromax ,Japan
20.	Particle size and zetasizer	Zetasizer nano ZS 90, Malvern Zetasizer Limited, Malvern, UK
21.	Field Emission Scanning Electron microscope	FESEM Joel JSM-7600 F, Tokyo, Japan

Serial No	Name	Source
22.	Transmission electron microscope	TEM, JEOL JEM-2010, JEOL, USA
23.	UV-VIS spectrophotometer	LI-295 UV VIS Single Beam, Lasany International, India
24.	Vortex mixture	Remi Sales & Engineering Ltd, Ganesh Chandra Avenue, Bando House, Dharmatala, Kolkata, India
25.	Zeiss Light microscope.	Carl Zeiss: Axiostar plus, Jena, Germany

5. Methodology

5.1. Estimation of absorbance maxima (λ_{max}) of Docetaxel by means of UV-Visible spectroscopy

A solution of docetaxel (10 µg/ml) was prepared in acetonitrile:water mixture in 60:40 v/v ratio. Then the absorbance maxima (λ_{max}) of the drug was determined by scanning the solution against acetonitrile:water mixture as blank in an absorption spectrum between 200 nm to 400 nm.

5.1.1. Preparation of stock solution of drug

The primary stock solution of docetaxel was prepared by dissolving 1 mg of docetaxel in 10 ml of acetonitrile:water mixture (60:40 v/v ratio). A high regression coefficient ($R^2 = 0.999$) was achieved, which suggested that the absorbance and concentration of drug were linearly related to each other, and it followed Beer's law.

5.1.2. Preparation of calibration curve of drug solution

From the stock solution of docetaxel (1 mg/10 ml), different aliquots (0.5, 1, 2, 4, 6, 8, 10 µg/ml) were prepared in acetonitrile:water solution. The absorption maxima (λ_{max}) was then determined at 229 nm, with acetonitrile:water kept as blank by UV-Visible spectrophotometer. All the data were measured in triplicate (Data is represented as mean±SD). The obtained absorbance was plotted against concentrations and the regression coefficient (R^2) and slope was obtained from the graph.

5.2. Drug excipients interaction study by FTIR

To ascertain whether there was any interaction between the drug and the chosen excipients, Fourier transform infrared (FTIR) spectroscopy was employed. Each sample (5 mg) was mixed at 1:100 ratio with IR grade KBr and punched to form pellets. An FTIR instrument (Magna-IR 750, Series II, Nicolet Instruments Inc, Madison, Wisconsin, USA) was then used to scan the pellets in the wavelength range of 4000-400 cm^{-1}. For the analysis, DTX, PLGA, PVA, PVA-PLGA mixture, a physical mixture of PLGA, PVA, and DTX, Blank NP, DTX NP and Cet-DTX NP were chosen.

5.3. Preparation of PLGA nanoparticles

The preparation of DTX-loaded PLGA nanoparticles and blank (without drug) nanoaparticles was done by the multiple emulsion solvent evaporation technique as per previously reported methods (Paul et al., 2018; Mandal et al., 2018). Briefly, 50 mg PLGA (75:25 grade carboxy terminated) and 5 mg drug was weighed and dissolved in a solvent mixture containing dichloromethane (DCM) and acetone in a ratio of 1:1 (2 ml). 2.5% w/v aqueous PVA solution was prepared and added dropwise to the beaker containing drug and PLGA solution, with homogenization at 16000 rpm with a high speed homogenizer. The primary emulsion thus formed was added dropwise to 1.5% w/v PVA solution (75 ml) and homogenized at 16000 rpm. Subsequently, w/o/w emulsion was formed after 5-6 min of homogenization. The beaker was then placed on a bath sonicator containing ice cold water, and sonicated for 30 min, and then stirred for overnight to remove and residual organic solvent. Next day, the formulation was centrifuged at 4°C at 5000 rpm for 10 min to separate the larger nanoparticles. Then the supernatant was centrifuged again at 16000 rpm for 45 min. The pellets thus collected were washed three times with distilled water, collected in a petridish and kept at -20 °C in a refrigerator. Then the nanoparticles were lyophilized at -40 °C for 8 h. and the final product was stored at -20 °C, for further use. The blank nanoparticles and were also prepared by the same method mentioned above, except the incorporation of drug in the organic phase. The schematic representation of the preparation of nanoparticles by multiple emulsion solvent evaporation technique is shown in **Figure 5.1**.

FITC conjugated nanoparticles were also prepared by the above mentioned method with few modifications. A stock solution of FITC (0.4% w/v) was prepared in ethanol:chloroform (1:3), and 100 µl of stock solution was added into organic phase during the process of formation of primary emulsion.
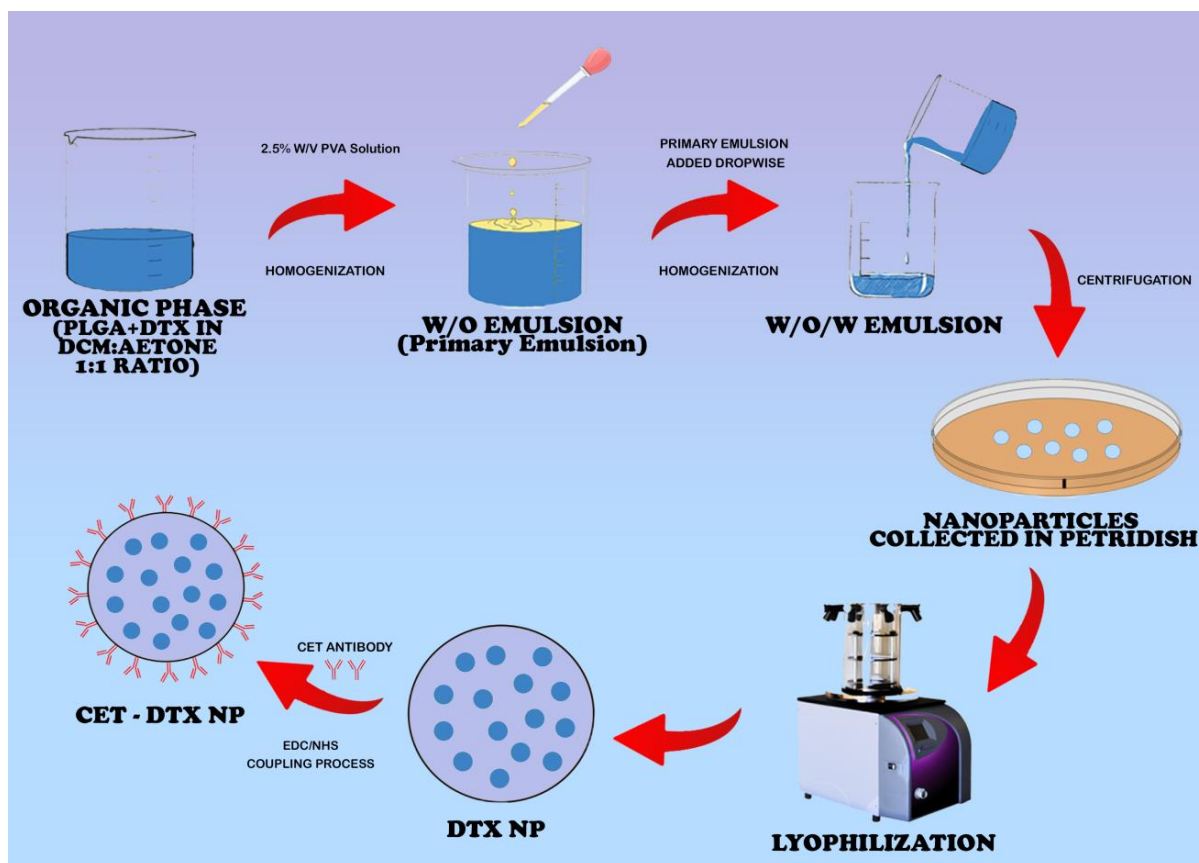
Figure 5.1. Schematic representation of the preparation of DTX NP by multiple emulsion solvent evaporation technique and its conjugation to Cet monoclonal antibody by EDC/NHS coupling chemistry

Antibody conjugation on the surface of the prepared nanoparticles

The anti-EGFR antibody (Cet) was conjugated onto the surface of prepared nanoparticles by means of 1-(3-dimethylaminopropyl)-3-ethylcarbodiimide hydrochloride (EDC) and N-hydroxysuccinimide (NHS) (EDC/NHS) coupling chemistry (Mondal et al., 2019; Ehsan et al., 2022). The lyophilized nanoparticles were resuspended in PBS (1 mg/ml). Then 1 µl of Cet antibody was withdrawn from the stock solution (100 µg/ml), and then added to the suspended nanoparticles. The suspension was then vortexed, and incubated at room temperature (25 °C) for 1 h, followed by centrifugation at 16000 rpm for 10 min to remove the unbound antibodies. The pellets thus obtained after centrifugation were collected, and resuspended in PBS and washed three times to remove the antibodies that remained unattached to the surface of the nanoparticles. The pellets were further lyophilized and kept at 4 °C in a refrigerator for further use.

5.4. Physicochemical characterization of the PLGA nanoparticles

5.4.1. Determination of particle size and zeta potential of the nanoparticles

The lyophilized nanoparticles were resuspended in distilled water, sonicated for 30 min and characterized for particle size, polydispersity index (PDI) and zeta potential values by using the Zetasizer Nano ZS 90 using Data Transfer Assistance (DTA) software (Malvern Zetasizer Limited, Malvern, UK).

5.4.2. Determination of drug loading and entrapment efficiency

Accurately weighted nanoparticles were placed in a centrifuge tube and mixed with an acetonitrile:water solution to determine the drug loading (Patel et al., 2018). The supernatant was filtered after the centrifuge tube has been vortexed, sonicated, and centrifuged. A UV spectrophotometer was used to assess the drug content quantitatively. The following equations were used to determine the drug loading of the experimental formulations:

$$\text{Actual drug loading (\%)} = \frac{Amount\ of\ drug\ present\ in\ nanoparticles}{Amount\ of\ nanoaprticles\ analyzed} \times 100 \qquad (1)$$

$$\text{Drug loading efficiency (\%)} = \frac{Actual\ drug\ laoding\ (\%)}{Theoretical\ drug\ lao\,ding\ (\%)} \times 100 \qquad (2)$$

5.4.3. Field emission scanning electron microscopy (FESEM) study

The morphology of outer surface of Cet-DTX NP was evaluated by placing Cet-DTX NP onto the metallic stubs having dual-sided adhesive carbon tape. After adding the nanoparticles, the excess sample was wiped off from the metallic stub. Subsequently, a platinum coating was done on the stub in vacuum by implementing JEOL JFC 1600 auto fine coater (JEOL, Tokyo, Japan) at an acceleration voltage of 5 kV. The nanoparticulate samples were observed under the Field emission scanning electron microscope (FESEM, JEOL JSM 6700 F, JEOL, Tokyo, Japan).

Energy dispersive X-ray (EDX) examination is done in a FESEM device to evaluate the elemental composition of the experimental nanoparticles (DTX NP and Cet-DTX NP). After being lyophilized and spread out on the metal stub, the nanoparticles were coated in platinum.

5.4.4. Transmission electron microscopy (TEM) study

The internal morphology of the nanoaprticles and the distribution of drug inside the core were assessed by TEM (JEOL JEM-2010, JEOL, USA). Briefly, the nanoparticles were resuspended in distilled water, and one drop of the suspension was put on the carbon-coated copper grid (300#; Ted Pella Inc., CA, USA). Further, the suspension drop was air-dried for 10-12 h and then analyzed through TEM instrument.

5.5. SDS-PAGE

The conjugation of antibodies on the surface of DTX NP was verified using SDS-PAGE. DTX, Cet-DTX, and Blank nanoparticles were resuspended in PBS at a concentration of 0.2 mg/ml, and standard Cet antibody was mixed individually with 2X Laemmli gel loading buffer (each 5 µL) at a concentration of 1 µL from the primary stock. DTX NP, Cet-DTX NP, and Blank NP were put onto a 10% SDS-PAGE gel along with the marker. Gel electrophoresis was carried out by running the gel (80V up to stacking and 100V up to resolving) (Aggarwal et al., 2013; Mondal et al., 2019).

5.6. *In vitro* drug release study

The *in vitro* drug release study was performed for Cet-DTX NP on various buffers, such as phosphate buffer saline (PBS) (pH 7.4) with 0.1% w/v tween 80, citrate buffer (pH 3), acetate buffer (pH 5) and bicarbonate buffer (pH 10). Cet-DTX NP was prepared as a suspension in various buffers (1 mg/ml, 2 ml) separately, and were shaken at 37 °C in an incubator shaker (Somax Incubator Shaker; ShenjhenPango Electronic Co. Ltd., Shenzhen, China). At various intervals (0.5 h, 1 h, 2 h, 4 h, 8 h, 24 h, 48 h, 96 h, 168 h, 336 h, 504 h and 672 h), the suspension (1 ml) was withdrawn from the vials, centrifuged, and the supernatant samples were examined for drug content using an UV-visible spectrophotometer at 229 nm (Bhattacharya et al., 2018). The centrifuged pellet after the each sample withdrawal was re-dispersed adding 1 ml of freshly prepared buffer before being replaced into the vial. The drug release curve was created as cumulative percent drug release vs. time graph. To understand the release profile of DTX from Cet-DTX NP, various kinetic models including zero order, first order, Highuchi, Hixson-Crowell and Korsmeyer-Peppas models were utilized (Dutta et al., 2019).

5.7. Stability study

Through accelerated stability study, the effect of temperature and humidity on the experimental nanoparticles was examined. The stability study was carried out in accordance with International Council of Harmonization (ICH) guidelines (2003) to determine the impact of temperature and relative humidity on the nanoformulations (DTX NP and Cet-DTX NP). Three months of stability tests were conducted on the optimized nanoparticles, with sampling intervals of one month. For the duration of 30 and 90 days, specific amounts of DTX NP and Cet-DTX NP were weighed and stored in zone III at 4-8°C (in the refrigerator), 30°C/75% RH, and 40°C/75% RH. The stability chamber samples were removed at the predetermined intervals (after 30 and 90 days). The stability parameters for those samples were examined using FESEM analysis and drug content.

5.8. Hydrolytic stability study

The hydrolytic breakdown of nanoparticles was compared in citrate buffer pH 3, acetate buffer pH 5, PBS pH 7.4, and bicarbonate buffer pH 10 (Bhattacharya et al., 2018). A required quantity (10 mg) of experimental nanoparticles and pure DTX were taken separately in 2 mL of different buffers in order to compare the hydrolytic breakdown of nanoparticles to that of free drug (citrate buffer pH 3, acetate buffer pH 5, phosphate buffer saline pH 7.4 and sodium bicarbonate buffer pH 9). The solutions were maintained at 37 °C with gentle shaking in an incubator. The samples were taken out of the incubator at the predetermined times (7, 14, 21, and 28 days), centrifuged, and then washed twice with double-distilled water before being dried in a speed vacuum for 30 min. The weight of the nanoparticles was then calculated. Fresh medium was used to replace the old medium entirely. Each sample's weight was precisely measured before the hydrolytic degradation assessment in order to calculate the weight loss. The weights of the samples were measured after drying in order to assess the weight change. The following formula was used to determine the change in weight (Maya et al., 2013):

$$\text{Weight change (\%)} = \frac{W_0 - W_t}{W_0} \times 100 \qquad (3)$$

where, W_0 and W_t, respectively, stand for the initial weight and the weight at time t.

5.9. *In vitro* cellular studies

5.9.1. Detection of mRNA by RT-PCR

The Trizol technique was used to isolate total RNA. Using a cDNA synthesis kit and following the manufacturer's instructions, the cDNA was transcribed (Biogenomics Asia). The Rotorgene Real-Time RT-PCR System was used to examine the expression levels of EGFR and the reference gene glyceraldehydes-3-phosphate dehydrogenase (GAPDH) in each cDNA sample (Qiagen, Germany). The **Table 5.1** contains a list of the specific primers involved in the study. Cycle conditions of the relative qRT-PCR were preincubated at 95 °C for 10 min, followed by 45 amplification cycles of 95 °C for 8 s, 62 °C for 15 s, 72 °C for 10 s, and a melting curve analysis, which ran Melt (65–95 °C), at 95 °C hold 0 s, at 65 °C hold 15 s and at 95 °C hold 0 s. Real-Time PCR software was used to analyse qRT-PCR data and determine quantification cycle values for relative quantification (Qiagen, Germany). The GAPDH gene expression was used to normalise the EGFR gene expression (Alfieri et al., 2011).

Table 5.1 :Primers used for RT-PCR and qPCR of EGFR and GAPDH

mRNA	Primers	Product size
EGFR	Forward primer: CGCCCTATGTCCCATTCACA Reverse primer: AAGGCCCATTTAGCCTCCAC	312bp
GAPDH	Forward primer: TGAGGGTAGGGCCTCCAAA Reverse primer: ATAGCCTAGGACTGGAGCGA	141bp

5.9.2. ELISA method for dissociation constant (K_D) determination

The dissociation constant (K_D) of Cet with EGFR overexpressed on the lung cancer cells (A549 and NCI-H23) was determined by cell based ELISA method (Patel et al., 2007; Eble, 2018). Falcon flexible 96-well flat bottomed plates were seeded with 100 µl (2×10^4 cells) of lung cancer cells per well at 37 ℃ overnight. The next day the plate was blocked with 1% BSA in PBS containing 0.1% w/v tween-20 for 2 h at room temperature. Various amounts of cetuximab in 100 µl were added. The plate was then washed 3x with PBS/Tween and 100 µl of horseradish peroxide (HRP) conjugated goat anti-human antibody (Biosource, Camarillo,

CA, USA) diluted at 1:5000 in 100 µl was added to the plate and incubated for 1 h at RT. The plate was then washed 3x and 50 µl/well of tetramethylbenzidine (TMB) (KPL, Gaithersburg, MD, USA) substrate was added to the plate. The plates were read at 450 nm using a microplate reader (Molecular Devices).

5.9.3. *In vitro* cytotoxicity assay

The MTT assay was used to assess the cytotoxic effects of free DTX, DTX NP, and Cet-DTX NP on human lung cancer cells (A549 and NCI-H23) and normal lung cells (L-132). 1.25 to 2.5×10^4 cells were seeded in each well of a 96-well plate, and they were then incubated with DMEM medium that had been supplemented overnight at 37 °C with 5% CO_2. Following the removal of the media, the cells were treated for 48 h in two separate groups with media containing free DTX suspension (200 µL, concentration range 5-150 nM) and Cet-DTX NP suspension (200 µL, equivalent DTX concentration range 5-150 nM). The cells in the control group did not receive any drug treatment. Each well received 20 µL of MTT solution (5 mg/mL in PBS) once the treatment period had ended, and then incubated for 3–4 h at 37 °C. Following the removal of the MTT solution, 100 µL of DMSO was added to each well, and the shaker was rotated for 15 min to extract the formazan crystals from the cells that had formed as a result of the reaction between the MTT solution and the mitochondrial reductase enzyme. After that, the plate was examined at 540 nm in an ELISA reader (Bio Rad, CA, USA). The IC_{50} value was calculated by plotting percentage of cell viability versus DTX/DTX NP/Cet-DTX NP concentration (Ehsan et al., 2022; Aggarwal et al., 2013).

Graph Pad Prism software was used to interpret the results graphically to assess the relevance of the results reported as the IC_{50} value (version 5, Graph Pad Prism software Inc, San Diego, CA, USA).

5.9.4. *In vitro* cellular uptake study

Using A549 and NCI-H23 cells, confocal laser microscopy was used to study the intracellular uptake of FITC-labeled DTX NP and Cet-DTX NP *in vitro* and to quantify it using flow cytometry. A 35 mm tissue culture dish with medium and approximately 10^4 cells were sown on a cover slip and cultured at 37 °C overnight for confocal laser imaging. Both the cells received the IC_{50} concentration of FITC-labeled Cet-DTX NP at 1 h and 4 h. The cells were rinsed in PBS after the treatment, fixed in 70% ethanol, co-stained with DAPI (for the nucleus), and mounted on a slide for observation under a confocal microscope (Olympus

FluoView FV10i, Olympus). Dual-color pictures were taken using the FITC (Ex/Em 495/519 nm) and DAPI (Ex/Em 359/461 nm) filters (Townsend et al., 2017).

The time-dependent intracellular absorption of PLGA nanoparticles was assessed using flow cytometry. Briefly, 10^6 A549 and NCI-H23 cells were grown in complete media for 24 h. The medium from each plate was replaced by incomplete medium and the treatment was conducted for 1 h, 2 h and 4 h. The cells, except the control group, were then exposed to FITC-loaded nanoparticles. Once the treatment was finished, the cells were taken from the plates and suspended in FACS tubes for analysis in a flow-cytometer (BD LSRFortessaTM, BD Biosciences, San Jose, USA). FACS Diva software (BD Biosciences) was used to collect the data (Dutta et al., 2019).

5.9.5. *In vitro* cellular apoptosis study

Apoptosis assay was conducted using a standard methodology to quantitatively assess the capacity of DTX/DTX NP/ Cet-DTX NP to induce apoptosis and/or necrosis in A549 and NCI-H23 cells. Briefly, the cells (2.5×10^5/ml) were cultured for 48 h at 37 °C in an atmosphere with 5% CO_2 and the IC_{50} concentration of the free drug and the formulations. Cells in the control group did not receive any treatment. Following the completion of the treatment period, the cells were detached using trypsin, cleaned with PBS (2X), and resuspended in 100 µL of Annexin V binding buffer (1X) (10 mM HEPES, 140 mM NaCl, 2.5 mM $CaCl_2$; pH 7.4). An additional 400 µL of binding buffer (1X) was added after adding 2 µL of annexin V-FITC to the cell suspension and incubated it in the dark for 15 minutes. Just prior to analysis, propidium iodide (PI) (5 µL, 50 g/ml) was added [31]. Data was obtained using an FACS Aria flow cytometer (Becton Dickinson, USA) using channels of FITC (excitation/emission 488 nm/530 nm) and PE-Texas red (excitation/emission 561 nm/616 nm) and post capturing analysis was done with BD FACS Diva software (Becton Dickinson, USA) (Chakraborty et al., 2020).

5.9.6. *In vitro* cell cycle analysis

The effect on cell cycle of DTX/DTX NP/Cet-DTX NP was examined using the methodology described in the literature (Maya et al., 2014; Wang et al., 2021). In a 12-well plate, 1×10^6 cells were seeded each well, and the plate was placed in a CO_2 incubator overnight. After being treated with free drug and various experimental formulations, cell cycle phase analysis

of nuclear DNA stained with PI were measured in a flow cytometer (Becton Dickinson FACS Fortessa 4 laser cytometer equipped with BD FACS Diva software).

5.10. Hemolysis study

The hemolytic studies were conducted using the previously described methodology, with a few alterations (Gaonkar et al., 2017; Liu et al., 2017). The freshly drawn blood from male swiss albino mice was placed in heparinized tubes and centrifuged at 4 °C for 5 minutes at 1000 g. The erythrocytes were rinsed three times with PBS after the supernatant was removed (pH 7.4). The resulting suspension (2%) was employed for a hemolysis study. A 96-well plate with 190 µL of the suspension in each well was then treated with 10 µL of the free drug (DTX) and experimental nanoparticles (DTX NP and Cet-DTX NP) (containing DTX at varying concentrations, such as 5, 10, 15, 30, 50, 100 and 150 nM) to assess the hemolytic effect. The unlysed erythrocytes were separated by centrifugation at 10,000 g for 5 min after being incubated at 37 °C for 1 h with gentle stirring. The optical density (OD) of the supernatant was then measured at 570 nm. By utilizing the procedure to compute the absorbance factor of a sample that was 100% hemolytic, the percentage of hemolysis was determined:

$$\text{Hemolysis (\%)} = \frac{(Abs - Abs_0)}{Abs_{100} - Abs_0} \times 100 \qquad (1)$$

where Abs, Abs_0, and Abs_{100}, respectively, represent the absorbance of samples, a solution with 0% and 100% hemolysis, respectively.

5.11. *In vivo* animal studies

5.11.1. Maximum tolerated dose (MTD)

Mice were administered DTX NPs, Cet-DTX NPs, and free DTX, and their *in vivo* tolerance to each treatment was compared. Male Swiss albino mice were randomly divided into six groups (n = 6). DTX NPs and Cet-DTX NPs were injected into 0.9% saline solution at dosages of 2.5, 5, 10, 20, and 40 mg/kg (corresponding to groups i, ii, iii, iv and v, respectively). Free DTX was dissolved in Tween 80 and 13% w/w ethanol in water at a ratio of 1:3 w/w to produce groups vi, vii, viii, ix, and x at DTX dosages of 2.5, 5, 10, and 40 mg/kg, respectively. The mice were given intravenous injections through tail vein on days 7, 14, 21, and 28. They were weighed before every injection and again on the first, second,

third, fourth, fifth, sixth, seventh, and eighth weeks. Blood samples were collected, and they were allowed to stand without any anticoagulant for 30 min. The blood samples were centrifuged at 2,500 rpm for 10 min before the serum was extracted. After 28 days, an automated clinical analyzer was used to measure and analyze the different biochemical parameters of liver and kidney, including SGOT, SGPT, ALP, urea, and creatinine, in accordance with the manufacturer's instructions (AU400, Olympus, Tokyo, Japan). The dose that resulted in a 20% weight loss was identified as the MTD (Tang et al., 2016; Qu et al., 2019; Choudhury et al., 2021).

5.11.2. Pharmacokinetic study in normal mice

Pharmacokinetic parameters of plasma and lung were analyzed in Swiss albino male normal mice (body weight 25-30 g) upon free DTX (10 mg/kg), DTX NP, and Cet-DTX NP (having an equivalent amount of DTX) i.v. administration. The treated animals were sacrificed at specific time points (0.5, 1, 2, 4, 6, 8, 10, 24, 48 and 72 h). The blood and the lung were collected. Tandem liquid chromatography and mass spectrophotometry (LC–MS/MS) was utilized to analyze the drug content in the separated plasma and the lung as per protocol. Paclitaxel was used as an internal standard.

In vivo pharmacokinetic studies of DTX NP, Cet-DTX NP and aqueous suspension containing free DTX were done in Swiss albino male mice (body weight 25-30 g). Three groups of the animals (n = 20 per group) were formed. Aqueous suspensions of free DTX, DTX NP, and Cet-DTX NP were injected intravenously into the animals in groups 1, 2, and 3 at doses of 10 mg DTX/kg body weight, respectively. At each time point, two mice were sacrificed, blood was probed, and plasma was collected. The same was done for lungs also. At specified intervals (0.5, 1, 2, 4, 6, 8, 10, 24, 48, and 72 h post injection), the blood and lungs were collected in heparinized tubes, and the plasma was separated by centrifuging the tubes at 10,000 rpm for 10 min. at 4 °C. Each 0.1 mL of plasma sample was mixed with 1 mL of ice-cold acetonitrile-methanol mixture and vortexed. The clear supernatant that was obtained after centrifugation was mixed with 100 µL of water and loaded into LC-MS/MS (LC: Shimadzu Model 20AC, MS: AB-SCIEX, Model: API4000), using software: Analyst 1.6. Analytes were eluted using YMC Triat C18 column (30 × 2.1 mm, 5 µ) and gradient elution technique of two mobile phases (mobile phase A: 0.1% formic acid in water and mobile phase B: 0.1% formic acid in methanol:acetonitrile:water (45:45:10)) was conducted

with an injection volume 20 µL, flow rate 0.8 mL/min and total run time 3.0 min (Das et al., 2015; Dutta et al., 2018; Ehsan et al., 2022).

5.11.3. Experimental animal model for *in vivo* anti-tumor efficacy

The Swiss albino mice used for the study were separated in five groups consisting of six mice in group. Group I served as normal control with oral administration of corn oil for four weeks. Group II animals were treated with benzo(a)pyrene (B(a)P, 50 mg/kg body weight dissolved in corn oil orally) weekly twice for 4 weeks, to induce lung cancer by 16th week, which served as carcinogen control. Group III animals were treated with DTX control for 4 weeks after they were administered with first dose of B(a)P. Group IV and Group V animals were treated with DTX NP and Cet-DTX NP (i.v., 10 mg DTX/kg body weight) for 4 weeks after they were treated with the first dose of B(a)P.

Group III, IV and V animals continued to receive the same treatment of B(a)P as received by group II animals. Administration dose of Cet with nanoparticles was 101.84 µg/mg of nanoparticle conjugate (Cet-DTX NP). Food and water was available *ad libitum*. During the study, the body weights were measured every week.

5.11.4. *In vivo* biodistribution study

The biodistribution study was conducted in B(a)P induced lung cancer mice model after injecting free DTX, DTX NP and Cet-DTX NP at predetermined time points. B(a)P induced lung cancer mice model were randomized into three groups (n=6 per group). Free DTX, DTX NP and Cet-DTX NP were injected as a single i.v. bolus injection into the tail vein of the mice at an equivalent dose of DTX (10 mg/kg body weight). After various time points (4 h, 24 h, 48 h and 72 h) post injection, the mice were sacrificed and the major tissues (whole blood, liver, kidney, heart, muscle and cancerous lung) were harvested from the mice. The tissue samples were homogenized with 1 mL of acetonitrile, followed by centrifugation for 30 min at 4 °C. 1 mL of supernatant was removed and dried under nitrogen. The dried samples were reconstituted with 0.1% formic acid in 100 µL of acetonitrile. The drug content in each organ was analyzed by LC–MS/MS (Li et al., 2019).

5.11.5. Survival time of mice

The survival analysis of experimental mice was regularly checked up until their mortality. Briefly, six separately treated mice from the carcinogen control and carcinogen treated received formulation treatment groups were allowed to live until natural death without

carrying out a required sacrifice. Kaplan-Meier survival analysis was used to calculate the mean survival time (MST). GraphPad Prism Software was used to conduct the statistical analysis (Choudhury et al., 2021).

5.11.6. Caspase-3 activity

A single i.v. bolus injection of DTX/DTX NP/Cet-DTX NP at a concentration equivalent to their respective IC_{50} values was administered to the various experimental animals. Lung tissues from various animal groups were removed after 24 h of treatment, collected, and processed for protein separation using RIPA buffer (Sigma). Caspase-3 activity was measured in accordance with the manufacturer's instructions using the caspase-3/7 colorimetric assay kit (Abcam kit no. ab39401) (Kim et al., 2010; Barua et al., 2022).

5.11.7. LPO and ROS study

Using a spectrofluorimeter of serum samples taken from the mice of the experimental normal control, carcinogen control, and carcinogen treated mice treated with various treatments, the relative estimation of ROS was examined. Using the thiobarbituric acid method, the amount of TBARS (thiobarbituric acid reactive substance), a product of lipid peroxidation under stress, was calculated in serum samples from the same experimental group of mice (BarathManiKanth et al., 2010; Zeb et al., 2016).

5.11.8. Lung histopathology analysis

For the fabrication of paraffin-embedded blocks, the lung tissues from the corresponding experimental groups (normal control, carcinogen control, and Carcinogen treated received formulation treatment) were fixed in 10% neutral buffered formalin. To examine tissue architecture and cancer morphology, 5 µm-thick slices were deparaffinized, rehydrated, and stained with hematoxylin and eosin in accordance with the recommended methodology (Pal et al., 2012). Zeiss light microscope and Axio Vision software 4.7.1 were used to view the histopathology slides.

5.12. Statistical analysis

Each experiment was carried out in triplicate. Student's t-test and one-way ANOVA was used for the statistical analysis, and Graph Pad Prism was used to generate the graphs (version 5, Graph Pad Prism software Inc, San Diego, CA, USA).

6. Results

6.1. Determination of absorbance maxima (λ_max) of Docetaxel

On the basis of scanning of Docetaxel by spectrophotometric method, the maximum wavelength (λ_max) was attained at 229 nm in acetonitrile:water, and therefore it has been selected as the analytical wavelength. The absorbance spectrum of Docetaxel was shown in **Figure 6.1**.
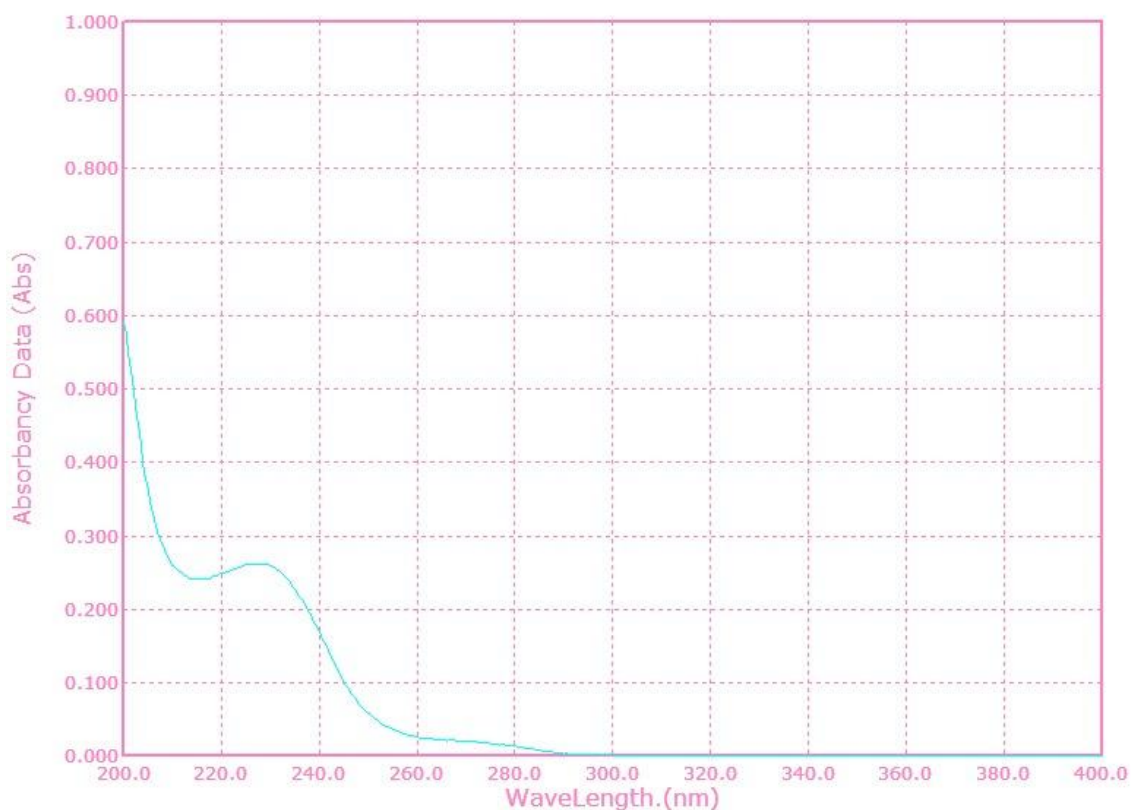
Figure 6.1. Absorbance maxima (λ_max) of Docetaxel

6.2. Estimation of calibration curve of Docetaxel

The absorbance values of the drug dissolved in acetonitrile:water were recorded at 229 nm in the concentration range of 0.5 to 10 µg/ml. A high regression coefficient (R^2=0.999) was achieved, which suggested that the absorbance and concentration of drug were linearly related to each other, and it followed Beer's law. The calibration curve of Docetaxel in acetonitrile:water is depicted in **Figure 6.2**.
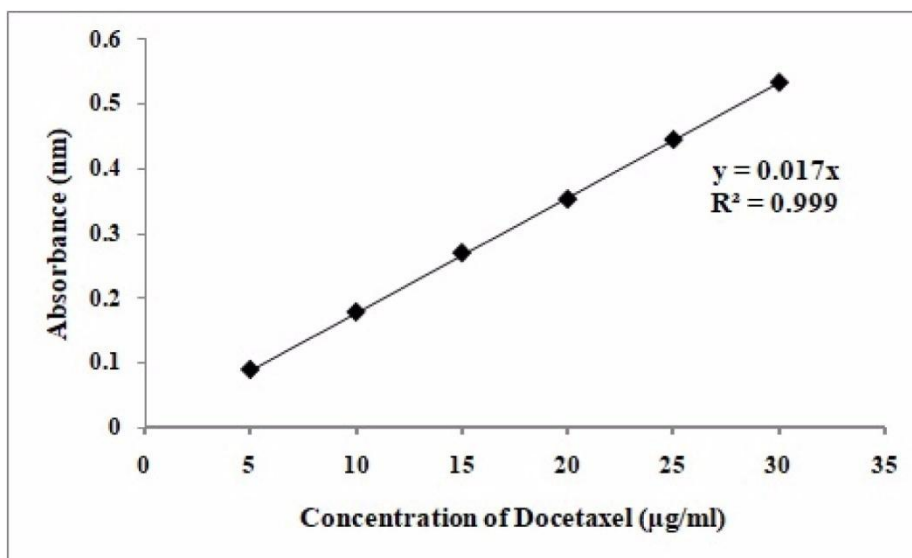
Figure 6.2. Calibration curve of Docetaxel in acetonitrile:water

6.3. Fourier Transform Infrared Spectroscopy (FTIR) analysis

The spectrophotometric investigation detected all the characteristic peaks of DTX and various excipients which were used to formulate DTX NP. No chemical interactions were observed between them **(Figure 6.3)**. N-H stretching at 3490 cm^{-1} and asymmetric and symmetric vibrations at 2947 cm^{-1} for CH$_2$ revealed for pure DTX. The C=O stretching vibrations of the ester group showed the peaks at 1725 cm^{-1}, C=N stretching at 1244 cm^{-1}, 1075 cm^{-1} for C=O stretching vibrations, respectively. For C-H in-plane and C-H out-of-plane C-C=O, the peaks were observed at 972 cm^{-1} and 712 cm^{-1}, respectively. PLGA displayed characteristic peaks at O-H at 3515 cm^{-1}; C-H at 2995 cm^{-1} and C=O at 1756 cm^{-1}, respectively.

Weak physicochemical interactions, such as the dipole-induced interaction, weak H-bonds, van der Waals force of attraction, etc., which may play significant roles in the formation of spherical shaped nanoparticles, were noted in the case of Blank NP and DTX NP, leading to some minor peak shiftings of the formulation components. In case of spectrum of physical mixture (PLGA, PVA and DTX) and DTX NP, the intensity of 712 cm^{-1} peak attributes the entrapment of DTX over blank NP.
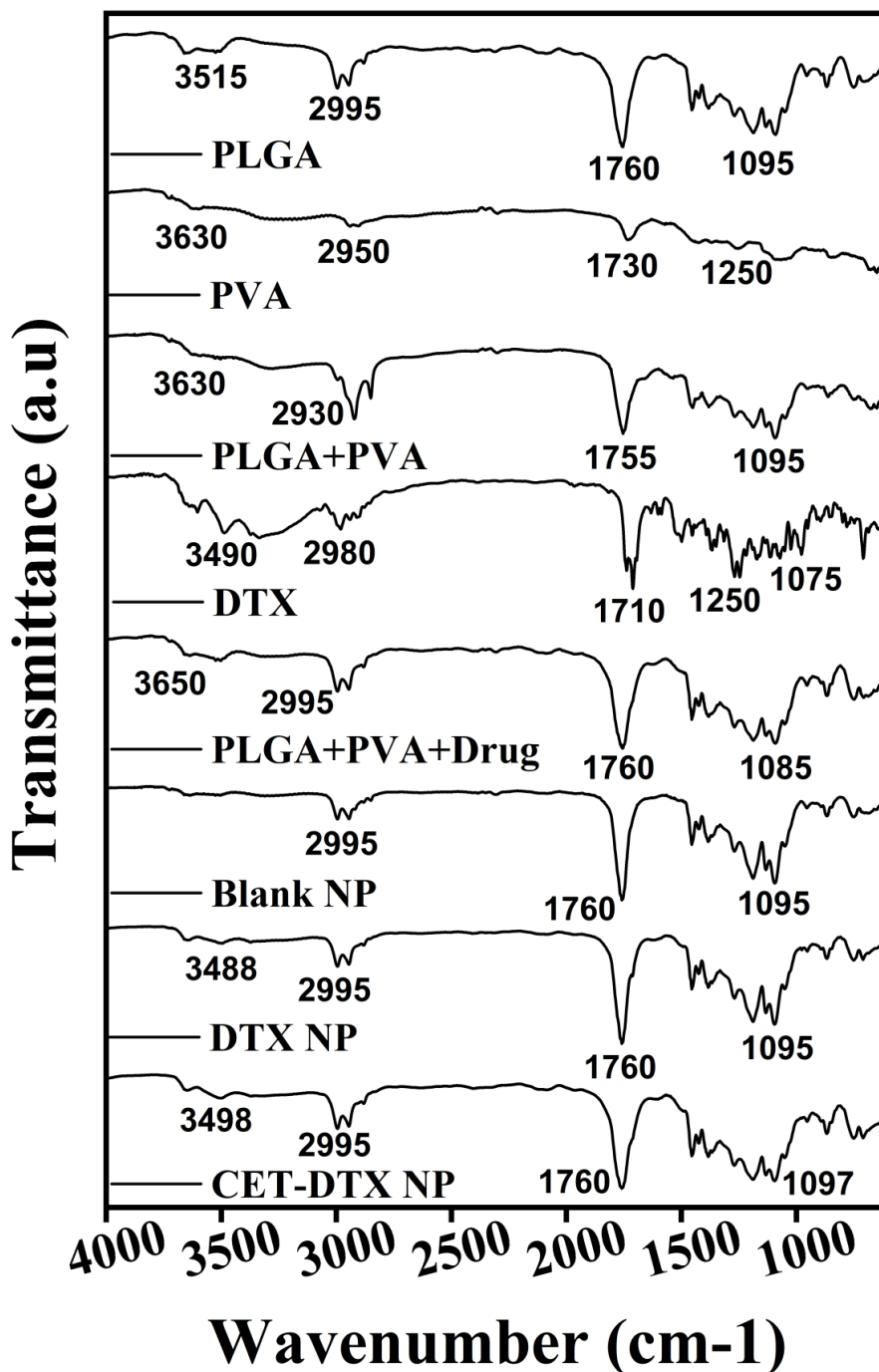
Figure 6.3. FTIR spectra of individual components, physical mixture, and nanoparticulate formulations. PLGA: Poly lactic-co-glycolic acid; PVA: Polyvinyl alcohol; DTX: Docetaxel; PLGA+PVA+Drug: Physical mixture of PLGA, PVA and Drug; BLANK NP: Blank nanoparticles; DTX NP: Docetaxel-loaded nanoparticles; CET-DTX NP: Cetuximab conjugated nanoparticles.

6.4. Preparation of the polymeric nanoparticles and conjugation with monoclonal antibody

The blank nanoparticles and different batches of drug loaded nanoparticles were prepared by multiple emulsion solvent evaporation technique. The nanoformulations were optimized by varying the drug polymer ratio to develop DTX-loaded PLGA nanoparticles. Further, the surface of the optimized nanoparticles was conjugated with Cetuximab monoclonal antibody for site-specific drug delivery to lung tumor cells.

6.5. Physicochemical characterization of the prepared nanoparticles

6.5.1. Drug loading and entrapment efficiency

The drug loading and encapsulation efficiency were assessed by varying the drug polymer ratio of the various nanoparticles, and the results were tabulated in **Table 6.1**. From the data, it was observed that the optimized DTX NP showed maximum drug loading, greater entrapment efficiency. The drug loading and encapsulation efficiency for DTX NP was 6.43% ± 0.25% and 70.76% ± 2.76%, respectively. In the case of Cet-DTX NP, the drug loading and encapsulation efficiency was found to be 5.86 ± 0.35% and 64.53% ±1.38%, respectively.

Table 6.1. Physicochemical characterization and optimization data of various experimental nanoparticles by varying drug:polymer ratio

Formulation	Drug:PLGA	Particle size (Z-average) (nm)[a]	Zeta potential (mV)[a]	Polydispersity index[a]	Drug loading (%)[a]	Encapsulation efficiency (%)[a]
DTX NP (optimized formulation)	1:10	225 ±3	-8.18±0.50	0.589±0.060	6.43%±0.25%	70.76% ± 2.76%
Cet-DTX NP (optimized formulation with antibody conjugation)	1:10	283± 2	-12.10±0.43	0.486±0.080	5.86%±0.35%	64.53% ±1.38%
DTX NP 1	2:10	400± 2	-5.10±0.47	0.663±0.060	5.06%±0.05%	55.73%± 0.50%
DTX NP 2	3:10	456± 2	-4.40±0.29	0.609±0.040	4.72%±0.07%	51.92%±0.78%

Note: DTX NP, PLGA nanoparticles encapsulating docetaxel; Cet-DTX NP, Antibody conjugated PLGA nanoparticle encapsulating docetaxel; PLGA, poly (lactide-co-glycolide); PVA, poly vinyl alcohol.[a] Each value represents mean ± SD (n = 3).

6.5.2. Particle size and zeta potential

The particle size, zeta potential, polydispersity index (PDI) values of the prepared NP is mentioned in **Table 6.1**. The physicochemical characterization of the optimized formulation DTX NP and Cet-DTX NP was carried out. It was found that the particle size of DTX NP and Cet-DTX NPs was 225 ± 3 nm and 283 ± 2 nm, respectively. The zeta potential value of DTX NP and Cet-DTX NPs was -8.18 ± 0.50 mV and -12.1 ± 0.43 mV, respectively **(Figure 6.4)**. The PDI value of DTX NP was 0.589 ± 0.060, while for Cet-DTX NP, the value was 0.486 ± 0.080.
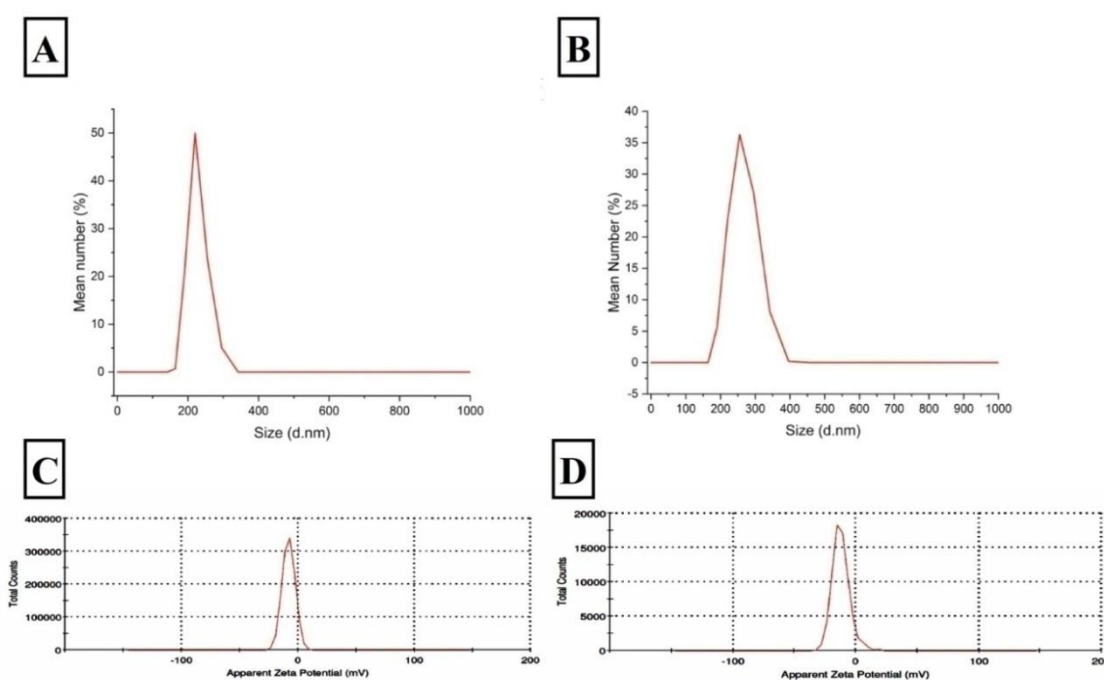
Figure 6.4. Particle size distribution and zeta potential data. (A) Particle size of DTX NP, (B) Particle size of Cet-DTX NP, (C) Zeta potential data of DTX NP, and (D) Zeta potential data of Cet-DTX NP

6.5.3. Surface morphology of the nanoparticles

The surface morphology was analyzed for Cet-DTX NP by Field emission scanning electron microscopy (FESEM) study **(Figure 6.5A)**. The figure revealed that Cet-DTX NPs had majority of spherical structure and densely distributed. Utilizing TEM analysis, the internal morphology of Cet-DTX NP was confirmed **(Figure 6.5B)**. The figures revealed that the drug was evenly and homogeneously distributed throughout the particles.
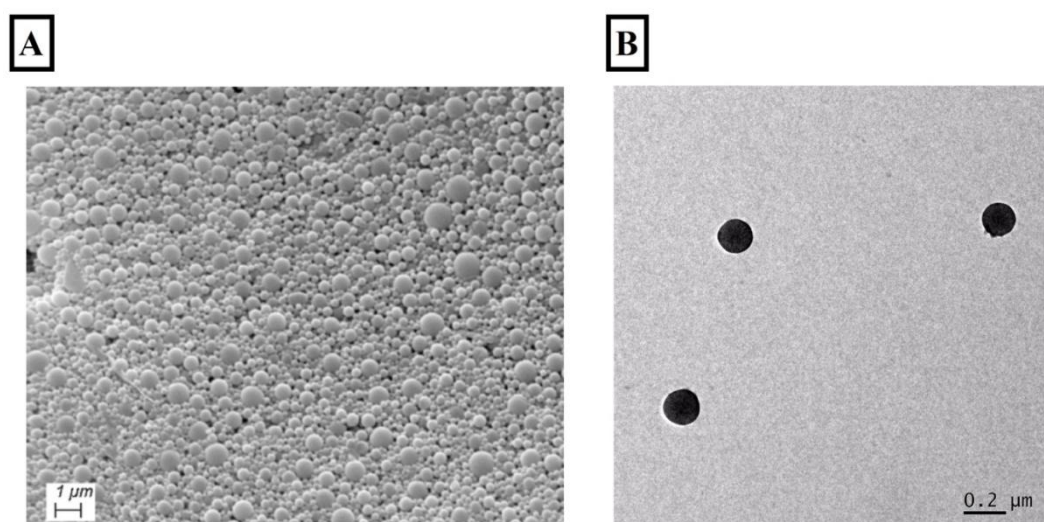
Figure 6.5. (A) Field emission scanning electron microscopy of Cet-DTX NP analyzed at 10,000× magnification, (B) Transmission electron microscopy of Cet-DTX NP

6.5.4. Energy dispersive X-ray (EDX) study

The EDX study for blank NP, DTX NP and Cet-DTX NP was carried out during FESEM analysis. Nitrogen in the case of DTX NP and its absence in the case of blank NP indicated the presence/lack of nitrogen of DTX in the two corresponding formulations. A high weight percentage of sulphur (2.02%) in case of Cet-DTX NP affirms the conjugation of the Cet to Cet-DTX NP **(Table 6.2)**. The other ingredients utilized to create DTX NP are devoid of sulphur. Because of the amide bond between the Cet and DTX NP, the Cet-DTX NP had a slightly greater weight percentage contribution from N (19.18%), which further supports the presence of Cet.

Table 6.2. Specific elemental composition (carbon, oxygen, nitrogen and sulphur) of nanoparticles.

Sample	CK		OK		NK		SK	
	Weight %	Atomic %	Weight %	Atomic %	Weight %	Atomic %	Weight %	Atomic %
Blank NP	39.37	58.59	60.63	41.41	-	-	-	-
DTX NP	43.57	49.22	41.56	30.19	14.87	15.61	-	-
Cet-DTX NP	49.09	55.41	29.71	20.72	19.18	21.89	2.02	1.99

Note: Weight % and atomic % of elements in Blank NP, DTX NP and Cet-DTX NP

Abbreviations: CK, carbon counts; OK, oxygen counts; NK, nitrogen count; SK sulphur count; Blank NP, blank nanoparticles; DTX NP, PLGA nanoparticle encapsulating docetaxel; Cet DTX NP, Antibody conjugated PLGA nanoparticle encapsulating docetaxel.

6.6. SDS-PAGE

We functionalized the surface of nanoparticles by conjugating Cet antibody against EGFR receptors which is generally overexpressed on the surface of lung cancer cells. The SDS-PAGE was run for both the DTX NP and Cet-DTX NP in comparison with the free antibody (**Figure 6.6**). It was demonstrated that the nanoparticles were conjugated well with the antibody and the antibody-conjugated particles ran slightly slowly, as compared to free antibody. It has demonstrated the effective conjugation of antibody onto the surface of DTX NP nanoparticles, which moved more slowly than free antibody due to the attachment to heavier nanoparticles. However, the lack of antibody on the surface of the DTX NP failed to produce any bands.
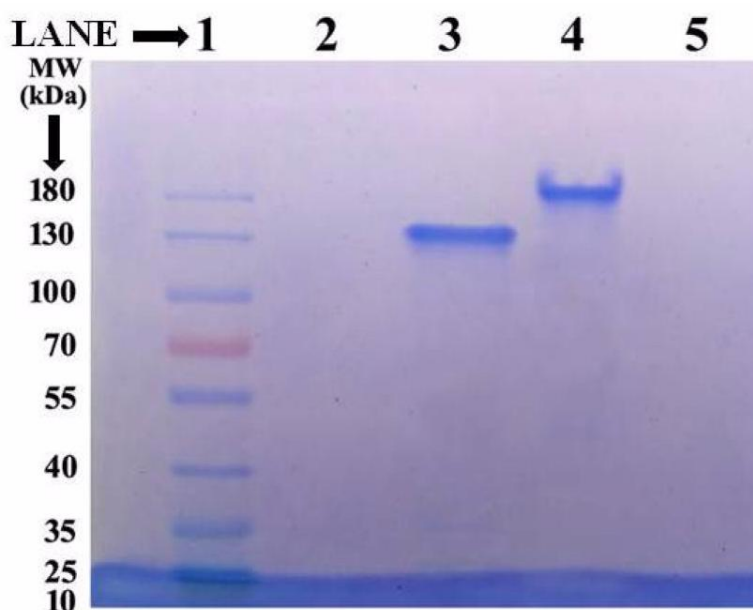
Figure 6.6. SDS-PAGE gel electrophoresis, Lane 1 represents protein marker, lane 2 showed unconjugated NP, lane 3 showed the standard anti-EGFR monoclonal antibody antibody (Cet), lane 4 represents antibody conjugated NP, lane 5 showed blank NP

6.7. *In vitro* drug release study

The different buffers and release media (citrate buffer pH 3, acetate buffer pH 5, phosphate buffer saline pH 7.4 with 0.1% w/v tween 80, and bicarbonate buffer pH 10) were used for the *in vitro* drug release investigation of Cet-DTX NP (as depicted in **Figure 6.7**). The nanoparticles deteriorated more quickly under an acidic pH, suggesting that rapid drug release (92.31% ± 2.37% in 24 h) in a citrate buffer (pH 3) rendered the formulation

unsuitable for oral administration. On the other hand, a slow and sustained release of the drug was seen in PBS with 0.1% w/v tween 80 (pH 7.4) (74.64% ± 2.83%) over the course of 28 days, showing that the produced nanoformulation would be stable in the blood for a prolonged period and would gradually and slowly degrade (since pH 7.4 simulates the environment of blood). The drug was only modestly (89.58% ± 2.47% in 28 days) released from the formulation in an acetate buffer (pH 5.5), implying that the nanoparticles would be stable in circulation and would deliver the drug more effectively in the tumor area, which is often an acidic milieu (pH ~4.5–5.5). The drug release from Cet-DTX NP was lower (32.11% ± 2.59%) in bicarbonate buffer (pH 10). Different regression coefficient (R^2) values for the kinetics were summarized after the drug release data were evaluated using zero-order, first-order, Hixson-Crowell, Korsmeyer-Peppas, and Higuchi kinetic models **(Table 6.3)**. The R^2 values indicate that, in all buffers and release media, drug release from the formulation adhered to Korsmeyer-Peppas kinetic model, thereby suggesting the release of drug from the nanoparticles by erosion, followed by slow diffusion from the eroded polymeric matrix. In case of PBS with 0.1% w/v tween 80, a good linearity ($R^2 = 0.979$) was obtained with a release exponent value (n) of the drug 0.29 for Cet-DTX NP, which suggests drug release followed Fickian diffusion.
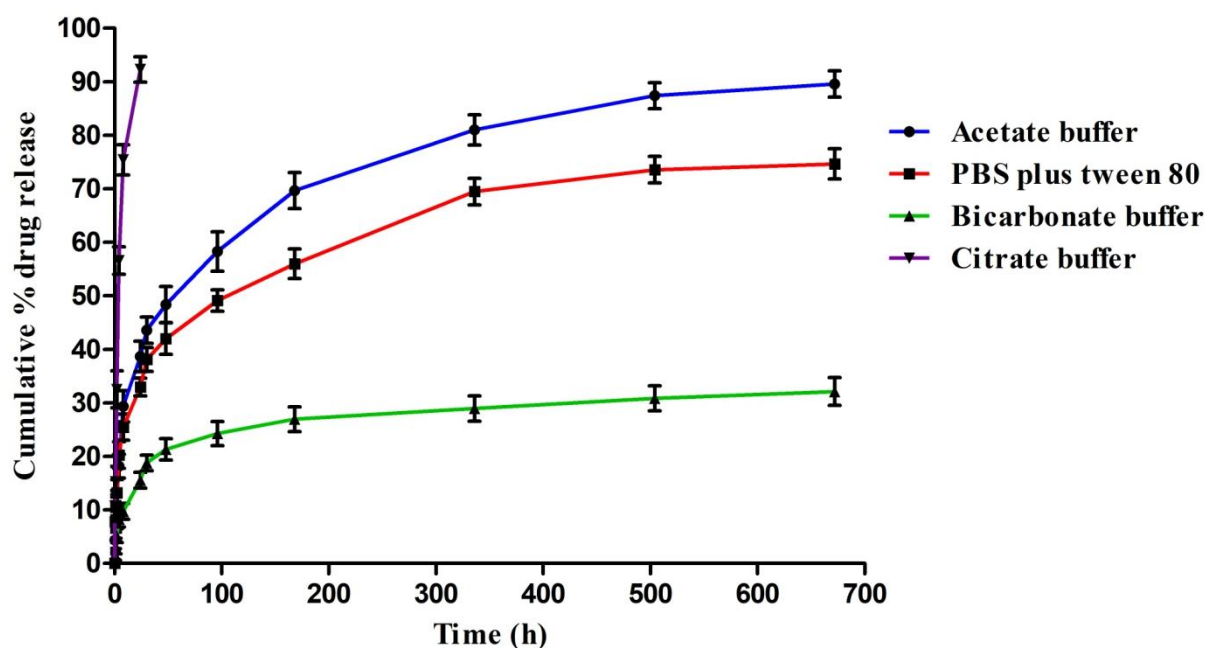
Figure 6.7. *In vitro* **drug release profile of DTX from Cet-DTX NP in phosphate buffer saline (PBS) pH 7.4 with tween 80, citrate buffer (pH 3), acetate buffer (pH 5), and bicarbonate buffer (pH 10). Data show mean±SD (n=3)**

Table 6.3. Depiction of *in vitro* drug release tested on different release kinetic models along with corresponding R^2 values and release exponent (n) (Korsmeyer–Peppas model).

Kinetic models	Cet-DTX NP release in Phosphate buffer saline pH 7.4 (with tween 80)	Cet-DTX NP release in Citrate buffer	Cet-DTX NP release in Acetate buffer	Cet-DTX NP release in Bicarbonate buffer
Zero order	y = 0.098x + 23.33 R² = 0.712	y = 3.501x + 20.64 R² = 0.727	y = 0.122x + 25.41 R² = 0.704	y = 0.041x + 10.58 R² = 0.610
First order	y = -0.000x + 1.88 R² = 0.850	y = -0.045x + 1.918 R² = 0.945	y = -0.001x + 1.87 R² = 0.913	y = -0.000x + 1.949 R² = 0.651
Higuchi model	y = 2.799x + 13.73 R² = 0.906	y = 20.63x + 2.527 R² = 0.917	y = 3.497x + 13.36 R² = 0.902	y = 1.223x + 6.186 R² = 0.833
Korsemeyer Peppas model	y = 0.296x + 1.091 R² = 0.979 n=0.29	y = 0.555x + 1.304 R² = 0.885 n=0.55	y = 0.364x + 1.018 R² = 0.943 n=0.36	y = 0.334x + 0.664 R² = 0.932 n=0.33
Hixson-Crowell model	y = 0.002x + 0.404 R² = 0.808	y = 0.107x + 0.325 R² = 0.881	y = 0.003x + 0.445 R² = 0.851	y = 0.000x + 0.173 R² = 0.637

6.8. Stability study

For the optimized formulation (DTX NP and Cet-DTX NP) in the freeze dried condition, stability studies were conducted to assess any alterations in the morphology during 3 months period at 4-8°C (refrigerated condition), 30°C, 75% RH, and 40°C, 75% RH. The stability study was also performed in terms of the changes in surface morphology of Cet-DTX NP by FE-SEM analysis **(Figure 6.8)**. The nanoformulation stored at 4-8°C maintained the surface morphology up to 3 months period. However, deformation of the formulation was observed at 30°C and 40°C during storage. A very significant changes in the surface morphology of the nanoformulation occurred during storage for 3 months, at these temperatures. Any notable changes in the drug content and encapsulation efficiency were not observed in case of DTX NP (Drug loading 6.25%, encapsulation efficiency 69.44%) and Cet-DTX NP (Drug loading 5.72%, encapsulation efficiency 62.93%) in the refrigerated condition at 4-8 ºC for 3 months **(Table 6.4)**. Thus, DTX NP and Cet-DTX NP should be stored between 2-8 ºC.

Table 6.4. Stability of DTX NP and Cet-DTX NP after 90 days of study stored at 4-8°C.

Formulation	Stability after 90 days at 4-8°C	
	Drug loading (%)*	Encapsulation efficiency (%)*
DTX NP (optimized formulation)	6.25%±1.09%	69.44%± 0.76%
Cet-DTX NP (optimized formulation)	5.72±0.73%	62.93%± 0.02%

*Data show mean ± SD (n=3).
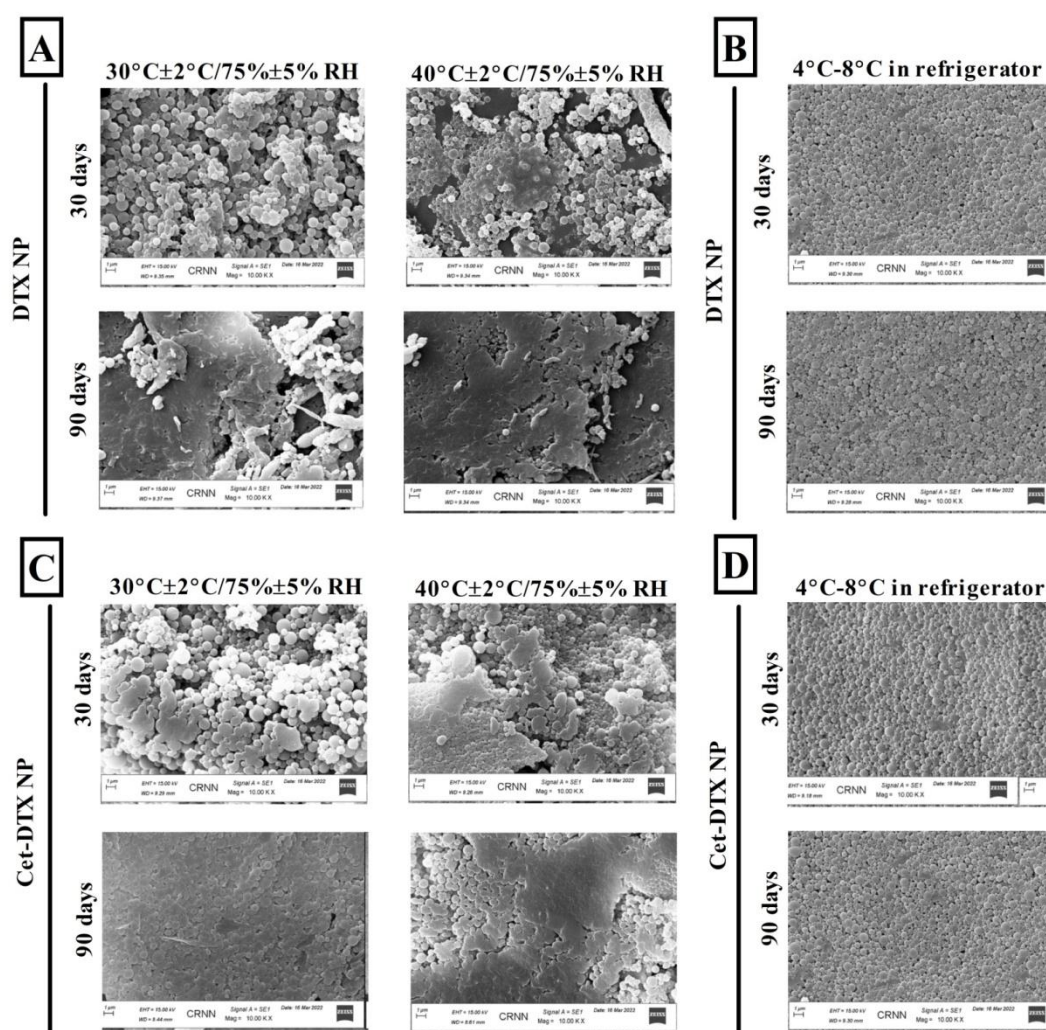
Figure 6.8. FESEM images of (A) DTX NP and (C) Cet-DTX NP stored at 30°C, 75% relative humidity, and at 40°C, 75% relative humidity after 30 days, and 90 days; and (B) DTX NP and (D) Cet-DTX NP stored at 4-8°C in a refrigerator for 30 days and 90 days.

6.9. Hydrolytic stability

The hydrolytic stability study of the optimized Cet-DTX NP was carried out in different pH media. An enhanced loss in the weight of nanoformulation was observed with the decrease in the pH of media **(Figure 6.9)**. Subsequent to 4 weeks of the experiment, the weight loss of Cet-DTX NP at pH 10 was 13.60% ± 1.14%, at pH 7.4 was 26.06% ± 1.66%, at pH 5 was 36.70% ± 1.57% and at pH 3 was 57.67% ± 1.56%, respectively.
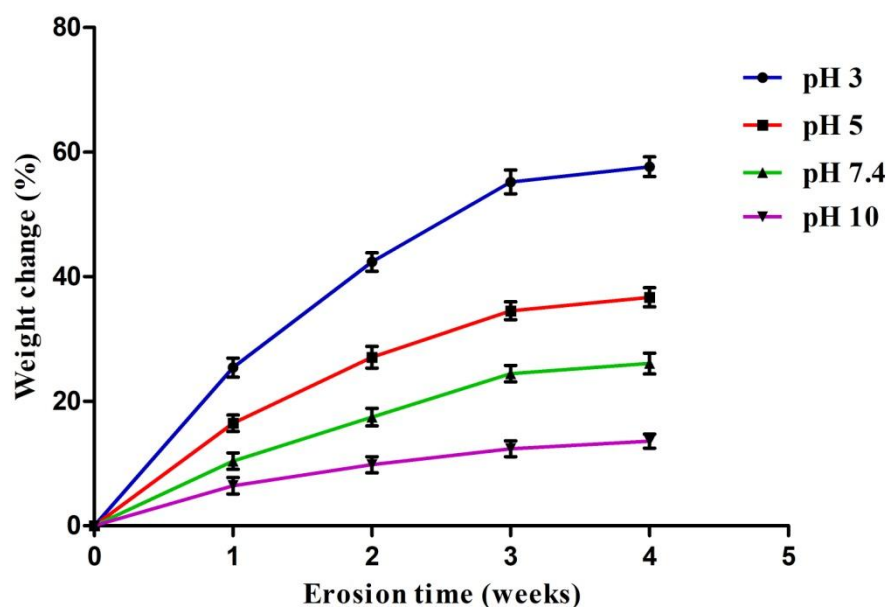
Figure 6.9. Percentage weight change of Cet-DTX NP at varying pH conditions (from pH 3 to pH 10). The values are mean of three batches with ±SD.

6.10. *In vitro* cellular studies

6.10.1. Detection of mRNA by RT-PCR

The results from RT-PCR study were summarized in **Figure 6.10**. The results indicate that lung cancer cell lines (A549 and NCI-H23) have overexpressed EGFR. However, A549 lung cancer cells have shown slightly greater expression than NCI-H23 cells. The Ct-median value of EGFR in both the cells (A549 and NCI-H23) were 17.89, for GAPDH the Ct-median value was 18.56, and for L-132 (normal lung epithelial cell line), the value was ≥35, respectively. The higher Ct-median value of L-132 cells clearly indicates the non-expression of EGFR.
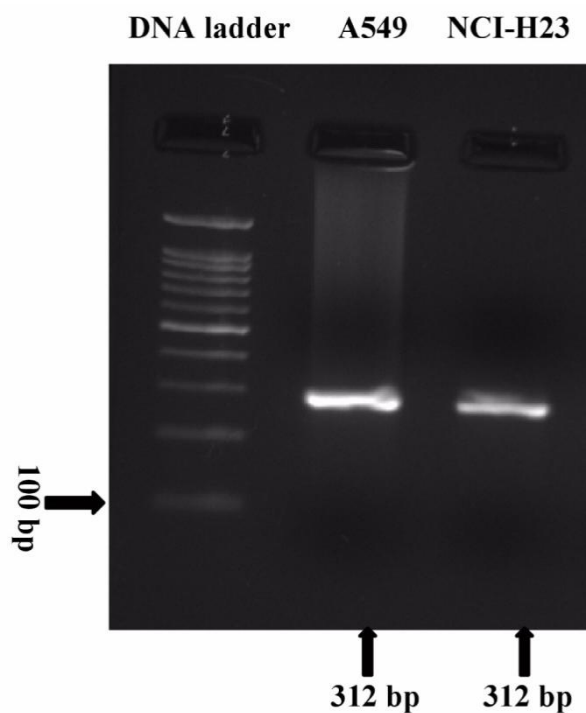
Figure 6.10. Analysis of EGFR mRNA expression in A549 and NCI-H23 lung cancer cells by RT-PCR study

6.10.2. Determination of dissociation constant (K_D) by binding experiment

The results obtained from titration ELISA along with mathematical evaluation demonstrated the interaction of cetuximab with EGFR receptors overexpressed on the lung cancer cells (A549 and NCI-H23) **(Figure 6.11)**. The dissociation constant (K_D) for the binding of cetuximab to the EGFR on A549 cells was 0.32 ± 0.016 nM, whereas cetuximab bound to the EGFR overexpressed on the NCI-H23 cells with a significantly lower affinity of 0.38 ± 0.019 nM.
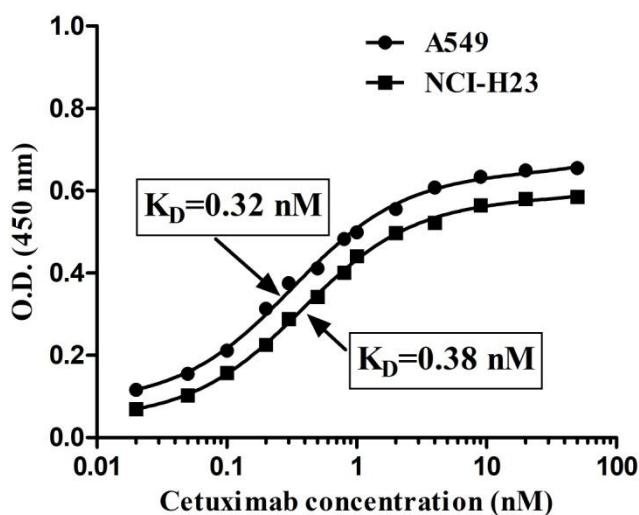
Figure 6.11. Representative titration curves showing dissociation constant (K_D) values for the interaction of Cet with EGFR overexpressed on A549 and NCI-H23 lung cancer cells (n=3).

6.10.3. *In vitro* cytotoxicity assay

In A549 and NCI-H23 cells, *in vitro* cytotoxicity investigation of free drug, DTX NP, and Cet-DTX NP was conducted. Cet-DTX NP was shown to have an IC_{50} value of 19.40 ±1.92 nM in A549 cells, which is much less than the IC_{50} values for the DTX (79.56 ± 2.46 nM) and DTX NP (39.90 ± 3.76 nM) **(Figure 6.12A)**. We also investigated Cet-DTX NP's ability to inhibit the proliferation of the NCI-H23 lung cancer cells. Cet-DTX NP IC_{50} value of 25.40 ± 1.54 nM, was much lower than the IC_{50} values for the DTX (109.64 ± 3.12 nM) and DTX NP (52.72 ± 2.85 nM) **(Figure 6.12B)**. DTX NP and Cet-DTX NP were shown to have very little cytotoxicity when tested against the normal lung epithelial cell line L-132 (percentage inhibition 8.23 ± 0.79% and 7.21 ± 1.20%, respectively), as compared to free drug (63.72 ± 2.68%) **(Table 6.5)**. Here for L-132 cells, percentage inhibition data were shown.
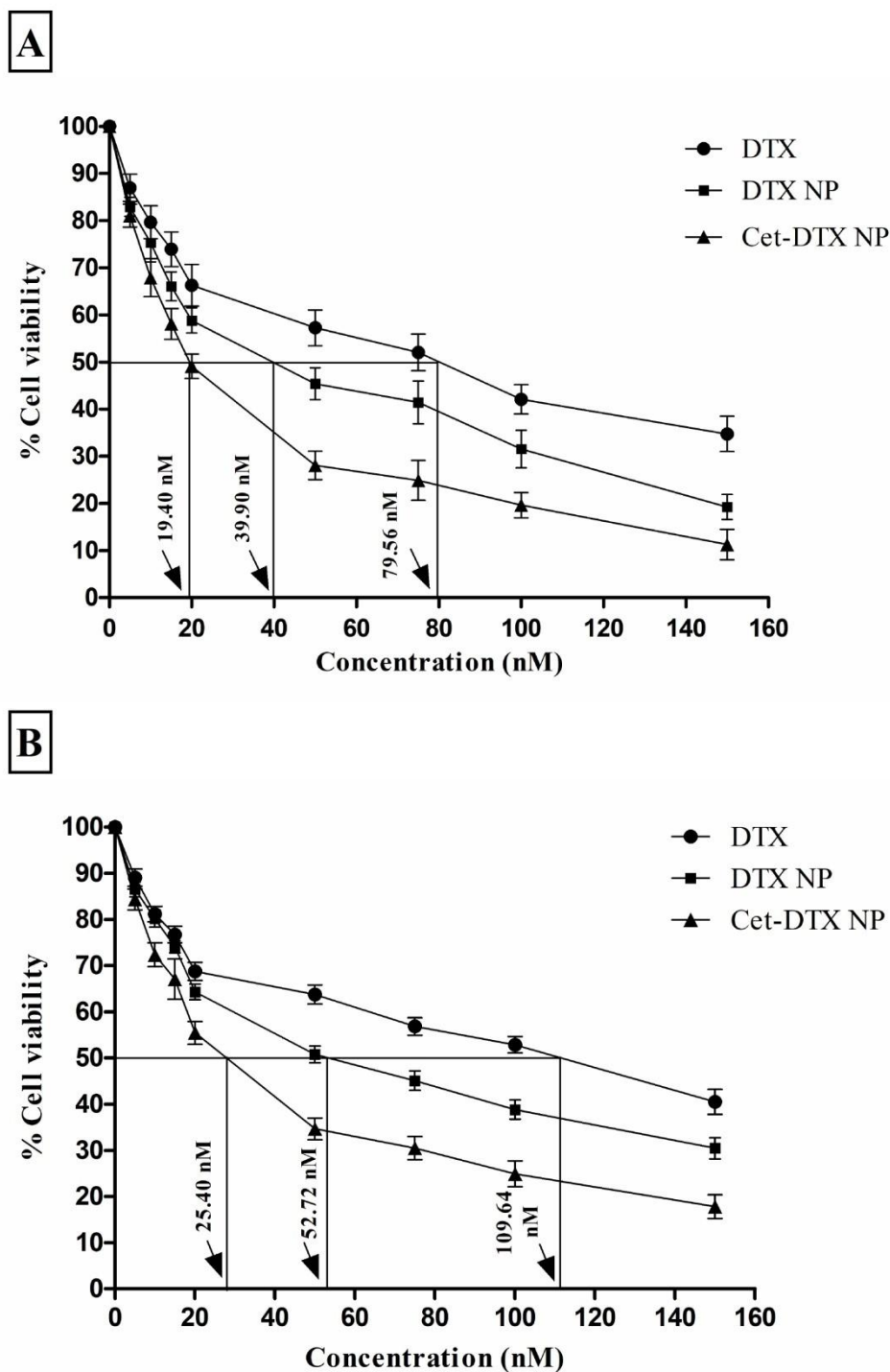
Figure 6.12. *In vitro* cytotoxixity assay of DTX, DTX NP and Cet-DTX NP on (A) A549 and (B) NCI-H23 lung cancer cells. Data show mean ± SD of three individual experiments.

Table 6.5. IC$_{50}$ doses and % inhibition in various cancerous and normal cell types, upon the treatment of free drug and experimental formulations.

Treatment groups	IC$_{50}$ dose in A549 cells (nM)*	IC$_{50}$ dose in NCI-H23 cells (nM)*	Percentage inhibition in L-132 cells (%)*
DTX	79.56±2.46	109.64±3.12	63.72±2.68
DTX NP	39.90±3.76[a]	52.72±2.85[a]	8.23±0.79[a]
Cet-DTX NP	19.40±1.92[a,b]	25.40±1.54[a,b]	7.21±1.20[a]

*Data show mean ± SD (n=3).

[a]($p<0.05$) when DTX is compared with DTX NP and DTX is compared to Cet-DTX NP.

[b]($p<0.05$) when DTX NP is compared to Cet-DTX NP.

6.10.4. Cellular uptake study

In vitro cellular uptake of FITC-conjugated formulations, DTX NP and Cet-DTX NP, was qualitatively evaluated by confocal microscopy. Following 1 h and 4 h incubations with FITC-conjugated DTX NP and Cet-DTX NP, respectively, confocal microscopy iamges of A549 and NCI-H23 cells were observed (**Figure 6.13A-6.13D**). The images showed that nanoparticle internalization in both the lung cancer cell lines were time-dependent.
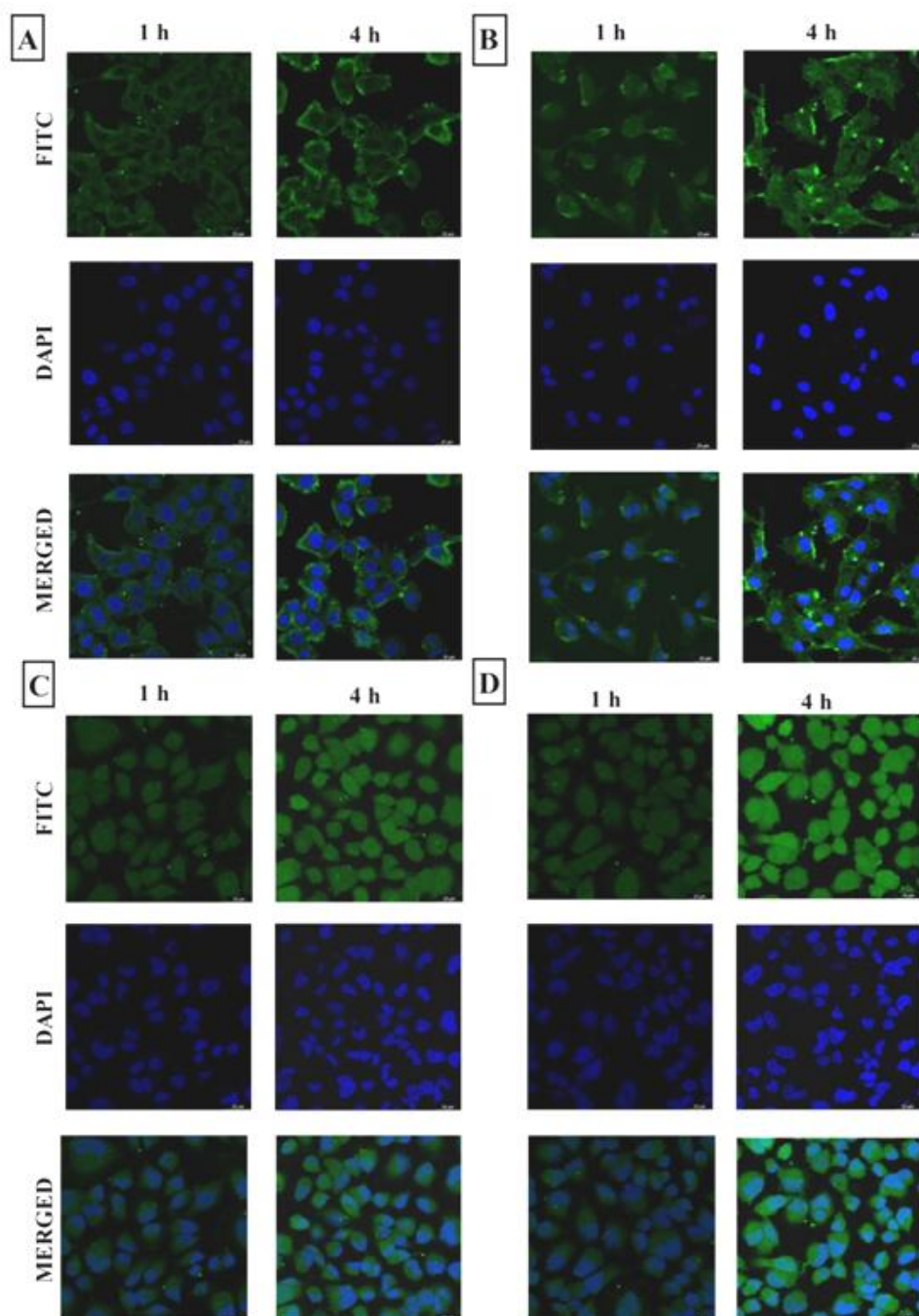
Figure 6.13. Qualitative evaluation of cellular uptake by confocal microscopy for (A) FITC-conjugated DTX NP (1 h and 4 h) in A549 cells, (B) FITC conjugated Cet-DTX NP (1h and 4 h) in A549 cells, (C) FITC-conjugated DTX NP (1 h and 4 h) in NCI-H23 cells, (D) FITC-conjugated Cet-DTX NP (1 h and 4 h) in NCI-H23 cells.

The quantification of cellular internalization of FITC-conjugated Cet-DTX NPs provided a clear-cut differentiation among the uptake pattern of the nanoparticles in terms of FITC mean-median values which were found to be 800 and 4067 (for DTX NP at 1 h and 4 h, respectively), 1164 and 5827 (for Cet-DTX NP at 1 h and 4 h, respectively) in A549 cells.

The FITC mean-median values in the case of NCI-H23 cells were found to be 442 and 1764 (for DTX NP at 1 h and 4 h, respectively), 646 and 2740 (for Cet-DTX NP at 1 h and 4 h, respectively) **(Figure 6.14A and 6.14B)**. Nanoparticle uptake within the cells was accelerated in a time-dependent way.
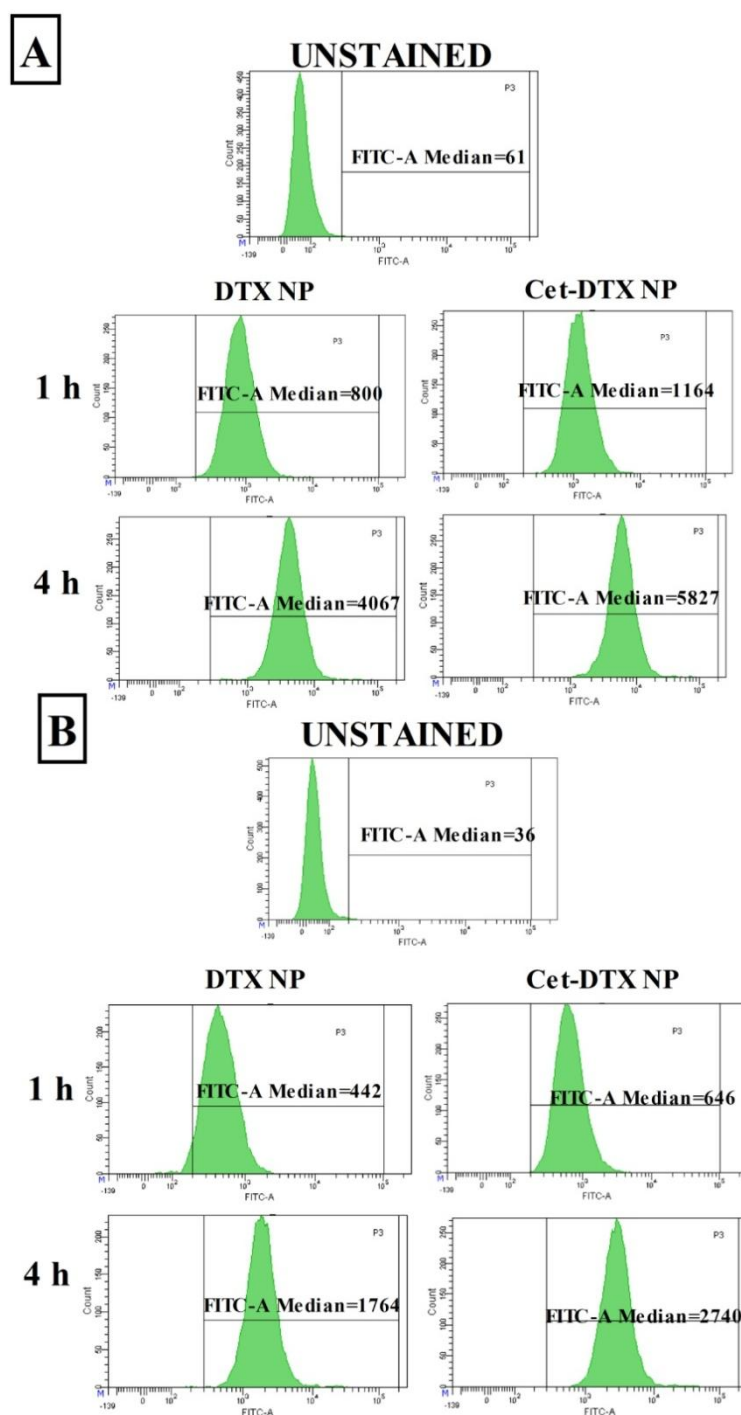
Figure 6.14. Quantitative estimation of the cellular internalization by flow cytometry for (A) FITC conjugated DTX NP and Cet-DTX NP for 1 and 4 h in A549 cells, (B) FITC conjugated DTX NP and Cet-DTX NP for 1 and 4 h in NCI-H23 cells.

6.10.5. Cellular apoptosis study

After being treated with DTX, DTX NPs, and Cet-DTX NPs, lung cancer cells (A549 and NCI-H23) underwent dual staining with Annexin V-FITC and propidium iodide (PI), which was followed by the quantification of apoptotic cells at various stages of apoptosis. A549 cells treated with Cet-DTX NP had apoptotic cell percentages of 50.7% (late apoptotic cells) and 45.6% (early apoptotic cells), whereas NCI-H23 cells treated with the same had apoptotic cell percentages of 58.6% (early apoptotic cells) and 37.9% (late apoptotic cells) **(Figure 6.15A and 6.15B)**. Comparing Cet-DTX NP to DTX NP and free DTX, the results showed that Cet-DTX NP increased more in the cells. Furthermore, a higher level of apoptosis in the FACS histogram of Cet-DTX NP-treated A549 cells and NCI-H23 cells compared to cells treated with DTX NP/free DTX (for 24 h) suggests that Cet-DTX NP is more efficacious to combat EGFR overexpressed lung cancer cells.
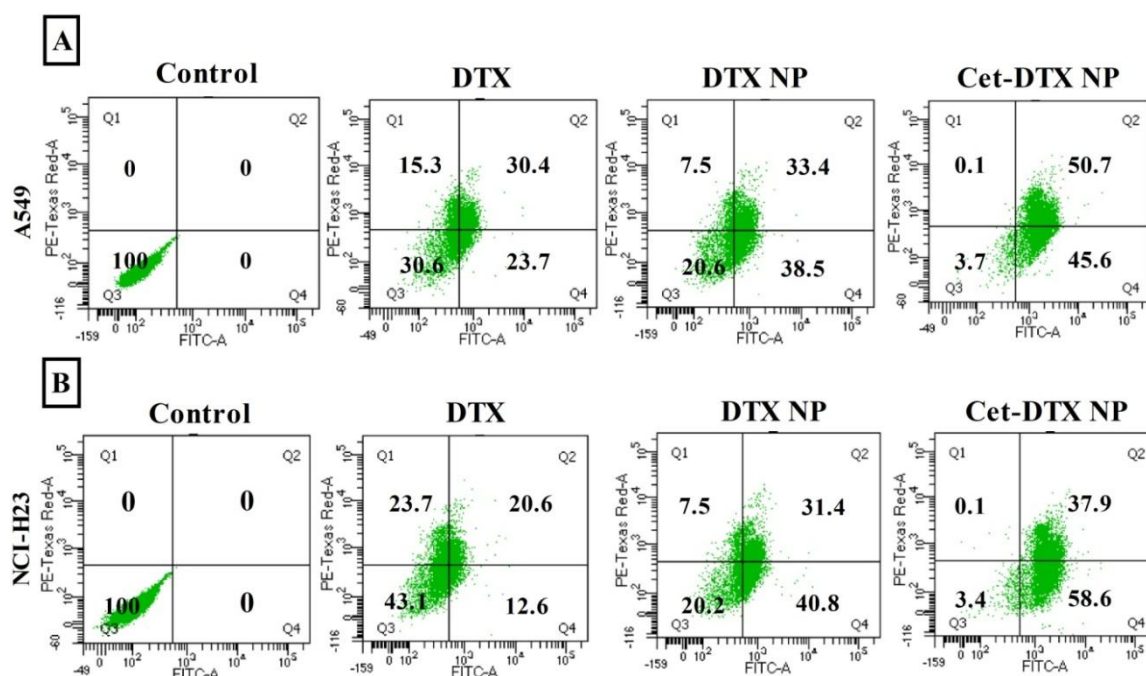
Figure 6.15. *In vitro* cellular apoptosis study (Annexin V/PI dual staining) in (A) A549 and (B) NCI-H23 lung cancer cells upon treatment with DTX, DTX NP and Cet-DTX NP.

6.10.6. Cell cycle analysis

The cell cycle regulatory pathway is crucial to the initiation and development of tumors. The mitotic arrest of cancer cells is caused by the strong binding of DTX to microtubules and the

promotion of its stability. It is well established that DTX causes cell cycle arrest by chromosomal breakage and mitotic impairment, leading to the normal G2/M phase arrest. A decrease in the percentage of cells in the S phase and an accumulation of cells in the G2/M phase were seen in A549 and NCI-H23 cells after treatment with DTX, DTX NP, and Cet-DTX NP. The cells were treated with DTX, DTX-NPs, and Cet-DTX-NPs before being incubated for 24 h. The control cells of the A549 and NCI-H23 cell lines were primarily in the G1 phase, with 8% and 9% of them, respectively, in the G2/M phase **(Figure 6.16A and 6.16B)**. Cet-DTX NP treatment, however, significantly arrested the G2/M phase (39.3% and 36.6% in A549 and NCI-H23 cells, respectively). The results suggest that after the treatment with Cet-DTX NP, the cells were inhibited in interphase (G2/M phase), which promotes the arrest of mitotic cell division. Chromosome damage might be the underlying cause of cell cycle arrest.
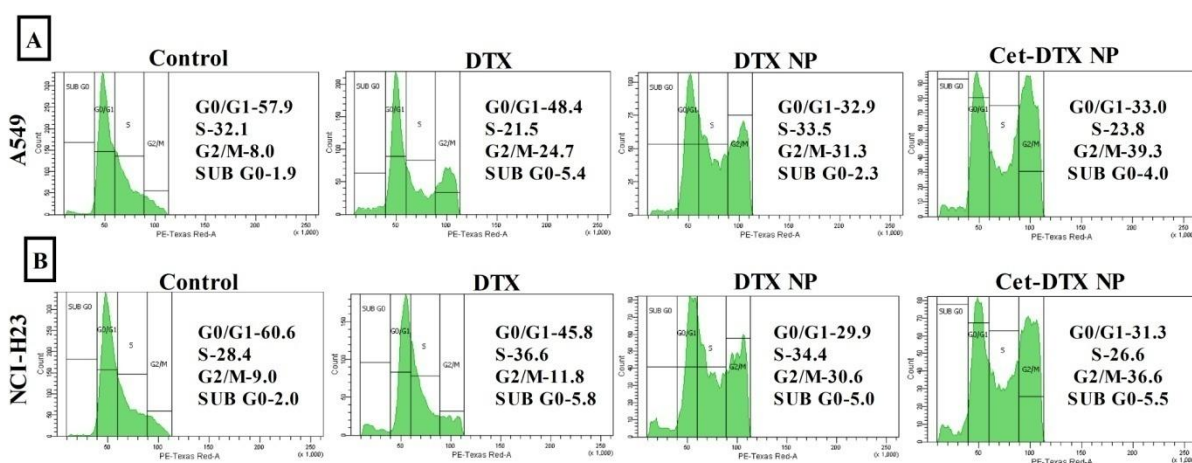
Figure 6.16. Cell cycle analysis by flow cytometry in (A) A549 and (B) NCI-H23 lung cancer cells upon treatment with DTX, DTX NP and Cet-DTX NP.

6.11. Hemolysis study

Cet-DTX NPs were tested for hemo-compatibility at various concentrations (5 to 150 nM) **(Figure 6.17)**. The nanoformulations (DTX NP and Cet-DTX NP) showed low hemolytic activity (<5%) between 5 and 150 nM. Since, the intended formulation's hemolysis rate was within the acceptable range of 5%, which is recognized for biomaterials with safe critical value identified by the International Organization for Standardization/Technical Report (ISO/TR 7406.46). Hence, Cet-DTX NP could be used safely for intravenous administration.
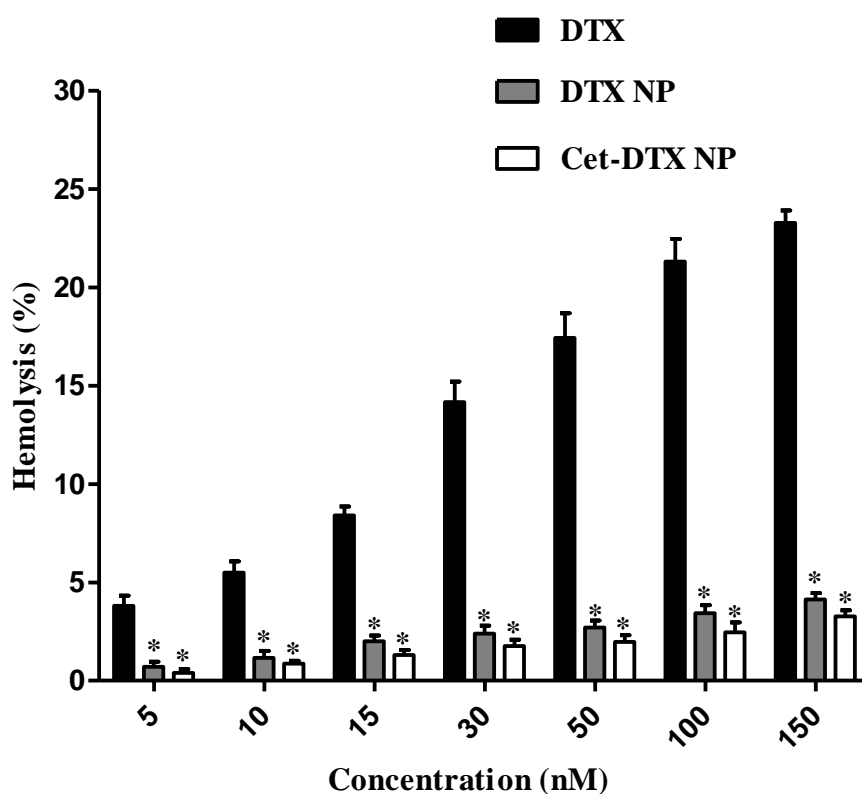
Figure 6.17. *In vitro* **hemolysis study after incubation of RBC with DTX, DTX NP and Cet-DTX NP at a concentration range from 5 nM to 150 nM [*(p<0.001) when DTX data were compared with those of DTX NP and Cet-DTX NP]**

6.12. *In vivo* **animal studies**

6.12.1. Maximum tolerated dose (MTD) in normal mice

The liver and kidney are the two crucial organs which are involved in the body's basic metabolism and excretion, respectively. As a result, aberrant liver and kidney functions are thought to be a sign of clinical symptoms, making the biochemical parameters that regulate the functions of these organs as a promising therapeutic target. The results of this study showed that the liver and kidney toxicity markers, ALP, SGPT, SGOT, urea, and creatinine, of the experimental mice treated with various nanoformulations revealed that levels of toxicity were in the order of DTX> DTX NP> Cet-DTX NP for a maximum dose, 40 mg/kg **(Table 6.6)**.

No substantial alterations in the body weight of normal mice treated with DTX NP and Cet-DTX NP were observed up to the dose of 10 mg/kg body weight, as compared to free DTX

which showed a marked change in body weight after the dose was increased to 10 mg/kg body weight (**Table 6.7**). A comparatively higher toxicity of free DTX, DTX NP and Cet-DTX NP in normal mice was observed when the dose of the drug was increased from 20 to 40 mg/kg body weight.

Table 6.6. Levels of various liver and kidney parameters in normal mice with various treatments.

S.No.	Group	Concentration (mg)	ALP (IU/L)[a]	SGOT (IU/L)[a]	SGPT (IU/L)[a]	Urea (mg/dL)[a]	Creatinine (mg/dL)[a]
1.	Normal control	-	175.22 ± 0.69	42.75 ± 0.37	35.69 ± 0.33	24.63 ± 0.41	0.27 ± 0.009
2.	DTX	2.5	176.19 ± 0.15	42.97 ± 0.46	36.02 ± 0.40	24.93 ± 0.35	0.28 ± 0.018
		5.0	176.60 ± 0.36	43.87 ± 0.39	36.92 ± 0.61	25.61 ± 0.30	0.29 ± 0.017
		10.0	179.06 ± 1.00*	44.94 ± 0.61*	37.68 ± 0.52*	27.21 ± 0.50*	0.34 ± 0.018*
		20.0	182.82 ± 1.17*	46.06 ± 0.56*	38.69 ± 0.38*	30.71 ± 0.65*	0.38 ± 0.008*
		40.0	183.73 ± 1.00*	49.30 ± 0.68*	41.07 ± 0.87*	32.49 ± 0.52*	0.39 ± 0.009*
3.	DTX NP	2.5	176.24 ± 0.51	43.17 ± 0.46	35.66 ± 0.46	25.23 ± 0.32	0.27 ± 0.005
		5.0	176.63 ± 0.61	43.82 ± 0.62	36.71 ± 0.40	25.76 ± 0.49	0.28 ± 0.006
		10.0	176.77 ± 0.47	43.86 ± 0.66	37.10 ± 0.42	26.03 ± 0.34	0.29 ± 0.009
		20.0	180.01 ± 0.98*	45.59 ± 0.97*	39.35 ± 1.10*	27.86 ± 0.50*	0.32 ± 0.019*
		40.0	181.44 ± 0.99*	47.98 ± 0.54*	41.61 ± 0.64*	29.64 ± 0.65*	0.34 ± 0.018*
4.	Cet-DTX NP	2.5	176.44 ± 0.41	43.09 ± 0.41	35.53 ± 0.74	25.13 ± 0.72	0.27 ± 0.007
		5.0	176.66 ± 0.47	43.39 ± 0.52	36.50 ± 0.46	25.82 ± 0.43	0.28 ± 0.005
		10.0	176.82 ± 0.31	43.96 ± 0.68	37.54 ± 0.52	25.88 ± 0.50	0.29 ± 0.008
		20.0	179.36 ± 0.90*	45.64 ± 0.90*	38.89 ± 0.85*	27.94 ± 0.74*	0.30 ± 0.012*
		40.0	181.11 ± 1.33*	46.55 ± 1.01*	41.32 ± 0.51*	29.11 ± 0.86*	0.32 ± 0.005*

[a]Data show mean ± SD (n=6) ;

* indicates $p < 0.05$ with respect to the value of control group of mice

Table 6.7. Changes in body weight of normal mice treated with different treatments.

S.No.	Group	Concentration (mg)	Day 0	Day 2	Day 4	Day 6	Day 8	Day 10	Day 12	Day 14
1.	Normal control[a,b]	-	25.16 ± 1.16	25.33 ± 1.03	26.17 ± 1.47	27.00 ± 1.09	26.33 ± 1.21	27.10 ± 0.54	28.66 ± 1.21	29.66 ± 0.81
2.	DTX[a,b]	2.5	25.83 ± 1.17	26.16 ± 0.98	26.50 ± 1.04	27.33 ± 1.36	26.83 ± 1.72	27.66 ± 1.36	28.16 ± 1.47	29.00 ± 0.89
		5.0	24.83 ± 0.75	25.66 ± 1.21	25.33 ± 1.21	26.00 ± 1.26	26.16 ± 0.75	27.33 ± 0.81	27.83 ± 1.16	28.83 ± 0.75
		10.0	24.66 ± 0.81	25.00 ± 0.89	25.66 ± 1.36	25.83 ± 1.83	23.50 ± 1.04*	23.00 ± 0.89*	22.83 ± 1.16*	21.83 ± 1.32*
		20.0	25.67 ± 0.51	25.16 ± 1.16	26.50 ± 1.04	23.83 ± 0.98*	23.33 ± 0.51*	22.50 ± 1.04*	21.83 ± 0.75*	21.00 ± 0.89*
		40.0	26.16 ± 1.16	25.16 ± 1.17	24.16 ± 1.16*	23.85 ± 0.73*	22.16 ± 0.75*	22.16 ± 0.75*	21.66 ± 1.21*	18.50 ± 0.54*
3.	DTX NP[a,b]	2.5	24.50 ± 0.83	24.33 ± 0.81	25.16 ± 0.75	25.33 ± 0.75	25.66 ± 0.81	27.50 ± 1.04	27.33 ± 1.50	29.83 ± 1.16
		5.0	24.83 ± 0.75	25.16 ± 0.75	26.83 ± 1.32	27.50 ± 1.51	27.16 ± 0.75	28.00 ± 0.89	28.16 ± 1.16	28.16 ± 1.17
		10.0	25.50 ± 1.04	26.83 ± 1.16	26.16 ± 0.75	26.50 ± 0.83	26.00 ± 0.89	27.16 ± 0.75	27.50 ± 0.54	28.17 ± 1.32
		20.0	24.83 ± 1.16	25.50 ± 0.54	24.66 ± 0.81	24.50 ± 1.04*	23.83 ± 0.75*	23.50 ± 0.54*	23.11 ± 0.75*	23.06 ± 0.51*
		40.0	25.50 ± 0.54	26.16 ± 0.75	25.67 ± 1.36	24.16 ± 0.75*	24.16 ± 0.75*	22.5 ± 0.54*	22.16 ± 1.17*	22.00 ± 1.10*
4.	Cet-DTX NP[a,b]	2.5	25.00 ± 0.89	26.83 ± 0.99	26.33 ± 0.82	27.50 ± 0.55	27.00 ± 0.91	27.18 ± 1.47	27.30 ± 0.52	27.28 ± 1.20
		5.0	25.83 ± 0.98	26.80 ± 0.75	27.33 ± 1.21	27.67 ± 0.81	27.31 ± 0.82	28.83 ± 0.70	29.00 ± 0.63	29.66 ± 0.81
		10.0	26.00 ± 1.10	26.17 ± 0.75	26.35 ± 0.84	25.67 ± 0.51	26.65 ± 1.21	26.50 ± 0.83	27.16 ± 0.76	27.16 ± 0.85
		20.0	25.16 ± 1.16	25.16 ± 1.18	25.68 ± 1.03*	24.50 ± 0.57*	23.60 ± 1.30*	23.50 ± 0.55*	22.83 ± 0.67*	21.67 ± 0.82*
		40.0	25.33 ± 0.81	26.34 ± 0.54	25.33 ± 0.81*	24.30 ± 0.85*	22.66 ± 0.82*	21.67 ± 1.00*	20.81 ± 1.33*	20.05 ± 1.06*

[a]weight of mice were expressed in gram,

[b]data were expressed as mean ± SD (n=6).

* (p<0.05) when the data of the treatment groups were compared with those of the normal control mice.

6.12.2. *In vivo* pharmacokinetics study in normal mice

Several pharmacokinetic parameters were examined using LC-MS/MS following intravenous administration of single doses of DTX, DTX NP and Cet-DTX NP (equivalent dose of 10 mg/kg of DTX). When compared to DTX NP/Cet-DTX NP treatment, the initial plasma DTX level was primarily higher for free-DTX treatment **(Figure 6.18A) (Table 6.8)**. However, a higher clearance rate indicated that the drug was removed from the body quicker. Drug concentration from free-DTX solution was much lower than that of the nanoformulations (DTX NP/Cet-DTX NP) that remained in the systemic circulation for a longer period of time for at least up to 72 h and released DTX steadily. DTX NP/Cet-DTX NP treatment extended the plasma half-life of DTX and significantly reduced the clearance rate (CL) compared to DTX treatment alone. MRT values provided additional support for the data **(Table 6.8)**.

Following i.v. treatment of the several nanoformulations, the concentration of DTX in murine lungs with time is shown in **Figure 6.18B**. The initial time points had a trend of elevated lung DTX concentrations (i.e., up to 2 h). Later, from time point 4 to 72 h, DTX levels demonstrated a considerable decline. **Table 6.8** lists the DTX pharmacokinetic parameters in mouse lung and plasma following i.v. bolus injection of free drug and different formulations.
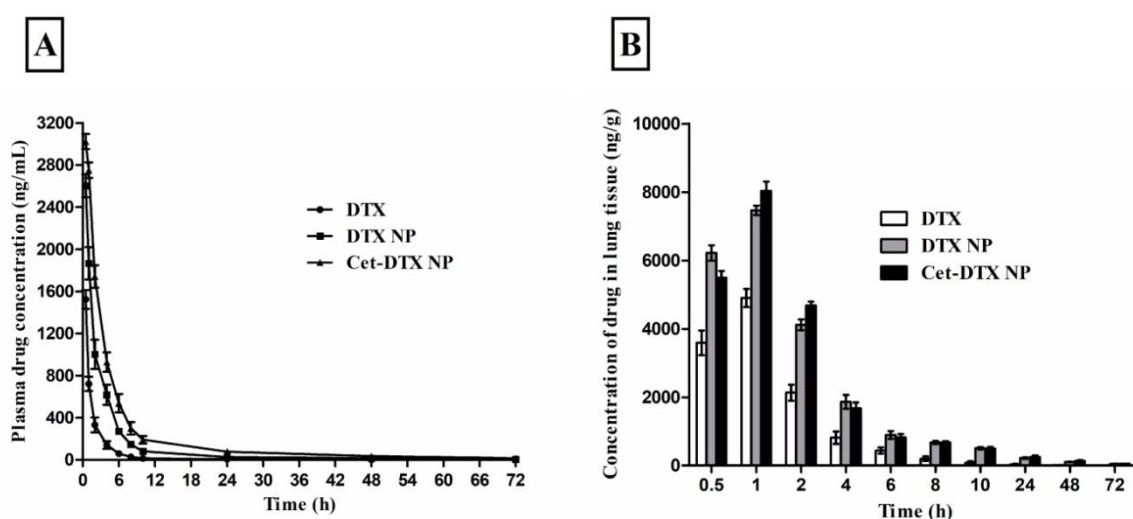
Figure 6.18. (A) *In vivo* **pharmacokinetic study of DTX in plasma upon administration of DTX/DTX NP/Cet-DTX NP by i.v. bolus route in mice, (B)** *In vivo* **pharmacokinetic study of DTX in lung after i.v. bolus administration of DTX/DTX NP/Cet-DTX NP in mice.**

Table 6.8. Plasma and lung pharmacokinetic parameters of DTX released from DTX-suspension, DTX NP, Cet-DTX NP after the i.v. bolus administration with an equivalent amount of drug in Swiss albino mice.

Pharmacokinetic parameters of Drug (Docetaxel)	Plasma profile			Lung profile		
	Upon DTX administration*	Upon DTX NP administration*	Upon Cet-DTX NP administration*	Upon DTX administration*	Upon DTX NP administration*	Upon Cet-DTX NP administration*
$t_{1/2}$ (h)	6.31 ± 2.53	16.73 ± 1.63[a]	20.56 ± 6.18[a]	8.309 ± 1.24	20.44 ± 2.34[a]	21.71 ± 2.28[a]
AUC_{0-t} (ng/mL.h)	3230.12 ± 282.16	8793.91 ± 1280.57[a]	14565 ± 2499.34[a,b]	13853.92 ± 2134.064	34590.17 ± 1856.18[a]	36113.42 ± 780.46[a]
$AUC_{0-\infty}$ (ng/mL.h)	3280.13 ± 296.57	8913.9 ± 1329.97[a]	15031.8 ± 2605.79[a,b]	13976.82 ± 2214.40	35933.34 ± 2217.57[a]	37793.69 ± 639.76[a]
$AUMC_{0-\infty}$ (ng/mL.h^2)	8016.74 ± 1993.09	67657.5 ± 21614.7[a]	179114 ± 50908.7[a,b]	59599.11 ± 24121.26	493364.4 ± 67421.51[a]	584522.9 ± 20019.27[a]
$MRT_{0-\infty}$ (h)	2.43 ± 0.51	7.47 ± 1.30[a]	11.804 ± 1.81[a,b]	4.16 ± 1.002	13.69 ± 1.007[a]	15.46 ± 0.33[a]
C_L (L/h/kg)	3.06 ± 28	1.13 ± 0.17[a]	0.67 ± 0.11[a,b]	0.72 ± 0.10	0.28 ± 0.02[a]	0.23 ± 0.02[a]

*Data show mean ± SD (n=6).

[a]($p<0.05$) The pharmacokinetics data of treatment of DTX group was compared with DTX NP treatment group and DTX treatment group was compared with Cet-DTX NP treatment group.

[b]($p<0.05$) The pharmacokinetic data of DTX NP and Cet-DTX NP groups were compared.

NB: $t_{1/2}$, half-life; AUC_{0-t}, area under the plasma concentration–time curve from time 0 to time of last measurable concentration; $AUC_{0-\infty}$, under the plasma concentration–time curve from time 0 to infinity; $AUMC_{0-\infty}$, area under the first moment curve from time 0 to infinity; MRT, mean resident time; CL, clearance.

6.12.3. *In vivo* **biodistribution study**

The *in vivo* biodistribution study was carried out in various vital organs (whole blood, liver, kidney, heart, muscle and cancerous lung) after 4 h, 24 h, 48 h and 72 h of treatment with free DTX and the different experimental nanoformulations (DTX NP and Cet-DTX NP) **(Figure 6.19)**. The drug content in each organ was determined by LC-MS/MS. The concentration of free DTX in tumors was very less after 4 h, and was almost negligible after 24 h post treatment. In contrast, the DTX concentration of DTX NP and Cet-DTX NP groups was much more elevated in cancerous lung, as compared to free DTX group. It was demonstrated that free DTX accumulated more in kidney and heart, as compared to blood, liver and muscles. On the other hand, after 72 h, very limited amount of Cet-DTX NP was accumulated in blood, liver, kidney, heart and muscles.

6.12.4. **Survival time of mice**

A Kaplan Meier curve was utilized to study the data in terms of animal survival **(Figure 6.20)**. All the experimental animals belonging to the carcinogen control group died within 35 days post treatment. However, a gradual increase in the survival rate was observed upon treatment with drug and different nanoformulations in the order: DTX<DTX NP<Cet-DTX NP. A significantly higher proportion of animals survived after the treatment with Cet-DTX NP (~67%), in comparison to the animals treated with DTX NP (~33%) and free DTX (~16.67%), at 120th day post treatment.
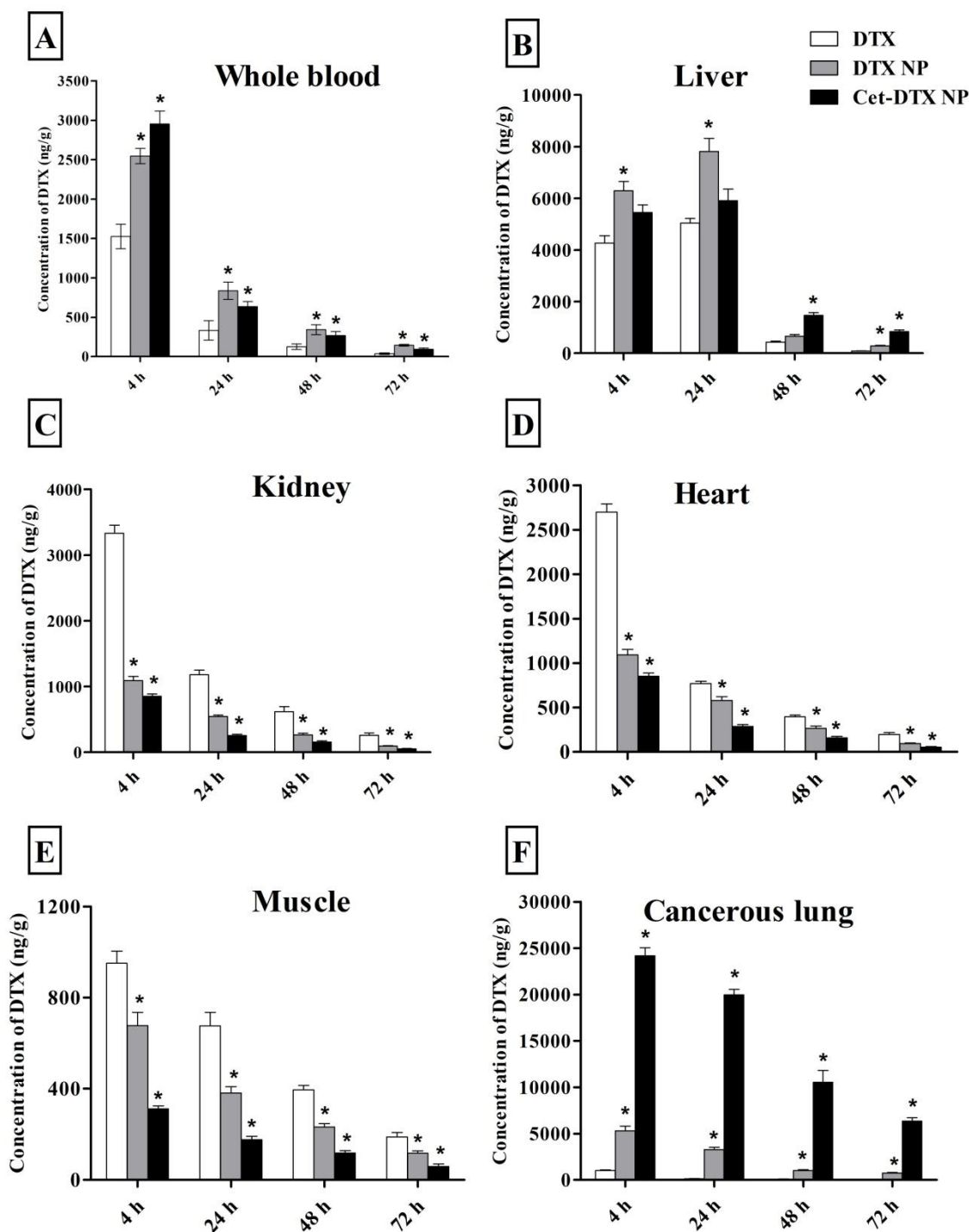
Figure 6.19. Biodistribution studies of DTX, DTX NP and Cet-DTX NP in B(a)P induced lung cancer mice model at 4 h, 24 h, 48 h and 72 h after i.v. bolus injection. Data were expressed as mean ± SD (n=6). *(p<0.05) when DTX data were compared with those of DTX NP and Cet-DTX NP.
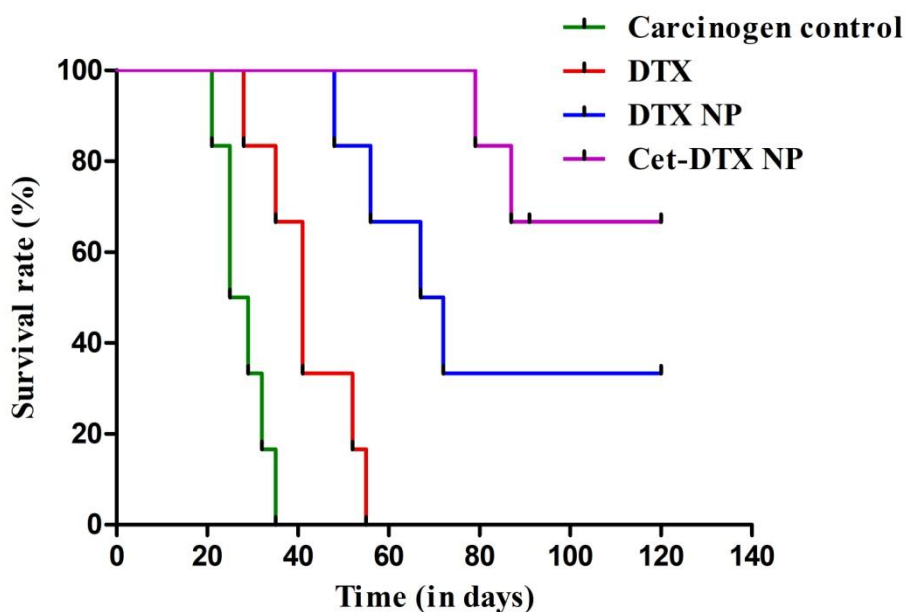
Figure 6.20. Percentage survival rate of mice after treatment with DTX, DTX NP, Cet-DTX NP and untreated lung carcinogenesis mice model (p<0.001).

6.12.5. Caspase-3 activity

Due to its role in the proteolytic cleavage of numerous vital proteins, caspase-3 is a crucial apoptosis biomarker. After the DTX/DTX NP/Cet-DTX NP treatment for 24 h, the degree of caspase-3 expression in lung homogenates was assessed using a colorimetric test. When compared to the normal control and carcinogen control mice, the investigation showed that the lung homogenates of mice exposed to Cet-DTX NP had higher levels of caspase-3 expression, as compared to free DTX and DTX NP **(Figure 6.21)**.
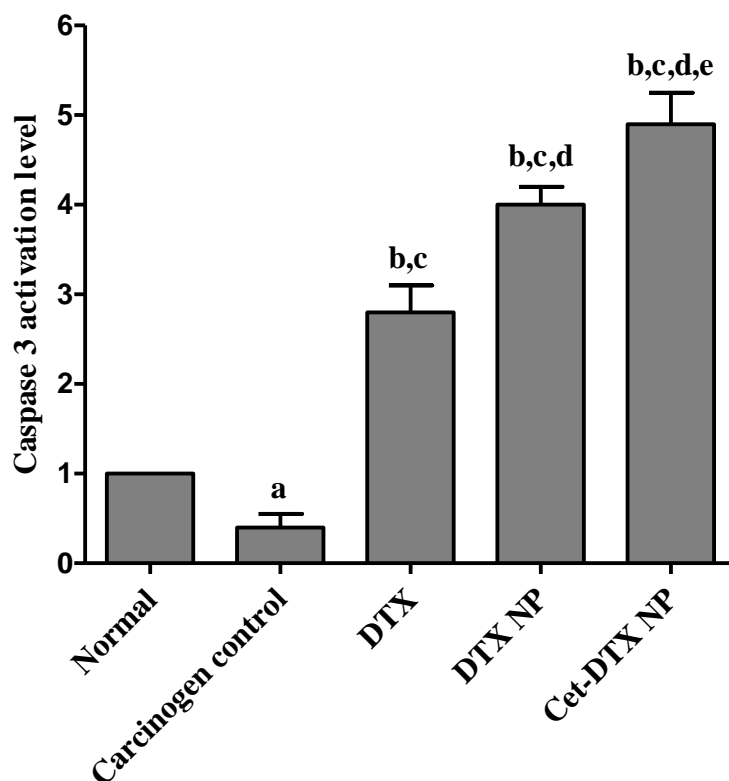
Figure 6.21. Comparative caspase-3 activation level in blood of normal and experimental mice [[a](p<0.05) when normal control group is compared with the carcinogen control group, [b](p<0.001) when normal control group is compared with those of DTX, DTX NP and Cet-DTX NP groups, [c](p<0.001) when carcinogen control group is compared with those of DTX, DTX NP and Cet-DTX NP group, [d](p<0.001) when DTX group is compared with those of DTX NP and Cet-DTX NP groups, [e](p<0.001) when DTX NP group is compared with the Cet-DTX NP group].

6.12.6. LPO and ROS study

Different lung tissues of experimental animals were examined for LPO and ROS levels. When compared to normal control animals, carcinogen control mice had considerably higher levels of LPO **(Figure 6.22A)** and ROS **(Figure 6.22B)**. However, following treatment with DTX, DTX NP, and Cet-DTX NP, the LPO and ROS levels decreased toward the normal group.
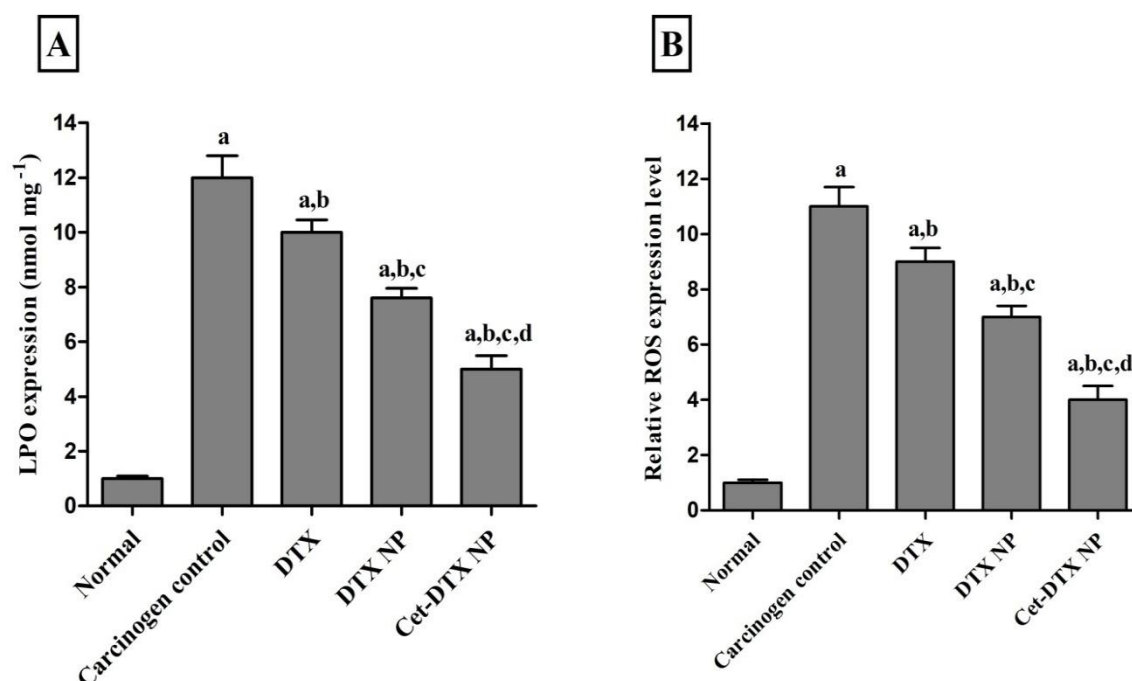
Figure 6.22. (A) Lipid peroxidation (LPO) in the *in vivo* lung carcinogenesis mice model after treatment with DTX, DTX NP and Cet-DTX NP [[a](p<0.05) when normal control group is compared with the carcinogen control, DTX, DTX NP and Cet-DTX NP groups, [b](p<0.05) when carcinogen control group is compared with those of DTX, DTX NP and Cet-DTX NP group, [c](p<0.05) when DTX group is compared with those of DTX NP and Cet-DTX NP groups, [d](p<0.05) when DTX NP group is compared with the Cet-DTX NP group]. The values are represented as mean ± SD (n = 6), (B) Changes in the level of Reactive oxygen species (ROS) in the *in vivo* lung carcinogenesis mice model after treatment with DTX, DTX NP and Cet-DTX NP, [b](p<0.05) when carcinogen control group is compared with those of DTX, DTX NP and Cet-DTX NP group, [c](p<0.05) when DTX group is compared with those of DTX NP and Cet-DTX NP groups, [d](p<0.05) when DTX NP group is compared with the Cet-DTX NP group].

6.12.7. Lung histopathology analysis

To evaluate histological alterations following therapy in B(a)P-challenged mice, the lungs were isolated 4 weeks after administration of free DTX, DTX NP, and Cet-DTX NP in the lung tissue. The lung tissues in the control group had a typical structure and showed no histological changes. The B(a)P group demonstrated severe stroma hemorrhagia, pulmonary oedema, mass inflammatory cell infiltrations and alveolar collapse, which were critically

damaging to the lung. The tumors in the lung were composed of large cells with eosinophilic cytoplasm. Nonetheless, the treatment with free DTX showed marginal improvement of the damaged lung. Upon treatment with nanoformulations (DTX NP and Cet-DTX NP, equivalent to 10 mg/kg body weight of DTX), deterioration of the lung's structural integrity was effectively reduced in Cet-DTX NP treated mice more than DTX NP-treated mice **(Figure 6.23A-6.23E)**.
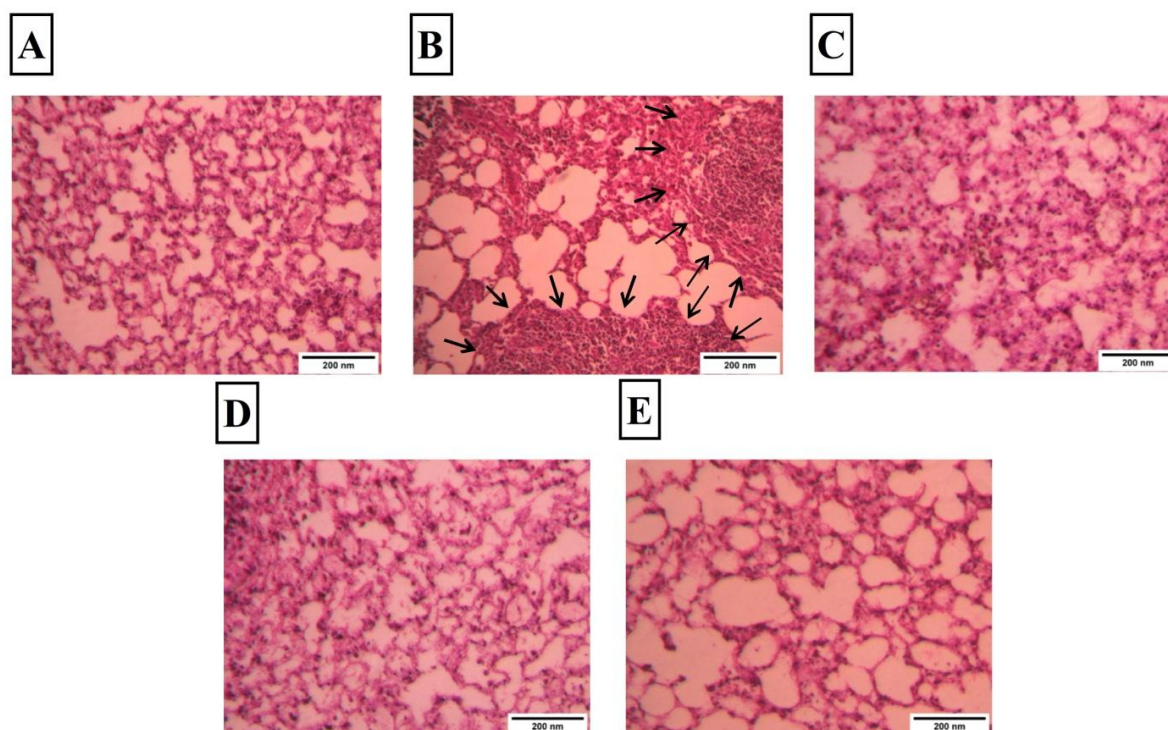
Figure 6.23. Histological sections (in 10× magnifications) of lungs of experimental mice. Microscopic images of lung section of (A) normal mice, (B) carcinogen control mice, solid tumor areas are shown by arrow heads, (C) carcinogen treated mice with DTX, (D) carcinogen treated mice with DTX NP, (E) carcinogen treated mice with Cet-DTX NP.

7. Discussion

Even though non-small cell lung cancer (NSCLC) is one of the most common tumors to be detected globally, treating it is still difficult. The epidermal growth factor receptor (EGFR) is reported to be overexpressed in the majority of NSCLC cases and to display aberrant signaling in a variety of human malignancies. Poor tumor differentiation, higher rates of lymph node metastases, and increased tumor proliferation has all been attributed to it (Hsu et al., 2019). It has also been associated with a worse prognosis. It is widely known that tumor-specific ligands, such as antibodies on the surface of nanoparticles against certain receptors, can be used to successfully target drugs at the site of the tumor (Tian et al., 2022). In order to develop a nanoformulation capable of transporting the drug for the afflicted cellular target, we have developed the antibody conjugated nanoparticles loaded with covalently bonded Cet antibody against EGFR to target malignant lung cells.

In order to improve the drug's potential for use in the treatment of cancer, DTX was incorporated into the PLGA nanoparticles due to its excellent anti-proliferative capabilities. In drug encapsulated formulation (DTX NP), FTIR study revealed modest shifting of the drug's non-typical peaks. This finding might be explained by physical interactions through bond formations including electrical forces such as van der Waals forces and dipole moments as well as weak hydrogen bond formation. However, all the characteristic peaks of DTX were seen in DTX NP, which suggests that the chemical integrity of the drug is maintained within the nanoparticles.

The EDC/NHS coupling chemistry successfully conjugated Cet antibody with the surface of the PLGA NP (Mondal et al., 2019). The nanoformulations were developed by varying the drug content with respect to the polymer content. Enhancement of drug content increased the size of the particles. Drug entrapment towards the core, and within and between the polymeric chains reduced the cohesiveness of the polymeric molecules, resulting in an increased size of the particles. Further, surface conjugation of Cetuximab (Cet) obviously enhance the size of the particles as reflected in the data **(Table 6.1)**. The surface morphology of the synthesized nanoparticles is of utmost significance, since it interacts with the biological membranes before getting absorbed. The nanoformulations had smooth surface and spherical shape with free of aggregation, and homogeneous drug distribution. Cet-DTX NPs must be stored as lyophilized powder and reconstituted in dispersed form before use, owing to their negative zeta potential (caused by the presence of a -COOH group in the polymer), within the

range of -30 to +30 mV (Dutta et al., 2019). Increasing drug content reduced the zeta potential of the polymeric nanoparticles. Free –COOH group of PLGA present on the surface of the particles causes negative zeta potential. More drug content might reduce the availability of free –COOH groups on the surface, causing reduction in zeta potential values. Further, conjugation of Cet antibody on the surface of the polymeric nanoparticles increased the zeta potential, as each molecule of Cet antibody contains additional free –COOH groups. The EDX detection of nitrogen in Cet-DTX NP suggested that DTX had been incorporated into the nanoparticles. The SDS-PAGE analysis confirms the conjugation of Cet antibody onto the surface of the PLGA nanoparticles. However, Cet-DTX NP band migrated slight lower in contrast to the Cet antibody because of the weight of DTX NP.

The drug released from the nanoformulation over time was assessed by the *in vitro* drug release study. An early burst release of the drug from Cet-DTX NP was demonstrated, which might have resulted due to the rapid dissociation of the drug adhered to the surface of the nanoparticles. Thereafter, a slow and sustained release of the drug takes place, probably due to the erosion of the polymeric core, followed by the diffusion of the drug from the polymeric matrix. The drug release pattern from the nanoparticles followed Korsemeyer Peppas model of kinetics with high linearity (Mandal et al., 2018; Mondal et al., 2019). Cet-DTX NP portrayed fast degradation in the acidic medium, which suggests ester hydrolysis of the polymeric core. The drug release was comparatively faster in acidic tumor environment (pH 5) while it depicted slow and sustained release in physiologically neutral media of blood (pH 7.4) (Bhattacharya et al., 2018; Ehsan et al., 2022). When DTX release from DTX NP and Cet-DTX NP was measured in PBS (pH 7.4) with 0.1% w/v tween 80, citrate buffer, acetate buffer, and bicarbonate buffer, it indicated acceptable linearity in the different kinetic models (as supported by R^2 value).

The experimental formulations (stored at 30°C and 40°C, and 75% RH) were agglomerated with slight structural deformation on storing for a period of 90 days probably due to the softening of polymer stored at higher temperature for a prolonged period. The nanoparticles were reasonably stable after being stored at 4–8 °C during this period, according to the data of accelerated stability experiments. Drug content did not vary significantly when stored at the refrigerated condition for a period of 90 days, which further suggests that the prepared nanoparticles should be stored at 4-8 ºC for long-term use.

RT-PCR analysis had confirmed the overexpression of EGFR in lung cancer cells (A549 and NCI-H23), whereas it is not significantly expressed in L-132 (normal lung epithelial cells). The overexpression of EGFR on both the lung cancer cells confirmed, that more ligand (anti-EGFR Cet antibody) will bind to these cells as compared to normal lung epithelial cells, resulting in more apoptosis in cancerous cells.

Cet prevents EGFR function by binding to the receptors overexpressed on the lung cancer cells. Cetuximab showed small K_D value (0.32 nM) for A549 cells, as compared to comparatively higher K_D value (0.38 nM) for NCI-H23. The lower K_D value in case of A549 cells suggests higher affinity and tighter binding of antibody with the receptors on the cell surface. This might be due to the various non-covalent interactions (hydrogen bonding, van der Waals forces and hydrophobic forces) that participate in the affinity of a binding site (Yao and Xu, 2012).

In vitro cytotoxicity study was performed using the MTT assay on A549 and NCI-H23 lung cancer cells, and L-132 normal lung epithelial cells. The lower IC_{50} values were observed after the lung cancer cells were treated with Cet-DTX NP, as compared to DTX NP and free drug. It might be due to the greater affinity of the Cet-DTX NP towards EGFR overexpressed lung cancer cells, thereby resulting in the greater uptake of nanoparticles within the cells. Owing to the limited expression of EGFR receptors on the surface of L-132 cells, the percentage viability of the cells was more when treated with the nanoformulations. Therefore, it indicates that the targeted nanoparticles exhibit cytotoxicity only towards lung cancer cells, and not toward the normal lung epithelial cells. Confocal microscopic study showed that FITC encapsulated nanoparticles (FITC-DTX NP and FITC-Cet-DTX NP) internalized well within the lung cancer cells (Patel et al., 2018). FACS analysis also showed time dependent quantitative uptake of DTX NP and Cet-DTX NP from 1 to 4 h in both the cancer cell types. The higher uptake of Cet-DTX NP within the cells might be due to its active targeting ability to EGFR-positive lung cancer cells.

Using the Annexin V-FITC staining procedure, apoptosis studies were carried out to check if EGFR mediated targeted nanoformulations caused the death of A549 and NCI-H23 cells. Comparing Cet-DTX NP to DTX NP and DTX using a site-specific sustained delivery pattern, it was found that Cet-DTX NP were more effective at inducing apoptosis in A549 and NCI-H23 cells. Cet-DTX NPs targeted delivery and improved cellular uptake cause a higher buildup of drug within lung cancer cells, leading to apoptosis.

The impact of site-specific and non-specific PLGA nanoparticles on the progression of the cell cycle in the A549 and NCI-H23 cells was examined using a flow cytometer. The outcomes demonstrated that DTX and its nanoformulations were accountable for the cell death brought on by the G2/M phase arrest. Typically, Cet-DTX NP caused mitotic arrest by releasing the drug that resulted in unstable microtubules, impairing the function of the mitotic spindle, and arresting the cells in the G2/M phase of mitosis (Jose et al., 2019). Thus, from the findings of cell cycle analysis, it can be interpreted that antibody conjugated nanoparticles are highly potent to arrest the cancer cell proliferation.

In case of MTD analysis, there is a substantial decrease in the level of liver and kidney toxicity markers (ALP, SGOT, SGPT, urea and creatinine) in normal mice treated with DTX NP and Cet-DTX NP, as compared to unbound DTX, indicating better tolerability of nano-encapsulated DTX, upto the dose of 10 mg/kg body weight. Moreover, there was no obvious change in the body weight of the normal mice treated with DTX NP and Cet-DTX NP, which further suggested 10 mg/kg body weight is the maximum tolerated dose of DTX when encapsulated in the form of nanoparticles. Cetuximab has a prolonged residential time in the body. The binding of Cet to EGFR on the cell surface internalizes at least 50% of the Cet-EGFR complex by first 3 h, at higher doses (here ≥20 mg/kg body weight) (Jutten et al., 2009), and this internalization of huge drug amount (50%) obviously showed toxicity in animals. Further, a longer stay of Cet-NPs as non-EGFR bound forms in the system dissociate Cet from the nanoparticles surface. Such free Cet in the cellular environment might produce non-specific toxicity which often reflects as Ca^{2+} level reduction in blood, loss of appetite and weight loss. Therefore, as a cumulative effect of greater internalization of the drug and toxicity produced by free Cet reduced the body weight of normal animals at higher doses.

The comparatively low hemolytic activity of the test nanoformulations (DTX NP and Cet-DTX NP) than free drug, suggest hemocompatibility. Therefore, it could be safely administered via intravenous route (Gaonkar et al., 2017). The administration of DTX NP/Cet-DTX NP to plasma and lung tissues resulted in elevated biological $t_{1/2}$, AUC, AUMC and MRT values, along with a decrease in elimination rate constants, which might be due to sustained release of the drug from the core of the nanoparticles for a prolonged duration.

The Cet-DTX NP showed higher amount of DTX at lung tumor sites than DTX NP and free DTX that was mainly attributed to the controlled and targeted DTX release of Cet-DTX NP

in cancerous lung, which resulted less DTX released in other organs (blood, liver, kidney, heart and muscles) and more DTX accumulated in the cancerous lung. On the contrary, the deposition of free DTX followed non-specific distribution pattern in liver, kidney, heart and muscles upto 72 h. Free DTX was found to be more accumulated in the heart and kidney, as compared to the liver. The possible reason for this observation might be due to the fact that liver is the organ of the reticuloendothelial system (RES), whose macrophages clear the drug and reduces the exposure to the parenchymal cells of liver (Fernandez-Urrusuno et al., 1996). The less accumulation of Cet-DTX NP confirmed its non-toxicity to cardiac tissues. However, the high concentration of DTX from Cet-DTX NP was observed in liver upto 72 h, which might be due to the known fact that liver exhibits a relatively higher levels of EGFR, thereby leading to an increased uptake of Cet conjugated nanoparticles in the liver. After 72 h, the negligible concentration of Cet-DTX NP in kidney suggests it to be the major route of the elimination of the experimental nanoparticles.

When carcinogen control animals were treated with DTX, Cet conjugated and unconjugated nanoparticles, there is an increase in the survival rate of animals treated with Cet-DTX NP. This is due to the targeting ability of Cet for DTX NPs, leading to the greater accumulation of DTX at the site of lung tumor (Karra et al., 2013). Moreover, there is a significant role of caspase-dependent apoptosis in the suppression of B(a)P-induced lung tumor development (Cui et al., 2020). There was an increased apoptosis by Cet-DTX NP when compared to free drug and DTX NP treatment. It might be due to the enhanced cellular internalization of the nanoparticles in EGFR-overexpressed lung cancer mice (Wathoni et al., 2022; Maya et al., 2013).

B(a)P-induced lung cancer is significantly influenced by ROS. ROS and LPO level play a significant role in the initiation, promotion, and progression of lung cancer (Majumder et al., 2021). These were markedly reduced after treatment with Cet-DTX NP, which is due to the enriched activity of detoxification enzyme in the treated animal group, as compared to carcinogen control group (Choudhury et al., 2021). The histopathological study revealed that Cet-DTX NP greatly reduced the growth of lung tumor and significantly restored the lung homogeneity, which may be contributed due to the site-specific targeting of antibody conjugated nanoparticles to the NSCLC, as compared to the normal cells.

8. Conclusion

In the present research investigation, we have developed a targeted nanoformulation (Cet-DTX NP) to deliver the anticancer drug, DTX to cancerous lung cells (A549 and NCI-H23) that overexpress the EGFR receptors. The PLGA nanoparticles were formulated by implementing multiple emulsion solvent evaporation technique to incorporate a higher concentration of drug. Moreover, the carboxyl terminated group of PLGA exposed to the surface of the nanoparticles permits further functionalization of antibody on its surface. The data of the present investigation demonstrated that the potent anti-cancer drug DTX was successfully incorporated into the biodegradable PLGA nanoparticles, fabricated with Cet with the requisite physicochemical properties. In addition, site-specific targeting of DTX to the lung cancer cells which overexpress EGFR receptors was accomplished by Cet coupling to the drug loaded nanoparticles, manifesting the drug release in a slow and sustained manner. From the results obtained by *in vitro* and *in vivo* studies, it was observed that the Cet-DTX NP was more efficacious than DTX NP and free DTX in terms of therapeutic improvement. Cet-DTX NP showed highest levels of cellular internalization and apoptotic potential, mostly due to its higher affinity towards the lung cancer cells.

In B(a)P-induced lung cancer-bearing mice, Cet-DTX NP significantly reduced the cancerous lesions of lungs. This might be attributable to an enhanced and sustained bioavailability of DTX in the lung tumor. The nanoencapsulated DTX resulted in reduced cytotoxicity in normal lung epithelial cells, and markedly enhance the therapeutic efficacy *in vivo*. To conclude, the present research study suggests that Cet-DTX NP should be further explored for its utilization to treat lung cancer, since it has the potential of delivering the drug more precisely to lung cancer cells and causes cellular apoptosis, in contrast to its activity in normal cells. Furthermore, more clinical studies will aid in estimating the human dose and study the potential of these nanoformulations in lung cancer patients.

9. Summary

Non small cell lung cancer (NSCLC) is one of the most prevalent cancers diagnosed worldwide, yet managing it is still challenging. It is responsible for approximately a quarter of all cancer fatalities, outnumbering colon, breast, and prostate cancers. Treatment of NSCLC patients with surgery and chemotherapy is hampered by late diagnosis. Moreover, the lack of tumor selectivity in these techniques leads to increased toxicity in patients, limiting the therapeutic efficacy. Platinum drugs, taxanes including paclitaxel (PTX) and docetaxel (DTX), albumin-bound paclitaxel, and other types of chemotherapy are all suggested for NSCLC. Among the taxane groups, DTX is quite effective to a wide spectrum of cancers. It has been shown to block microtubule depolymerization of free tubulins in preclinical experiments in a range of murine malignancies and human tumor xenografts, including lung adenocarcinoma.

In NSCLC, the epidermal growth factor receptor (EGFR) is a popular target. It belongs to the family of receptor tyrosine kinases, which stimulates several signaling pathways to encourage growth of cells, cellular proliferation, and survival. Targeting lung tumors with EGFR expression can be an important strategy because EGFR expression is often low in most organs (such as benign tumor nodules). Numerous drugs that target the EGFR pathway have been developed. They include small molecule tyrosine kinase inhibitors, (such as afatinib, gefitinib, and erlotinib) and EGFR-inhibiting antibodies [e.g. cetuximab (Cet)], in light of the fact that EGFR plays such an important role in lung adenocarcinoma. Anti-EGFR humanized monoclonal antibody, Cetuximab (Cet), blocks binding of activating ligands to EGFR and prevents the downstream signaling of EGFR-dependent growth and survival to provide anti-tumor activity. Cet binding to EGFR causes membrane clearance, internalization and EGFR degradation for signal termination.

During the last few decades, nanoparticles for cancer chemotherapy are gaining popularity. Enhanced permeability and the retention effect (EPR effect) of the cancerous tumors make the tumor accumulation of NP feasible. In order to conjugate ligands onto the surface of nanoparticles, the 1-ethyl-3-[3-dimethylaminopropyl] carbodiimide hydrochloride/ N-hydroxysuccinimide (EDC/NHS) coupling process is one of the highly efficient techniques. It is commonly used to attach a variety of DNA or antibodies to the nanoparticles. Several studies have shown that the anti-EGFR monoclonal antibody Cet can be conjugated

to nanoparticles, allowing the drug-loaded nanoparticles to be delivered specifically to lung cancer cells.

The focus of this research work is to develop antibody-conjugated nanoparticles (Cet-DTX NP) with site-specific targeting that can provide clear therapeutic benefits against lung tumors. We have synthesized DTX-loaded Poly (D, L-lactide-co-glycolide) (PLGA) nanoparticles conjugated with Cet using EDC/NHS coupling chemistry for lung tumor-specific nanoparticle accumulation in an experimental mouse model. We tried to focus on *in vivo* results to prove intended use of the experimental nanoformulation, which affirmed our hypothesis as the drug reached the affected tissues with an increased and sustained availability, with an enhanced anti-tumor efficacy against lung cancer.
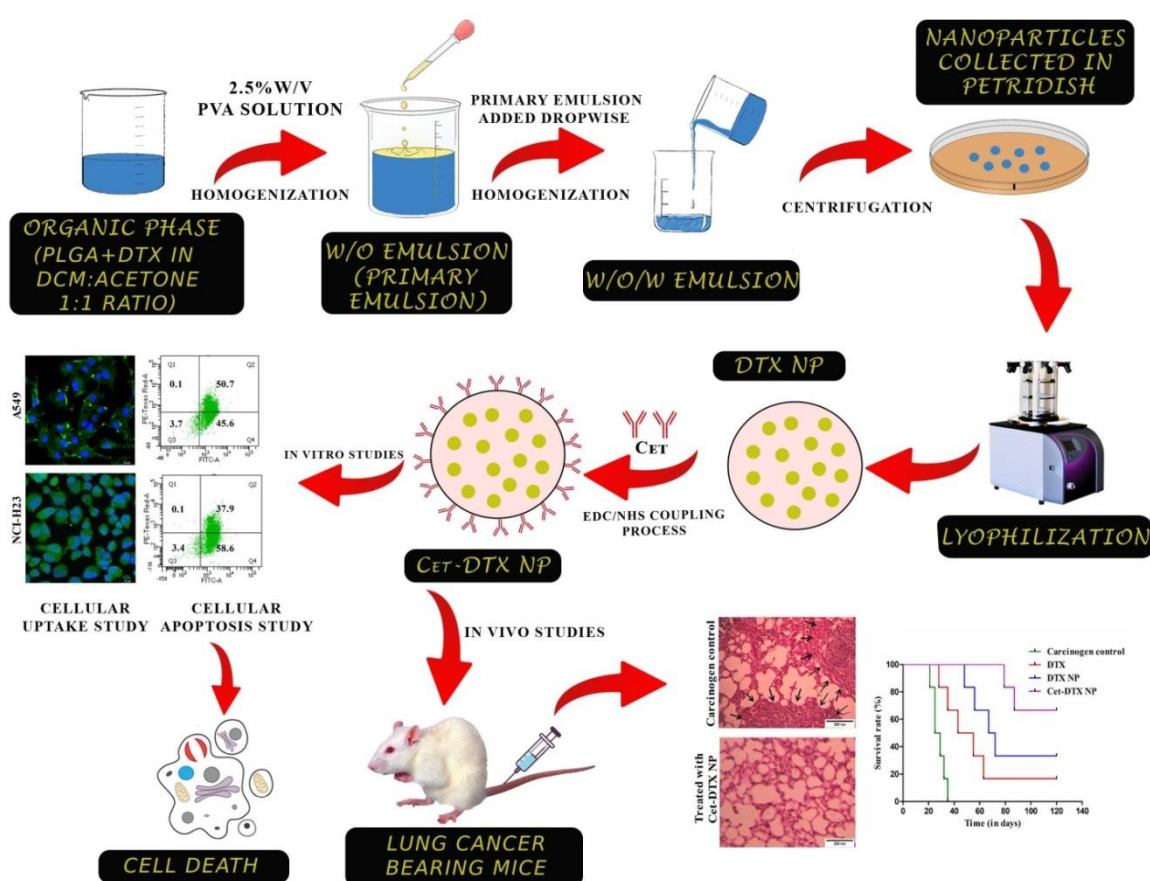
Figure 9.1. Schematic diagram representing the summary of the present research study

On the basis of scanning of DTX by spectrophotometric method, the maximum wavelength (λ_{max}) was attained at 229 nm in acetonitrile:water, and therefore it has been selected as the analytical wavelength. The FTIR investigation detected that no chemical interactions were observed between the drug and the excipients. Weak physicochemical interactions, such as

the dipole-induced interaction, weak H-bonds, van der Waals force of attraction, etc., which may play significant roles in the formation of spherical shaped nanoparticles, were noted in the case of Blank NP and DTX NP, leading to some minor peak shiftings of the formulation components.

It was observed that the optimized DTX NP showed maximum drug loading, greater entrapment efficiency, smaller particle size and greater zeta potential values. The FESEM study revealed that Cet-DTX NPs had majority of spherical structure and densely distributed. TEM analysis showed the internal morphology of Cet-DTX NP. The figure revealed that the drug was evenly and homogeneously distributed throughout the particles. SDS-PAGE study demonstrated that the antibody was effectively conjugated onto the surface of DTX NP nanoparticles, which moved more slowly than free antibody due to the attachment to heavier nanoparticles. However, the lack of antibody on the surface of the DTX NP failed to produce any bands. In case of EDX study, nitrogen in the case of DTX NP and its absence in the case of blank NP indicated the presence/lack of nitrogen of DTX in the two corresponding formulations. A higher weight percentage of sulphur in case of Cet-DTX NP affirms the conjugation of the Cet to Cet-DTX NP. Because of the amide bond between the Cet and DTX NP, the Cet-DTX NP had a slightly greater weight percentage contribution from nitrogen, which further supports the presence of Cet.

The drug released from the nanoformulation over time was assessed by the *in vitro* drug release study. An early burst release of the drug from Cet-DTX NP was demonstrated, which might have resulted due to the rapid dissociation of the drug adhered to the surface of the nanoparticles. Thereafter, a slow and sustained release of the drug takes place, probably due to the erosion of the polymeric core, followed by the diffusion of the drug from the polymeric matrix. The drug release pattern from the nanoparticles followed Korsemeyer Peppas model of kinetics with high linearity. Cet-DTX NP portrayed fast degradation in the acidic medium, which suggests ester hydrolysis of the polymeric core. The drug release was comparatively faster in acidic tumor environment (pH 5) while it depicted slow and sustained release in physiologically neutral media of blood (pH 7.4). When DTX release from DTX NP and Cet-DTX NP was measured in PBS (pH 7.4) with 0.1% w/v tween 80, citrate buffer, acetate buffer, and bicarbonate buffer, it indicated acceptable linearity in the different kinetic models (as supported by R^2 value).

The experimental formulations (stored at 30°C and 40°C, and 75% RH) were agglomerated with slight structural deformation on storing for a period of 90 days probably due to the softening of polymer stored at higher temperature for a prolonged period. The nanoparticles were reasonably stable after being stored at 4–8 °C during this period, according to the data of accelerated stability experiments. Drug content did not vary significantly when stored at the refrigerated condition for a period of 90 days, which further suggests that the prepared nanoparticles should be stored at 4-8 ℃ for long-term use.

RT-PCR analysis had confirmed the overexpression of EGFR in lung cancer cells (A549 and NCI-H23), whereas it is not significantly expressed in L-132 (normal lung epithelial cells). The overexpression of EGFR on both the lung cancer cells confirmed, that more ligand (anti-EGFR Cet antibody) will bind to these cells as compared to normal lung epithelial cells, resulting in more apoptosis in cancerous cells. Cet prevents EGFR function by binding to the receptors overexpressed on the lung cancer cells. The lower K_D value in case of A549 cells, as compared to NCI-H23 cells suggests higher affinity and tighter binding of antibody with the receptors on the cell surface. This could be due to the various non-covalent interactions (hydrogen bonding, van der Waals forces and hydrophobic forces) that participate in the affinity of a binding site.

In vitro cytotoxicity study exhibited lower IC_{50} values after the lung cancer cells were treated with Cet-DTX NP, as compared to DTX NP and free drug. It might be due to the greater affinity of the Cet-DTX NP towards EGFR overexpressed lung cancer cells, thereby resulting in the greater uptake of nanoparticles within the cells. Moreover, the targeted nanoparticles exhibit cytotoxicity only towards lung cancer cells, and not toward the normal lung epithelial cells. Confocal microscopic study showed that FITC encapsulated nanoparticles (FITC-DTX NP and FITC-Cet-DTX NP) internalized well within the lung cancer cells. FACS analysis also showed time dependent quantitative uptake of DTX NP and Cet-DTX NP from 1 to 4 h in both the cancer cell types. Comparing Cet-DTX NP to DTX NP and DTX using a site-specific sustained delivery pattern, it was found that Cet-DTX NP were more effective at inducing apoptosis in A549 and NCI-H23 cells. Cet-DTX NPs targeted delivery and improved cellular uptake cause a higher buildup of drug within lung cancer cells, leading to apoptosis. The outcomes of the cell cycle analysis in the A549 and NCI-H23 cells demonstrated that DTX and its nanoformulations were accountable for the cell death brought

on by the G2/M phase arrest. It could be interpreted that antibody conjugated nanoparticles are highly potent to arrest the cancer cell proliferation.

In case of MTD analysis, there is a substantial decrease in the level of liver and kidney toxicity markers (ALP, SGOT, SGPT, urea and creatinine) in normal mice treated with DTX NP and Cet-DTX NP, as compared to unbound DTX, indicating better tolerability of nano-encapsulated DTX, upto the dose of 10 mg/kg body weight. Moreover, there was no obvious change in the body weight of the normal mice treated with DTX NP and Cet-DTX NP, which further suggested 10 mg/kg body weight is the maximum tolerated dose of DTX when encapsulated in the form of nanoparticles. Cetuximab has a prolonged residential time in the body. Therefore, as a cumulative effect of greater internalization of the drug and toxicity produced by free Cet reduced the body weight of normal animals at higher doses.

The comparatively low hemolytic activity of the test nanoformulations (DTX NP and Cet-DTX NP) than free drug, suggest hemocompatibility. Therefore, it could be safely administered via intravenous route. The administration of DTX NP/Cet-DTX NP to plasma and lung tissues resulted in elevated biological $t_{1/2}$, AUC, AUMC and MRT values, along with a decrease in elimination rate constants, which might be due to sustained release of the drug from the core of the nanoparticles for a prolonged duration.

The Cet-DTX NP showed higher amount of DTX at lung tumor sites than DTX NP and free DTX that was mainly attributed to the controlled and targeted DTX release of Cet-DTX NP in cancerous lung, which resulted less DTX released in other organs (blood, liver, kidney, heart and muscles) and more DTX accumulated in the cancerous lung. Free DTX was found to be more accumulated in the heart and kidney, as compared to the liver, which might be due to the fact that liver is the organ of the reticuloendothelial system (RES), whose macrophages clear the drug and reduces the exposure to the parenchymal cells of liver [53]. The less accumulation of Cet-DTX NP confirmed its non-toxicity to cardiac tissues.

When carcinogen control animals were treated with DTX, Cet conjugated and unconjugated nanoparticles, there is an increase in the survival rate of animals treated with Cet-DTX NP. This is due to the targeting ability of Cet for DTX NPs, leading to the greater accumulation of DTX at the site of lung tumor. Moreover, there is a significant role of caspase-dependent apoptosis in the suppression of B(a)P-induced lung tumor development.

ROS and LPO level play a significant role in the initiation, promotion, and progression of lung cancer. These were markedly reduced after treatment with Cet-DTX NP, which is due to the enriched activity of detoxification enzyme in the treated animal group, as compared to carcinogen control group. The histopathological study revealed that Cet-DTX NP greatly reduced the growth of lung tumor and significantly restored the lung homogeneity, which may be contributed due to the site-specific targeting of antibody conjugated nanoparticles to the NSCLC, as compared to the normal cells.

In summary, the present research study recommends that Cet-DTX NP be further investigated for application in the treatment of lung cancer since it has the ability to deliver the drug more specifically to lung cancer cells and triggers cellular apoptosis, as opposed to its effects on normal cells. Additionally, further clinical investigations will assist to determine the human dose and explore the effectiveness of these nanoformulations in patients with lung cancer.

10. References

Abou-El-Naga AM, Mutawa G, El-Sherbiny IM, Mousa SA. Activation of Polymeric Nanoparticle Intracellular Targeting Overcomes Chemodrug Resistance in Human Primary Patient Breast Cancer Cells [Retraction]. Int. J. Nanomedicine 2022;17:2555-2556.

Aggarwal S, Gupta S, Pabla D, Murthy RS. Gemcitabine-loaded PLGA-PEG immunonanoparticles for targeted chemotherapy of pancreatic cancer. Cancer Nanotechnol. 2013;4:145-157.

Ahmed MM, Fatima F, Anwer MK, Aldawsari MF, Alsaidan YS, Alfaiz SA, Haque A, Alanazi AZ, Alhazzani K. Development and characterization of Brigatinib loaded solid lipid nanoparticles: In-vitro cytotoxicity against human carcinoma A549 lung cell lines. Chem. Phys. Lipids 2020;233:105003.

Alexis F, Rhee JW, Richie JP, Radovic-Moreno AF, Langer R, Farokhzad OC. New frontiers in nanotechnology for cancer treatment. In: Urologic Oncology: Seminars and Original Investigations 2008 (Vol. 26, No. 1, pp. 74-85). Elsevier.

Alfieri RR, Galetti M, Tramonti S, Andreoli R, Mozzoni P, Cavazzoni A, Bonelli M, Fumarola C, La Monica S, Galvani E, De Palma G. Metabolism of the EGFR tyrosin kinase inhibitor gefitinib by cytochrome P450 1A1 enzyme in EGFR-wild type non small cell lung cancer cell lines. Mol. Cancer 2011;10:1-14.

Aran V, Omerovic J. Current approaches in NSCLC targeting K-RAS and EGFR. Int. J. Mol. Sci. 2019;20:5701.

Assoun S, Brosseau S, Steinmetz C, Gounant V, Zalcman G. Bevacizumab in advanced lung cancer: state of the art. Future Oncol. 2017;13:2515-2535.

Attia MF, Anton N, Wallyn J, Omran Z, Vandamme TF. An overview of active and passive targeting strategies to improve the nanocarriers efficiency to tumour sites. J. Pharm. Pharmacol. 2019;71:1185-1198.

Azimi B, Nourpanah P, Rabiee M, Arbab S. Poly (lactide -co- glycolide) Fiber: An Overview. J. Eng. Fiber. Fabr. 2014; 9:47-66.

Bagnardi V, Rota M, Botteri E, Scotti L, Jenab M, Bellocco R, Tramacere I, Pelucchi C, Negri E, La Vecchia C, Corrao G. Alcohol consumption and lung cancer risk in never smokers: a meta-analysis. Ann. Oncol. 2011;22:2631-2639.

Baker S, Dahele M, Lagerwaard FJ, Senan S. A critical review of recent developments in radiotherapy for non-small cell lung cancer. Radiat. Oncol. 2016;11:1-14.

Barak D, Engelberg S, Assaraf YG, Livney YD. Selective Targeting and Eradication of Various Human Non-Small Cell Lung Cancer Cell Lines Using Self-Assembled Aptamer-Decorated Nanoparticles. Pharmaceutics 2022;14:1650.

BarathManiKanth S, Kalishwaralal K, Sriram M, Pandian SR, Youn HS, Eom S, Gurunathan S. Anti-oxidant effect of gold nanoparticles restrains hyperglycemic conditions in diabetic mice. J. Nanobiotechnology 2010;8:1-15.

Barua A, Choudhury P, Nag N, Nath A, Kundagrami S, Pal A, Panda CK, Saha P. Xanthone from Swertia chirata exerts chemotherapeutic potential against colon carcinoma. Curr. Sci. 2022;122:47-55.

Baskar R, Lee KA, Yeo R, Yeoh KW. Cancer and radiation therapy: current advances and future directions. Int. J. Med. Sci. 2012;9:193-199.

Belani CP. Paclitaxel and docetaxel combinations in non-small cell lung cancer. Chest;117:144S-151S.

Bhattacharya S, Mondal L, Mukherjee B, Dutta L, Ehsan I, Debnath MC, Gaonkar RH, Pal MM, Majumdar S. Apigenin loaded nanoparticle delayed development of hepatocellular carcinoma in rats. Nanomedicine 2018;14:1905-1917.

Blumenschein Jr GR, Paulus R, Curran WJ, Robert F, Fossella F, Werner-Wasik M, Herbst RS, Doescher PO, Choy H, Komaki R. Phase II study of cetuximab in combination with chemoradiation in patients with stage IIIA/B non–small-cell lung cancer: RTOG 0324. J. Clin. Oncol. 2011;29:2312-2318.

Bonomi PD, Mace J, Mandanas RA, Min M, Olsen M, Youssoufian H, Katz TL, Sheth G, Lee HJ. Randomized phase II study of cetuximab and bevacizumab in combination with two regimens of paclitaxel and carboplatin in chemonaive patients with stage IIIB/IV non–small-cell lung cancer. J. Thorac. Oncol. 2013;8:338-345.

Bou-Assaly W, Mukherji S. Cetuximab (erbitux). Am. J. Neuroradiol. 2010;31:626-627.

Brennan P, Hainaut P, Boffetta P. Genetics of lung-cancer susceptibility. Lancet Oncol. 2011;12:399-408.

Butler LM, Montague JA, Koh WP, Wang R, Yu MC, Yuan JM. Fried meat intake is a risk factor for lung adenocarcinoma in a prospective cohort of Chinese men and women in Singapore. Carcinogenesis 2013;34:1794-1799.

Chakraborty S, Dlie ZY, Chakraborty S, Roy S, Mukherjee B, Besra SE, Dewanjee S, Mukherjee A, Ojha PK, Kumar V, Sen R. Aptamer-functionalized drug nanocarrier improves hepatocellular carcinoma toward normal by targeting neoplastic hepatocytes. Mol. Ther. Nucleic Acids 2020;20:34-49.

Che CL, Zhang YM, Zhang HH, Sang YL, Lu B, Dong FS, Zhang LJ, Lv FZ. DNA microarray reveals different pathways responding to paclitaxel and docetaxel in non-small cell lung cancer cell line. Int. J. Clin. Exp. Pathol. 2013;6:1538-1548.

Chen R, Khatri P, Mazur PK, Polin M, Zheng Y, Vaka D, Hoang CD, Shrager J, Xu Y, Vicent S, Butte AJ. A meta-analysis of lung cancer gene expression identifies PTK7 as a survival gene in lung adenocarcinoma. Cancer Res. 2014;74:2892-2902.

Chishti N, Jagwani S, Dhamecha D, Jalalpure S, Dehghan MH. Preparation, optimization, and in vivo evaluation of nanoparticle-based formulation for pulmonary delivery of anticancer drug. Medicina 2019;55:294.

Chittasupho C, Lirdprapamongkol K, Kewsuwan P, Sarisuta N. Targeted delivery of doxorubicin to A549 lung cancer cells by CXCR4 antagonist conjugated PLGA nanoparticles. Eur. J. Pharm. Biopharm. 2014;88:529-538.

Choudhury P, Barua A, Roy A, Pattanayak R, Bhattacharyya M, Saha P. Eugenol emerges as an elixir by targeting β-catenin, the central cancer stem cell regulator in lung carcinogenesis: An in vivo and in vitro rationale. Food Funct. 2021;12:1063-1078.

Christiani DC. Ambient air pollution and lung cancer: nature and nurture. Am. J. Respir. Crit. Care Med. 2021;204:752-753.

Chung CH, Mirakhur B, Chan E, Le QT, Berlin J, Morse M, Murphy BA, Satinover SM, Hosen J, Mauro D, Slebos RJ. Cetuximab-induced anaphylaxis and IgE specific for galactose-α-1, 3-galactose. N. Engl. J. Med. 2008;358:1109-1117.

Chung EK, Yong SH, Lee EH, Kim EY, Chang YS, Lee SH. New targeted therapy for non-small cell lung cancer. Tuberc. Respir. Dis. 2023;86:1-13.

Cortés ÁA, Urquizu LC, Cubero JH. Adjuvant chemotherapy in non-small cell lung cancer: state-of-the-art. Transl. Lung Cancer Res. 2015;4:191-197.

Couraud S, Zalcman G, Milleron B, Morin F, Souquet PJ. Lung cancer in never smokers–a review. Eur. J. Cancer 2012;48:1299-1311.

Cui XY, Park SH, Park WH. Auranofin inhibits the proliferation of lung cancer cells via necrosis and caspase-dependent apoptosis. Oncol. Rep. 2020;44:2715-2724.

Das PJ, Paul P, Mukherjee B, Mazumder B, Mondal L, Baishya R, Debnath MC, Dey KS. Pulmonary delivery of voriconazole loaded nanoparticles providing a prolonged drug level in lungs: a promise for treating fungal infection. Mol. Pharm. 2015;12:2651-2664.

Dassonville O, Bozec A, Fischel JL, Milano G. EGFR targeting therapies: monoclonal antibodies versus tyrosine kinase inhibitors: similarities and differences. Crit. Rev. Oncol. Hematol. 2007;62:53-61.

Denisenko TV, Budkevich IN, Zhivotovsky B. Cell death-based treatment of lung adenocarcinoma. Cell Death Dis. 2018;9:117.

Du Z, Lovly CM. Mechanisms of receptor tyrosine kinase activation in cancer. Mol. Cancer 2018;17:58.

Dutta D, Chakraborty A, Mukherjee B, Gupta S. Aptamer-conjugated apigenin nanoparticles to target colorectal carcinoma: a promising safe alternative of colorectal cancer chemotherapy. ACS Appl. Bio Mater. 2018;1:1538-1556.

Dutta D, Paul B, Mukherjee B, Mondal L, Sen S, Chowdhury C, Debnath MC. Nanoencapsulated betulinic acid analogue distinctively improves colorectal carcinoma in vitro and in vivo. Sci. Rep. 2019;9:1-20.

Eble JA. Titration ELISA as a method to determine the dissociation constant of receptor ligand interaction. J. Vis. Exp. 2018;(132):e57334.

Ehsan I, Kumari L, Sen R, Al Hoque A, Mukherjee B, Mukherjee A, Ghosh P, Bhattacharya S. J591 functionalized paclitaxel-loaded PLGA nanoparticles successfully inhibited PSMA overexpressing LNCaP cells. J. Drug Deliv. Sci. Technol. 2022;75:103689.

Elmowafy EM, Tiboni M, Soliman ME. Biocompatibility, biodegradation and biomedical applications of poly (lactic acid)/poly (lactic-co-glycolic acid) micro and nanoparticles. J. Pharm. Investig. 2019;49:347-380.

Farjadian F, Ghasemi A, Gohari O, Roointan A, Karimi M, Hamblin MR. Nanopharmaceuticals and nanomedicines currently on the market: challenges and opportunities. Nanomedicine 2019;14:93-126.

Fehringer G, Brenner DR, Zhang ZF, Lee YC, Matsuo K, Ito H, Lan Q, Vineis P, Johansson M, Overvad K, Riboli E. Alcohol and lung cancer risk among never smokers: A pooled analysis from the international lung cancer consortium and the SYNERGY study. Int J Cancer 2017;140:1976-1984.

Fernandez-Urrusuno R, Fattal E, Rodrigues Jr JM, Feger J, Bedossa P, Couvreur P. Effect of polymeric nanoparticle administration on the clearance activity of the mononuclear phagocyte system in mice. J. Biomed. Mater. Res. 1996;31:401-408.

Furrukh M. Tobacco smoking and lung cancer: perception-changing facts. Sultan Qaboos Univ. Med. J. 2013;13:345-358.

Gaio E, Conte C, Esposito D, Reddi E, Quaglia F, Moret F. CD44 targeting mediated by polymeric nanoparticles and combination of chlorine TPCS2a-PDT and docetaxel-chemotherapy for efficient killing of breast differentiated and stem cancer cells in vitro. Cancers 2020;12:278.

Gaonkar RH, Ganguly S, Dewanjee S, Sinha S, Gupta A, Ganguly S, Chattopadhyay D, Chatterjee Debnath M. Garcinol loaded vitamin E TPGS emulsified PLGA nanoparticles: preparation, physicochemical characterization, in vitro and in vivo studies. Sci. Rep. 2017;7:1-14.

Garg A. Polymeric Nanoparticles to Target Lung Cancer. Polymeric nanoparticles for the treatment of solid tumors. In: Environmental Chemistry for a Sustainable World book series (ECSW,volume 71) 2022:351-371.

Guo S, Zhang Y, Wu Z, Zhang L, He D, Li X, Wang Z. Synergistic combination therapy of lung cancer: Cetuximab functionalized nanostructured lipid carriers for the co-delivery of paclitaxel and 5-Demethylnobiletin. Biomed Pharmacother 2019;118:109225.

Guo X, Szoka FC. Chemical approaches to triggerable lipid vesicles for drug and gene delivery. Acc. Chem. Res. 2003;36:335-341.

Haleem A, Javaid M, Singh RP, Rab S, Suman R. Applications of Nanotechnology in Medical field. Global Health Journal (GHJ) 2023;7:70-77.

Hecht SS. Cigarette smoking and lung cancer: chemical mechanisms and approaches to prevention. Lancet Oncol. 2002;3:461-469.

Herbst RS, Morgensztern D, Boshoff C. The biology and management of non-small cell lung cancer. Nature 2018;553:446-454.

Hines DJ, Kaplan DL. Poly (lactic-co-glycolic) acid− controlled-release systems: experimental and modeling insights. Crit. Rev. Ther. Drug Carr. Syst. 2013;30:257-276.

Hoy H, Lynch T, Beck M. Surgical treatment of lung cancer. Crit. Care Nurs. Clin. North Am. 2019;31:303-313.

Hsu PC, Jablons DM, Yang CT, You L. Epidermal growth factor receptor (EGFR) pathway, yes-associated protein (YAP) and the regulation of programmed death-ligand 1 (PD-L1) in non-small cell lung cancer (NSCLC). Int. J. Mol. Sci. 2019;20:3821.

Huang WT, Larsson M, Wang YJ, Chiou SH, Lin HY, Liu DM. Demethoxycurcumin-carrying chitosan–antibody core–shell nanoparticles with multitherapeutic efficacy toward malignant A549 lung tumor: From in vitro characterization to in vivo evaluation. Mol. Pharm 2015;12:1242-1249.

Hussein AS, Abdullah N, Ahmadun FL. In vitro degradation of poly (D, L-lactide-co-glycolide) nanoparticles loaded with linamarin. IET Nanobiotechnol. 2013;7:33-41.

Imran M, Saleem S, Chaudhuri A, Ali J, Baboota S. Docetaxel: An update on its molecular mechanisms, therapeutic trajectory and nanotechnology in the treatment of breast, lung and prostate cancer. J. Drug Deliv. Sci. Technol. 2020;60:101959.

Imyanitov EN, Iyevleva AG, Levchenko EV. Molecular testing and targeted therapy for non-small cell lung cancer: Current status and perspectives. Crit. Rev. Oncol. Hematol. 2021;157:103194.

Jose S, Cinu TA, Sebastian R, Shoja MH, Aleykutty NA, Durazzo A, Lucarini M, Santini A, Souto EB. Transferrin-conjugated docetaxel–PLGA nanoparticles for tumor targeting: influence on MCF-7 cell cycle. Polymers 2019;11:1905.

Jutten B, Dubois L, Li Y, Aerts H, Wouters BG, Lambin P, Theys J, Lammering G. Binding of cetuximab to the EGFRvIII deletion mutant and its biological consequences in malignant glioma cells. Radiother. Oncol. 2009;92:393-398.

Kanwal M, Ding XJ, Cao Y. Familial risk for lung cancer. Oncol. Lett. 2017;13:535-542.

Kapoor DN, Bhatia A, Kaur R, Sharma R, Kaur G, Dhawan S. PLGA: a unique polymer for drug delivery. Ther. Deliv. 2015;6:41-58.

Karra N, Nassar T, Ripin AN, Schwob O, Borlak J, Benita S. Antibody conjugated PLGA nanoparticles for targeted delivery of paclitaxel palmitate: efficacy and biofate in a lung cancer mouse model. Small 2013;9:4221-4236.

Keedy VL, Sandler AB. Inhibition of angiogenesis in the treatment of non- small cell lung cancer. Cancer Sci. 2007;98:1825-1830.

Keles H, Naylor A, Clegg F, Sammon C. Investigation of factors influencing the hydrolytic degradation of single PLGA microparticles. Polym. Degrad. Stab. 2015;119:228-241.

Kim HK, Choi YH, Verpoorte R. NMR-based metabolomic analysis of plants. Nat. Protoc. 2010;5:536-549.

Kraus LA, Samuel SK, Schmid SM, Dykes DJ, Waud WR, Bissery MC. The mechanism of action of docetaxel (Taxotere®) in xenograft models is not limited to bcl-2 phosphorylation. Invest. New Drugs 2003;21:259-268.

Kwak K, Paek D, Park JT. Occupational exposure to formaldehyde and risk of lung cancer: A systematic review and meta-analysis. Am. J. Ind. Med. 2020;63:312-327.

Lang-Lazdunski L. Surgery for nonsmall cell lung cancer. Eur. Respir. Rev. 2013;22:382-404.

Li K, Zhan W, Chen Y, Jha RK, Chen X. Docetaxel and doxorubicin codelivery by nanocarriers for synergistic treatment of prostate cancer. Front. Pharmacol. 2019;10:1436.

Li K, Zhan W, Jia M, Zhao Y, Liu Y, Jha RK, Zhou L. Dual loading of nanoparticles with doxorubicin and icotinib for the synergistic suppression of non-small cell lung cancer. Int. J. Med. Sci. 2020;17:390-402.

Li S, Xu S, Liang X, Xue Y, Mei J, Ma Y, Liu Y, Liu Y. Nanotechnology: breaking the current treatment limits of lung cancer. Adv. Healthc. Mater. 2021;10:2100078.

Li W, Yalcin M, Bharali DJ, Lin Q, Godugu K, Fujioka K, Keating KA, Mousa SA. Pharmacokinetics, biodistribution, and anti-angiogenesis efficacy of diamino propane tetraiodothyroacetic acid-conjugated biodegradable polymeric nanoparticle. Sci. Rep. 2019;9:9006.

Li X, Li J, Wu P, Zhou L, Lu B, Ying K, Chen E, Lu Y, Liu P. Smoker and non-smoker lung adenocarcinoma is characterized by distinct tumor immune microenvironments. Oncoimmunology 2018;7:e1494677.

Li X, Li J, Wu P, Zhou L, Lu B, Ying K, Chen E, Lu Y, Liu P. Paclitaxel and quercetin nanoparticles co-loaded in microspheres to prolong retention time for pulmonary drug delivery. Int. J. Nanomedicine 2017;12:8239-8255.

Liu TC, Jin X, Wang Y, Wang K. Role of epidermal growth factor receptor in lung cancer and targeted therapies. Am. J. Cancer Res. 2017;7:187-202.

Liu Y, Cheng W, Xin H, Liu R, Wang Q, Cai W, Peng X, Yang F, Xin H. Nanoparticles advanced from preclinical studies to clinical trials for lung cancer therapy. Cancer Nanotechnol. 2023;14:1-25.

Loiseau A, Boudon J, Oudot A, Moreau M, Boidot R, Chassagnon R, Mohamed Saïd N, Roux S, Mirjolet C, Millot N. Titanate nanotubes engineered with gold nanoparticles and docetaxel to enhance radiotherapy on xenografted prostate tumors. Cancers 2019;11:1962.

Ma P, Mumper RJ. Paclitaxel nano-delivery systems: a comprehensive review. J. Nanomed. Nanotechnol. 2013;4:1000164.

Mahmood MA, Madni A, Rehman M, Rahim MA, Jabar A. Ionically cross-linked chitosan nanoparticles for sustained delivery of docetaxel: fabrication, post-formulation and acute oral toxicity evaluation. Int. J. Nanomedicine 2019,14:10035-10046.

Majeed U, Manochakian R, Zhao Y, Lou Y. Targeted therapy in advanced non-small cell lung cancer: current advances and future trends. J Hematol Oncol 2021;14:1-20.

Majumder D, Debnath R, Nath P, Libin Kumar KV, Debnath M, Tribedi P, Maiti D. Bromelain and Olea europaea (L.) leaf extract mediated alleviation of benzo (a) pyrene induced lung cancer through Nrf2 and NFκB pathway. Environ. Sci. Pollut. Res. 2021;28:47306-47326.

Makadia HK, Siegel SJ. Poly lactic-co-glycolic acid (PLGA) as biodegradable controlled drug delivery carrier. Polymers 2011;3:1377-1397.

Malek-Khatabi A, Razavi MS, Abdollahi A, Rahimzadeghan M, Moammeri F, Sheikhi M, Tavakoli M, Rad-Malekshahi M, Rad ZF. Recent progress in PLGA-based microneedle-mediated transdermal drug and vaccine delivery. Biomater. Sci. 2023 (Accepted).

Mandal D, Shaw TK, Dey G, Pal MM, Mukherjee B, Bandyopadhyay AK, Mandal M. Preferential hepatic uptake of paclitaxel-loaded poly-(DL-lactide-co-glycolide) nanoparticles—A possibility for hepatic drug targeting: Pharmacokinetics and biodistribution. Int. J. Biol. Macromol. 2018;112:818-830.

Mattu C, Brachi G, Menichetti L, Flori A, Armanetti P, Ranzato E, Martinotti S, Nizzero S, Ferrari M, Ciardelli G. Alternating block copolymer-based nanoparticles as tools to modulate the loading of multiple chemotherapeutics and imaging probes. Acta Biomater. 2018;80:341-351.

Maya S, Kumar LG, Sarmento B, Rejinold NS, Menon D, Nair SV, Jayakumar R. Cetuximab conjugated O-carboxymethyl chitosan nanoparticles for targeting EGFR overexpressing cancer cells. Carbohydr. Polym. 2013;93:661-669.

Maya S, Sarmento B, Lakshmanan VK, Menon D, Seabra V, Jayakumar R. Chitosan cross-linked docetaxel loaded EGF receptor targeted nanoparticles for lung cancer cells. Int. J. Biol. Macromol. 2014;69:532-541.

Mithoowani H, Febbraro M. Non-small-cell lung cancer in 2022: A review for general practitioners in oncology. Curr. Oncol. 2022;29:1828-1839.

Molina JR, Adjei AA, Jett JR. Advances in chemotherapy of non-small cell lung cancer. Chest 2006;130:1211-1219.

Mondal L, Mukherjee B, Das K, Bhattacharya S, Dutta D, Chakraborty S, Pal MM, Gaonkar RH, Debnath MC. CD-340 functionalized doxorubicin-loaded nanoparticle induces apoptosis and reduces tumor volume along with drug-related cardiotoxicity in mice. Int. J. Nanomedicine 2019;14:8073-8094.

Montero A, Fossella F, Hortobagyi G, Valero V. Docetaxel for treatment of solid tumours: a systematic review of clinical data. Lancet Oncol. 2005;6:229-239.

Morse DL, Gray H, Payne CM, Gillies RJ. Docetaxel induces cell death through mitotic catastrophe in human breast cancer cells. Mol. Cancer Ther. 2005;4:1495-1504.

Najlah M, Ahmed Z, Iqbal M, Wang Z, Tawari P, Wang W, McConville C. Development and characterisation of disulfiram-loaded PLGA nanoparticles for the treatment of non-small cell lung cancer. Eur. J. Pharm. Biopharm. 2017;112:224-233.

Oerlemans C, Bult W, Bos M, Storm G, Nijsen JF, Hennink WE. Polymeric micelles in anticancer therapy: targeting, imaging and triggered release. Pharm. Res. 2010;27:2569-2589.

Pal D, Sur S, Mandal S, Das A, Roy A, Das S, Panda CK. Prevention of liver carcinogenesis by amarogentin through modulation of G 1/S cell cycle check point and induction of apoptosis. Carcinogenesis 2012;33:2424-2431.

Park YI, Kwon SH, Lee G, Motoyama K, Kim MW, Lin M, Niidome T, Choi JH, Lee R. pH-sensitive multi-drug liposomes targeting folate receptor β for efficient treatment of non-small cell lung cancer. J Control Release 2021;330:1-14.

Parmar K, Patel J, Pathak Y. Factors Affecting the Clearance and Biodistribution of Polymeric Nanoparticles. InPharmacokinetics and Pharmacodynamics of

Nanoparticulate Drug Delivery Systems 2022 Mar 8 (pp. 261-272). Cham: Springer International Publishing.

Patel D, Lahiji A, Patel S, Franklin M, Jimenez X, Hicklin DJ, Kang X. Monoclonal antibody cetuximab binds to and down-regulates constitutively activated epidermal growth factor receptor vIII on the cell surface. Anticancer Res. 2007;27(5A):3355-3366.

Patel J, Amrutiya J, Bhatt P, Javia A, Jain M, Misra A. Targeted delivery of monoclonal antibody conjugated docetaxel loaded PLGA nanoparticles into EGFR overexpressed lung tumour cells. J. Microencapsul. 2018;35:204-217.

Patra JK, Das G, Fraceto LF, Campos EV, Rodriguez-Torres MD, Acosta-Torres LS, Diaz-Torres LA, Grillo R, Swamy MK, Sharma S, Habtemariam S. Nano based drug delivery systems: recent developments and future prospects. J. Nanobiotechnology 2018;16:1-33.

Paul P, Sengupta S, Mukherjee B, Shaw TK, Gaonkar RH, Debnath MC. Chitosan-coated nanoparticles enhanced lung pharmacokinetic profile of voriconazole upon pulmonary delivery in mice. Nanomedicine 2018;13:501-520.

Pesch B, Kendzia B, Gustavsson P, Jöckel KH, Johnen G, Pohlabeln H, Olsson A, Ahrens W, Gross IM, Brüske I, Wichmann HE. Cigarette smoking and lung cancer—relative risk estimates for the major histological types from a pooled analysis of case–control studies. Int. J. Cancer 2012;131:1210-1219.

Pirker R, Filipits M. Monoclonal antibodies against EGFR in non-small cell lung cancer. Crit. Rev. Oncol. Hematol. 2011;80:1-9.

Prabhakar CN. Epidermal growth factor receptor in non-small cell lung cancer. Transl. Lung Cancer Res. 2015;4:110-118.

Qu N, Sun Y, Li Y, Hao F, Qiu P, Teng L, Xie J, Gao Y. Docetaxel-loaded human serum albumin (HSA) nanoparticles: synthesis, characterization, and evaluation. Biomed. Eng. Online 2019;18:1-14.

Rafiei P, Haddadi A. Pharmacokinetic consequences of PLGA nanoparticles in docetaxel drug delivery. Pharm. Nanotechnol. 2017;5:3-23.

Rajdev K, Siddiqui AH, Ibrahim U, Patibandla P, Khan T, El-Sayegh D, Khan TM. An unusually aggressive large cell carcinoma of the lung: undiagnosed until autopsy. Cureus 2018;10:e2202.

Rawal S, Bora V, Patel B, Patel M. Surface-engineered nanostructured lipid carrier systems for synergistic combination oncotherapy of non-small cell lung cancer. Drug Deliv. Transl. Res. 2021;11:2030-2051.

Rossi A, Maione P, Gridelli C. Cetuximab in advanced non-small cell lung cancer. Crit. Rev. Oncol. Hematol. 2006;59:139-149.

Rudnik LA, Farago PV, Manfron Budel J, Lyra A, Barboza FM, Klein T, Kanunfre CC, Nadal JM, Bandéca MC, Raman V, Novatski A. Co-loaded curcumin and methotrexate nanocapsules enhance cytotoxicity against non-small-cell lung cancer cells. Molecules 2020;25:1913.

Ryman JT, Meibohm B. Pharmacokinetics of monoclonal antibodies. CPT Pharmacometrics Syst. Pharmacol. 2017;6:576-588.

Sabit H, Abdel-Hakeem M, Shoala T, Abdel-Ghany S, Abdel-Latif MM, Almulhim J, Mansy M. Nanocarriers: A Reliable Tool for the Delivery of Anticancer Drugs. Pharmaceutics 2022;14:1566.

Saif MW, Kim R. Incidence and management of cutaneous toxicities associated with cetuximab. Expert Opin. Drug Saf. 2007;6:175-182.

Sarkar S, Osama K, Mohammad Sajid Jamal Q, Amjad Kamal M, Sayeed U, Khan KA, Siddiqui H, Akhtar S. Advances and implications in nanotechnology for lung cancer management. Curr. Drug Metab. 2017;18:30-38.

Selvaggi G, Novello S, Torri V, Leonardo E, De Giuli P, Borasio P, Mossetti C, Ardissone F, Lausi P, Scagliotti GV. Epidermal growth factor receptor overexpression correlates with a poor prognosis in completely resected non-small-cell lung cancer. Ann. Oncol. 2004;15:28-32.

Shankar A, Dubey A, Saini D, Singh M, Prasad CP, Roy S, Bharati SJ, Rinki M, Singh N, Seth T, Khanna M. Environmental and occupational determinants of lung cancer. Transl. Lung Cancer Res. 2019;8:S31-S49.

Shareck M, Rousseau MC, Koushik A, Siemiatycki J, Parent ME. Inverse association between dietary intake of selected carotenoids and vitamin C and risk of lung cancer. Front. Oncol. 2017;7:23.

Sharma A, Shambhwani D, Pandey S, Singh J, Lalhlenmawia H, Kumarasamy M, Singh SK, Chellappan DK, Gupta G, Prasher P, Dua K. Advances in lung cancer treatment using nanomedicines. ACS Omega 2022;8:10-41.

Shen Q, Peng L, Zhang Y, Wang R. Application of nanotechnology in diagnosis and/or therapy of non-small cell lung cancer. Front. Oncol. 2023;13:1234727.

Shukla SK, Kulkarni NS, Farrales P, Kanabar DD, Parvathaneni V, Kunda NK, Muth A, Gupta V. Sorafenib loaded inhalable polymeric nanocarriers against non-small cell lung cancer. Pharm. Res. 2020;37:1-9.

Simone CB, Jones JA. Palliative care for patients with locally advanced and metastatic non-small cell lung cancer. Ann Palliat Med. 2013;2:178-188.

Singh G, Pai RS. Pharmacokinetics and in vivo biodistribution of optimized PLGA nanoparticulate drug delivery system for controlled release of emtricitabine. Drug Deliv. 2014;21:627-635.

Sohail MF, Rehman M, Sarwar HS, Naveed S, Salman O, Bukhari NI, Hussain I, Webster TJ, Shahnaz G. Advancements in the oral delivery of Docetaxel: challenges, current state-of-the-art and future trends. Int. J. Nanomedicine 2018;13:3145-3161.

Sokol MB, Nikolskaya ED, Yabbarov NG, Zenin VA, Faustova MR, Belov AV, Zhunina OA, Mollaev MD, Zabolotsky AI, Tereshchenko OG, Severin ES. Development of novel PLGA nanoparticles with co-encapsulation of docetaxel and abiraterone acetate for a highly efficient delivery into tumor cells. J. Biomed. Mater. Res. B Appl. Biomater. 2019;107:1150-1158.

Song Z, Shi Y, Han Q, Dai G. Endothelial growth factor receptor-targeted and reactive oxygen species-responsive lung cancer therapy by docetaxel and resveratrol encapsulated lipid-polymer hybrid nanoparticles. Biomed. Pharmacother. 2018;105:18-26.

Takata Y, Xiang YB, Yang G, Li H, Gao J, Cai H, Gao YT, Zheng W, Shu XO. Intakes of fruits, vegetables, and related vitamins and lung cancer risk: results from the Shanghai Men's Health Study (2002–2009). Nutr. Cancer 2013;65:51-61.

Takeda M, Nakagawa K. Role of EGFR monoclonal antibodies in the management of non–small cell lung cancer. Curr. Cancer Drug Targets 2015;15:792-802.

Tang X, Wang G, Shi R, Jiang K, Meng L, Ren H, Wu J, Hu Y. Enhanced tolerance and antitumor efficacy by docetaxel-loaded albumin nanoparticles. Drug Del. 2016;23:2686-2696.

Thandra KC, Barsouk A, Saginala K, Aluru JS, Barsouk A. Epidemiology of lung cancer. Contemp. Oncol. (Pozn.) 2021;25:45-52.

Thomas A, Rajan A, Giaccone G. Tyrosine kinase inhibitors in lung cancer. Hematol. Oncol. Clin. North Am. 2012;26:589-605.

Tian H, Zhang T, Qin S, Huang Z, Zhou L, Shi J, Nice EC, Xie N, Huang C, Shen Z. Enhancing the therapeutic efficacy of nanoparticles for cancer treatment using versatile targeted strategies. J. Hematol. Oncol. 2022;15:1-40.

Townsend MH, Anderson MD, Weagel EG, Velazquez EJ, Weber KS, Robison RA, O'Neill KL. Non-small-cell lung cancer cell lines A549 and NCI-H460 express hypoxanthine guanine phosphoribosyltransferase on the plasma membrane. Onco Targets Ther. 2017;10:1921-1932.

Vinod SK, Hau E. Radiotherapy treatment for lung cancer: Current status and future directions. Respirology 2020;25:61-71.

Wang S, Gou J, Wang Y, Tan X, Zhao L, Jin X, Tang X. Synergistic antitumor efficacy mediated by liposomal co-delivery of polymeric micelles of vinorelbine and cisplatin in non-small cell lung cancer. Int. J. Nanomedicine 2021;16:2357-2372.

Wang Y, Guo M, Lin D, Liang D, Zhao L, Zhao R, Wang Y. Docetaxel-loaded exosomes for targeting non-small cell lung cancer: preparation and evaluation in vitro and in vivo. Drug Deliv. 2021;28:1510-1523.

Wang Y, Zuo A, Huang X, Ying Y, Shu X, Chen X, Yang Y, Ma J, Lin G, Wang X, Mei L. Docetaxel-loaded PAMAM-based poly (γ-benzyl-l-glutamate)-bd-α-tocopheryl

polyethylene glycol 1000 succinate nanoparticles in human breast cancer and human cervical cancer therapy. J. Microencapsul. 2019;36:552-565.

Wang Z, Xing Y, Li B, Li X, Liu B, Wang Y. Molecular pathways, resistance mechanisms and targeted interventions in non-small-cell lung cancer. Mol. Biomed. 2022;3:42.

Wathoni N, Puluhulawa LE, Joni IM, Muchtaridi M, Mohammed AF, Elamin KM, Milanda T, Gozali D. Monoclonal antibody as a targeting mediator for nanoparticle targeted delivery system for lung cancer. Drug Deliv. 2022;29:2959-2970.

Wieduwilt MJ, Moasser M. The epidermal growth factor receptor family: biology driving targeted therapeutics. Cell. Mol. Life Sci. 2008;65:1566-1584.

Wistuba II, Gazdar AF. Characteristic genetic alterations in lung cancer. Lung Cancer: Volume 1: Molecular Pathology Methods and Reviews. 2003:3-28.

Xu Y, Kim CS, Saylor DM, Koo D. Polymer degradation and drug delivery in PLGA- based drug–polymer applications: A review of experiments and theories. J. Biomed. Mater. Res. B Appl. Biomater. 2017;105:1692-1716.

Xue Y, Wang L, Zhang Y, Zhao Y, Liu Y. Air pollution: A culprit of lung cancer. J. Hazard. Mater. 2022;434:128937.

Yao L, Xu S. Force-induced selective dissociation of noncovalent antibody–antigen bonds. J. Phys. Chem. B 2012;116:9944-9948.

Yao Y, Zhou Y, Liu L, Xu Y, Chen Q, Wang Y, Wu S, Deng Y, Zhang J, Shao A. Nanoparticle-based drug delivery in cancer therapy and its role in overcoming drug resistance. Front. Mol. Biosci. 2020;7:193.

Yetisgin AA, Cetinel S, Zuvin M, Kosar A, Kutlu O. Therapeutic nanoparticles and their targeted delivery applications. Molecules 2020;25:2193.

Yu BO, Tai HC, Xue W, Lee LJ, Lee RJ. Receptor-targeted nanocarriers for therapeutic delivery to cancer. Mol. Membr. Biol. 2010;27:286-298.

Yuan M, Huang LL, Chen JH, Wu J, Xu Q. The emerging treatment landscape of targeted therapy in non-small-cell lung cancer. Signal Transduct. Target Ther. 2019;4:61.

Zappa C, Mousa SA. Non-small cell lung cancer: current treatment and future advances. Transl. Lung Cancer Res. 2016;5:288-300.

Zeb A, Ullah F. A simple spectrophotometric method for the determination of thiobarbituric acid reactive substances in fried fast foods. J. Anal. Methods Chem. 2016;2016:1-5.

Zhang L, Zhang N. How nanotechnology can enhance docetaxel therapy. Int. J. Nanomedicine 2013;8:2927-2941.

Zhang M, Hagan IV CT, Foley H, Tian X, Yang F, Au KM, Mi Y, Medik Y, Roche K, Wagner K, Rodgers Z. Co-delivery of etoposide and cisplatin in dual-drug loaded nanoparticles synergistically improves chemoradiotherapy in non-small cell lung cancer models. Acta Biomater. 2021;124:327-335.

Zhang W, Chen Y, Wang B, Feng X, Zhang L, Liu S. Facile preparation of paclitaxel nano-suspensions to treat lung cancer. J. Biomater. Tissue Eng. 2022;12:690-694.

Zhang X, Liu J, Li X, Li F, Lee RJ, Sun F, Li Y, Liu Z, Teng L. Trastuzumab-coated nanoparticles loaded with docetaxel for breast cancer therapy. Dose-Response 2019;17:1559325819872583.

Zhao J, Zhuo M, Wang Z, Duan J, Wang Y, Wang S, An T, Wu M, Wang J. A phase I study of nimotuzumab plus docetaxel in chemotherapy-refractory/resistant patients with advanced non-small-cell lung cancer. Chin. J. Cancer Res. 2016;28:12-18.

Zhao T, Qin S, Li P, Feng T, Wan J, Yuan P, Zhang L. Novel hyaluronic acid-modified temperature-sensitive nanoparticles for synergistic chemo-photothermal therapy. Carbohydr. Polym. 2019;214:221-233.

Ref. No. P-1|RS|81|16

Date: 23.02.2016
~~62.03~~

To
Sm. Leena Kumari,
'SHYAMALAYA'
Arya Kanya Saroni,
Murgasol, Asansol,
West Bengal,
Pin code: 713303

Dear Sir/ Madam,

I am pleased to inform you that you have been selected **Junior Research Fellow** to work in the DST PURSE -II Programme in the PHARMACEUTICAL TECHNOLOGY Department, Jadavpur University.
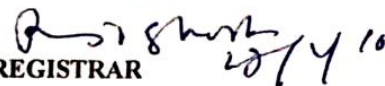
You will be paid a fellowship of **Rs.25,000/-** with admissible allowances as per DST rules. The tenure of your fellowship is two years from the date of joining. You are required to be present in the department on a regular basis during University hours to assist in the on-going projects of the department under DST PURSE -II Programme. The fellowship will be paid to you only on production of Attendance- cum- work certificate as per rules.

Your service will be governed by the same terms and conditions as may be applicable to the temporary staff of the University and you will be under the administrative control of the undersigned.

You are requested to join the post within ten days from the date of receipt of this letter and submit your joining report in duplicate through proper channel to the undersigned with a declaration stating that you are not a recipient of any emoluments from any other source from the date of your joining the Fellowship.

The duplicate copy of this appointment letter duly signed by you should also be submitted at the time of joining the Fellowship.

Yours faithfully,

REGISTRAR

Declaration and Undertaking

I do hereby declare that I am fully aware of the above-noted terms and conditions mentioned in the appointment letter towards the post of JRF in the Pharmacy Department, JU purely on temporary basis. I understand that I shall not be part of permanent staff and my appointment is co-terminus with the necessity of the Department and as such all the rights and privileges of permanent staff shall not be available to me on my joining the post.

I agree to accept the above terms and conditions of service.

I shall report for duty in the forenoon of ....16.03.2016..................................

Name & Signature   *LEENA KUMARI*

দূরভাষ : ২৪১৪-৬৬৬৬/৬১৯৪/৬৬৪৩/৬৪৯৫/৬৪৪৩
দূরবাণী : (৯১)-০৩৩-২৪১৪-৬৪১৪/২৪১৩-৭১২১

Website : www.jadavpur.edu
E-mail : registrar@admin.jdvu.ac.in

Phone : 2414-6666/6194/6643/6495/6443
Fax : (91)-033-2414-6414/2413-7121

ACK. No.: 111536/2K17/1
FILE No. : 09/096 (0928)/2018-EMR-I

Dated: 26-4-2018

LEENA KUMARI
C/O-PROF BISWAJIT MUKHERJEE
PHARMACEUTICS RESEARCH LABORATORY,
2ND FLOOR, DEPARTMENT OF
PHARMACEUTICAL TECHNOLOGY, JADAVPUR
UNIVERSITY, 188, RAJA SC MALLICK
ROAD,KOLKATA-700032, WEST BENGAL,
INDIA NA
KOLKATA-700032

Award Letter

Sir/Madam,

With reference to your application and subsequent interview, I am happy to inform you that you have been selected for the award on the terms and conditions (as mentioned in the Hindi Version). The award will be effective from the date mentioned above or from the date of joining research **whichever is later.** The duration of CSIR SRF, ▓▓▓▓▓▓▓ and Research Associate is as mentioned in the Hindi version. This award letter is valid only for the institute as given in the table of Hindi version of the award letter. If any recipient of the fellowship/associateship joins in an institute other than the one given in the Hindi Version of the award letter, this award letter will automatically be deemed cancelled.

Any further extension is at the discretion of CSIR, based on a three member Assessment Committee Report & Annual Progress Report. A copy of Terms & Conditions of CSIR Fellowship/ Associateship is available on HRDG website (http://www.csirhrdg.res.in). In case, the terms & conditions are acceptable to you, you may join the Fellowship/Associateship within the validity period under intimation to this office.

The Director General, CSIR has also been pleased to sanction the Stipend and Contingency as stated above. In addition to Stipend & Contingency, House Rent Allowance will be payable as per rules of the host Institute. In no case, it will exceed the rates payable to Central Govt. employees.

Please note that the validity of the award is for **six months** only from the effective date of award.

The award of CSIR Fellowship / Associateship does not imply any assurance or guarantee to subsequent employment by CSIR.

Yours faithfully,

SECTION OFFICER
(011-25842074)

Copy to :- Jadavpur University, Kolkata -700032
1. Registrar/Principal/Director, with the request to send the following documents to this office.
(A) Joining Report in the enclosed prescribed from.
(B) Undertaking in the enclosed prescribed form.
2. Sr. F&AO (EMR). The expenditure will be debitable to the Budget Head 'P-81-101'.
3. Bill File.
4. Office Copy.

- P.T.O.-

* You are kindly advised to visit the HRDG (CSIR) website (www.csirhrdg.res.in) for rules/regulations governing the CSIR fellowship/associateship. You are also advised to submit Annual Progress Report alongwith other requisite documents well in time. Noncompliance of CSIR norms for submission of annual progress report alongwith other requisite documents within six months after completion of yearly tenure may result in termination of fellowship/associateship.

Institutional Animal Ethics Committee (IAEC)

Department of Pharmaceutical Technology

Jadavpur University

Kolkata-700032
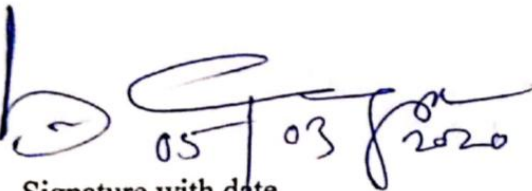
Ref No: AEC/PHARM/1704/05/2020   Date: 05.03.2020

This is to certify that Project title **"Site-specific targeting of biodegradable polymeric nanoparticles for the treatment of lung cancer:** *an in vitro and in vivo* **approach"** has been approved by the Institutional Animal Ethical Committee (IAEC), Jadavpur University in the meeting held on 3rd March, 2020.

Prof. (Dr.) Biswajit Mukherjee

Chairman/Member Secretary IAEC

Signature with date

The NEW ENGLAND
JOURNAL of MEDICINE

Permissions

About NEJM

Submit Your Permission Request Using RightsLink

If you are seeking permission to copy, reproduce, or republish content from the *New England Journal of Medicine* (NEJM) and you are not the author of the content, you may use the Copyright Clearance Center's RightsLink® service. Simply visit NEJM.org and locate the article or video from which you seek to reuse content.

Once you have located and accessed the article you are looking for on NEJM.org:
- Click on the Permissions link © in the toolbar to the left of the article.
- The RightsLink window will pop up with information about the content you have selected.
- Follow the prompts to select the options that best suit your needs.
- The system will either provide you with an immediate price quote or direct your request to the NEJM Permissions Department for further processing through the RightsLink interface.

If you are the author of an article that has been published in NEJM, see **Author Permissions**.

> Note: All commercial reuse examples discussed in section above also apply to authors of NEJM Group manuscripts that are employed by industry and distributing/exposing content on behalf of their employers.

Reuse of Content Within a Thesis or Dissertation

Content (full-text or portions thereof) may be used in print and electronic versions of a dissertation or thesis without formal permission from the Massachusetts Medical Society (MMS), Publisher of the *New England Journal of Medicine*.

> The following credit line must be printed along with the copyrighted material:
>
> Reproduced with permission from (scientific reference citation), Copyright Massachusetts Medical Society.

Third-Party Content

Grants of permissions apply only to copyrighted materials that the MMS owns and not to copyrighted texts or illustrations from other sources.

Prohibited Uses

The *New England Journal of Medicine* (and its logo design) are registered trademarks of the Massachusetts Medical Society. NEJM does not grant permission for its logo, cover, or brand identity to be used in materials. Permission will not be granted for photographs depicting identifiable individuals.

ELSEVIER LICENSE
TERMS AND CONDITIONS

Jul 09, 2023

This Agreement between Department of Pharmaceutical Technology, Jadavpur University, Kolkata, India -- Leena Kumari ("You") and Elsevier ("Elsevier") consists of your license details and the terms and conditions provided by Elsevier and Copyright Clearance Center.

License Number	5584660607766
License date	Jul 09, 2023
Licensed Content Publisher	Elsevier
Licensed Content Publication	Journal of Drug Delivery Science and Technology
Licensed Content Title	Docetaxel: An update on its molecular mechanisms, therapeutic trajectory and nanotechnology in the treatment of breast, lung and prostate cancer
Licensed Content Author	Mohammad Imran,Sadaf Saleem,Aiswarya Chaudhuri,Javed Ali,Sanjula Baboota
Licensed Content Date	Dec 1, 2020
Licensed Content Volume	60
Licensed Content Issue	n/a
Licensed Content Pages	1
Start Page	101959
End Page	
Type of Use	reuse in a thesis/dissertation

Portion	figures/tables/illustrations
Number of figures/tables/illustrations	1
Format	both print and electronic
Are you the author of this Elsevier article?	No
Will you be translating?	No
Title	Fabrication of a Biodegradable Polymeric Nanostructural Carrier Mediated Target Specific Drug Delivery System for the Treatment of Lung Cancer
Institution name	Department of Pharmaceutical Technology, Jadavpur University, Kolkata, India
Expected presentation date	Aug 2023
Portions	Figure 3
Requestor Location	Department of Pharmaceutical Technology, Jadavpur University, Kolkata, India Department of Pharmaceutical Technology, Jadavpur University, Kolkata, India Kolkata, 700032 India Attn: Department of Pharmaceutical Technology, Jadavpur University, Kolkata, India
Publisher Tax ID	GB 494 6272 12
Billing Type	Invoice
Billing Address	Department of Pharmaceutical Technology, Jadavpur University, Kolkata, India Department of Pharmaceutical Technology, Jadavpur University, Kolkata, India Kolkata, India 700032 Attn: Department of Pharmaceutical Technology, Jadavpur University, Kolkata, India

JOHN WILEY AND SONS LICENSE
TERMS AND CONDITIONS

Jul 09, 2023

This Agreement between Department of Pharmaceutical Technology, Jadavpur University, Kolkata, India -- Leena Kumari ("You") and John Wiley and Sons ("John Wiley and Sons") consists of your license details and the terms and conditions provided by John Wiley and Sons and Copyright Clearance Center.

License Number	5584660962498
License date	Jul 09, 2023
Licensed Content Publisher	John Wiley and Sons
Licensed Content Publication	Advanced Healthcare Materials
Licensed Content Title	Nanotechnology: Breaking the Current Treatment Limits of Lung Cancer
Licensed Content Author	Ying Liu, Yang Liu, Yongfu Ma, et al
Licensed Content Date	May 21, 2021
Licensed Content Volume	10
Licensed Content Issue	12
Licensed Content Pages	18
Type of use	Dissertation/Thesis

Requestor type	University/Academic
Format	Print and electronic
Portion	Figure/table
Number of figures/tables	1
Will you be translating?	No
Title	Fabrication of a Biodegradable Polymeric Nanostructural Carrier Mediated Target Specific Drug Delivery System for the Treatment of Lung Cancer
Institution name	Department of Pharmaceutical Technology, Jadavpur University, Kolkata, India
Expected presentation date	Aug 2023
Portions	Figure 1
Requestor Location	Department of Pharmaceutical Technology, Jadavpur University, Kolkata, India Department of Pharmaceutical Technology, Jadavpur University, Kolkata, India Kolkata, 700032 India Attn: Department of Pharmaceutical Technology, Jadavpur University, Kolkata, India
Publisher Tax ID	EU826007151
Billing Type	Invoice
Billing Address	Department of Pharmaceutical Technology, Jadavpur University, Kolkata, India Department of Pharmaceutical Technology, Jadavpur University, Kolkata, India Kolkata, India 700032

ELSEVIER LICENSE
TERMS AND CONDITIONS

Jul 09, 2023

This Agreement between Department of Pharmaceutical Technology, Jadavpur University, Kolkata, India -- Leena Kumari ("You") and Elsevier ("Elsevier") consists of your license details and the terms and conditions provided by Elsevier and Copyright Clearance Center.

License Number	5584670442420
License date	Jul 09, 2023
Licensed Content Publisher	Elsevier
Licensed Content Publication	Urologic Oncology: Seminars and Original Investigations
Licensed Content Title	New frontiers in nanotechnology for cancer treatment
Licensed Content Author	Frank Alexis,June-Wha Rhee,Jerome P. Richie,Aleksandar F. Radovic-Moreno,Robert Langer,Omid C. Farokhzad
Licensed Content Date	January–February 2008
Licensed Content Volume	26
Licensed Content Issue	1
Licensed Content Pages	12
Start Page	74
End Page	85
Type of Use	reuse in a thesis/dissertation

Portion	figures/tables/illustrations
Number of figures/tables/illustrations	1
Format	both print and electronic
Are you the author of this Elsevier article?	No
Will you be translating?	No
Title	Fabrication of a Biodegradable Polymeric Nanostructural Carrier Mediated Target Specific Drug Delivery System for the Treatment of Lung Cancer
Institution name	Department of Pharmaceutical Technology, Jadavpur University, Kolkata, India
Expected presentation date	Aug 2023
Portions	Figure 1
Requestor Location	Department of Pharmaceutical Technology, Jadavpur University, Kolkata, India Department of Pharmaceutical Technology, Jadavpur University, Kolkata, India Kolkata, 700032 India Attn: Department of Pharmaceutical Technology, Jadavpur University, Kolkata, India
Publisher Tax ID	GB 494 6272 12
Billing Type	Invoice
Billing Address	Department of Pharmaceutical Technology, Jadavpur University, Kolkata, India Department of Pharmaceutical Technology, Jadavpur University, Kolkata, India Kolkata, India 700032 Attn: Department of Pharmaceutical Technology, Jadavpur University, Kolkata, India

Taylor & Francis
Taylor & Francis Group

Check for updates

RESEARCH ARTICLE

Cetuximab-conjugated PLGA nanoparticles as a prospective targeting therapeutics for non-small cell lung cancer

Leena Kumari[a], Iman Ehsan[a], Arunima Mondal[b], Ashique Al Hoque[a], Biswajit Mukherjee[a], Pritha Choudhury[c], Arunima Sengupta[b], Ramkrishna Sen[a] and Prasanta Ghosh[a]

[a]Department of Pharmaceutical Technology, Jadavpur University, Kolkata, India; [b]Department of Life Science and Biotechnology, Jadavpur University, Kolkata, India; [c]Department of Cardiovascular and Metabolic Sciences, Lerner Research Institute, Cleveland Clinic, Ohio, USA

ABSTRACT

Non-small cell lung cancer (NSCLC) is one of the most prevalent cancers diagnosed worldwide, yet managing it is still challenging. The epidermal growth factor receptor (EGFR) exhibits aberrant signalling in a wide range of human cancers, and it is reported to overexpress in most NSCLC cases. The monoclonal antibody [Cetuximab (Cet)] was conjugated onto the surface of the poly (lactide-co-glycolide) (PLGA) nanoparticles which were loaded with docetaxel (DTX) for the development of targeted therapy against lung cancer. This site-specific delivery system exhibited an enhanced cellular uptake in lung cancer cells which overexpress EGFR (A549 and NCI-H23). The nanoparticles also showed better therapeutic effectiveness against NSCLC cells, as evidenced by reduced IC_{50} values, cell cycle arrest at the G2/M phase, and increased apoptosis. The improved efficacy and *in vivo* tolerance of Cet-DTX NPs were demonstrated in benzo(a)pyrene (BaP)-induced lung cancer mice model. Histopathological analysis showed that intravenous injection of Cet-DTX NP to mice carrying lung cancer greatly reduced tumour development and proliferation. Comparing Cet-DTX NP to free drug and unconjugated nanoparticles, it also had negligible side effects and improved survival rates. Therefore, Cet-DTX NPs present a promising active targeting carrier for lung tumour-NSCLC-selective treatment.

GRAPHICAL ABSTRACT
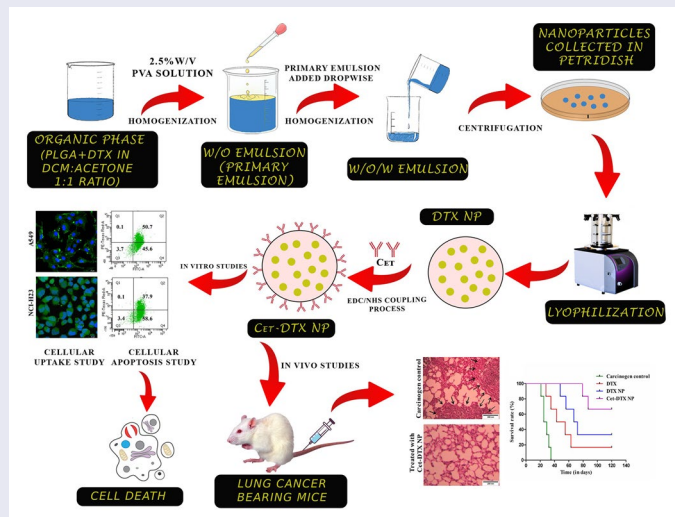
Introduction

Non-small cell lung cancer (NSCLC), which makes up more than 80% of all lung cancer cases, is still the most common cancer-related fatality globally. NSCLC is responsible for approximately a quarter of all cancer fatalities, outnumbering colon, breast, and prostate cancers [1]. Treatment of NSCLC patients with surgery and chemotherapy is hampered by late diagnosis. Furthermore, the lack of tumour selectivity in these techniques leads to increased toxicity in patients, limiting the therapeutic efficacy [2]. Platinum drugs, taxanes including paclitaxel (PTX) and docetaxel (DTX), albumin-bound PTX, and other types of chemotherapy are all suggested for NSCLC. Among the taxane groups, DTX is quite effective for a wide spectrum of cancers. It has been shown to block microtubule depolymerisation of free tubulin in preclinical experiments in a range of murine malignancies and human tumour xenografts, including NSCLC [3].

In NSCLC, the epidermal growth factor receptor (EGFR) is a popular target. It belongs to the family of receptor tyrosine kinases, which stimulates several signalling pathways to encourage growth of cells, cellular proliferation, and survival [4]. The EGFR gene can be upregulated or can become oncogenicly active, which results in uncontrolled development and tumour progression. It is already reported in the literature that in case of normal cells, the expression of EGFR is estimated to be from 40,000 to 100,000 receptors per cell, whereas overexpression of more than 10^6 receptors per cell is observed in the cancer cells [5]. Between 40% and 80% of adenocarcinoma demonstrates EGFR overexpression, and lung cancer patients have an activating mutation in the EGFR gene [6]. Targeting lung tumours with EGFR expression can be an important strategy because EGFR expression is often low in most organs (such as benign tumour nodules). Numerous drugs that target the EGFR pathway have been developed. They include small molecule tyrosine kinase inhibitors, (such as afatinib, gefitinib, and erlotinib) and EGFR-inhibiting antibodies [e.g. cetuximab (Cet)], in light of the fact that EGFR plays such an important role in lung adenocarcinoma [4]. Anti-EGFR humanised monoclonal antibody, Cetuximab (Cet), blocks binding of activating ligands to EGFR and prevents the downstream signalling of EGFR-dependent growth and survival to provide anti-tumour activity [7–9]. Cet binding to EGFR causes membrane clearance, internalisation and EGFR degradation for signal termination [10–12].

The limitations of a conventional chemotherapy for the treatment of NSCLC can be efficiently overcome by using site-specific targeted drug delivery. Nanotechnology has made significant progress in early detection and preventive bio-imaging, multifunctional medicines, and drug delivery system. During the last few decades, nanoparticles for cancer chemotherapy are gaining popularity. Enhanced permeability and the retention effect of the cancerous tumours make the tumour accumulation of NP feasible [13]. In order to conjugate ligands onto the surface of nanoparticles, the 1-ethyl-3-[3-dimethylaminopropyl] carbodiimide hydrochloride/N-hydroxysuccinimide (EDC/NHS) coupling process is one of the highly efficient techniques. It is commonly used to attach a variety of DNA or antibodies to the nanoparticles. Several studies have shown that the anti-EGFR monoclonal antibody cetuximab can be conjugated to nanoparticles, allowing the drug-loaded nanoparticles to be delivered specifically to lung cancer cells [14,15].

This research work focuses on developing antibody-conjugated nanoparticles (Cet-DTX NP) with site-specific targeting that can provide clear therapeutic benefits against lung tumours. We have synthesised DTX-loaded Poly (D, L-lactide-co-glycolide) (PLGA) nanoparticles conjugated with anti-EGFR antibody (Cet) using EDC/NHS coupling chemistry for lung tumour-specific nanoparticle accumulation in an experimental mouse model. Cet is already identified as a predictive marker against EGFR-targeted site-specific delivery [9,10]. PLGA is a biodegradable polymer for human use, and the potency of DTX is already established. We tried to focus on *in vivo* results to prove the intended use of our formulation, which affirmed our hypothesis as the drug reached the affected tissues with an increased and sustained availability, with enhanced antitumor efficacy against lung non-small cell adenocarcinoma.

Materials and methods

Materials

Docetaxel (DTX) with 99.95% purity was obtained from Fresenius Kabi Oncology Ltd., Kolkata, India. Acid-terminated PLGA {poly (lactide-co-glycolide) ratio 75:25, MW 4,000–15,000}, fluorescein isothiocyanate (FITC), 3-(4, 5-dimers dimethylthiazol-2-yl)-2,

5-diphenyltetrazolium bromide (MTT dye), and benzo(a)pyrene (BaP) were purchased from Sigma-Aldrich Co., St Louis, MO, USA. Polyvinyl alcohol (M.W. 1,25,000) was bought from SD Fine-Chemicals Limited, Mumbai, India. Cetuximab monoclonal antibody (Cet) was procured from Ideal Chemicals, Kolkata, West Bengal. N-hydroxysuccinimide (NHS) and 1-(3-dimethylaminopropyl)-3-ethyl carbodiimidehydrochloride (EDC) were purchased from Himedia Laboratories (Mumbai, Maharashtra, India). Two different human lung cancer cells (A549 and NCI-H23), and a normal human lung epithelial cell line (L-132) were obtained from the National Centre for Cell Science (NCCS), Pune, India. Cells were maintained in Dulbecco's Modified Eagle Medium (DMEM) and Roswell Park Memorial Institute Medium (RPMI 1640) (Hi-Media). 4',6' Diamidino-2-phenylindole (DAPI) dye, other culture media, foetal bovine serum (FBS), and other associated constituents for *in vitro* cell culture were obtained from Thermo Fisher Scientific, Waltham, USA. All additional reagents/chemicals procured/used were of analytical or molecular biology grade and were further used without any other purification. All aqueous solutions were prepared using Milli-Q water (18 M-cm) from a Millipore Gradient Milli-Q water system.

Swiss albino male mice (20-25 g) were obtained from the National Institute of Nutrition, Hyderabad, India, and all the animal studies followed the protocol of the Animal Ethics Committee (AEC), Jadavpur University, Kolkata, India.

Drug excipients interaction study

To ascertain whether there was any interaction between the drug and the chosen excipients, Fourier transforms infra-red (FTIR) spectroscopy was employed. Each sample (5 mg) was mixed at a 1:100 ratio with IR grade KBr and punched to form pellets. An FTIR instrument (Magna-IR 750, Series II, Nicolet Instruments Inc, Madison, Wisconsin, USA) was then used to scan the pellets in the wavelength range of 4000-400 cm^{-1}. For the analysis, DTX, PLGA, PVA, PVA-PLGA mixture, a physical mixture of PLGA, PVA, and DTX, Blank NP, DTX NP, and Cet-DTX NP were chosen.

Preparation and physicochemical characterisation of the PLGA nanoparticles

DTX-loaded PLGA nanoparticles and blank (without drug) nanoparticles were prepared by the multiple emulsion solvent evaporation technique as per previously reported methods [16,17]. The resultant lyophilised nanoparticles was further conjugated with Cet monoclonal antibody using N-hydroxysuccinimide (NHS) and 1-(3-dimethylaminopropyl)-3-ethylcarbodiimide hydrochloride (EDC) coupling chemistry [18,19]. The preparation and conjugation of the experimental formulations and their physicochemical characterisations are elaborately described in the Supplementary file.

SDS-PAGE

The conjugation of antibodies on the surface of DTX NP was verified using SDS-PAGE. DTX, Cet-DTX, and Blank nanoparticles were resuspended in PBS at a concentration of 0.2 mg/ml, and standard anti-EGFR monoclonal antibody (Cet) was mixed individually with 2X Laemmli gel loading buffer (each 5 μL) at a concentration of 1 μL from the primary stock. DTX NP, Cet-DTX NP, and Blank NP were put onto a 10% SDS-PAGE gel along with the marker. Gel electrophoresis was carried out by running the gel (80V up to stacking and 100V up to resolving) [18,20].

In vitro drug release study

The *in vitro* drug release study was performed for Cet-DTX NP on various buffers, such as phosphate buffer saline (PBS) (pH 7.4) with 0.1% w/v tween 80, citrate buffer (pH 3), acetate buffer (pH 5) and bicarbonate buffer (pH 10). Cet-DTX NP was prepared as a suspension in various buffers (1 mg/ml, 2 ml) separately and was shaken at 37 °C in an incubator shaker (Somax Incubator Shaker; Shenjhen Pango Electronic Co. Ltd., Shenzhen, China). At various intervals (0.5 h, 1 h, 2 h, 4 h, 8 h, 24 h, 48 h, 96 h, 168 h, 336 h, 504 h, and 672 h), the suspension (1 ml) was withdrawn from the vials, centrifuged, and the supernatant samples were examined for drug content using a UV-visible spectrophotometer at 229 nm [21]. The centrifuged pellet after each sample withdrawal was re-dispersed, adding 1 ml of freshly prepared buffer before being replaced into the vial. The drug release curve was created as cumulative percent drug release vs. time graph. To understand the release profile of DTX from Cet-DTX NP, various kinetic models, including zero order, first order, Higuchi, Hixson-Crowell, and Korsmeyer-Peppas models, were utilised [22].

Stability study

The effect of temperature and humidity on the experimental nanoparticles was examined through an accelerated stability study. The nanoformulations were kept in Zone-III temperature conditions (30 °C, 75% RH and 40 °C, 75% RH) and also at the refrigerated condition (4-8 °C) and were withdrawn at different time points (at 30 days and 90 days), according to the International Conference on Harmonisation (ICH) guidelines (2003), after which the FESEM analysis and drug content were analysed.

Additionally, in citrate buffer pH 3, acetate buffer pH 5, PBS pH 7.4, and bicarbonate buffer pH 10, the hydrolytic breakdown of nanoparticles was compared [21]. The supplementary file describes in detail the methods of accelerated stability study and hydrolytic study.

Detection of mRNA by RT-PCR

RNA extraction and isolation was done by the Trizol technique. Manufacturer's instructions were followed for cDNA synthesis kit to transcribe the cDNA (Biogenomics Asia). The Rotorgene Real-Time PCR System was used to examine the expression levels of EGFR and the reference gene, glyceraldehyde-3-phosphase dehydrogenase (GAPDH), in each cDNA sample (Qiagen, Germany). Procedure is mentioned in the supplementary section along with details of the specific primers are mentioned in the Table S1 [23].

ELISA method for dissociation constant (K$_D$) determination

The dissociation constant (K$_D$) of Cet with EGFR overexpressed on the lung cancer cells (A549 and NCI-H23) was determined by cell based ELISA method, as per the protocol described in supplementary section [24,25].

In vitro cytotoxicity assay

To assess the growth inhibitory capacity or the cytotoxicity of free DTX, DTX NP, and Cet-DTX NP, the 3-[4,5-dimethylthiazol-2-yl]-3,5-diphenyl tetrazolium bromide (MTT) assay was used in human lung cancer cells (A549 and NCI-H23) and normal lung cells (L-132). The absorbance ratio between the cells treated with nanoparticles and untreated control cells was used to assess the proportion of viable cells in each well [26,27]. The supplementary file contains a detailed explanation of the MTT assay methodology.

In vitro cellular uptake study

Using A549 and NCI-H23 cells, confocal laser microscopy was used to study the intracellular uptake of FITC-labeled DTX NP and Cet-DTX NP *in vitro* and to quantify it using flow cytometry. A 35 mm tissue culture dish with medium and approximately 10^4 cells were sown on a cover slip and cultured at 37 °C overnight for confocal laser imaging. Both the cells received the IC$_{50}$ concentration of FITC-labeled Cet-DTX NP at 1 h and 4 h. The cells were rinsed in PBS after the treatment, fixed in 70% ethanol, co-stained with DAPI (for the nucleus), and mounted on a slide for observation under a confocal microscope (Olympus FluoView FV10i, Olympus). Dual-color pictures were taken using the FITC (Ex/Em 495/519 nm) and DAPI (Ex/Em 359/461 nm) filters [28].

The time-dependent intracellular absorption of PLGA nanoparticles was assessed using flow cytometry. Briefly, 10^6 A549 and NCI-H23 cells were grown in complete media for 24 h. The medium from each plate was replaced by an incomplete medium and the treatment was conducted for 1 h, 2 h and 4 h. The cells, except the control group, were then exposed to FITC-loaded nanoparticles. Once the treatment was finished, the cells were taken from the plates and suspended in FACS tubes for analysis in a flow cytometer (BD LSRFortessaTM, BD Biosciences, San Jose, USA). FACS Diva software (BD Biosciences) was used to collect the data [22].

In vitro cellular apoptosis study

Apoptosis assay was conducted using a standard methodology to quantitatively assess the capacity of DTX/DTX NP/Cet-DTX NP to induce apoptosis and/or necrosis in A549 and NCI-H23 cells. Briefly, the cells (2.5×10^5/ml) were cultured for 48 h at 37 °C in an atmosphere with 5% CO$_2$ and the IC$_{50}$ concentration of the free drug and the formulations. Cells in the control group did not receive any treatment. Following the completion of the treatment period, the cells were detached using trypsin, cleaned with PBS (2X), and resuspended in 100 µL of Annexin V binding buffer (1X) (10 mM HEPES, 140 mM NaCl, 2.5 mM CaCl$_2$; pH 7.4). An additional 400 µL of binding buffer (1X) was added after adding 2 µL of annexin V-FITC to the cell suspension and incubating it in the dark for 15 min. Before analysis, propidium iodide (PI) (5 µL, 50 µg/ml) was added [29]. Data were obtained using a FACS Aria flow cytometer (Becton Dickinson, USA) using channels of FITC (excitation/emission 488 nm/530 nm), and PE-Texas red (excitation/emission 561 nm/616 nm) and post-capturing analysis was done with BD FACS Diva software (Becton Dickinson, USA) [30].

In vitro cell cycle analysis

The effect on the cell cycle of DTX/DTX NP/Cet-DTX NP was examined using the methodology described in the literature [31,32]. In a 12-well plate, 1×10^6 cells were seeded each well, and the plate was placed in a CO$_2$ incubator overnight. After being treated with the free drug and various experimental formulations, cell cycle phase analysis of nuclear DNA stained with PI was measured in a flow cytometer (Becton Dickinson FACS Fortessa 4 laser cytometer equipped with BD FACS Diva software).

Haemolysis study

The haemolytic studies were conducted using the previously described methodology, with a few alterations [33,34]. The freshly drawn blood from male Swiss albino mice was placed in heparinised tubes and centrifuged at 4 °C for 5 min at 1000 g. The

erythrocytes were rinsed three times with PBS after removing the supernatant (pH 7.4). The resulting suspension (2%) was employed for a haemolysis study. A 96-well plate with 190 μL of the suspension in each well was then treated with 10 μL of the free drug (DTX) and experimental nanoparticles (DTX NP and Cet-DTX NP) (containing DTX at varying concentrations, such as 0.5, 1, 2.5, 10, 15, 30, 50, 100, and 150 nM) to assess the haemolytic effect. The unlysed erythrocytes were separated by centrifugation at 10,000 g for 5 min after incubating at 37 °C for 1 h with gentle stirring. The optical density (OD) of the supernatant was then measured at 570 nm. By utilising the procedure to compute the absorbance factor of a sample that was 100% haemolytic, the percentage of haemolysis was determined:

$$Haemolysis(\%) = \frac{(Abs - Abs_0)}{Abs_{100} - Abs_0} \times 100 \qquad (1)$$

where Abs, Abs_0, and Abs_{100}, respectively, represent the absorbance of samples, a solution with 0% and 100% haemolysis, respectively.

Maximum tolerated dose (MTD)

Mice were administered DTX NPs, Cet-DTX NPs, and free DTX, and their *in vivo* tolerance to each treatment was compared. Male Swiss albino mice were randomly divided into six groups (n = 6). DTX NPs and Cet-DTX NPs were injected into 0.9% saline solution at dosages of 2.5, 5, 10, 20, and 40 mg/kg (corresponding to groups i, ii, iii, iv, and v, respectively). Free DTX was dissolved in Tween 80 and 13% w/w ethanol in water at a ratio of 1:3 w/w to produce groups vi, vii, viii, ix, and x at DTX dosages of 2.5, 5, 10, and 40 mg/kg, respectively. The mice were given intravenous injections through tail vein on days 7, 14, 21, and 28. They were weighed before every injection and again on the first, second, third, fourth, fifth, sixth, seventh, and eighth weeks. Blood samples were collected, and they were allowed to stand without anticoagulant for 30 min. The blood samples were centrifuged at 2,500 rpm for 10 min before the serum was extracted. After 28 days, an automated clinical analyser was used to measure and analyse the different biochemical parameters of liver and kidney, including SGOT, SGPT, ALP, urea, and creatinine, in accordance with the manufacturer's instructions (AU400, Olympus, Tokyo, Japan). The dose that resulted in a 20% weight loss was identified as the MTD [35–37].

Pharmacokinetic study in normal mice

Pharmacokinetic parameters of plasma and lung were analysed in Swiss albino male normal mice (body weight 25-30 g) upon free DTX (10 mg/kg), DTX NP, and Cet-DTX NP (having an equivalent amount of DTX) i.v. administration. The treated animals were sacrificed at specific time points (0.5, 1, 2, 4, 6, 8, 10, 24, 48, and 72 h). The blood and the lung were collected. Tandem liquid chromatography and mass spectrophotometry (LC–MS/MS) was utilised to analyse the drug content in the separated plasma and the lung as per protocol. Paclitaxel was used as an internal standard.

In vivo pharmacokinetic studies of DTX NP, Cet-DTX NP and aqueous suspension containing free DTX were done in Swiss albino male mice (body weight 25-30 g). Three groups of the animals (n = 20 per group) were formed. Aqueous suspensions of free DTX, DTX NP, and Cet-DTX NP were injected intravenously into the animals in groups 1, 2, and 3 at doses of 10 mg DTX/ kg body weight, respectively. At each time point, two mice were sacrificed, blood was probed, and plasma was collected. The same was done for lungs also. At specified intervals (0.5, 1, 2, 4, 6, 8, 10, 24, 48, and 72 h post injection), the blood and lungs were collected in heparinised tubes, and the plasma was separated by centrifuging the tubes at 10,000 rpm for 10 mins at 4 °C. Each 0.1 ml of plasma sample was mixed with 1 ml of ice-cold acetonitrile-methanol mixture and vortexed. The clear supernatant that was obtained after centrifugation was mixed with 100 μL of water and loaded into LC-MS/MS (LC: Shimadzu Model 20AC, MS: AB-SCIEX, Model: API4000), using software: Analyst 1.6. Analytes were eluted using YMC Triat C18 column (30 × 2.1 mm, 5 μ) and gradient elution technique of two mobile phases (mobile phase A: 0.1% formic acid in water and mobile phase B: 0.1% formic acid in methanol:acetonitrile:water (45:45:10)) was conducted with an injection volume 20 μL, flow rate 0.8 ml/min and total run time 3.0 min [19,38,39].

Experimental animal model for in vivo anti-tumour efficacy

The Swiss albino mice used for the study were separated in five groups consisting of six mice in group. Group I served as normal control with oral administration of corn oil for four weeks. Group II animals were treated with benzo(a)pyrene (B(a) P, 50 mg/kg body weight dissolved in corn oil orally) weekly twice for 4 weeks, to induce lung cancer by 16th week, which served as carcinogen control. Group III animals were treated with DTX control for 4 weeks after they were administered with first dose of B(a)P. Group IV and Group V animals were treated with DTX NP and Cet-DTX NP (i.v., 10 mg DTX/kg body weight) for 4 weeks after they were treated with the first dose of B(a) P. Groups III, IV and V animals continued to receive the same treatment of B(a)P as received by group II animals. Administration dose of Cet with nanoparticles was 101.84 μg/mg of nanoparticle conjugate (Cet-DTX NP). Food and water was available *ad libitum*. During the study, the body weights were measured every week.

In vivo biodistribution study

The biodistribution study was conducted in B(a)P induced lung cancer mice model after injecting free DTX, DTX NP and Cet-DTX NP at predetermined time points. Elaborated protocol is described in the supplementary section [40].

Survival time of mice

The survival analysis of experimental mice was regularly checked up until their mortality. Briefly, six separately treated mice from the carcinogen control and carcinogen treated received formulation treatment groups were allowed to live until natural death without carrying out a required sacrifice. Kaplan-Meier survival analysis was used to calculate the mean survival time (MST). GraphPad Prism Software was used to conduct the statistical analysis [37].

Caspase-3 activity

A single i.v. bolus injection of DTX/DTX NP/Cet-DTX NP at a concentration equivalent to their respective IC_{50} values was administered to the various experimental animals. Lung tissues from various animal groups were removed after 24 h of treatment, collected, and processed for protein separation using RIPA buffer (Sigma). Caspase-3 activity was measured in accordance with the

manufacturer's instructions using the caspase-3/7 colorimetric assay kit (Abcam kit no. ab39401) [41,42].

LPO and ROS study

The relative estimation of ROS was examined using a spectrofluorimeter of serum samples taken from the mice of the experimental normal control, carcinogen control, and carcinogen treated mice treated with various treatments. Using the thiobarbituric acid method, the amount of TBARS (thiobarbituric acid reactive substance), a product of lipid peroxidation under stress, was calculated in serum samples from the same experimental groups of mice [43,44].

Lung histopathology analysis

For the fabrication of paraffin-embedded blocks, the lung tissues from the corresponding experimental groups (normal control, carcinogen control, and carcinogen-treated received formulation treatment) were fixed in 10% neutral buffered formalin. To examine tissue architecture and cancer morphology, 5 μm-thick slices were deparaffinized, rehydrated, and stained with haematoxylin and eosin in accordance with the recommended methodology [45]. Zeiss light microscope and Axio Vision software 4.7.1 were used to view the histopathology slides.

Statistical analysis

Each experiment was carried out in triplicate. Student's t-test and one-way ANOVA was used for the statistical analysis, and Graph Pad Prism was used to generate the graphs (version 5, Graph Pad Prism software Inc, San Diego, CA, USA).

Results

Fourier transform infrared spectroscopy (FTIR) analysis

The spectrophotometric investigation detected all the characteristic peaks of DTX and various excipients which were used to formulate DTX NP. No chemical interactions were observed between them (Supplementary Figure 1). N-H stretching at $3490\,cm^{-1}$ and asymmetric and symmetric vibrations at $2947\,cm^{-1}$ for CH_2 revealed for pure DTX. The C=O stretching vibrations of the ester group showed peaks at $1725\,cm^{-1}$, C=N stretching at $1244\,cm^{-1}$, and $1075\,cm^{-1}$ for C=O stretching vibrations, respectively. For C-H in-plane and C-H out-of-plane C-C=O, the peaks were observed at $972\,cm^{-1}$ and $712\,cm^{-1}$, respectively. PLGA displayed characteristic peaks at O-H at $3515\,cm^{-1}$; C-H at $2995\,cm^{-1}$ and C=O at $1756\,cm^{-1}$, respectively.

Weak physicochemical interactions, such as the dipole-induced interaction, weak H-bonds, van der Waals force of attraction, etc., which may play significant roles in the formation of spherical-shaped nanoparticles, were noted in the case of Blank NP and DTX NP,

leading to some minor peak shifting of the formulation components. In the spectrum of the physical mixture (PLGA, PVA, and DTX) and DTX NP, the intensity of $712\,cm^{-1}$ peak is attributed to the entrapment of DTX over blank NP.

Preparation and characterisation of nanoparticles

Our formulation developed and optimised the drug-polymer ratio to develop DTX-loaded PLGA nanoparticles. Physicochemical characterisations such as the size, zeta potential, and polydispersity index (PDI) values of the prepared NP, along with its drug loading and encapsulation efficiency, are mentioned in Table 1. The above data showed that the optimised DTX NP showed maximum drug loading, greater entrapment efficiency, smaller particle size, and greater zeta potential values. The physicochemical characterisation of the optimised formulation DTX NP and Cet-DTX NP was carried out. It was found that the particle size of DTX NP and Cet-DTX NPs was $225 \pm 3\,nm$ and $283 \pm 2\,nm$, respectively. The zeta potential value of DTX NP and Cet-DTX NPs was $-8.18 \pm 0.50\,mV$ and $-12.1 \pm 0.43\,mV$, respectively (Supplementary Figure 2). The PDI value of DTX NP was 0.589 ± 0.06, while for Cet-DTX NP, the value was 0.486 ± 0.08. The drug loading and encapsulation efficiency for DTX NP was 6.43% ± 0.25% and 70.76% ± 2.76%, respectively. In the case of Cet-DTX NP, the drug loading and encapsulation efficiency were found to be $5.86 \pm 0.35\%$ and 64.53% ±1.38%, respectively (Table 1). In our research study, DTX was the chemotherapeutic drug, which showed anti-cancer efficacy against lung cancer cells. Cet antibody was conjugated onto the surface of our nanoparticles at a very low dose. It was used as a ligand to target our nanoparticles to the EGFR overexpressed lung cancer cells. Therefore, drug loading and encapsulation efficiency were determined for DTX and not for Cet antibody.

We have developed formulations by varying the drug content with respect to the polymer content. Enhancement of drug content increased the size of the particles. Drug entrapment towards the core, and within and between the polymeric chains reduced the cohesiveness of the polymeric molecules, resulting in an increased size of the particles. Further, surface conjugation of Cetuximab (Cet) obviously enhanced the size of the particles as reflected in the data (Table 1). Increasing drug content reduced the zeta potential of the polymeric nanoparticles. Free –COOH group of PLGA present on the surface of the particles causes negative zeta potential. More drug content might reduce the availability of free –COOH groups on the surface, causing reduction in zeta potential values. Further, conjugation of Cet antibody on the surface of the polymeric nanoparticles increased the zeta potential, as each molecule of Cet antibody contains additional free –COOH groups.

The surface morphology was analysed for Cet-DTX NP by Field emission scanning electron microscopy (FESEM) study (Figure 1A). The figure revealed that Cet-DTX NPs had the majority of spherical structure and were densely distributed. Utilising TEM analysis, the internal morphology of Cet-DTX NP was confirmed (Figure 1B). The figure revealed that the drug was evenly and homogeneously distributed throughout the particles.

Table 1. Physicochemical characterisation and optimisation data of various experimental nanoparticles by varying drug: polymer ratio.

Formulation	Drug: PLGA	Particle size (Z-average) (nm)[a]	Zeta potential (mV)[a]	Polydispersity index[a]	Drug loading (%)[a]	Encapsulation efficiency (%)[a]
DTX NP (optimised formulation)	1:10	225 ± 3	−8.18 ± 0.50	0.589 ± 0.06	6.43% ± 0.25%	70.76% ± 2.76%
Cet-DTX NP (optimised formulation with antibody conjugation)	1:10	283 ± 2	−12.10 ± 0.43	0.486 ± 0.08	5.86% ± 0.35%	64.53% ± 1.38%
DTX NP 1	2:10	400 ± 2	−5.10 ± 0.47	0.663 ± 0.06	5.06% ± 0.05%	55.73% ± 0.50%
DTX NP 2	3:10	456 ± 2	−4.40 ± 0.29	0.609 ± 0.04	4.72% ± 0.07%	51.92% ± 0.78%

Note: DTX NP, PLGA nanoparticles encapsulating docetaxel; Cet-DTX NP, Antibody conjugated PLGA nanoparticle encapsulating docetaxel; PLGA, poly (lactide-co-glycolide); PVA, poly vinyl alcohol.
[a] Each value represents mean ± SD ($n = 3$).

SDS-PAGE

We functionalised the surface of nanoparticles by conjugating the Cet antibody against EGFR receptors which are generally overexpressed on the surface of lung cancer cells. The SDS-PAGE was run for both the DTX NP and Cet-DTX NP compared to the free antibody (Figure 1C). It was demonstrated that the nanoparticles were conjugated well with the antibody and the antibody-conjugated particles ran slightly slowly, as compared to free antibody. It has demonstrated the effective conjugation of antibodies onto the

surface of DTX NP nanoparticles, which moved more slowly than free antibodies due to the attachment to heavier nanoparticles. However, the lack of antibodies on the surface of the DTX NP failed to produce any bands.

Energy dispersive X-ray (EDX) study

The EDX study for blank NP, DTX NP, and Cet-DTX NP was carried out during FESEM analysis. Nitrogen in the case of DTX NP and
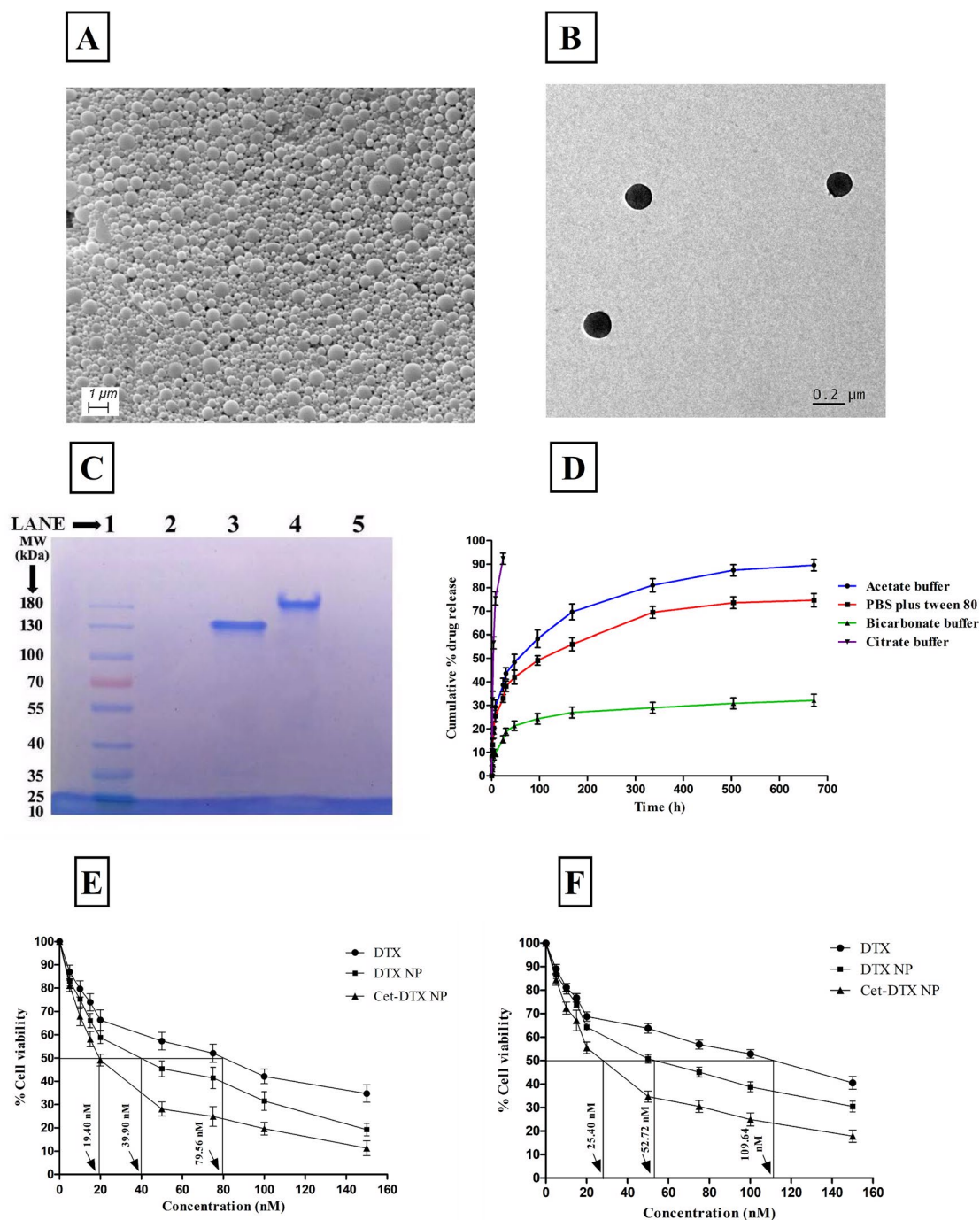
Figure 1. Morphological study of Cet-DTX NP. (A) Field emission scanning electron microscopy; (B) Transmission electron microscopy; (C) SDS-PAGE gel electrophoresis, Lane 1 represents protein marker, and lane 2 showed unconjugated NP, lane 3 shows the standard anti-EGFR monoclonal antibody (Cet), lane 4 represents antibody conjugated NP, lane 5 showed blank NP; (D) *In vitro* drug release profile of DTX from Cet-DTX NP in phosphate buffer saline (PBS), pH 7.4, with tween 80, citrate buffer (pH 3), acetate buffer (pH 5), and bicarbonate buffer (pH 10). Data show mean ± SD ($n = 3$); *In vitro* cytotoxicity assay of DTX, DTX NP, and Cet-DTX NP on (E) A549 and (F) NCI-H23 lung cancer cells. Data show the mean ± SD of three individual experiments.

its absence in the case of blank NP indicated the presence/lack of nitrogen of DTX in the two corresponding formulations. A high weight percentage of sulphur (2.02%) in the case of Cet-DTX NP affirms the conjugation of the Cet to Cet-DTX NP (Table S2). The other ingredients utilised to create DTX NP are devoid of sulphur. Because of the amide bond between the Cet and DTX NP, the Cet-DTX NP had a slightly greater weight percentage contribution from N (19.18%), which further supports the presence of Cet.

In vitro drug release study

The different buffers and release media (citrate buffer pH 3, acetate buffer pH 5, phosphate buffer saline pH 7.4 with 0.1% w/v tween 80, and bicarbonate buffer pH 10) were used for the *in vitro* drug release investigation of Cet-DTX NP (as depicted in Figure 1D). The nanoparticles deteriorated more quickly under an acidic pH, suggesting that rapid drug release (92.31% ± 2.37% in 24 h) in a citrate buffer (pH 3) rendered the formulation unsuitable for oral administration. On the other hand, a slow and sustained release of the drug was seen in PBS with 0.1% w/v tween 80 (pH 7.4) (74.64% ± 2.83%) over the course of 28 days, showing that the produced nanoformulation would be stable in the blood for a prolonged period and would gradually and slowly degrade (since pH 7.4 simulates the environment of blood). The drug was only modestly (89.58% ± 2.47% in 28 days) released from the formulation in an acetate buffer (pH 5.5), implying that the nanoparticles would be stable in circulation and would deliver the drug more effectively in the tumour area, which is often an acidic milieu (pH ~4.5–5.5). The drug release from Cet-DTX NP was lower (32.11% ± 2.59%) in bicarbonate buffer (pH 10). Different regression coefficient (R^2) values for the kinetics were summarised after the drug release data were evaluated using zero-order, first-order, Hixson-Crowell, Korsmeyer-Peppas, and Higuchi kinetic models (Table 2). The R^2 values indicate that, in all buffers and release media, drug release from the formulation adhered to Korsmeyer-Peppas kinetic model, thereby suggesting drug release from the nanoparticles by erosion, followed by slow diffusion from the eroded polymeric matrix. In the case of PBS with 0.1% w/v tween 80, a good linearity ($R^2 = 0.979$) was obtained with a release exponent value (n) of the drug 0.29 for Cet-DTX NP, which suggests drug release followed Fickian diffusion.

Stability study

For the optimised formulation (DTX NP and Cet-DTX NP) in the freeze-dried condition, stability studies were conducted to assess any alterations in the morphology during 3 months period at 4-8 °C

(refrigerated condition), 30 °C, 75% RH, and 40 °C, 75% RH. The stability study was also performed in terms of the changes in surface morphology of Cet-DTX NP by FESEM analysis (Supplementary Figure 3). The nanoformulation stored at 4-8 °C maintained the surface morphology up to 3 months period. However, deformation of the formulation was observed at 30 °C and 40 °C during storage. Very significant changes in the surface morphology of the nanoformulation occurred during storage for 3 months at these temperatures. Any notable changes in the drug content and encapsulation efficiency were not observed in the case of DTX NP (Drug loading 6.25%, encapsulation efficiency 69.44%) and Cet-DTX-NP (Drug loading 5.72%, encapsulation efficiency 62.93%) in the refrigerated condition at 4-8 °C for 3 months (Table S3). Thus, DTX NP and Cet-DTX NP should be stored between 2-8 °C.

Hydrolytic stability

The hydrolytic stability study of the optimised Cet-DTX NP was carried out in different pH media. An enhanced loss in the weight of nanoformulation was observed with the decrease in the pH of media (Supplementary Figure 4). After 4 weeks of the experiment, the weight loss of Cet-DTX NP at pH 10 was 13.60% ± 1.14%, at pH 7.4 was 26.06% ± 1.66%, at pH 5 was 36.70% ± 1.57% and at pH 3 was 57.67% ± 1.56%, respectively.

Detection of mRNA by RT-PCR

The results from RT-PCR study were summarised in Supplementary Figure 5. Our results indicate that lung cancer cell lines (A549 and NCI-H23) have overexpressed EGFR. However, A549 lung cancer cells have shown slightly greater expression than NCI-H23 cells. The Ct-median values of EGFR in both the cells (A549 and NCI-H23) were 17.89, for GAPDH the Ct-median value was 18.56, and for L-132 (normal lung epithelial cell line), the value was ≥35, respectively. The higher Ct-median value of L-132 cells clearly indicates the non-expression of EGFR.

Determination of dissociation constant (K_D) by binding experiment

The results obtained from titration ELISA along with mathematical evaluation demonstrated the interaction of cetuximab with EGFR receptors overexpressed on the lung cancer cells (A549 and NCI-H23) (Supplementary Figure 6). The dissociation constant (K_D) for the binding of cetuximab to the EGFR on A549 cells was 0.32 ± 0.016 nM, whereas cetuximab bound to the EGFR overexpressed on the NCI-H23 cells with a significantly lower affinity of 0.38 ± 0.019 nM.

Table 2. Depiction of *in vitro* drug release tested on different release kinetic models along with corresponding R^2 values and release exponent (n) (Korsmeyer–Peppas model).

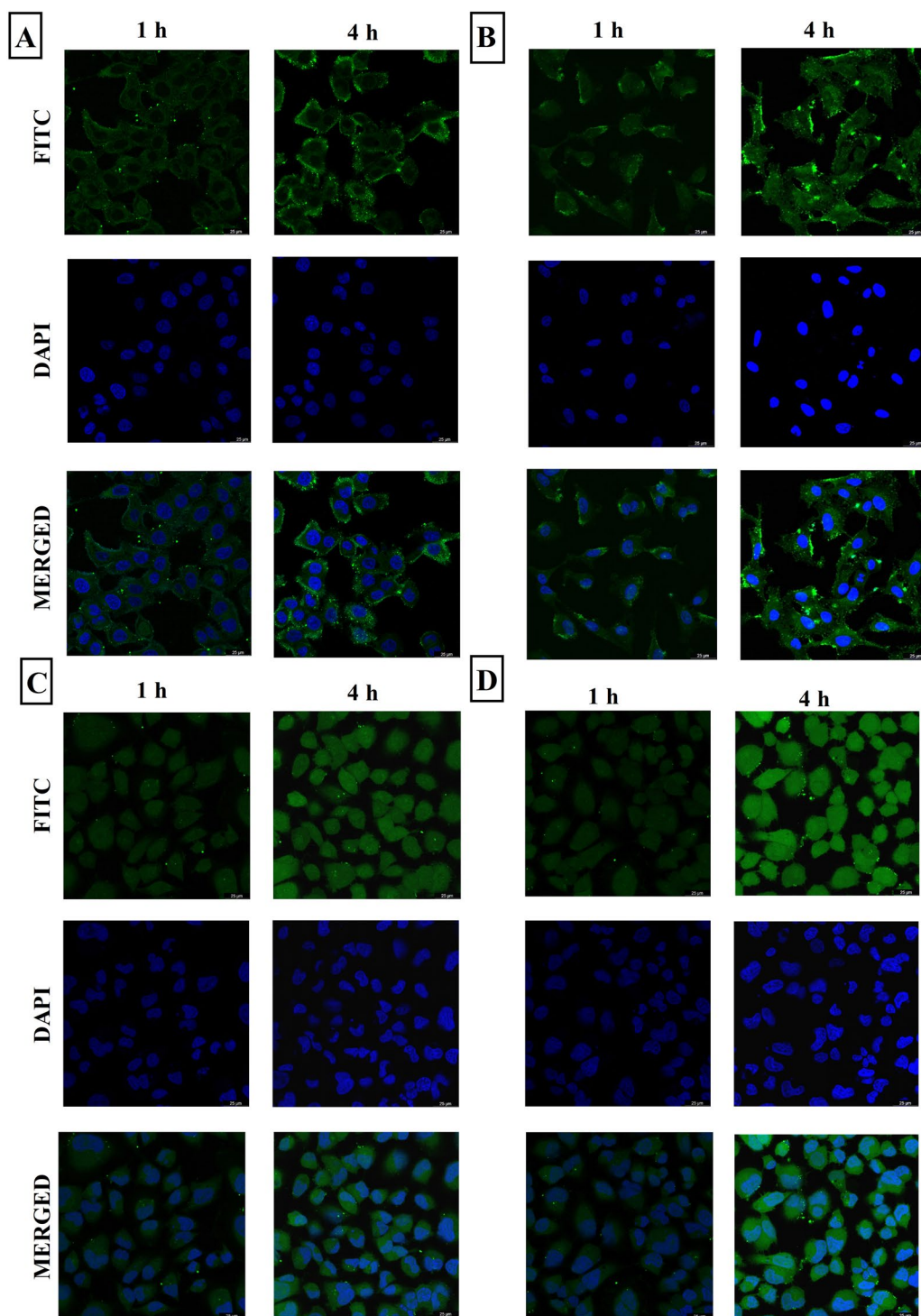| Kinetic models	Cet-DTX NP release in Phosphate buffer saline pH 7.4 (with tween 80)	Cet-DTX NP release in Citrate buffer	Cet-DTX NP release in Acetate buffer	Cet-DTX NP release in Bicarbonate buffer
Zero order	y = 0.098x + 23.33 $R^2 = 0.712$	y = 3.501x + 20.64 $R^2 = 0.727$	y = 0.122x + 25.41 $R^2 = 0.704$	y = 0.041x + 10.58 $R^2 = 0.610$
First order	y = −0.000x + 1.88 $R^2 = 0.850$	y = −0.045x + 1.918 $R^2 = 0.945$	y = −0.001x + 1.87 $R^2 = 0.913$	y = −0.000x + 1.949 $R^2 = 0.651$
Higuchi model	y = 2.799x + 13.73 $R^2 = 0.906$	y = 20.63x + 2.527 $R^2 = 0.917$	y = 3.497x + 13.36 $R^2 = 0.902$	y = 1.223x + 6.186 $R^2 = 0.833$
Korsemeyer-Peppas model	y = 0.296x + 1.091 $R^2 = 0.979$ n = 0.29	y = 0.555x + 1.304 $R^2 = 0.885$ n = 0.55	y = 0.364x + 1.018 $R^2 = 0.943$ n = 0.36	y = 0.334x + 0.664 $R^2 = 0.932$ n = 0.33
Hixson-Crowell model	y = 0.002x + 0.404 $R^2 = 0.808$	y = 0.107x + 0.325 $R^2 = 0.881$	y = 0.003x + 0.445 $R^2 = 0.851$	y = 0.000x + 0.173 $R^2 = 0.637$

Figure 2. Qualitative evaluation of cellular uptake by confocal microscopy for (A) FITC-conjugated DTX NP (1 h and 4 h) in A549 cells, (B) FITC-conjugated Cet-DTX NP (1h and 4 h) in A549 cells, (C) FITC-conjugated DTX NP (1 h and 4 h) in NCI-H23 cells, (D) FITC-conjugated Cet-DTX NP (1 h and 4 h) in NCI-H23 cells.

In vitro cytotoxicity assay

In A549 and NCI-H23 cells, *in vitro* cytotoxicity investigation of free drug, DTX NP, and Cet-DTX NP was conducted. Cet-DTX NP was shown to have an IC_{50} value of 19.40 ± 1.92 nM in A549 cells, which is much less than the IC_{50} values for the DTX (79.56 ± 2.46 nM) and DTX NP (39.90 ± 3.76 nM) (Figure 1E). We also investigated Cet-DTX NP's ability to inhibit the proliferation of the NCI-H23 lung cancer cells. Cet-DTX NP IC_{50} value of 25.40 ± 1.54 nM, was much lower than the IC_{50} values for the DTX (109.64 ± 3.12 nM)

and DTX NP (52.72 ± 2.85 nM) (Figure 1F). Due to the conjugation of antibodies on the surface of nanoparticles, Cet-DTX NP is more target-specific, as compared to DTX NP. The surface modification of Cet-DTX NP led to the greater internalisation of drug loaded nanoparticles into the lung cancer cells and increased apoptosis, as shown by flow cytometer data. Hence, Cet-DTX NP is more effective at a lower concentration (as shown by lower IC_{50} value) than DTX NP. DTX NP and Cet-DTX NP were shown to have very little cytotoxicity when tested against the normal lung epithelial
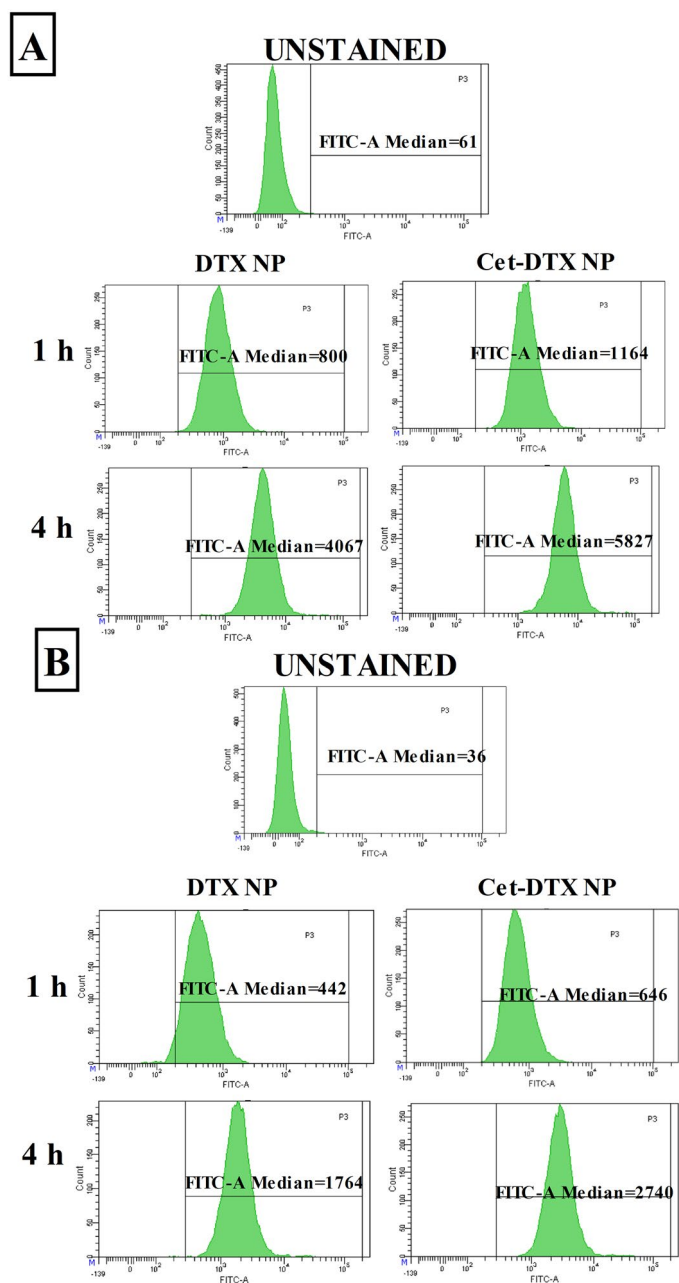
Figure 3. Quantitative estimation of the cellular internalisation by flow cytometry for (A) FITC conjugated DTX NP and Cet-DTX NP for 1 and 4 h in A549 cells, (B) FITC conjugated DTX NP and Cet-DTX NP for 1 and 4 h in NCI-H23 cells.

cell line L-132 (percentage inhibition 8.23 ± 0.79% and 7.21 ± 1.20%, respectively), as compared to free drug (63.72 ± 2.68%) (Table S4). Here for L-132 cells, percentage inhibition data were shown.

Cellular uptake study

In vitro cellular uptake of FITC-conjugated formulations, DTX NP and Cet-DTX NP, was qualitatively evaluated by confocal microscopy. Following 1 h and 4 h incubations with FITC-conjugated DTX NP and Cet-DTX NP, respectively, confocal microscopy images of A549 and NCI-H23 cells were observed (Figure 2A–D). The images showed time-dependent nanoparticle internalisation in both lung cancer cell lines.

The quantification of cellular internalisation of FITC-conjugated Cet-DTX NPs provided a clear-cut differentiation among the uptake pattern of the nanoparticles in terms of FITC mean-median values

which were found to be 800 and 4067 (for DTX NP at 1 h and 4 h, respectively), 1164 and 5827 (for Cet-DTX NP at 1 h and 4 h, respectively) in A549 cells. The FITC mean-median values in the case of NCI-H23 cells were found to be 442 and 1764 (for DTX NP at 1 h and 4 h, respectively), 646 and 2740 (for Cet-DTX NP at 1 h and 4 h, respectively) (Figure 3A and B). Nanoparticle uptake within the cells was accelerated in a time-dependent way. The site-specific targeting ability of Cet-DTX NP to EGFR overexpressed lung cancer cells led to a greater internalisation within the cells (as shown by flow cytometer data), and, therefore, it has higher mean FITC fluorescence values than DTX NP.

Cellular apoptosis study

After being treated with DTX, DTX NPs, and Cet-DTX NPs, lung cancer cells (A549 and NCI-H23) underwent dual staining with Annexin V-FITC and propidium iodide (PI), which was followed by the quantification of apoptotic cells at various stages of apoptosis. A549 cells treated with Cet-DTX NP had apoptotic cell percentages of 50.7% (late apoptotic cells) and 45.6% (early apoptotic cells), whereas NCI-H23 cells treated with the same had apoptotic cell percentages of 58.6% (early apoptotic cells) and 37.9% (late apoptotic cells) (Figure 4A and B). Comparing Cet-DTX NP to DTX NP and free DTX, the results showed that Cet-DTX NP increased more in the cells. Furthermore, a higher level of apoptosis in the FACS histogram of Cet-DTX NP-treated A549 cells and NCI-H23 cells compared to cells treated with DTX NP/free DTX (for 24 h) suggests that Cet-DTX NP is more efficacious to combat EGFR overexpressed lung cancer cells.

Cell cycle analysis

The cell cycle regulatory pathway is crucial to the initiation and development of tumours. The strong binding of DTX causes the mitotic arrest of cancer cells to microtubules and promotes its stability. It is well established that DTX causes cell cycle arrest by chromosomal breakage and mitotic impairment, leading to normal G2/M phase arrest. A decrease in the percentage of cells in the S phase and an accumulation of cells in the G2/M phase was seen in A549 and NCI-H23 cells after treatment with DTX, DTX NP, and Cet-DTX NP. The cells were treated with DTX, DTX-NPs, and Cet-DTX-NPs before incubating for 24 h. The control cells of the A549 and NCI-H23 cell lines were primarily in the G1 phase, with 8% and 9% of them in the G2/M phase (Figure 4C and D). Cet-DTX NP treatment significantly arrested the G2/M phase (39.3% and 36.6% in A549 and NCI-H23 cells, respectively). The results suggest that after the treatment with Cet-DTX NP, the cells were inhibited in interphase (G2/M phase), which promotes the arrest of mitotic cell division. Chromosome damage might be the underlying cause of cell cycle arrest.

Haemolysis study

Cet-DTX NPs were tested for hemocompatibility at various concentrations (5 to 150 nM) (Figure 5A). The nanoformulations (DTX NP and Cet-DTX NP) showed low haemolytic activity (<5%) between 5 and 150 nM. Since the intended formulation's haemolysis rate was within the acceptable range of 5%, which is recognised for biomaterials with safe critical value identified by the International Organisation for Standardization/Technical Report (ISO/TR 7406.46), hence, Cet-DTX NP could be used safely for intravenous administration.
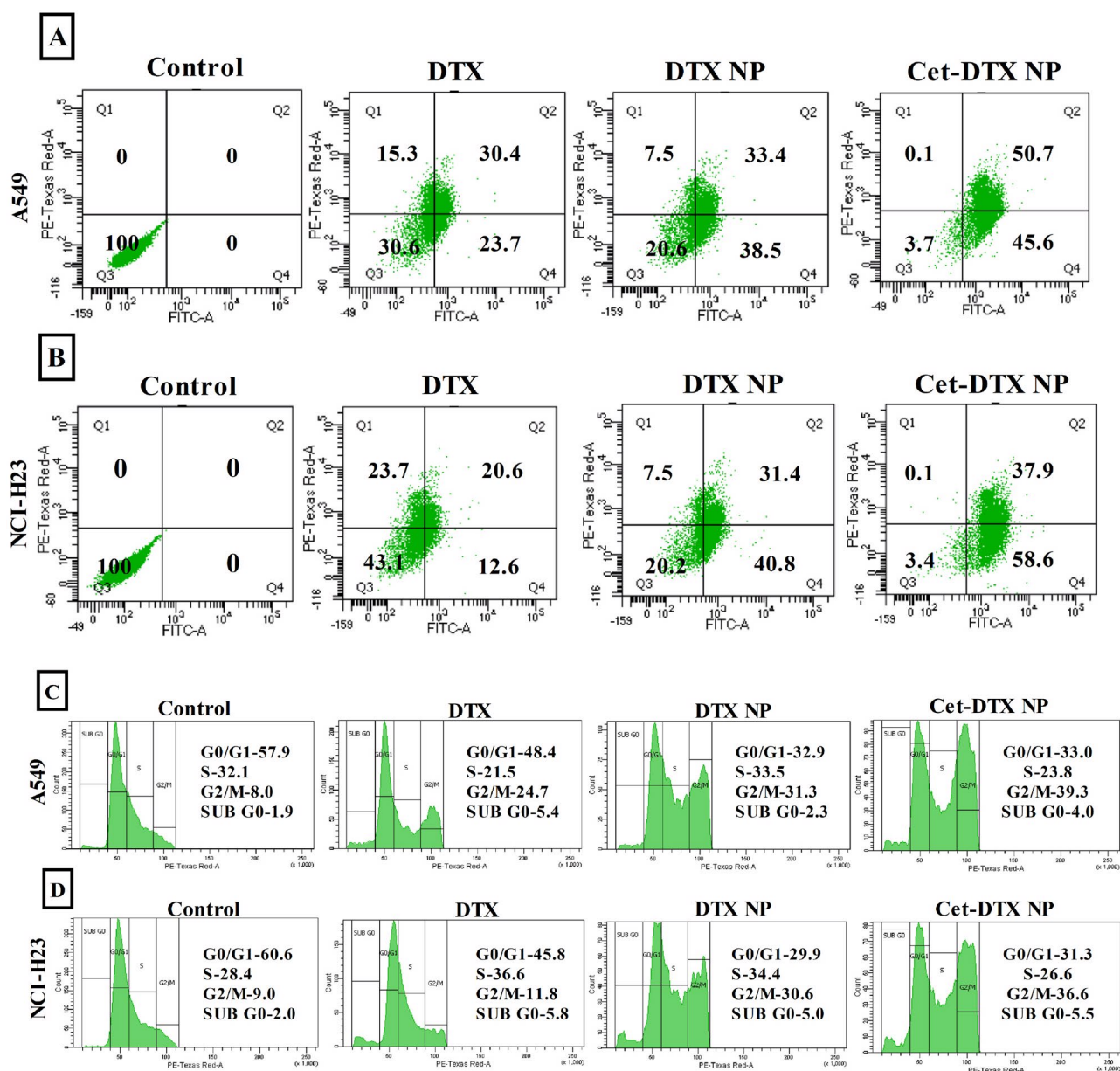
Figure 4. *In vitro* cellular apoptosis study (Annexin V/PI dual staining) in (A) A549 and (B) NCI-H23 lung cancer cells upon treatment with DTX, DTX NP and Cet-DTX NP. Cell cycle analysis by flow cytometry in (C) A549 and (D) NCI-H23 lung cancer cells upon treatment with DTX, DTX NP and Cet-DTX NP.

Maximum tolerated dose (MTD) in normal mice

The liver and kidney are the two crucial organs involved in the body's primary metabolism and excretion, respectively. As a result, aberrant liver and kidney functions are thought to be a sign of clinical symptoms, making the biochemical parameters that regulate the functions of these organs as a promising therapeutic target. The results of this study showed that the liver and kidney toxicity markers, ALP, SGPT, SGOT, urea, and creatinine, of the experimental mice treated with various nanoformulations revealed that levels of toxicity were in the order of DTX > DTX NP > Cet-DTX NP for a maximum dose, 40 mg/kg (Table S5). Moreover, no substantial alterations in the body weight of normal mice treated with DTX NP and Cet-DTX NP were observed up to the dose of 10 mg/kg body weight, as compared to free DTX which showed a marked change in body weight after the dose was increased to 10 mg/kg body weight (Table S6). Comparatively higher toxicity of free DTX, DTX NP, and Cet-DTX NP in normal mice was observed when the dose of the drug was increased from 20 to 40 mg/kg body weight.

In vivo pharmacokinetics study in normal mice

Several pharmacokinetic parameters were examined using LC-MS/MS following intravenous administration of single doses of DTX, DTX NP and Cet-DTX NP (equivalent dose of 10 mg/kg of DTX). When compared to DTX NP/Cet-DTX NP treatment, the initial plasma DTX level was primarily higher for free-DTX treatment (Figure 5B) (Table 3). However, a higher clearance rate indicated that the drug was removed from the body quicker. Drug concentration from free-DTX solution was much lower than that of the nanoformulations (DTX NP/Cet-DTX NP) that remained in the systemic circulation for a longer period of time for at least up to 72 h and released DTX steadily. DTX NP/Cet-DTX NP treatment extended the plasma half-life of DTX and significantly reduced the clearance rate (CL) compared to DTX treatment alone. MRT values provided additional support for the data (Table 3).

Following i.v. treatment of the several nanoformulations, the concentration of DTX in murine lungs with time is shown in Figure 5C. The initial time points had a trend of elevated lung DTX concentrations
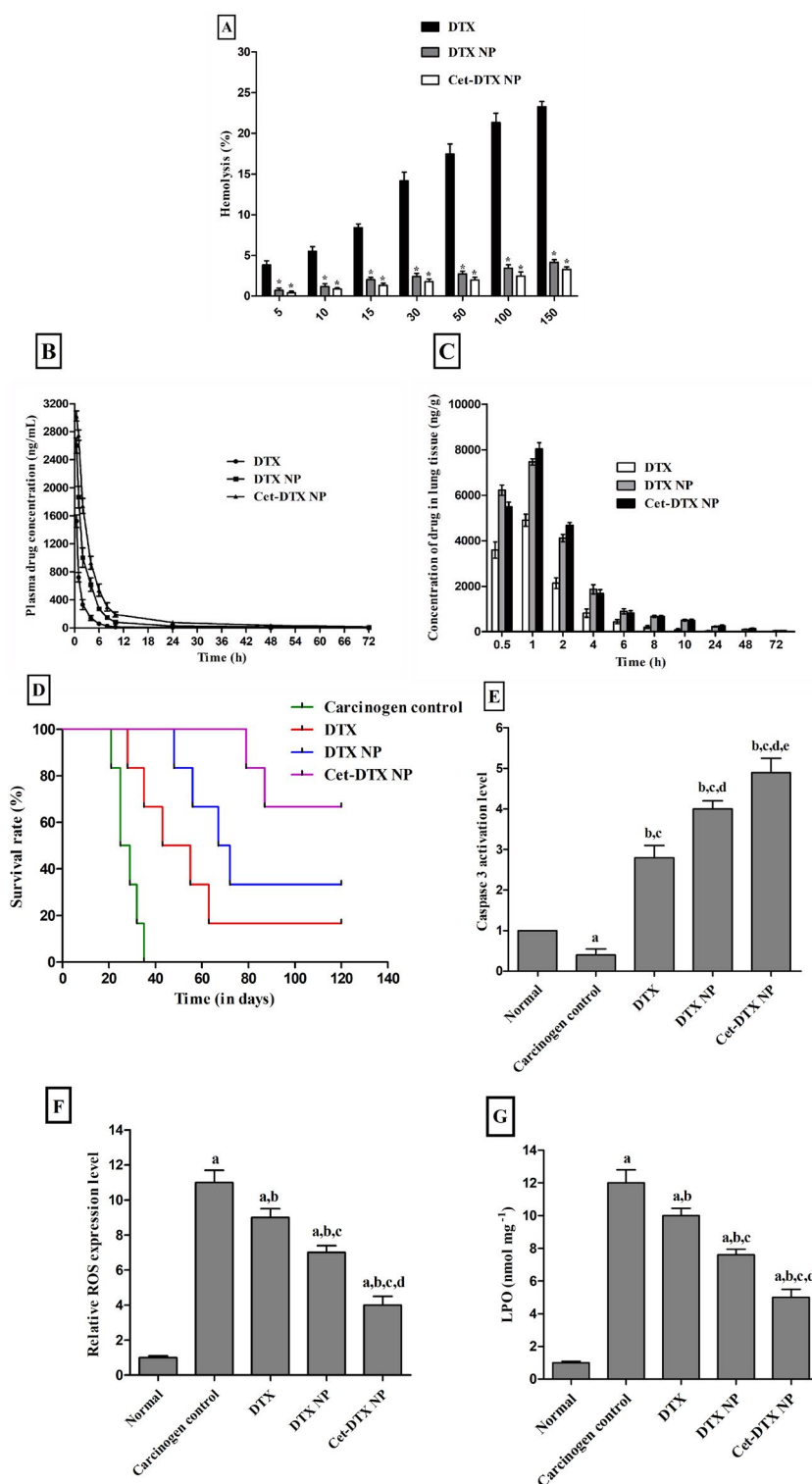
Figure 5. (A) *In vitro* haemolysis study after incubation of RBC with DTX, DTX NP and Cet-DTX NP at a concentration range from 5 nM to 150 nM [*($p < 0.001$) when DTX data were compared with those of DTX NP and Cet-DTX NP], (B) *In vivo* pharmacokinetic study of DTX in plasma upon administration of DTX/DTX NP/Cet-DTX NP by i.v. bolus route in mice, (C) *In vivo* pharmacokinetic study of DTX in the lung after i.v. bolus administration of DTX/DTX NP/Cet-DTX NP in mice, (D) Percentage survival rate of mice after treatment with DTX, DTX NP, Cet-DTX NP and untreated lung carcinogenesis mice model ($p < 0.001$), (E) Comparative caspase 3 activation level in blood of normal and experimental mice [[a]($p < 0.05$) when normal control group is compared with the carcinogen control group, [b]($p < 0.001$) when normal control group is compared with those of DTX, DTX NP and Cet-DTX NP groups, [c]($p < 0.001$) when carcinogen control group is compared with those of DTX, DTX NP and Cet-DTX NP group, [d]($p < 0.001$) when DTX group is compared with those of DTX NP and Cet-DTX NP groups, [e]($p < 0.001$) when DTX NP group is compared with the Cet-DTX NP group], (F) Changes in the level of Reactive oxygen species (ROS) in the *in vivo* lung carcinogenesis mice model after treatment with DTX, DTX NP and Cet-DTX NP [[a]($p < 0.05$) when normal control group is compared with the carcinogen control, DTX, DTX NP and Cet-DTX NP groups, [b]($p < 0.05$) when carcinogen control group is compared with those of DTX, DTX NP and Cet-DTX NP group, [c]($p < 0.05$) when DTX group is compared with those of DTX NP and Cet-DTX NP groups, [d]($p < 0.05$) when DTX NP group is compared with the Cet-DTX NP group], (G) Lipid peroxidation (LPO) in the *in vivo* lung carcinogenesis mice model after treatment with DTX, DTX NP and Cet-DTX NP [[a]($p < 0.05$) when normal control group is compared with the carcinogen control, DTX, DTX NP and Cet-DTX NP groups, [b]($p < 0.05$) when carcinogen control group is compared with those of DTX, DTX NP and Cet-DTX NP group, [c]($p < 0.05$) when DTX group is compared with those of DTX NP and Cet-DTX NP groups, [d]($p < 0.05$) when DTX NP group is compared with the Cet-DTX NP group]. The values are represented as mean ± SD ($n = 6$).

Table 3. Plasma and lung pharmacokinetic parameters of DTX released from DTX-suspension, DTX NP, and Cet-DTX NP after the intravenous bolus administration with an equivalent amount of drug in Swiss albino mice.

Pharmacokinetic parameters of Drug (Docetaxel)	Plasma profile			Lung profile		
	Upon DTX administration*	Upon DTX NP administration*	Upon Cet-DTX NP administration*	Upon DTX administration*	Upon DTX NP administration*	Upon Cet-DTX NP administration*
$t_{1/2}$ (h)	6.31 ± 2.53	16.73 ± 1.63^a	20.56 ± 6.18^a	8.309 ± 1.24	20.44 ± 2.34^a	21.71 ± 2.28^a
AUC_{0-t} (ng/mL.h)	3230.12 ± 282.16	8793.91 ± 1280.57^a	$14565 \pm 2499.34^{a,b}$	13853.92 ± 2134.064	34590.17 ± 1856.18^a	36113.42 ± 780.46^a
$AUC_{0-\infty}$ (ng/mL.h)	3280.13 ± 296.57	8913.9 ± 1329.97^a	$15031.8 \pm 2605.79^{a,b}$	13976.82 ± 2214.40	35933.34 ± 2217.57^a	37793.69 ± 639.76^a
$AUMC_{0-\infty}$ (ng/mL.h^2)	8016.74 ± 1993.09	67657.5 ± 21614.7^a	$179114 \pm 50908.7^{a,b}$	59599.11 ± 24121.26	493364.4 ± 67421.51^a	584522.9 ± 20019.27^a
$MRT_{0-\infty}$ (h)	2.43 ± 0.51	7.47 ± 1.30^a	$11.804 \pm 1.81^{a,b}$	4.16 ± 1.002	13.69 ± 1.007^a	15.46 ± 0.33^a
C_L (L/h/kg)	3.06 ± 28	1.13 ± 0.17^a	$0.67 \pm 0.11^{a,b}$	0.72 ± 0.10	0.28 ± 0.02^a	0.23 ± 0.02^a

NB: $t_{1/2}$, half-life; AUC_{0-t}, area under the plasma concentration–time curve from time 0 to time of last measurable concentration; $AUC_{0-\infty}$, under the plasma concentration–time curve from time 0 to infinity; $AUMC_{0-\infty}$, area under the first moment curve from time 0 to infinity; MRT, mean resident time; CL, clearance.
*Data show mean $\pm$ SD ($n = 6$).
[a]($p < 0.05$) The pharmacokinetics data of treatment of DTX group was compared with DTX NP treatment group and DTX treatment group was compared with Cet-DTX NP treatment group.
[b]($p < 0.05$) The pharmacokinetic data of DTX NP and Cet-DTX NP groups were compared.

(i.e. up to 2h). Later, from time point 4 to 72h, DTX levels demonstrated a considerable decline. Table 3 lists the DTX pharmacokinetic parameters in mouse lung and plasma following i.v. bolus injection of free drug and different formulations.

In vivo biodistribution study

The *in vivo* biodistribution study was carried out in various vital organs (whole blood, liver, kidney, heart, muscle and cancerous lung) after 4h, 24h, 48h and 72h of treatment with free DTX and the different experimental nanoformulations (DTX NP and Cet-DTX NP) (Supplementary Figure 7). The drug content in each organ was determined by LC-MS/MS. The concentration of free DTX in tumours was very less after 4h, and was almost negligible after 24h post treatment. In contrast, the DTX concentration of DTX NP and Cet-DTX NP groups was much more elevated in cancerous lung, as compared to free DTX group. It was demonstrated that free DTX accumulated more in kidney and heart, as compared to blood, liver and muscles. On the other hand, after 72h, very limited amount of Cet-DTX NP was accumulated in blood, liver, kidney, heart and muscles.

Survival time of mice

A Kaplan Meier curve was utilised to study the data in terms of animal survival (Figure 5D). All the experimental animals belonging to the carcinogen control group died within 35days post-treatment. However, a gradual increase in the survival rate was observed upon treatment with the drug and different nanoformulations in the order: DTX < DTX NP < Cet-DTX NP. A significantly higher proportion of animals survived after the treatment with Cet-DTX NP (~67%), in comparison to the animals treated with DTX NP (~33%) and free DTX (~16.67%), at 120th-day post-treatment.

Caspase-3 activity

Due to its role in the proteolytic cleavage of numerous vital proteins, caspase-3 is a crucial apoptosis biomarker. After the DTX/DTX NP/Cet-DTX NP treatment for 24h, the degree of caspase-3 expression in lung homogenates was assessed using a colorimetric test. Compared to the normal control and carcinogen control mice, the investigation showed that the lung homogenates of mice exposed to Cet-DTX NP had higher caspase-3 expression levels than free DTX and DTX NP (Figure 5E).

LPO and ROS study

Different lung tissues of experimental animals were examined for LPO and ROS levels. Compared to normal control animals, carcinogen control mice had considerably higher levels of ROS (Figure 5F) and LPO (Figure 5G). However, following treatment with DTX, DTX NP, and Cet-DTX NP, the LPO and ROS levels decreased towards the normal group.

Lung histopathology analysis

To evaluate histological alterations following therapy in BaP-challenged mice, the lungs were isolated 4weeks after free DTX, DTX NP, and Cet-DTX NP administration. The lung tissues in the control group had a typical structure and showed no histological changes. The BaP group demonstrated severe stroma hemorrhagia, pulmonary oedema, mass inflammatory cell infiltrations, and alveolar collapse, which were critically damaging to the lung. The tumours in the lung were composed of large cells with eosinophilic cytoplasm. Nonetheless, the treatment with free DTX showed marginal improvement in the damaged lung. Upon treatment with nanoformulations (DTX NP and Cet-DTX NP, equivalent to 10mg/kg body weight of DTX), deterioration of the lung's structural integrity was effectively reduced in Cet-DTX NP treated mice more than DTX NP-treated mice (Figure 6A–E).

Discussion

The utilisation of tumour-specific ligands like antibodies on the surface of the nanoparticles against specific receptors for successful drug targeting at the tumour site is well known [46]. Non-small-cell lung cancer (NSCLC) has elevated levels of EGFR. The cancer type has been linked to a worse prognosis, poor tumour differentiation, greater rates of lymph node metastases, and enhanced tumour proliferation [47]. Therefore, antibody-conjugated nanoparticles equipped with covalently bonded Cet antibody against EGFR to target cancerous lung cells have been produced here to provide a formulation competent to transport the drug for the affected cellular target.

Due to the remarkable anti-proliferative properties of DTX, PLGA nanoparticles were prepared in this research to increase the drug's potential for utilisation in cancer treatment. FTIR analysis showed minor shifting of the drug's non-typical peaks in drug encapsulated formulation (DTX NP), which might be attributed to physical interactions through bond formations such as electrical forces like van der Waals forces and dipole moments, as well as weak hydrogen bond formation. However, the presence of all characteristic peaks of DTX in DTX NP suggests the chemical integrity of DTX inside the nanoformulation.

The EDC/NHS coupling chemistry successfully conjugated the Cet antibody with the surface of the PLGA NP [18]. The surface
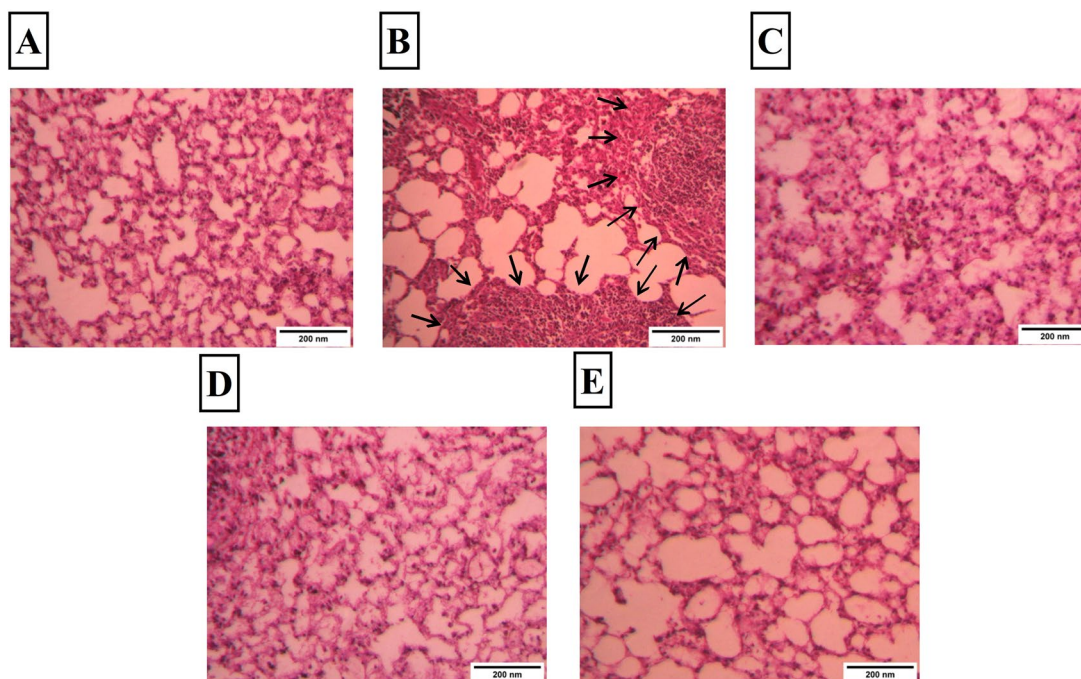
Figure 6. Histological sections (in 10× magnifications) of lungs of experimental mice. Microscopic images of lung section of (A) normal mice, (B) carcinogen control mice, arrowheads show solid tumour areas, (C) carcinogen-treated mice with DTX, (D) carcinogen-treated mice with DTX NP, (E) carcinogen-treated mice with Cet-DTX NP.

morphology of the synthesised nanoparticles is of utmost significance since it interacts with the biological membranes before getting absorbed. The nanoformulations had a smooth surface, spherical shape free of aggregation, and homogeneous drug distribution. Cet-DTX NPs must be stored as lyophilised powder and reconstituted in the dispersed form before use, owing to their negative zeta potential (caused by -COOH group in the polymer), within the range of −30 to +30 mV [22]. The EDX detection of nitrogen in Cet-DTX NP suggested that DTX had been incorporated into the nanoparticles. The SDS-PAGE analysis confirms the conjugation of the Cet antibody onto the surface of the PLGA nanoparticles. However, the Cet-DTX NP band migrated slightly lower in contrast to the Cet antibody because of the heavier Cet-DTX NP.

The drug released from the nanoformulation over time was assessed by the *in vitro* drug release study. An early burst release of the drug from Cet-DTX NP was demonstrated, which might have resulted due to the rapid dissociation of the drug adhered to the surface of the nanoparticles. Thereafter, a slow and sustained release of the drug occurred, probably due to the erosion of the polymeric core, followed by the diffusion of the drug from the polymeric matrix. The nanoparticle drug release pattern followed the Korsemeyer-Peppas kinetic model with a high level of linearity [16,17]. Cet-DTX NP portrayed fast degradation in the acidic medium, which suggests ester hydrolysis of the polymeric core. The drug release was comparatively faster in an acidic tumour environment (pH 5), while it depicted slow and sustained release in physiologically neutral media of blood (pH 7.4) [19,21]. When DTX release from DTX NP and Cet-DTX NP was measured in PBS (pH 7.4) with 0.1% w/v tween 80, citrate buffer, acetate buffer, and bicarbonate buffer, it indicated acceptable linearity in the different kinetic models (as supported by R^2 value).

The experimental formulations (stored at 30 °C and 40 °C, and 75% RH) were agglomerated with slight structural deformation on storing for a period of 90 days, probably due to the softening of polymer stored at higher temperatures for a prolonged period. The nanoparticles were reasonably stable after being stored at

4–8 °C during this period, according to the data of accelerated stability experiments. Drug content did not vary significantly when stored at the refrigerated condition for a period of 90 days, which further suggests that the prepared nanoparticles should be stored at 4-8 °C for long-term use.

RT-PCR analysis had confirmed the overexpression of EGFR in lung cancer cells (A549 and NCI-H23), whereas it is not significantly expressed in L-132 (normal lung epithelial cells). The overexpression of EGFR on both the lung cancer cells confirmed, that more ligand (anti-EGFR Cet antibody) will bind to these cells as compared to normal lung epithelial cells, resulting in more apoptosis in cancerous cells.

Cet prevents EGFR function by binding to the receptors overexpressed on the lung cancer cells. Cetuximab showed small K_D value (0.32 nM) for A549 cells, as compared to comparatively higher K_D value (0.38 nM) for NCI-H23. The lower K_D value in case of A549 cells suggests higher affinity and tighter binding of antibody with the receptors on the cell surface. This might be due to the various non-covalent interactions (hydrogen bonding, van der Waals forces and hydrophobic forces) that participate in the affinity of a binding site [48].

In vitro cytotoxicity study was performed using the MTT assay on A549 and NCI-H23 lung cancer cells and L-132 normal lung epithelial cells. The lower IC_{50} values were observed after the lung cancer cells were treated with Cet-DTX NP, as compared to DTX NP and free drug. It might be due to the greater affinity of the Cet-DTX NP towards EGFR overexpressed lung cancer cells, thereby resulting in the greater uptake of nanoparticles within the cells. Owing to the limited expression of EGFR receptors on the surface of L-132 cells, the percentage viability of the cells was more when treated with our nanoformulations. Therefore, it indicates that our targeted nanoparticles exhibit cytotoxicity only towards lung cancer cells and not towards normal lung epithelial cells. A confocal microscopic study showed that FITC encapsulated nanoparticles (FITC-DTX NP and FITC-Cet-DTX NP) were internalised well by the lung cancer cells [14]. FACS analysis also showed time-dependent quantitative DTX NP and Cet-DTX NP uptake from 1 to 4 h in both cancer cell

types. The higher uptake of Cet-DTX NP within the cells might be due to its active targeting ability to EGFR-positive lung cancer cells.

Using the Annexin V-FITC staining procedure, apoptosis studies were carried out to check if EGFR-mediated targeted nanoformulations caused the death of A549 and NCI-H23 cells. Comparing Cet-DTX NP to DTX NP and DTX using a site-specific sustained delivery pattern, it was found that Cet-DTX NP was more effective at inducing apoptosis in A549 and NCI-H23 cells. Cet-DTX NP-targeted delivery improved cellular uptake and caused a higher drug buildup within lung cancer cells, leading to apoptosis.

The impact of site-specific and non-specific PLGA nanoparticles on the cell cycle progression in the A549 and NCI-H23 cells was examined using a flow cytometer. The outcomes demonstrated that DTX and its nanoformulations were accountable for the cell death brought on by the G2/M phase arrest. Typically, Cet-DTX NP caused mitotic arrest by releasing the drug that resulted in unstable microtubules, impairing the function of the mitotic spindle and arresting the cells in the G2/M phase of mitosis [49]. Thus, from the findings of cell cycle analysis, it can be interpreted that antibody-conjugated nanoparticles are highly potent in arresting cancer cell proliferation.

In the case of MTD analysis, there is a substantial decrease in the level of liver and kidney toxicity markers (ALP, SGOT, SGPT, urea, and creatinine) in normal mice treated with DTX NP and Cet-DTX NP, as compared to unbound DTX, indicating better tolerability of nano-encapsulated DTX, up to the dose of 10 mg/kg body weight. Moreover, there was no obvious change in the body weight of the normal mice treated with DTX NP and Cet-DTX NP, which further suggested 10 mg/kg body weight is the maximum tolerated dose of DTX when encapsulated in the form of nanoparticles. Cetuximab has a prolonged residential time in the body. The binding of Cet to EGFR on the cell surface internalises at least 50% of the Cet-EGFR complex by first 3 h, at higher doses (here ≥20 mg/kg body weight) [50], and this internalisation of huge drug amount (50%) obviously showed toxicity in animals. Further, a longer stay of Cet-NPs as non-EGFR bound forms in the system dissociates Cet from the nanoparticles surface. Such free Cet in the cellular environment might produce non-specific toxicity which often reflects as Ca^{2+} level reduction in blood, loss of appetite and weight loss. Therefore, as a cumulative effect of greater internalisation of the drug and toxicity produced by free Cet reduced the body weight of normal animals at higher doses.

The comparatively low haemolytic activity of the test nanoformulations (DTX NP and Cet-DTX NP) than free drug suggests hemocompatibility. Therefore, it could be safely administered intravenously [33]. The administration of DTX NP/Cet-DTX NP to plasma and lung tissues resulted in elevated biological $t_{1/2}$, AUC, AUMC, and MRT values, along with a decrease in elimination rate constants, which might be due to sustained release of the drug from the core of the nanoparticles for a prolonged duration.

The Cet-DTX NP showed higher amount of DTX at lung tumour sites than DTX NP and free DTX that was mainly attributed to the controlled and targeted DTX release of Cet-DTX NP in cancerous lung, which resulted less DTX released in other organs (blood, liver, kidney, heart and muscles) and more DTX accumulated in the cancerous lung. On the contrary, the deposition of free DTX followed non-specific distribution pattern in liver, kidney, heart and muscles up to 72 h. Free DTX was found to be more accumulated in the heart and kidney, as compared to the liver. The possible reason for this observation might be due to the fact that liver is the organ of the reticuloendothelial system, whose macrophages clear the drug and reduce the exposure to the parenchymal cells of liver [51]. The less accumulation of Cet-DTX NP confirmed its non-toxicity to cardiac tissues. However, the high

concentration of DTX from Cet-DTX NP was observed in liver up to 72 h, which might be due to the known fact that liver exhibits a relatively higher levels of EGFR, thereby leading to an increased uptake of Cet conjugated nanoparticles in the liver. After 72 h, the negligible concentration of Cet-DTX NP in kidney suggests it to be the major route of the elimination of our experimental nanoparticles.

When carcinogen control animals were treated with DTX, Cet conjugated and unconjugated nanoparticles, there was an increase in the survival rate of animals treated with Cet-DTX NP. This was due to the targeting ability of Cet for DTX NPs, leading to the greater accumulation of DTX at the site of lung tumour [52]. Moreover, caspase-dependent apoptosis plays a significant role in suppressing BaP-induced lung tumour development [53]. There was increased apoptosis by Cet-DTX NP when compared to free drug and DTX NP treatment. It might be due to the enhanced cellular internalisation of the nanoparticles in EGFR-overexpressed lung cancer mice [54,55].

ROS significantly influences BaP-induced lung cancer. ROS and LPO levels play a significant role in lung cancer initiation, promotion, and progression [56]. They were markedly reduced after the treatment with Cet-DTX NP, which might be due to the enriched activity of detoxification enzymes in the treated animal group, as compared to the carcinogen control group [37]. The histopathological study revealed that Cet-DTX NP greatly reduced the growth of lung tumours and significantly restored lung homogeneity, which may be attributed to the site-specific targeting of antibody-conjugated nanoparticles to the NSCLC, as compared to the normal cells.

Conclusion

In our research study, a targeted nanoformulation (Cet-DTX NP) was developed to deliver the chemotherapeutic drug, DTX to cancerous lung cells (A549 and NCI-H23) that overexpress the EGFR gene. The ability of PLGA-based nanoparticles prepared by using the multiple emulsion solvent evaporation method to retain a greater percentage of DTX and to also give carboxyl functionality for further antibody tagging has been demonstrated to be successful. The results of the current studies suggested that the potent anti-cancer drug DTX was successfully incorporated into biodegradable PLGA nanoparticles fabricated with Cet with the requisite physicochemical properties. Additionally, targeted drug delivery of DTX to the lung cancer cells that overexpress the EGFR was demonstrated by the coupling of Cet to nanoparticles manifesting the release of the drug sustainably to lung cancer cells. The results of the current *in vitro* and *in vivo* studies demonstrated that Cet-DTX NP performed better than DTX NP in terms of therapeutic improvement. Cet-DTX NP had the highest levels of cellular internalisation and apoptotic potential, most likely due to its highly-selective affinity for lung cancer cells.

Cet-DTX NP significantly reduced the malignant lung region in BaP-induced lung cancer-bearing mice. We assumed that this occurred due to an increased and sustained bioavailability of DTX in the lung tumour. When DTX was nanoencapsulated, the *in vitro* cytotoxicity was considerably reduced in normal cells, and the therapeutic efficacy *in vivo* was markedly enhanced. Overall, the study suggests that Cet-DTX NP might be investigated for use in developing potential nanoformulations to treat lung cancer, since it could deliver the drug to lung cancer cells more precisely and cause apoptosis, as opposed to its activity in healthy cells. Moreover, additional clinical research will help anticipate the dose in humans and explore the prospects of these nanoformulations in lung cancer patients.

Acknowledgements

Disclosure statement

No potential conflict of interest was reported by the authors.

Authors' contributions

Leena Kumari and Biswajit Mukherjee contributed to funding acquisition, study conception and design, manuscript drafting, and critical revision; Leena Kumari, Iman Ehsan, Arunima Mondal, and Ashique Al Hoque contributed to the analysis and interpretation of data; Pritha Choudhury, Arunima Sengupta, Ramkrishna Sen, and Prasanta Ghosh contributed in experiments, drafting and revising the work; Leena Kumari contributed in agreement to be accountable for all aspects of the work in ensuring that questions related to the accuracy or integrity of any part of the work are appropriately investigated and resolved.

Funding

References

[1]   Yuan M, Huang LL, Chen JH, et al. The emerging treatment landscape of targeted therapy in non-small-cell lung cancer. Signal Transduct. Target Ther. 2019;4(1):1–14.

[2]   Sebastian M, Reck M, Waller CF, et al. The efficacy and safety of BI 2536, a novel plk-1 inhibitor, in patients with stage IIIB/IV non-small cell lung cancer who had relapsed after, or failed, chemotherapy: results from an open-label, randomized phase II clinical trial. J Thorac Oncol. 2010;5(7):1060–1067.

[3]   Chen R, Manochakian R, James L, et al. Emerging therapeutic agents for advanced non-small cell lung cancer. J Hematol Oncol. 2020;13(1):1–23.

[4]   Hsu WH, Yang JH, Mok TS, et al. Overview of current systemic management of EGFR-mutant NSCLC. Ann Oncol. 2018;29(suppl_1):i3–i9.

[5]   Wee P, Wang Z. Epidermal growth factor receptor cell proliferation signaling pathways. Cancers. 2017;9(5):52.

[6]   Bethune G, Bethune D, Ridgway N, et al. Epidermal growth factor receptor (EGFR) in lung cancer: an overview and update. J. Thorac. Dis. 2010;2(1):48–51.

[7]   Ciardiello F, Tortora G. EGFR antagonists in cancer treatment. N Engl J Med. 2008;358(11):1160–1174.

[8]   Kawaguchi Y, Kono K, Mimura K, et al. Cetuximab induce antibody-dependent cellular cytotoxicity against EGFR-expressing esophageal squamous cell carcinoma. Int J Cancer. 2007;120(4):781–787.

[9]   Correale P, Botta C, Cusi MG, et al. Cetuximab ± chemotherapy enhances dendritic cell-mediated phagocytosis of Colon cancer cells and ignites a highly efficient Colon cancer antigen-specific cytotoxic T-cell response in vitro. Int J Cancer. 2012;130(7):1577–1589.

[10]   Sunada H, Magun BE, Mendelsohn J, et al. Monoclonal antibody against epidermal growth factor receptor is internalized without stimulating receptor phosphorylation. Proc Natl Acad Sci U S A. 1986;83(11):3825–3829.

[11]   Jaramillo ML, Leon Z, Grothe S, et al. Effect of the anti-receptor ligand-blocking 225 monoclonal antibody on EGF receptor endocytosis and sorting. Exp Cell Res. 2006;312(15):2778–2790.

[12]   Sunada H, Yu P, Peacock JS, et al. Modulation of tyrosine, serine, and threonine phosphorylation and intracellular processing of the epidermal growth factor receptor by antireceptor monoclonal antibody. J Cell Physiol. 1990;142(2):284–292.

[13]   Gavas S, Quazi S, Karpiński TM. Nanoparticles for cancer therapy: current progress and challenges. Nanoscale Res. Lett. 2021;16(1):1–21.

[14]   Patel J, Amrutiya J, Bhatt P, et al. Targeted delivery of monoclonal antibody conjugated docetaxel loaded PLGA nanoparticles into EGFR overexpressed lung tumour cells. J Microencapsul. 2018;35(2):204–217.

[15]   Viswanadh MK, Jha A, Reddy Adena SK, et al. Formulation and in vivo efficacy study of cetuximab decorated targeted bioadhesive nanomedicine for non-small-cell lung cancer therapy. Nanomedicine (Lond). 2020;15(24):2345–2367.

[16]   Paul P, Sengupta S, Mukherjee B, et al. Chitosan-coated nanoparticles enhanced lung pharmacokinetic profile of voriconazole upon pulmonary delivery in mice. Nanomedicine (Lond). 2018;13(5):501–520.

[17]   Mandal D, Shaw TK, Dey G, et al. Preferential hepatic uptake of paclitaxel-loaded poly-(DL-lactide-co-glycolide) nanoparticles—a possibility for hepatic drug targeting: pharmacokinetics and biodistribution. Int J Biol Macromol. 2018;112:818–830.

[18]   Mondal L, Mukherjee B, Das K, et al. CD-340 functionalized doxorubicin-loaded nanoparticle induces apoptosis and reduces tumor volume along with drug-related cardiotoxicity in mice. Int J Nanomedicine. 2019;14:8073–8094.

[19]   Ehsan I, Kumari L, Sen R, et al. J591 functionalized paclitaxel loaded PLGA nanoparticles successfully inhibited PSMA overexpressing LNCaP cells. J. Drug Deliv. Sci. Technol. 2022;75:103689.

[20]   Aggarwal S, Gupta S, Pabla D, et al. Gemcitabine-loaded PLGA-PEG immunonanoparticles for targeted chemotherapy of pancreatic cancer. Cancer Nanotechnol. 2013;4(6):145–157.

[21]   Bhattacharya S, Mondal L, Mukherjee B, et al. Apigenin loaded nanoparticle delayed development of hepatocellular carcinoma in rats. Nanomedicine. 2018;14(6):1905–1917.

[22]   Dutta D, Paul B, Mukherjee B, et al. Nanoencapsulated betulinic acid analogue distinctively improves colorectal carcinoma in vitro and in vivo. Sci Rep. 2019;9(1):1–20.

[23]   Alfieri RR, Galetti M, Tramonti S, et al. Metabolism of the EGFR tyrosin kinase inhibitor gefitinib by cytochrome P450 1A1 enzyme in EGFR-wild type non small cell lung cancer cell lines. Mol Cancer. 2011;10(1):143.

[24]   Patel D, Lahiji A, Patel S, et al. Monoclonal antibody cetuximab binds to and down-regulates constitutively activated epidermal growth factor receptor vIII on the cell surface. Anticancer Res. 2007;27(5A):3355–3366.

[25]   Eble JA. Titration ELISA as a method to determine the dissociation constant of receptor ligand interaction. J Vis. Exp. 2018;132:e57334.

[26]   Chakraborty S, Dlie ZY, Mukherjee B, et al. A comparative investigation of the ability of various aptamer-Functionalized drug nanocarriers to induce selective apoptosis in neoplastic hepatocytes: in vitro and in vivo outcome. AAPS PharmSciTech. 2020;21(3):1–13.

[27]   Shahrad S, Rajabi M, Javadi H, et al. Targeting lung cancer cells with MUC1 aptamer-functionalized PLA-PEG nanocarriers. Sci Rep. 2022;12(1):1–11.

[28] Townsend MH, Anderson MD, Weagel EG, et al. Non-small-cell lung cancer cell lines A549 and NCI-H460 express hypoxanthine guanine phosphoribosyltransferase on the plasma membrane. Onco Targets Ther. 2017;10:1921–1932.

[29] Nandi D, Besra SE, Vedasiromoni JR, et al. Anti-leukemic activity of *Wattakaka volubilis* leaf extract against human myeloid leukemia cell lines. J Ethnopharmacol. 2012;144(3):466–473.

[30] Chakraborty S, Dlie ZY, Chakraborty S, et al. Aptamer-functionalized drug nanocarrier improves hepatocellular carcinoma toward normal by targeting neoplastic hepatocytes. Mol Ther Nucleic Acids. 2020;20:34–49.

[31] Maya S, Sarmento B, Lakshmanan VK, et al. Chitosan cross-linked docetaxel loaded EGF receptor targeted nanoparticles for lung cancer cells. Int J Biol Macromol. 2014;69:532–541.

[32] Wang Y, Guo M, Lin D, et al. Docetaxel-loaded exosomes for targeting non-small cell lung cancer: preparation and evaluation in vitro and in vivo. Drug Deliv. 2021;28(1):1510–1523.

[33] Gaonkar RH, Ganguly S, Dewanjee S, et al. Garcinol loaded vitamin E TPGS emulsified PLGA nanoparticles: preparation, physicochemical characterization, in vitro and in vivo studies. Sci Rep. 2017;7(1):1–14.

[34] Liu K, Chen W, Yang T, et al. Paclitaxel and quercetin nanoparticles co-loaded in microspheres to prolong retention time for pulmonary drug delivery. Int J Nanomedicine. 2017;12:8239–8255.

[35] Tang X, Wang G, Shi R, et al. Enhanced tolerance and antitumor efficacy by docetaxel-loaded albumin nanoparticles. Drug Deliv. 2016;23(8):2686–2696.

[36] Qu N, Sun Y, Li Y, et al. Docetaxel-loaded human serum albumin (HSA) nanoparticles: synthesis, characterization, and evaluation. BioMed Eng OnLine. 2019;18(1):1–14.

[37] Choudhury P, Barua A, Roy A, et al. Eugenol emerges as an elixir by targeting β-catenin, the central cancer stem cell regulator in lung carcinogenesis: an in vivo and in vitro rationale. Food Funct. 2021;12(3):1063–1078.

[38] Das PJ, Paul P, Mukherjee B, et al. Pulmonary delivery of voriconazole loaded nanoparticles providing a prolonged drug level in lungs: a promise for treating fungal infection. Mol Pharm. 2015;12(8):2651–2664.

[39] Dutta D, Chakraborty A, Mukherjee B, et al. Aptamer-conjugated apigenin nanoparticles to target colorectal carcinoma: a promising safe alternative of colorectal cancer chemotherapy. ACS Appl Bio Mater. 2018;1(5):1538–1556.

[40] Li W, Yalcin M, Bharali DJ, et al. Pharmacokinetics, biodistribution, and anti-angiogenesis efficacy of diamino propane tetraiodothyroacetic acid-conjugated biodegradable polymeric nanoparticle. Sci Rep. 2019;9(1):9006.

[41] Kim HK, Choi YH, Verpoorte R. NMR-based metabolomic analysis of plants. Nat Protoc. 2010;5(3):536–549.

[42] Barua A, Choudhury P, Nag N, et al. Xanthone from *Swertia chirata* exerts chemotherapeutic potential against Colon carcinoma. Curr. Sci. 2022;122(1):47–55.

[43] BarathManiKanth S, Kalishwaralal K, Sriram M, et al. Anti-oxidant effect of gold nanoparticles restrains hyperglycemic conditions in diabetic mice. J Nanobiotechnol. 2010;8(1):1–15.

[44] Zeb A, Ullah F. A simple spectrophotometric method for the determination of thiobarbituric acid reactive substances in fried fast foods. J. Anal. Methods Chem. 2016;2016:1–5.

[45] Pal D, Sur S, Mandal S, et al. Prevention of liver carcinogenesis by amarogentin through modulation of G 1/S cell cycle check point and induction of apoptosis. Carcinogenesis. 2012;33(12):2424–2431.

[46] Tian H, Zhang T, Qin S, et al. Enhancing the therapeutic efficacy of nanoparticles for cancer treatment using versatile targeted strategies. J Hematol Oncol. 2022;15(1):1–40.

[47] Hsu PC, Jablons DM, Yang CT, et al. Epidermal growth factor receptor (EGFR) pathway, yes-associated protein (Yap) and the regulation of programmed death-ligand 1 (PD-L1) in non-small cell lung cancer (NSCLC). IJMS. 2019;20(15):3821.

[48] Yao L, Xu S. Force-induced selective dissociation of non-covalent antibody–antigen bonds. J Phys Chem B. 2012;116(33):9944–9948.

[49] Jose, A Sebastian. Transferrin-conjugated docetaxel–PLGA nanoparticles for tumor targeting: influence on MCF-7 cell cycle. Polymers. 2019;11(11):1905.

[50] Jutten B, Dubois L, Li Y, et al. Binding of cetuximab to the EGFRvIII deletion mutant and its biological consequences in malignant glioma cells. Radiother Oncol. 2009;92(3):393–398.

[51] Fernández-Urrusuno R, Fattal E, Rodrigues JM, et al. Effect of polymeric nanoparticle administration on the clearance activity of the mononuclear phagocyte system in mice. J Biomed Mater Res. 1996;31(3):401–408.

[52] Karra N, Nassar T, Ripin AN, et al. Antibody conjugated PLGA nanoparticles for targeted delivery of paclitaxel palmitate: efficacy and biofate in a lung cancer mouse model. Small. 2013;9(24):4221–4236.

[53] Cui XY, Park SH, Park WH. Auranofin inhibits the proliferation of lung cancer cells via necrosis and caspase-dependent apoptosis. Oncol Rep. 2020;44(6):2715–2724.

[54] Wathoni N, Puluhulawa LE, Joni IM, et al. Monoclonal antibody as a targeting mediator for nanoparticle targeted delivery system for lung cancer. Drug Deliv. 2022;29(1):2959–2970.

[55] Maya S, Kumar LG, Sarmento B, et al. Cetuximab conjugated O-carboxymethyl chitosan nanoparticles for targeting EGFR overexpressing cancer cells. Carbohydr Polym. 2013;93(2):661–669.

[56] Majumder D, Debnath R, Nath P, et al. Bromelain and Olea europaea (L.) leaf extract mediated alleviation of benzo (a) pyrene induced lung cancer through Nrf2 and NFκB pathway. Environ Sci Pollut Res Int. 2021;28(34):47306–47326.
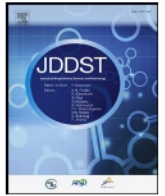
J591 functionalized paclitaxel-loaded PLGA nanoparticles successfully inhibited PSMA overexpressing LNCaP cells

Iman Ehsan [a], Leena Kumari [a,1], Ramkrishna Sen [a,1], Ashique Al Hoque [a], Biswajit Mukherjee [a,*], Alankar Mukherjee [a], Prasanta Ghosh [a], Sanchari Bhattacharya [b]

[a] Department of Pharmaceutical Technology, Jadavpur University, Kolkata, India
[b] Guru Nanak Institute of Pharmaceutical Science and Technology, Panihati, Kolkata, India

ARTICLE INFO

ABSTRACT

To evaluate the chemotherapeutic efficacy of J591 fabricated poly(d,l)-lactic-*co*-glycolic acid (PLGA) nanoparticles containing paclitaxel (Ab-PTX-NP) *in vitro* in PSMA (prostate specific membrane antigen) expressing prostate cancer cells, increase the solubility, bioavailability, circulation time, and limit systemic toxicity to achieve the maximum curative effect accompanied by controlled dosing, we formulated Ab-PTX-NP. Physicochemical characterizations such as Field emission scanning electron microscopy, Transmission electron microscopy, and Atomic force microscopy revealed that the particles were smooth-surfaced, with homogeneous distribution of drug within the particles and size were in the nano range. The encapsulation efficiency of Ab-PTX-NP was found to be 70.85%. This study acknowledges the effectiveness of Ab-PTX-NP *in vitro*, which displays elevated cellular cytotoxicity and internalization, maximum apoptosis (74.1%) in PSMA-abundant LNCaP cells, in comparison to PSMA negative PC3 cells. Pharmacokinetic data revealed the bioavailability of paclitaxel upon i.v. administration in the systemic circulation of male Balb/c mice. Herein, J591 was maneuvered in a neoteric way to carry the prepared chemotherapeutic nanoparticles directly to the affected prostate cancer cells.

1. Introduction

Prostate cancer is a common and recurrent cancer type in males globally, with a growing incidence of mortality [1]. International management of prostate cancer is still obscure and remains a global challenge to manage in spite of our perceptive of its biology and growth regulation. Recent treatments include surgical elimination of the prostate, radiation and androgen ablation (early stage), and chemotherapy (secondary treatment). Normally, androgen regulates the prostate and most of its malignancies, development, growth, and function [2,3]. Our study will utilize the ubiquitous overexpression of the prostate-specific membrane-antigen PSMA on cancerous prostate cells. PSMA plays an imperative role in diagnosis, managing as well as treating prostate cancer. The aggrandized PSMA glutamate carboxypeptidase II, having a molecular weight of about 100 kDa, is enhanced and progressively elevated in prostate adenocarcinoma and in the neovasculature of solid tumors and positively correlates with tumor progression or metastasis in prostate cancer tissue, thus, differentiating benign tumors from

malignant disease [4,5]. More crucially, the presence of internalization motif in the cytoplasmic tail of PSMA might suggest that the ligand-attached nanotherapeutics may get internalised into the cell [6].

J591, an anti-PSMA monoclonal antibody (Ab), has already been developed to target PSMA and has been demonstrated in cellular internalization [7,8]. The absence of the majority of extra-prostatic expression of PSMA on normal vasculature endothelium makes it target-specific. Paclitaxel (PTX) is the best microtubule stabilized drug licensed by the United States Food and Drug Administration (USFDA) for the therapeutic treatment of a range of malignancies, including prostate cancer. PTX inhibits mitosis and is effective in eradicating cancer cells during the interphase of the cell cycle [9]. It can be hypothesized that delivering paclitaxel (PTX) as a chemotherapeutic payload by encapsulating it in a designed PLGA (USFDA approved biodegradable polymer for human use by i.v. route) nanoparticle (PTX-NP), and further conjugating it with J591 Ab (Ab-PTX-NP), aids in the higher cellular internalization of PTX to PSMA expressed prostate cancer cells.

Elevated cellular uptake of PTX by the prostate cancer cells was

---

SEARCH FOR NEW ANTILEISHMANIAL CHEMOTHERAPEUTICS

NABANITA KAR[1], SANTANU GHOSH[1], LEENA KUMARI[1], SHREYASI CHAKRABORTY[1], TANMOY BERA[1*]

[1]Laboratory of Nanomedicine, Division of Pharmaceutical Biotechnology, Department of Pharmaceutical Technology, Jadavpur University, Kolkata 700032, India
Email: proftanmoybera@gmail.com

ABSTRACT

Objective: The objective of this work was to screen a number of compounds for their antileishmanial efficacy and cytotoxicity profiling.

Methods: Curry leaf oil, cypress oil and spikenard oil were identified by gas chromatography-mass spectrometry (GC/MS) analysis. Betulinic acid, spikenard oil, cypress oil and curry leaf oil were evaluated for their *in vitro* antileishmanial activity against *Leishmania donovani* AG83 wild-type, sodium stibogluconate resistant (SSG-resistant), paromomycin (PMM-resistant) and GE1 field type strains on axenic and cellular amastigote model and compared the results with standard drugs used to treat leishmaniasis.

Results: Betulinic acid showed strong antileishmanial activity against wild-type (SI= 192.8), SSG-resistant (SI= 19.3) and GE1 strains (SI= 100), whereas cypress oil has produced highest antileishmanial activity against PMM-resistant strains (SI= 15.09) among all the tested drugs. The data obtained also revealed that cypress oil had the maximum CC_{50} value of 452.9 µl among all standard and tested drugs.

Conclusion: All tested drugs had antileishmanial property but among them, betulinic acid possess strong antileishmanial activity in case of both wild-type and drug-resistant leishmaniasis.

Keywords: Betulinic acid, Spikenard oil, Cypress oil, Curry leaf oil, GC/MS, *In vitro* antileishmanial activity

INTRODUCTION

Leishmaniasis is a vector-borne parasitic disease caused by a protozoan parasite of the genus *Leishmania* [1]. The parasite is generally transmitted to human beings by the bite of a previously infected phlebotomine sandfly. The parasite of the disease occurs in two distinct forms: the flagellated, extracellular promastigotes that resides in the gut of female sandfly vector; and the nonflagellated, nonmotile amastigote form that exists and multiplies within the phagolysosomal compartment of macrophages [2, 3]. Depending on the causative species involved, human leishmaniasis may manifest in various forms that include cutaneous leishmaniasis (CL), mucocutaneous leishmaniasis (MCL), diffused cutaneous leishmaniasis (DCL), and visceral leishmaniasis (VL), of which visceral leishmaniasis is the most lethal form of disease caused by the species of *Leishmania donovani* [4].

Pentavalent antimonials such as meglumine antimoniate (Glucantime, Sanofi-Aventis) and sodium stibogluconate (Pentostan, GlaxoSmithKline) are variably effective against both VL and CL and may be administered via intravenous (IV), intramuscular (IM) or intralymphatic (IL) route. Unfortunately, the increased risk of cardiotoxicity, nephrotoxicity and widespread antimonial resistance has limited their use [5]. Recently, four new potential therapies are developed for the treatment of VL, such as an amphotericin B liposomal formulation (AmBisome), oral miltefosine, a parenteral formulation of aminosidine (paromomycin), and oral sitamaquine. However, individual users of these drugs have several drawbacks [6]. According to recent clinical studies, combination therapies possess potential benefits against VL in India, in which short-course multidrug treatment is compared with standard therapy [7]. Nevertheless, inadequate mode of administration of current therapies, resistance and cost-related issues have prevented their widespread use. Therefore, it is imperative to develop new antileishmanial compounds with reduced side effects and toxicity. The terpenoids also referred to as terpenes obtained from the plants might be an alternative source of potent new molecules for the treatment of several critical diseases since they are a rich source of therapeutically active constituents [8, 9].

The genus *Cupressus* (commonly known as Cypress), belonging to the family Cupressaceae [10] is traditionally known to possess several beneficial activities for the treatment of stomach ache, toothache, diabetes, inflammation, laryngitis and as astringent and contraceptive [11, 12]. *Murraya koenigii*, commonly known as 'Curry patta' in India, belongs to the member of family Rutaceae. Traditionally, the plant has been found to exhibit potent antioxidant [13], antimicrobial [14], hypoglycemic [15], antidiarrhoeal [16], hepatoprotective [17], melanogenesis inhibitory [18], antiobesity and lipid-lowering [19] activities. Spikenard, also known as 'Muskroot' is a class of aromatic amber-coloured essential oil obtained from the dried roots and rhizomes of a flowering plant *Nardostachys jatamansi*, belonging to the Valerian family [20]. Traditionally, the roots of jatamansi exhibited antimicrobial [21], antioxidant and anticholinesterase activity [22], anxiolytic [23], neuroprotective [24], anticancer [25], anti-diabetic [26] and anti-androgenic [27] activity. Betulinic acid (3-β-hydroxy-lup-20(29)-en-28-oic acid) is a pentacyclic lupane-type triterpene obtained from various plants such as *Tryphyllum peltatum*, *Ancistrocladus heyneaus*, *Diospyros leucomelas*, *Tetracera boliviana*, *Zizyphus joazeiro*, *Syzygium formosanum*, etc. [28]. It exhibits a wide range of biological activities which includes antibacterial [29], antiprotozoal [30], antiviral [31], anticancer [32], anti-inflammatory and immune-modulatory [33], and anti-HIV [34] activity.

Based on the significant biological activities and medicinal properties of several bioactive terpenoids, our present study was aimed to investigate the *in vitro* antileishmanial properties and toxicity profile of few selected terpenoids, which include cypress oil, spikenard oil, curry leaf oil, betulinic acid and to compare their activity against some conventional antileishmanial agents like amphotericin B, sodium stibogluconate (SSG), paromomycin (PMM) and miltefosine.

MATERIALS AND METHODS

Chemicals and reagents

Curry leaf oil (CAS no. 8008-52-4) was procured from Mother Herbs Pvt. ltd. (India), Spikenard oil (CAS no. 8022-22-8) was procured

ORIGINAL RESEARCH

Inhibitory effect of a new orally active cedrol-loaded nanostructured lipid carrier on compound 48/80-induced mast cell degranulation and anaphylactic shock in mice

Shreyasi Chakraborty
Nabanita Kar
Leena Kumari
Asit De
Tanmoy Bera

Laboratory of Nanomedicine, Department of Pharmaceutical Technology, Jadavpur University, Kolkata, West Bengal, India

Background: Type I hypersensitivity is an allergic reaction characterized by the overactivity of the immune system provoked by normally harmless substances. Glucocorticoids, anti-histamines, or mast cell stabilizers are the choices of treatment for type I hypersensitivity. Even though these drugs have the anti-allergic effect, they can have several side effects in prolong use. Cedrol is the main bioactive compound of *Cedrus atlantica* with anti-tumor, anti-oxidative, and platelet-activating factor inhibiting properties.

Methods: In this study, the preparation and anti-anaphylactic effect of cedrol-loaded nanostructured lipid carriers (NLCs) were evaluated. NLCs were prepared using Compritol® 888 ATO and triolein as lipid phase and vitamin E D-α-tocopherylpolyethyleneglycol 1000 succinate, soya lecithin, and sodium deoxycholate as nanoparticle stabilizers.

Results: The average diameter of cedrol-NLCs (CR-NLCs) was 71.2 nm (NLC-C_1) and 91.93 nm (NLC-C_2). The particle had negative zeta potential values of -31.9 mV (NLC-C_1) and -44.5 mV (NLC-C_2). Type I anaphylactoid reaction in the animal model is significantly reduced by cedrol and cedrol-NLC. This in vivo activity of cedrol resulted that cedrol suppressed compound 48/80-induced peritoneal mast cell degranulation and histamine release from mast cells. Furthermore, compound 48/80-evoked Ca^{2+} uptake into mast cells was reduced in a dose-dependent manner by cedrol and cedrol-NLC. Studies confirmed that the inhibition of type I anaphylactoid response in vivo in mice and compound 48/80-induced mast cell activation in vitro are greatly enhanced by the loading of cedrol into the NLCs. The safety of cedrol and CR-NLC was evaluated as selectivity index (SI) with prednisolone and cromolyn sodium as positive control. SI of CR-NLC-C_2 was found to be 11.5-fold greater than both prednisolone and cromolyn sodium.

Conclusion: Administration of CR-NLC 24 hours before the onset of anaphylaxis can prevent an anaphylactoid reaction. NLCs could be a promising vehicle for the oral delivery of cedrol to protect anaphylactic reactions.

Keywords: mast cell, degranulation, allergy, NLC, cedrol, anaphylaxis

Introduction

Over the last few decades, the occurrence of allergic asthma, rhinitis, conjunctivitis, food allergy, and anaphylaxis has increased in both the developing and the developed world.[1,2] Systemic anaphylaxis is the most deadly one among them.[3] Around 300 million people suffer from asthma globally. The World Health Organization (WHO) has estimated that worldwide mortality due to asthma has reached >180,000

Correspondence: Tanmoy Bera
Department of Pharmaceutical Technology, Jadavpur University, 188, Raja S.C Mullick Road, Kolkata 700032, West Bengal, India
Tel +91 98314 70041
Email proftanmoybera@gmail.com

Nonionic surfactant nanovesicles for cosmeceutical applications

Biswajit Mukherjee[a], Lopamudra Dutta[b,*],
Leena Kumari[a], Manasadeepa Rajagopalan[c],
Sanchari Bhattacharya[d], Manisheeta Ray[a], and
Shreyasi Chakraborty[e]

[a]Department of Pharmaceutical Technology, Jadavpur University, Kolkata, India, [b]Department of Bioengineering and Therapeutic Sciences, University of California San Francisco (UCSF), San Francisco, CA, United States, [c]East West College of Pharmacy, Bengaluru, Karnataka, India, [d]Guru Nanak Institute of Pharmaceutical Science and Technology, Panihati, Kolkata, India, [e]School of Pharmacy, Techno India University, Kolkata, India

1 Introduction

Newer cosmeceuticals have slowly occupied the cosmetic market, and the estimated cosmeceutical global market was US$51.7 Billion in 2020 despite the COVID-19 crisis. By 2027, it is expected to be US$81.8 Billion with 6.8% growth (CAGR 2020–2027) [1,2]. Cosmeceuticals mean cosmetics containing bioactive ingredients having a therapeutic effect on the surface of application [2,3]. Nanostructured substances have different physical and chemical properties along with biological activities as compared to conventional ones. In cosmeceutical products, transparency, distinctive texture, better performance, more stability, target specificity, and enhanced consumer acceptance are followed when it is structured as nanosize [4]. There is no strict scrutiny involved for the approval of nanocosmeceuticals, and clinical trials are also not required in this area, raising

*Current address: Thermo Fisher Scientific, Fremont, CA, United States

327

Chapter 6 - Guar gum-based nanomaterials in drug delivery and biomedical applications

Biswajit Mukherjee, Leena Kumari, Iman Ehsan, Prasanta Ghosh, Soumyabrata Banerjee, Samrat Chakraborty, Manisheeta Ray, Ashique Al Hoque, Ratan Sahoo

Show more ∨

+ Add to Mendeley ⁂ Share ❞ Cite

Get rights and content

Abstract

Guar gum is a natural polymer possessing various unique features such as biodegradability, biocompatibility, biosafety, etc. and it is widely used in various biomedical industries. However, the native form of guar gum exhibits difficulties in formulating biomedical devices due to its excessive swelling ability, instability, and likelihood of microbial contamination. These drawbacks could be overcome by tailoring the functional groups of guar gum to accomplish its derivatives with improved physicochemical properties. The various derivatizations of guar gum include cross-linking, carboxymethylation, amination, and grafting with other natural, synthetic, or semisynthetic polymers. Recently, various modified forms of guar gum are exploited to develop an array of nanomaterials for biomedical applications. In this book chapter, we have summarized the source and physicochemical properties of guar gum, its modification approaches, and its utilization in nanomaterial fabrication for drug delivery and biomedical applications. The limitations and future scopes of such nanomaterials are also discussed.
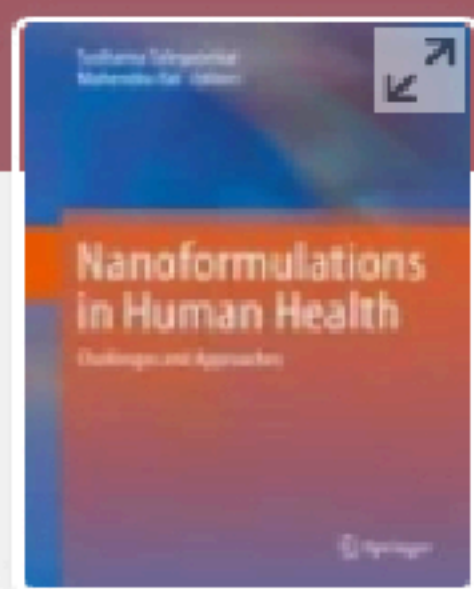
Conventional and Nonconventional Approaches to Site-Specific Targeting of Nanotherapeutics in Some Infectious Diseases and Metabolic Disorders

Biswajit Mukherjee ✉, Samrat Chakraborty, Iman Ehsan, Apala Chakraborty, Leena Kumari, Alankar Mukherjee & Shounak Sarkhel

Chapter | First Online: 31 July 2020

241 Accesses

Abstract

Systemic fungal infection in pulmonary tissue and viral infections affecting peripheral nerve claim millions of lives every year. The inability of therapeutics to reach the diseased sites at an optimum concentration, lack of patient-friendly delivery strategies, and inability of delivery strategies to penetrate and/or release the therapeutic payload at the diseased sites, keeping the normal cells unaffected, are some of the reasons which demand alternative or other methods to successfully deliver drug to affected sites. Since the end of the last century, a novel drug delivery system (drug-nanocarrier system) has reached a new benchmark with the application of nanomedicine in the treatment of fatal metabolic disorders and infectious diseases. Despite its ability to increase permeability and penetrability to cells/tissues/organs, its uncontrolled biodistribution may cause cytotoxicity to nontargeted cells, resulting in improper therapeutic management. Therefore, ligand-based active targeting strategies are most popularly exploited by researchers around the world to develop site-specific targeting of diseased sites. A plethora of site-specific nanomedicines has been developed on the laboratory scale based on conventional active targeting strategies with ligands. Even after a lot of sincere efforts, the translation of laboratory to clinic is very limited due to toxicity, stability, and the nonspecific nature of ligands. Therefore, certain nonconventional approaches of targeting therapeutics, such as gene-silencing technology, management of glioma by incorporation of brain-mimicking lipid in nanoliposomal formulations, chemical-mediated nanoliposomal formulations specifically targeted to peripheral nervous systems (PNS), and innovation of novel delivery devices, offer significant promise for effective therapeutic management. This chapter focuses on the pros and cons and future prospects of various conventional and nonconventional approaches of drug targeting with an insight to develop powerful therapeutic weapons for effective therapeutic management of deadly diseases.

Transdermal Nanomedicines for Reduction of Dose and Site-Specific Drug Delivery

8

Biswajit Mukherjee, Soma Sengupta, Soumyabrata Banerjee, Moumita Dhara, Ashique Al Hoque, Leena Kumari, Manisheeta Ray, Iman Ehsan, and Alankar Mukherjee

Abstract

The emergence of new technologies provides unique opportunities to exploit novel approaches in drug delivery. Transdermal drug delivery systems (TDDS) are one of the imperative technologies of increasing interest with the benefits of sustained/controlled drug delivery leading to patient convenience and compliance. By definition, TDDS are topically administered medications, for example, patches or semisolids, which permeate the active ingredient through the intact skin for systemic effects in a sustained manner. Transdermal drug deliveries, therefore, are the noninvasive administration of active ingredients from the skin surface across its layers, to the systemic circulation. Nanomedicinal approaches through TDDS can be utilized for site-specific delivery of drugs which can lead to the reduction of dose, too. We have reported here TDDS providing nanomedicinal strategies to deliver drug(s) to the target tissues.

Keywords

Skin · Transdermal delivery · Nanomedicine · Dose · Site-specific delivery

8.1   Introduction

Skin, being the largest organ of our body, protects us as a physiological barrier from different infections, environmental stress, such as heat or cold, and permeates the sensation with the help of nerve endings residing beneath the skin. Certain active ingredients having the potency to cross this physiological barrier can even reach the

---

B. Mukherjee (✉) · S. Sengupta · S. Banerjee · M. Dhara · A. Al Hoque · L. Kumari · M. Ray · I. Ehsan · A. Mukherjee

Department of Pharmaceutical Technology, Jadavpur University, Kolkata, India

CHAPTER 6

Nanomedicine: Could It Be a Boon for Pulmonary Fungal Infections?

BISWAJIT MUKHERJEE*, ASHIQUE AL HOQUE,
SHREYASI CHAKRABORTY, LEENA KUMARI, SOMDATTA ROY, and
PARAMITA PAUL

*Department of Pharmaceutical Technology, Jadavpur University,
Kolkata–700032, India, Tel.: +91-33-2457-2588/2414-6677/2457-2274,
E-mail: biswajit55@yahoo.com*

Corresponding author. E-mail: biswajit55@yahoo.com

ABSTRACT

Pulmonary fungal infections cover a broad spectrum related to a variety of fungal sources. They can particularly affect immune-compromised individuals. Fungi may cause lung infection when fungal material or fungal spores are inhaled. The incidence of pulmonary fungal infection has been increasing globally in the last few decades. There are a variety of fungal infections such as histoplasmosis, sporotrichosis, blastomycosis, coccidioidomycosis, paracoccidioidomycosis, cryptococcosis, aspergillosis, candidiasis, pneumonia, etc. that can cause severe pulmonary injury. The advancement of nanotechnology has revolutionized the field of pharmacotherapy because of its therapeutic potential specifically in the treatment of pulmonary fungal infections. Nanotechnology offers a plethora of advantages over conventional therapy including smaller size, larger surface area, capability of surface modification, site-specific targeting to increase local drug concentration, thereby reducing dose-related side effects, potential to entrap both hydrophilic and hydrophobic drugs, and improved pharmacokinetic profile such as extended retention time, increased half-life of drugs, etc. In this chapter, we will mainly focus on the current treatment regimen, approaches of various nanoformulations for the treatment of pulmonary fungal infections via different routes of

Certificate of Appreciation

This is to certify that

Prof. / Dr./ Mr./ Ms. __Leena Kumari__ has been awarded __Second__ prize for Poster presentation / Oral presentation in the International e-Conference on "RESEARCH ADVANCEMENT RESILIENCE IN THE PANDEMIC ERA- A Drive for Innovative Transformation"

Organized by
School of Health Sciences,

NSHM Knowledge Campus on 26th & 27th August, 2021.

Musfiqua Mookerjee
Dr. Musfiqua Mookerjee
Convener
(e-NATCONPH 2021)

Prof. Dr. Subhasis Maity
Chairman
(e-NATCONPH 2021)

3RD PHARM. TECH. IAPST INTERNATIONAL CONFERENCE ON

MOLECULAR MECHANISM OF DISEASES AND NOVEL THERAPEUTIC APPROACHES

19th-20th January, 2019

Certificate

This Certificate is awarded to Ms. / Mr. / Dr. / Prof. _Leena Kumari_

for participation as Delegate / Resource Person / Chairing a Session /

Presenting a Paper (Oral / Poster).

Prof. Gurudutta Pattnaik
Local Organizing Secretary

Mr. Anup Pal
Secretary, IAPST

Prof. Biswajit Mukherjee
Organizing Secretary

Jointly Organized by:

School of Pharmacy and Life Sciences,
Centurion University of Technology and
Management, Bhubaneswar, India

Indian Association of Pharmaceutical
Scientists and Technologists (IAPST),
Kolkata, India

Centurion
UNIVERSITY

NATIONAL SEMINAR

on

Pharmacy & Healthcare:
Traditional Knowledge to Modern Techniques

14ᵗʰ September, 2018

Certificate

This certificate is awarded to Prof. / Dr. / Mr. / Mrs. / Ms.

.... LEENA KUMARI ....

for participation as Delegate/ ~~Resource Person~~/ ~~Chairing a session~~/

Presenting a paper (~~Oral~~/ Poster).

Prof. Biswajit Mukherjee
Co-Chairman

Dr. Saikat Dewanjee
Organizing Secretary

Sponsored by:

NSERB INDIA

Science and Engineering Research Board
Department of Science and Technology
Government of India, New Delhi

Organized by:

Advanced Pharmacognosy Research Laboratory
Department of Pharmaceutical Technology
Jadavpur University, Kolkata 700032

Leena Kumari
19/07/23